

MODELING AND DESIGN OF  
IRON-CORE SHUNT REACTORS  
WITH DISCRETELY DISTRIBUTED AIR-GAPS

A THESIS SUBMITTED TO  
THE GRADUATE SCHOOL OF NATURAL AND APPLIED SCIENCES  
OF  
MIDDLE EAST TECHNICAL UNIVERSITY

BY

ATILLA DÖNÜK

IN PARTIAL FULFILLMENT OF THE REQUIREMENTS  
FOR  
THE DEGREE OF DOCTOR OF PHILOSOPHY  
IN  
ELECTRICAL AND ELECTRONICS ENGINEERING

SEPTEMBER 2012

Approval of the thesis:

**MODELING AND DESIGN OF  
IRON-CORE SHUNT REACTORS  
WITH DISCRETELY DISTRIBUTED AIR-GAPS**

submitted by **ATILLA DÖNÜK** in partial fulfillment of the requirements for the degree of **Doctor of Philosophy in Electrical and Electronics Engineering Department, Middle East Technical University** by,

Prof. Dr. Canan Özgen  
Dean, Graduate School of **Natural and Applied Sciences**

\_\_\_\_\_

Prof. Dr. İsmet Erkmen  
Head of Department, **Electrical and Electronics Engineering**

\_\_\_\_\_

Prof. Dr. Muammer Ermiş  
Supervisor, **Electrical and Electronics Eng. Dept., METU**

\_\_\_\_\_

Dr. H. Faruk Bilgin  
Co-Supervisor, **Tubitak Uzay / METU EEE (Part-Time)**

\_\_\_\_\_

**Examining Committee Members:**

Prof. Dr. H. Bülent Ertan  
Electrical and Electronics Eng. Dept., METU

\_\_\_\_\_

Prof. Dr. Muammer Ermiş  
Electrical and Electronics Eng. Dept., METU

\_\_\_\_\_

Prof. Dr. Işık Çadircı  
Electrical and Electronics Eng. Dept., HU

\_\_\_\_\_

Prof. Dr. Arif Ertuş  
Electrical and Electronics Eng. Dept., METU

\_\_\_\_\_

Assoc. Prof. Dr. İres İskender  
Electrical and Electronics Eng. Dept., GU

\_\_\_\_\_

**Date:**

14 / 09 / 2012

**I hereby declare that all information in this document has been obtained and presented in accordance with academic rules and ethical conduct. I also declare that, as required by these rules and conduct, I have fully cited and referenced all material and results that are not original to this work.**

Name Surname : Atilla DÖNÜK

Signature :

## ABSTRACT

### MODELING AND DESIGN OF IRON-CORE SHUNT REACTORS WITH DISCRETELY DISTRIBUTED AIR-GAPS

DÖNÜK, Atilla

Ph.D., Department of Electrical and Electronics Engineering

Supervisor: Prof. Dr. Muammer ERMIŞ

Co-Supervisor: Dr. H. Faruk BİLGİN

September 2012, 188 pages

In this research work detailed parallel and series equivalent circuits of a gapped iron-core shunt reactor with discretely distributed gaps are derived. The validity of the recommended equivalent circuits is verified by Finite Element Analysis and laboratory tests. Effects of fringing flux and discretely distributed gaps on inductance parameters and reactor losses are also investigated. Moving Strip Method for discretely distributed gapped shunt reactors is recommended. Two design procedures for shunt reactor with discretely distributed gaps are developed within the scope of this thesis. A simple and practical design approach is also developed which does not need any Finite Element Analysis software. This practical method is very useful for design engineers and researchers. The results of practical design approach are shown to be in good agreement with Finite Element Analysis and experimental work.

**Keywords:** Iron-Core Shunt Reactor, Air-Gap, Finite Element Method, Leakage Inductance

## ÖZ

### HAVA ARALIKLARI EŞİT DAĞITILMIŞ DEMİR-ÇEKİRDEKLİ ŞÖNT REAKTÖRLERİN MODELLENMESİ VE TASARIMI

DÖNÜK, Atilla

Doktora, Elektrik ve Elektronik Mühendisliği Bölümü

Tez Yöneticisi: Prof. Dr. Muammer ERMİŞ

Ortak Tez Yöneticisi: Dr. H. Faruk BİLGİN

Eylül 2012, 188 sayfa

Bu çalışmada hava aralıkları eşit dağıtılmış demir-çekirdekli şönt reaktörün paralel ve seri eşdeğer devreleri detaylı bir şekilde tanımlanmıştır. Önerilen eşdeğer devrelerin geçerliliği Sonlu Elemanlar Analiz yöntemi ve deneysel çalışmalarla doğrulanmıştır. Ayrıca kaçak akıların ve dağıtılmış hava aralıklarının endüktans parametreleri ve reaktör kayıpları üzerine etkisi araştırılmıştır. Hava aralıkları eşit dağıtılmış şönt reaktörler için Hareketli Şerit Metodu önerilmiştir. Bu tez kapsamında hava aralıkları eşit dağıtılmış şönt reaktör için iki tasarım yöntemi geliştirilmiştir. Herhangi bir Sonlu Elemanlar Analiz yöntemi yazılımı gerektirmeyen basit ve pratik bir tasarım yöntemi de geliştirilmiştir. Bu pratik metod tasarım ve mühendisleri ve araştırmacılar için çok kullanışlıdır. Önerilen pratik tasarım yönteminin sonuçları Sonlu Elemanlar Analizi yöntemi ve deneysel çalışmaların sonuçlarıyla tutarlı olduğu gösterilmiştir.

**Anahtar Kelimeler:** Demir-Çekirdekli Şönt Reaktör, Hava-Aralığı, Sonlu Elemanlar Yöntemi, Kaçak Endüktans

*To My Wife and My Parents,*

## ACKNOWLEDGMENTS

I would like to express my sincerest thanks and my deepest respect to my supervisor, Prof. Dr. Muammer Ermiř, for his guidance, technical and mental support, encouragement and valuable contributions during my graduate studies.

I express my sincerest thanks to my co-supervisor, Dr. H. Faruk Bilgin, for his guidance, support and encouragement during my graduate studies.

I wish to express my special thanks to Prof. Dr. Jan K. Sykulski and Dr. Mihai Rotaru for their guidance and support during my studies in University of Southampton, UK.

I would like to thank to Prof. Dr. Iřık adırcı, for her guidance and support during my graduate studies.

I would like to thank to Prof. Dr. H. Bülent Ertan and Assoc. Prof. Dr. İres İskender for their comments in my thesis progress committee.

I would like to acknowledge the valuable staff of TÜBİTAK-UZAY Power Electronics Department for their technical support during my graduate program.

Special thanks to Cem Özgür Gerçek, Alper Terciyanlı and Adnan Açık for sharing their knowledge and valuable times with me during my studies.

I am also grateful to Burhan Gültekin, Tülay Avcı and Bilge Mutluer for their encouragements and support.

I would like to express my deepest gratitude to my parents, Ayhan and Dođan Dönük and my mother and father in law, Sabiha and Muammer Gürel for their support and encouragement.

Finally, I would like to express my deepest gratitude to my wife, Gizem Gürel Dönük, for her patience, moral support and encouragement.

## TABLE OF CONTENTS

ABSTRACT .....	iv
ÖZ .....	v
ACKNOWLEDGMENTS.....	vii
TABLE OF CONTENTS.....	viii
LIST OF TABLES.....	xi
LIST OF FIGURES .....	xiv

### CHAPTERS

1. INTRODUCTION.....	1
1.1. General Overview.....	1
1.2. Shunt Reactor Studies in the Literature .....	2
1.2.1. Gapped Iron-Core Shunt Reactor .....	2
1.2.2. Reactor Design.....	4
1.2.2.1. Finite Element Method in the Design of Electrical Machines.....	5
1.2.2.2. Reactor Losses .....	6
1.2.2.3. Analytical Methods Used for Reactor Design .....	8
1.3. Scope of the Thesis.....	10
2. EQUIVALENT CIRCUIT OF A DISCRETELY DISTRIBUTED- GAPPED IRON-CORE SHUNT REACTOR .....	13
2.1. Introduction.....	13
2.2. Definition of Inductance Parameters and Equivalent Circuits of a Discretely Distributed Gapped Iron-Core Reactor .....	14
2.2.1. General Definitions.....	14
2.2.2. Parallel Equivalent Circuit Based on Magnetic Flux Distribution.....	16
2.2.3. Series Equivalent Circuit Based on Energy Definition.....	18



2.2.4. Calculation of Equivalent Inductances Based on Energy Distribution.....	19
2.2.5. Conversion of Series Equivalent Circuit into Parallel Equivalent Circuit .....	20
2.2.6. Maxwell 3D FEA Software .....	22
2.2.6.1. Magnetostatic Solution .....	22
2.2.6.1.1. Inductance Calculation.....	22
2.2.6.1.2. Analysis.....	25
2.2.6.2. Transient Solution .....	27
2.2.6.2.1. Core Loss Coefficients for Electrical Steel.....	27
2.2.7. Numerical Investigation of the Proposed Method Using Finite Element Analysis .....	29
2.3. Effects of Distributing Air-Gap into Several Discrete Air-Gaps on Inductance Parameters .....	32
2.4. Effects of Distributing Air-Gap into Several Discrete Air-Gaps on Reactor Losses .....	36
2.5. Conclusions .....	47
3. REACTOR DESIGN BY THE AID OF FINITE ELEMENT ANALYSIS.....	48
3.1. Introduction.....	48
3.2. Comparison of Sinusoidal Current and Voltage Excitation Methods .....	49
3.3. Design Procedure .....	53
3.3.1. Assumptions.....	55
3.3.2. Flowchart of the Design Procedure.....	59
3.4. Results of FEA Aided Design Work .....	67
3.4.1. Design Work According to Minimum Initial Cost Criterion.....	67
3.4.2. Design Work According to Minimum Total Loss Criterion .....	73
3.4.3. Design Work According to Minimum Present Value Cost Criterion.....	79
3.5. Comparison of Three Design Criteria .....	86
3.6. Effects of Leakage Inductance Percentage on Reactor Cost and Losses .....	89

3.7. Discussions.....	92
4. A PRACTICAL APPROACH TO THE REACTOR DESIGN.....	94
4.1. Introduction.....	94
4.2. Design Procedure and Assumptions.....	94
4.2.1. Definition of the Optimized Reactor.....	94
4.2.2. Graphical Tools Required For Practical Design Approach.....	96
4.3. Proposed Practical Design Approach .....	100
4.4. Verification of the Practical Design Approach.....	116
4.5. Discussions.....	118
5. CONCLUSIONS.....	120
REFERENCES .....	124
APPENDICES	
A. Magnetization and Core Loss Curves of M330-35AP Non-Grain Oriented Steel.....	131
B. Iteration Results for the Three Design Criteria Given in Chapter 3 .....	132
C. Various Shunt Reactor Designs Optimized According to Min PVC Design Objective .....	147
D. The Most Common Standard Transformer Ratings.....	183
E. Maxwell Software Overview .....	185
VITA.....	188

## LIST OF TABLES

### TABLES

Table 2.1	Dimensions and specifications of the two reactors .....	15
Table 2.2	Technical Specifications of the Optimized Single-Phase Shunt Reactor .....	33
Table 2.3	Equivalent Inductance Parameters of a $1/\sqrt{3}$ kV, 73 A, 50 Hz, 28 mH Single-Phase Shunt Reactor with G=32 Gaps.....	36
Table 2.4	Power Loss Components of Optimized $1/\sqrt{3}$ Kv, 73 A, 50 Hz, 28 mh Single-Phase Shunt Reactor with G=32 Gaps.....	45
Table 3.1	Harmonic current components and THD of the reactor current .....	52
Table 3.2	Execution times of the Magnetostatic and Transient Analysis tools ....	53
Table 3.3	Leakage inductance estimations used in design procedure .....	57
Table 3.4	Clearances used in design procedure.....	58
Table 3.5	Core dimensions of the optimized shunt reactors for 5% and 15% leakage inductance estimations (G=2).....	91
Table 4.1	Specifications used in design phase .....	104
Table 4.2	Technical specs, reactor parameters and performance figures of the optimized shunt reactors designed according to the FEA and Practical Approaches .....	117
Table B.1	Design parameters of minimum total loss criterion for 0.8 T.....	132
Table B.2	Design parameters of minimum total loss criterion for 1 T.....	133
Table B.3	Design parameters of minimum total loss criterion for 1.2 T.....	134
Table B.4	Design parameters of minimum total loss criterion for 1.4 T.....	135
Table B.5	Selected design parameters from iterations given for minimum total loss criterion.....	136
Table B.6	Design parameters of minimum present value cost criterion for 0.8 T .....	137

Table B.7	Design parameters of minimum present value cost criterion for 1 T .....	138
Table B.8	Design parameters of minimum present value cost criterion for 1.2 T .....	139
Table B.9	Design parameters of minimum present value cost criterion for 1.4 T .....	140
Table B.10	Selected design parameters from iterations given for minimum present value cost criterion.....	141
Table B.11	Design parameters of minimum initial cost criterion for 0.8 T .....	142
Table B.12	Design parameters of minimum initial cost criterion for 1 T .....	143
Table B.13	Design parameters of minimum initial cost criterion for 1.2 T .....	144
Table B.14	Design parameters of minimum initial cost criterion for 1.4 T .....	145
Table B.15	Selected design parameters from iterations given for minimum initial cost criterion .....	146
Table C.1	Selected design parameters for 60 K temperature rise at 1.1 kV.....	173
Table C.2	Selected design parameters for 60 K temperature rise at 13.8 kV.....	174
Table C.3	Selected design parameters for 60 K temperature rise at 34.5 kV.....	175
Table C.4	Selected design parameters for 60 K temperature rise at 1.1/13.8/34.5 kV .....	176
Table C.5	Selected design parameters for 80 K temperature rise at 1.1 kV.....	177
Table C.6	Selected design parameters for 80 K temperature rise at 13.8 kV.....	178
Table C.7	Selected design parameters for 80 K temperature rise at 34.5 kV.....	179
Table C.8	Selected design parameters for 100 K temperature rise at 1.1 kV.....	180
Table C.9	Selected design parameters for 100 K temperature rise at 13.8 kV.....	181
Table C.10	Selected design parameters for 100 K temperature rise at 34.5 kV.....	182

Table D.1	Distribution Transformers of Beyoglu Region .....	183
Table D.2	Dispersion of MV/LV Distribution Transformers Installed in Turkish Electricity Grid Related to Voltage Levels .....	183
Table D.3	ABB Oil Immersed Transformer Power Rating (34.5/0.4 kV).....	184
Table D.4	Standard Ratings of Distribution Transformers .....	184

## LIST OF FIGURES

### FIGURES

Figure 1.1	Concept of several discrete gaps and equivalent electric circuit of a gapped iron-core shunt reactor given in [5] .....	2
Figure 1.2	Equivalent electric circuit of a single-phase gapped iron-core shunt reactor given in [6] .....	3
Figure 1.3	Equivalent circuit of a gapped iron-core shunt reactor given in [7] .....	3
Figure 1.4	Parallel and series connected inductance components given in [8] .....	4
Figure 2.1	Upper halves of the two reactors having the same inductance value, a) no air-gap in the core, b) an air-gap in each limb .....	14
Figure 2.2	Single-phase shunt reactor having a laminated core with discretely distributed gaps. (a) Schematic diagram (b) Magnetic equivalent circuit .....	15
Figure 2.3	Electric equivalent circuit of a single-phase lossless reactor .....	17
Figure 2.4	Equivalent circuit of a single-phase shunt reactor with distributed gaps in its laminated core .....	18
Figure 2.5	(a) Magnetic flux pattern in a three-limb reactor, (b) a detail showing fringing, (c) energy distribution .....	18
Figure 2.6	Series equivalent circuit of a lossless reactor .....	19
Figure 2.7	Variation of inductances of a gapped iron core reactor with increasing current from completely unsaturated to highly saturated magnetic circuit .....	30
Figure 2.8	Variation of inductances of a gapped iron core reactor with increasing current in the magnetically linear region (as Fig. 2.7 but with linear scale and for smaller values of current) .....	31
Figure 2.9	Single-phase shunt reactor as specified in Table 2.2 .....	33
Figure 2.10	Variations in inductance parameters in Fig.2.6 against G .....	34
Figure 2.11	Magnetic flux density distributions of the reactor along the core for different number of distributed gaps for	

	single-phase shunt reactor (FEM results) .....	37
Figure 2.12	Variation of core loss for different number of distributed gaps for single-phase shunt reactor (Calculated by Maxwell Transient Analyses) .....	38
Figure 2.13	Variation of total core loss against number of distributed gaps for single phase shunt reactor (FEM results) .....	40
Figure 2.14	Illustration of moving strip method.....	42
Figure 2.15	Flux density distribution, (a) in the core for $G=2$ , (b) in the air-layer for $G=2$ , (c) in the core for $G=32$ and (d) in the air-layer for $G=32$ .....	42
Figure 2.16	Estimation of additional eddy-current loss arising from fringing flux around air-gaps for $G=2$ and $G=32$ , (a) Variations in fringing flux determined by moving strip method, (b) Illustration of areas corresponding to gap-losses.....	44
Figure 3.1	Excitation models of the target shunt reactor for Magnetostatic and Transient Analysis Tools .....	49
Figure 3.2	Magnetic field distributions in the magnetic cores for $B_m=1$ T .....	50
Figure 3.3	Magnetic field distributions in the magnetic cores for $B_m=1.4$ T .....	51
Figure 3.4	Magnetic field distributions in the magnetic cores for $B_m=1.6$ T .....	51
Figure 3.5	Illustration of core and winding dimensions.....	58
Figure 3.6	Flowchart of the design procedure (Matlab).....	61
Figure 3.7	Flowchart of the design procedure (FEA) .....	66
Figure 3.8	Variations in initial cost of the optimum reactor against design value of $B_m$ (min IC (N, J, t)).....	67
Figure 3.9	Variations in design parameters against $B_m$ for the optimized reactor in Fig.3.4 (min IC (N, J, t)) .....	68
Figure 3.10	Variations in PVC against $B_m$ for the optimized reactor in Fig.3.4 .....	71
Figure 3.11	Flux density distributions in the core of the optimized reactors for different peak flux densities both for $G=2$ and $G=20$ (min IC (N, J, t)) .....	72
Figure 3.12	Variations in design parameters of the optimum reactor against design value of $B_m$ (min Pt (N, J, t)) .....	73

Figure 3.13	Variations in Present Value Cost of the optimum reactor against design value of $B_m$ (min Pt (N, J, t)) .....	76
Figure 3.14	Variations in Initial Cost of the optimum reactor against design value of $B_m$ (min Pt (N, J, t)) .....	77
Figure 3.15	Flux density distributions in the core of the optimized reactors for different peak flux densities both for $G=2$ and $G=20$ (min Pt (N, J, t)).....	78
Figure 3.16	Variations in design parameters of the optimum reactor against design value of $B_m$ (min PVC (N, J, t)).....	79
Figure 3.17	Flux density distributions in the core of the optimized reactors for different peak flux densities both for $G=2$ and $G=20$ (min PVC (N, J, t)).....	85
Figure 3.18	Variations in Initial Cost against $B_m$ for three design criteria ( $G=2$ ) .....	86
Figure 3.19	Variations in Initial Cost against $B_m$ for three design criteria ( $G=20$ ) .....	86
Figure 3.20	Variations in total loss against $B_m$ for three design criteria ( $G=2$ ) .....	87
Figure 3.21	Variations in total loss against $B_m$ for three design criteria ( $G=20$ ) .....	87
Figure 3.22	Variations in Present Value Cost against $B_m$ for three design criteria ( $G=2$ ) .....	88
Figure 3.23	Variations in Present Value Cost against $B_m$ for three design criteria ( $G=20$ ) .....	88
Figure 3.24	Variations in Initial Cost against $B_m$ for 5% and 15% leakage inductance ( $G=2$ ) .....	90
Figure 3.25	Variations in total loss against $B_m$ for 5% and 15% leakage inductance ( $G=2$ ).....	90
Figure 3.26	Variations in Present Value Cost against $B_m$ for 5% and 15% leakage inductance ( $G=2$ ).....	91
Figure 3.27	Flux density distributions in the core of the reactors designed for different leakage percentages ( $G=2$ ) .....	92
Figure 4.1	Equivalent circuit of a single-phase shunt reactor with Distributed gaps in its laminated core .....	94



Figure 4.2	Leakage inductance percentage variations against kVAr rating of the reactor for 60 K temperature rise above the ambient .....	97
Figure 4.3	Leakage inductance percentage variations against kVAr rating of the reactor for 80 K temperature rise above the ambient .....	97
Figure 4.4	Leakage inductance percentage variations against kVAr rating of the reactor for 100 K temperature rise above the ambient .....	99
Figure 4.5	Leakage inductance percentage variations against kVAr rating of the reactor for 0.4 kV operating voltage.....	99
Figure 4.6	Leakage inductance percentage variations against kVAr rating of the reactor for 1.1 kV operating voltage.....	99
Figure 4.7	Leakage inductance percentage variations against kVAr rating of the reactor for 13.8 kV operating voltage.....	99
Figure 4.8	Leakage inductance percentage variations against kVAr rating of the reactor for 34.5 kV operating voltage.....	100
Figure 4.9	Simplified equivalent circuit of a single-phase shunt reactor with Several discretely distributed air-gaps.....	101
Figure 4.10	Illustration of core and winding dimensions.....	102
Figure 4.11	Flowchart of the proposed practical design approach.....	106
Figure 4.12	Flowchart of the proposed practical design approach by energy method .....	111
Figure A.1	Magnetization Curve of M330-35 AP NGO Steel.....	131
Figure A.2	Loss Curves of M330-35 AP NGO Steel .....	131
Figure C.1	Initial Cost variations against kVAr rating of the reactor for 60 K temperature rise above the ambient .....	147
Figure C.2	Initial Cost variations against kVAr rating of the reactor for 80 K temperature rise above the ambient .....	148
Figure C.3	Initial Cost variations against kVAr rating of the reactor for 100 K temperature rise above the ambient .....	149
Figure C.4	Initial Cost variations against kVAr rating of the reactor for 0.4 kV operating voltage.....	150
Figure C.5	Initial Cost variations against kVAr rating of the reactor for 1.1 kV operating voltage.....	150

Figure C.6	Initial Cost variations against kVAr rating of the reactor for 13.8 kV operating voltage.....	150
Figure C.7	Initial Cost variations against kVAr rating of the reactor for 34.5 kV operating voltage.....	151
Figure C.8	Present Value Cost variations against kVAr rating of the reactor for 60 K temperature rise above the ambient.....	151
Figure C.9	Present Value Cost variations against kVAr rating of the reactor for 80 K temperature rise above the ambient.....	152
Figure C.10	Present Value Cost variations against kVAr rating of the reactor for 100 K temperature rise above the ambient.....	153
Figure C.11	Present Value Cost variations against kVAr rating of the reactor for 0.4 kV operating voltage .....	154
Figure C.12	Present Value Cost variations against kVAr rating of the reactor for 1.1 kV operating voltage .....	154
Figure C.13	Present Value Cost variations against kVAr rating of the reactor for 13.8 kV operating voltage .....	154
Figure C.14	Present Value Cost variations against kVAr rating of the reactor for 34.5 kV operating voltage .....	155
Figure C.15	PVC/kVAr variations against kVAr rating of the reactor for 60 K temperature rise above the ambient.....	155
Figure C.16	PVC/kVAr variations against kVAr rating of the reactor for 80 K temperature rise above the ambient.....	156
Figure C.17	PVC/kVAr variations against kVAr rating of the reactor for 100 K temperature rise above the ambient.....	156
Figure C.18	PVC/kVAr variations against kVAr rating of the reactor for 0.4 kV operating voltage .....	156
Figure C.19	PVC/kVAr variations against kVAr rating of the reactor for 1.1 kV operating voltage .....	156
Figure C.20	PVC/kVAr variations against kVAr rating of the reactor for 13.8 kV operating voltage .....	157
Figure C.21	PVC/kVAr variations against kVAr rating of the reactor for 34.5 kV operating voltage .....	157
Figure C.22	Number of turns variations against kVAr rating of the reactor for 60 K temperature rise above the ambient.....	158

Figure C.23	Number of turns variations against kVAr rating of the reactor for 80 K temperature rise above the ambient.....	158
Figure C.24	Number of turns variations against kVAr rating of the reactor for 100 K temperature rise above the ambient.....	159
Figure C.25	Number of turns variations against kVAr rating of the reactor for 0.4 kV operating voltage.....	159
Figure C.26	Number of turns variations against kVAr rating of the reactor for 1.1 kV operating voltage.....	159
Figure C.27	Number of turns variations against kVAr rating of the reactor for 13.8 kV operating voltage.....	159
Figure C.28	Number of turns variations against kVAr rating of the reactor for 34.5 kV operating voltage.....	160
Figure C.29	Foil thickness variations against kVAr rating of the reactor for 60 K temperature rise above the ambient.....	160
Figure C.30	Foil thickness variations against kVAr rating of the reactor for 80 K temperature rise above the ambient.....	160
Figure C.31	Foil thickness variations against kVAr rating of the reactor for 100 K temperature rise above the ambient.....	161
Figure C.32	Foil thickness variations against kVAr rating of the reactor for 0.4 kV operating voltage.....	161
Figure C.33	Foil thickness variations against kVAr rating of the reactor for 1.1 kV operating voltage.....	161
Figure C.34	Foil thickness variations against kVAr rating of the reactor for 13.8 kV operating voltage.....	162
Figure C.35	Foil thickness variations against kVAr rating of the reactor for 34.5 kV operating voltage.....	162
Figure C.36	Current density variations against kVAr rating of the reactor for 60 K temperature rise above the ambient.....	162
Figure C.37	Current density variations against kVAr rating of the reactor for 80 K temperature rise above the ambient.....	163
Figure C.38	Current density variations against kVAr rating of the reactor for 100 K temperature rise above the ambient.....	163
Figure C.39	Current density variations against kVAr rating of the reactor for 0.4 kV operating voltage.....	163

Figure C.40	Current density variations against kVAr rating of the reactor for 1.1 kV operating voltage .....	164
Figure C.41	Current density variations against kVAr rating of the reactor for 13.8 kV operating voltage .....	164
Figure C.42	Current density variations against kVAr rating of the reactor for 34.5 kV operating voltage .....	164
Figure C.43	Variations in reactor current against kVAr rating of the reactor .....	165
Figure C.44	Leakage inductance percentage variations against total inductance of the reactor for 60 K temperature rise above the ambient .....	165
Figure C.45	Leakage inductance percentage variations against total inductance of the reactor for 80 K temperature rise above the ambient .....	166
Figure C.46	Leakage inductance percentage variations against total inductance of the reactor for 100 K temperature rise above the ambient .....	167
Figure C.47	Leakage inductance percentage variations against total inductance of the reactor for 0.4 kV operating voltage.....	167
Figure C.48	Leakage inductance percentage variations against total inductance of the reactor for 1.1 kV operating voltage.....	168
Figure C.49	Leakage inductance percentage variations against total inductance of the reactor for 13.8 kV operating voltage.....	168
Figure C.50	Leakage inductance percentage variations against total inductance of the reactor for 34.5 kV operating voltage.....	168
Figure C.51	Number of turns variations against total inductance of the reactor for 60 K temperature rise above the ambient .....	169
Figure C.52	Number of turns variations against total inductance of the reactor for 80 K temperature rise above the ambient .....	169
Figure C.53	Number of turns variations against total inductance of the reactor for 100 K temperature rise above the ambient .....	170
Figure C.54	Number of turns variations against total inductance of the reactor for 0.4 kV operating voltage.....	171
Figure C.55	Number of turns variations against total inductance of the reactor for 1.1 kV operating voltage.....	171
Figure C.56	Number of turns variations against total inductance of the reactor for 13.8 kV operating voltage.....	171
Figure C.57	Number of turns variations against total inductance of the reactor for 34.5 kV operating voltage.....	172

# CHAPTER 1

## INTRODUCTION

### 1.1 General Overview

Reactors are widely used in power engineering area at different voltage levels due to several reasons, such as reactive power compensation, filtration of harmonics, preventing lightly loaded cables or over-headed lines against dangerous over-voltages, limiting short-circuit currents, etc. [1]. They are classified and named in accordance with their function.

“The large inherent capacitance of lightly loaded transmission systems can cause two types of overvoltage in the system that can be controlled by employing shunt reactors. The first type of overvoltage occurs when the leading capacitive charging current of a lightly loaded, long transmission line flows through the inductance of the line and the system. This is referred to as the Ferranti effect; operating voltage increases with distance along the transmission line. Lagging reactive current consumed by a shunt reactor reduces the leading capacitive charging current of the line and thus reduces the voltage rise. Another type of overvoltage is caused by the interaction of line capacitance with any saturable portion of system inductive reactance, or ferroresonance. When switching a transformer-terminated line, the voltage at the end of the line can rise to a sufficient value to saturate the transformer inductance. Interaction between this inductance and the capacitance of the line can generate harmonics, causing over-voltages. Application of a shunt reactor on the tertiary of the transformer can mitigate this type of overvoltage by reducing the voltage to values below that at which saturation of the transformer core can occur,

while also providing a low non-saturable inductance in parallel with the transformer impedance” [1]. Shunt reactors are also used in Static Synchronous Compensator (STATCOM) applications. In a Voltage Source Converter (VSC) STATCOM reactors are used on the ac side and capacitors are used in the dc-link whereas in a Current Source Converter (CSC) STATCOM reactors are connected in dc-link and capacitors are on the ac side [2-4].

Shunt reactors are manufactured as single-phase or three-phase units being dry type or oil-immersed depending on the application they are used. The material used as magnetic core can be either air or iron [1]. Iron-core reactors can be built up with air-gaps in their magnetic cores, concentrically placed or discretely distributed along the limb, in order to ensure linearity and to reduce the volume of the magnetic core.

## 1.2 Shunt Reactor Studies in the Literature

### 1.2.1 Gapped Iron-Core Shunt Reactor

The equivalent electric circuit of an extra high voltage, gapped iron-core shunt reactor is given in Fig.1.1 [5]. In this work, the derivation of the equivalent circuit has not been given and losses have been neglected in the equivalent electric circuit of the shunt reactor. Leakage inductance calculation has not been discussed in [5]. On the other hand, the concept of several discrete gaps has also been introduced as illustrated in Fig.1.1.

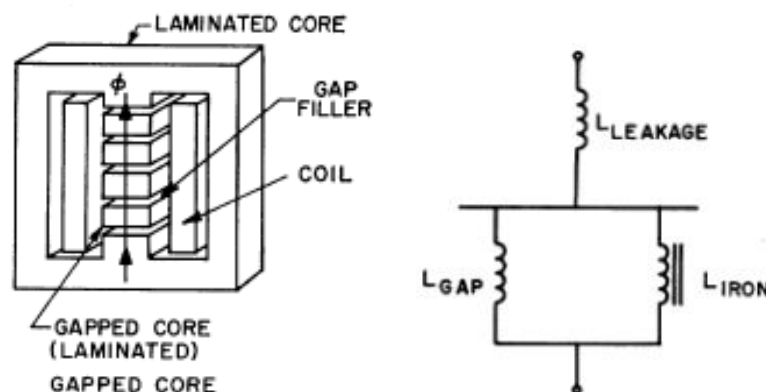


Figure 1.1 Concept of several discrete gaps and equivalent electric circuit of a gapped iron-core shunt reactor given in [5]

The derivation of the equivalent electric circuit for a single-phase, gapped shunt reactor has been presented in [6] for use in harmonic analysis. This model takes into

account nonlinearity of the iron-core and includes most of the reactor loss components as illustrated in Fig.1.2. Although leakage inductance has been defined, its calculation has not been given in [6].

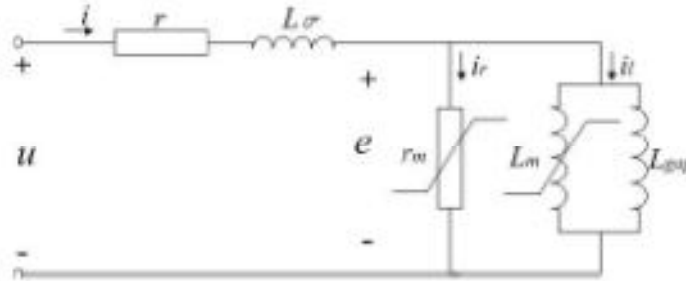


Figure 1.2 Equivalent electric circuit of a single-phase gapped iron-core shunt reactor given in [6]

A  $500/\sqrt{3}$  kV, 50 MVA shunt reactor with discretely distributed air-gaps and its power loss components have been described in [7]. Some empirical expressions have also been given in [7] for the calculation of self-inductance and its leakage inductance component. Unfortunately, the coefficients used in empirical expressions have not been clearly described so calculation of leakage inductance component is complicated. The equivalent circuit of a gapped iron-core shunt reactor described in [7] is illustrated in Fig.1.3.

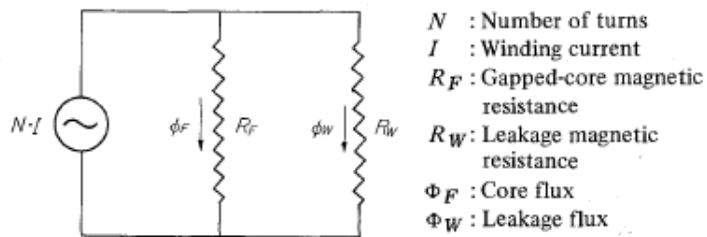


Figure 1.3 Equivalent circuit of a gapped iron-core shunt reactor given in [7]

The alternative electric equivalent circuits: parallel and series connected inductance components of an iron core reactor with discretely distributed gaps have been given in [8] by neglecting reactor losses as illustrated in Fig.1.4.

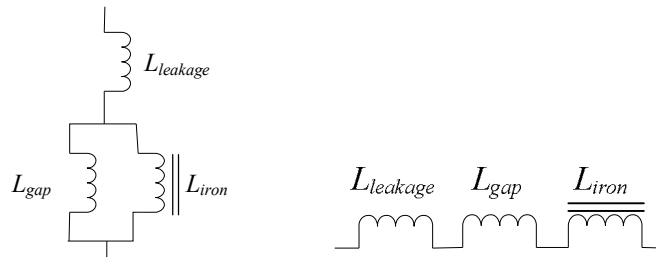


Figure 1.4 Parallel and series connected inductance components given in [8]

### 1.2.2 Reactor Design

Reactor design has been studied by many researchers since early 1900's. A method of designing air-gap in transformers and chokes to obtain a constant inductance has been introduced in [9] by experimental studies with superimposed dc and ac excitations. Calculation of apparent inductance of a gapped iron-core reactor under superimposed dc and ac excitation has been presented in [10]. An analytical design approach to gapped C-core inductor has been described using flowcharts in [11] for superimposed dc and ac currents. In [11], the standard core dimensions already produced by the manufacturers have been used in design process, the air-gap has not been distributed and leakage inductance has been neglected. A design procedure for air-gapped reactors for nine different dc-to-dc converters has been presented in [12]. The operating frequency of the reactor in [12] was 2 kHz and power rating was 400 W, fringing has been neglected, leakage inductance has not been considered, a single air-gap has been inserted in the core and core has been selected from manufacturer's catalog. A computer-aided method for design of gapped inductors operating with dc bias current has been proposed in [13]. Leakage inductance, distributing the air-gaps and a specific core design issues have not been discussed in [13]. The design of ac and dc inductors for three different types of inductors and for different excitation types has been discussed in [14]. In the equivalent circuit of the reactor given in [14] leakage inductance has been neglected and distributing the air-gaps have not been discussed. A design procedure aiming at constructing the power inductors with minimum total loss by using an iterative process has been given in [15]. Effect of leakage inductance and distributing the air-gaps have not been considered, design method has been decided to be area product method (this method is presented in section 1.2.2.3).



### **1.2.2.1 Finite Element Method in the Design of Electrical Machines**

Finite Element Method (FEM) is one of the famous numerical techniques and a very sophisticated tool widely used by engineers, scientists and researchers to solve partial differential equations arising from various engineering problems [16-17]. “Currently the finite element method is clearly the dominant numerical analysis method for the simulation of physical field distributions, with success not paralleled by any other numerical technique. In essence, the finite element method finds the solution to any engineering problem that can be described by a finite set of spatial partial derivative equations with appropriate boundary and initial conditions. It is used to solve problems for an extremely wide variety of static, steady state, and transient engineering applications from diverse markets such as automotive, aerospace, nuclear, biomedical, etc.” [16]. In practical applications, instead of using the term ‘FEM Analysis’ usually the term ‘Finite Element Analysis (FEA)’ is used. Many FEA software developed by different companies are widely used by design engineers or researchers for several purposes. Maxwell, Ansys, MagNet, Opera, Flux, FEMM, JMAG, Comsol are examples of well-known commercial FEA software.

FEA software is widely used in design of reactors. A design criterion based on energy for gapped-core magnetic micro-actuators has been presented in [18]. Analyses based on FEM have also been used in [18]. Another design study including 3D FEM analyses has been presented in [19] for saturable reactors. In [19] a single air-gap has been used and the effect of the air-gap shape on inductance characteristics has been presented, fringing or leakage flux have not been discussed. In [20] a cost-effective design of a reactor for adjustable speed drive applications has been introduced. The reactor in [20] has been designed for high-frequency application but design method has not been defined clearly. Leakage inductance and distribution of air-gap has been ignored, on the other hand FEA has been used to illustrate flux distributions. Effects of fringing flux and its calculations for gapped inductors have been presented in [21] using FEM. However, the method defined in [21] has been tested for only single-gap case, distributed gap case and leakage inductance has not been discussed. The behavior of the magnetic flux in a shunt reactor with a toroidal core, neglecting leakage flux, has been studied by 3D FEM analysis in [22]. In [23] optimization of smoothing inductors for electric traction by

obtaining the magnetic field distribution using FEA has been introduced for only single air-gap case. A foil winding model for FEA simulations has been developed and introduced in [24]. The reluctances of a gapped core inductor has been calculated in [25] using Schwarz-Christoffel Transformation. Effect of fringing flux has been considered and inductance calculated by FEA, however distribution of air-gap and leakage inductance have not been defined in [25].

In high frequency design studies the problem of fringing fields on winding losses has been investigated by some researchers. Effect of air-gap size and winding position on magnetic stray field in a gapped toroidal reactor which has a rectangular cross-section has been investigated in [26] using a single air-gap. Fringing fields due to a single air-gap in the core of a magnetic component has been presented in [27] for different winding arrangements using numerical FEM calculations.

FEA software is not only used in design of reactors but also in other electrical machines such as AC and DC rotating machines and transformers [28-41].

### **1.2.2.2 Reactor Losses**

Total loss of a gapped iron-core shunt reactor is composed of core loss, winding loss and gap loss as defined in [42]. The core material of a reactor is usually a ferromagnetic material and this material dissipates electrical energy when an alternating current is applied on it. This energy is called core loss. Core loss (also called iron loss in literature) is the sum of hysteresis loss, eddy-current loss and excess loss of the magnetic material used to built up the core.

Hysteresis loss is due to the movements of atomic dipoles in the domain walls (region separating the magnetic domains) of the material during cyclical excitation [10, 17]. When an alternating current is applied to a magnetic material, circulating currents called Eddy-currents (or Foucault-currents), are induced in the material. Eddy-current loss is due to these circulating currents within the magnetic material. These currents usually circulates normal to the width of the core, so to reduce the effect of eddy-currents, cores are usually built up with thin laminated steels and a thin insulating coating [1]. Eddy-current loss has been investigated by many

researchers in the past and the most detailed results have been presented in [43] and [44].

Excess loss is also caused by eddy-currents due to domain wall motion (based on micro-structural physical properties of the magnetic material) and has been defined in [45] by experimental work.

Gap loss is also caused by eddy-currents. Fringing flux around the air-gaps leaves and re-enters the core perpendicular to the laminations and causes eddy-currents as defined in [42] and [46].

A simplified model for core loss in EI laminated transformer cores has been presented in [47] for computer aided design. Frequency dependency in hysteresis loss of magnetic materials has been introduced in [48] as a new modeling approach. Iron loss distributions of a 3-phase reactor with a core built of grain-oriented silicon steel have been analyzed in [49] by FEA. The effect of air-gap design on foil winding losses (eddy-current losses induced in windings due to fringing fluxes) of a reactor used in high-frequency applications has been investigated in [50] by FEA. An analytical method to calculate eddy-current losses in air-core reactors has been introduced in [51]. An extension to the Steinmetz equation, used in core loss calculation with non-sinusoidal waveforms, has been proposed in [52]. A method of core loss calculation in rotating electrical machines by FEA for a wide range of frequencies has been proposed in [53]. A modified formula to represent the change in core loss coefficients has been proposed in [54] for electrical machines operating with high frequency. A method of calculating core loss of a single-phase reactor connected to an inverter power supply taking eddy-currents into account has been proposed in [55]. Core loss has been calculated for both laminated core and solid core modeling in [55]. After giving a survey of core loss measurement techniques used for magnetic materials, a novel technique to measure the core loss of low permeability magnetic materials has been given in [56] for high-frequency applications. Eddy losses in the coil of a high-voltage dry type smoothing reactor under harmonic magnetic fields has been analyzed and presented in [57]. Core loss calculation of a reactor both for laminated and solid core modeling for FEA applications have been introduced in [58] and [59] for lumped (not distributed) air-

gap. The core loss of a distributed-gapped core reactor has been analyzed in [60] for different powder core materials at high-frequency excitations by using FEA. The behavior of laminated iron-core inductors used in switching converters at high-frequencies has been presented in [61]. Losses and parameters of a three-phase five-limb inductor structure with distributed air-gaps and with a hybrid magnetic core, used in hybrid active power filter application, has been presented in [62]. Laminated core modeling of a three-phase, lumped gapped, iron-core reactor and eddy-current loss reduction in reactor core have been investigated by using 3D FEA in [63]. An improved presentation of winding losses in lumped gapped inductors using analytical FEM calculations has been reported in [65]. The skin effect in resistance of foil windings composed of rectangular conductors has been studied for microwave applications in [65]. Core losses of six kinds of core structure for a controllable reactor by FEA have been compared and presented in [66]. Analysis of a macroscopic modeling method for laminated steel used in iron cores and iron loss measurements have been presented in [67]. The use of non-oriented electrical steel in automobile motors and reactors has been presented in [68]. A 3D FEA approach to consider the effects of the lamination core loss on the transient magnetic field and its validation test on electrical motors and transformers have been proposed in [69]. A dynamic core loss model to estimate the core loss coefficients in FEA in both soft ferromagnetic materials and power ferrite materials has been improved and proposed in [70]. This model has been tested in calculating the core loss of a five limb transformer and core loss of a brushless DC motor by Maxwell 3D transient analysis.

The proposed method described in [70] is used in this thesis to calculate the core losses of the designed reactors in Maxwell FEA software.

### **1.2.2.3 Analytical Methods Used For Reactor Design**

Two approaches are widely used in ac and dc inductor design. First one is Area Product ( $A_p$ ) approach and second one is Core Geometry ( $K_g$ ) approach [42].

Area product ( $A_p$ ) has been defined in [42] as the product of effective cross-sectional area of the core ( $A_c$ ) and the winding area of the core ( $W_a$ ). In this approach the volt-

ampere (VA) capability, in other words the power of the inductor, is related to  $A_p$  as given in (1.1) [42].

$$A_p = \frac{VA (10^4)}{K_f K_u B_{ac} f J} [cm^4] \quad (1.1)$$

where;  $K_f$  is the wave form factor (4 for square wave, 4.44 for sine wave),  $K_u$  is window utilization factor,  $B_{ac}$  is the operating flux density in Tesla,  $f$  is the operating frequency in Hz and  $J$  is the current density in A/cm<sup>2</sup>.

Inductors are usually designed for a temperature rise goal, on the other hand it is also possible to design inductors for an efficiency goal [42]. If this is the case, VA of the reactor can be related to efficiency as given in (1.2) [42].

$$\alpha = \frac{VA}{K_g K_e} [\%] \quad (1.2)$$

where;  $\alpha$  is regulation in percentage.  $K_g$  and  $K_e$  are determined by core geometry and operating conditions, respectively and are defined in [42] as given in (1.3).

$$K_g = \frac{W_a A_c^2 K_u}{MLT} [cm^5] \quad (1.3)$$

$$K_e = 0.145 K_f^2 f^2 B_m^2 (10^{-4})$$

where; MLT is the mean length turn of the winding,  $B_m$  is the peak flux density in the core.  $K_f$  is the wave form factor (4 for square wave, 4.44 for sine wave),  $K_u$  is window utilization factor,  $f$  is the operating frequency.

Inductor design using above approaches are straightforward since manufacturers provide the available core dimensions in their catalogs. The VA rating of the inductor is already specified at the beginning of the design phase, after obtaining  $A_p$  from the equations given above, the suitable core satisfying this  $A_p$  value can be easily selected from the catalogs provided by the core manufacturers. These approaches are widely used in high-frequency design studies but they have limitations for low-frequency design studies especially at moderate and high power

ratings. Since the commercially available cores have been produced in specific dimensions, it is very difficult to find a core for a design at random power and voltage rating, in low-frequency design researches. Therefore, cores of such designs are needed to be produced on order with the dimensions obtained in design phase.

### **1.3 Scope of the Thesis**

The equivalent magnetic and electric circuits of shunt reactors have been defined in many studies in the literature, however derivation of the circuits, definition and calculation of inductance parameters of the shunt reactor have not been clearly defined. Moreover, the design methods given in the literature are mostly based on area product method which does not include a specific core design, that is, the core used in this design method is chosen from manufacturers' catalogs. The leakage inductance percentage in the design phase of the shunt reactor has usually been ignored and has not been considered in the literature. There is no doubt that reactor manufacturers have developed their own design methods by experience and know-how. They design and produce reactors by the aid of FEA software but they do not share or publish these methods and their details because of commercial concerns. Therefore, in this study it is aimed at developing a robust design method for gapped iron-core shunt reactors with brief descriptions and calculation of its parameters. The reliability of the proposed design approach has been tested for low voltage and medium voltage applications and also for a wide range of power rating between 50 kVAr and 5 MVAR, by using FEA software (Maxwell) simulations.

The following contributions are made to the shunt reactor design by this study;

- Derivation of equivalent circuit of a gapped iron-core shunt reactor, brief description of inductance components and their calculations
- Effects of fringing flux and discretely distributed air-gaps on inductance parameters and losses of shunt reactors
- Moving Strip Method for gap loss calculation of discretely distributed gapped iron-core shunt reactors

- Design approach by the aid of Finite Element Analysis
- A simple and short-cut Practical Design Approach for researchers and design engineers without need of any FEA software

The outline of the thesis is as given below;

Chapter 2 describes the fundamental definitions and explores the computational alternatives of equivalent inductances of discretely distributed-gapped iron-core shunt reactors. It is argued that a definition based on flux distribution may not be reliable and calculations based on energy or co-energy are thus preferable. The behaviour of all inductance components in both series and parallel equivalent circuit representations of the reactor is studied numerically using 3D finite element simulation for a wide range of currents encompassing both linear regime and extreme saturation. Effects of dividing the air-gap in the iron-core of shunt reactors into several discrete gaps on inductance parameters of the equivalent circuit, core losses and gap losses are also investigated both quantitatively and qualitatively. An optimum range for the number of discrete gaps is defined which minimizes fringing flux and hence leakage inductance. A new method called Moving Strip Method is also introduced to estimate the gap-loss in the iron-core of shunt reactors having discretely distributed small air-gaps relative to those with large air-gaps. For an optimized shunt reactor, parameters of the equivalent electric circuit are obtained by both analytical calculations and FEM analyses and then verified by measurements on the implemented reactor.

In Chapter 3, Finite Element Analysis (FEA) aided reactor design is described. A single-phase shunt reactor is designed and optimized for three design criteria, minimum Initial Cost (min IC), minimum Total Loss (min Pt) and minimum Present Value Cost (min PVC), respectively and each individual design case is repeated for four different time maximum values of flux density in the core, ( $B_m$ ); 0.8 T, 1 T, 1.2 T and 1.4 T. Inductance parameters and core losses are calculated by using Maxwell 3D simulations. Finally, the results of these three different design criteria obtained

from FEA optimizations are compared and min PVC design criterion is found to be optimum criterion for shunt reactor design.

In Chapter 4, a practical approach to the design of shunt reactors with discretely distributed air-gaps is developed. Graphical constructions for percentage leakage inductance, which have been obtained according to min PVC design criterion by using FEA optimizations, are defined for the Practical Design Approach. The verification of the proposed design approach is carried out for two different shunt reactors by using FEA tools.

In Chapter 5, general conclusions are given.

B-H curve and the loss curves of the magnetic material used in reactor core are illustrated in Appendix-A.

In Appendix-B, the results of iterations and inductance calculations performed in Maxwell for the reactors designed in Chapter 3 are presented.

The results of iterations and inductance calculations performed in Maxwell for the reactors designed in Chapter 4 are presented in Appendix C.

The most common standard transformer ratings with low voltage and medium voltage secondary windings are given in Appendix-D.



## CHAPTER 2

### EQUIVALENT CIRCUIT OF A DISCRETELY DISTRIBUTED-GAPPED IRON-CORE SHUNT REACTOR

#### 2.1 Introduction

This chapter describes the fundamental definitions and explores computational alternatives of equivalent inductances of discretely distributed-gapped iron-core reactors. It is argued that a definition based on flux distribution may not be reliable and calculations based on energy or co-energy are thus preferable. The behaviour of all inductance components in both series and parallel equivalent circuit representations of the reactor has been studied numerically using 3D finite element simulation for a wide range of currents encompassing both linear regime and extreme saturation.

Effects of dividing the air-gap in the iron-core of shunt reactors into several discrete gaps on inductance parameters of the equivalent circuit, core losses and gap losses are also investigated both quantitatively and qualitatively. An optimum range for the number of discrete gaps is defined which minimizes fringing flux and hence leakage inductance.

A new method called Moving Strip Method is also introduced to estimate the gap-loss in the iron-core of shunt reactors having discretely distributed small air-gaps relative to those with large air-gaps. For an optimized shunt reactor, parameters of the equivalent electric circuit have been obtained by both analytical calculations and FEM analyses and then verified by measurements on the implemented reactor.

## 2.2 Definition of Inductance Parameters and Equivalent Circuits of a Discretely Distributed-Gapped Iron-Core Reactor

### 2.2.1. General Definitions

Iron-core reactors are usually built up with air-gaps in their magnetic cores in order to ensure linearity and to reduce the volume of the core. In order to illustrate the effect of air-gaps on reactor volume and dimensions, a single-phase shunt reactor has been designed and simulated for two cases, one with no gaps and the other with air-gaps in the core. The magnetic flux density distributions on the cores of the two reactors are as shown in Fig.2.1.

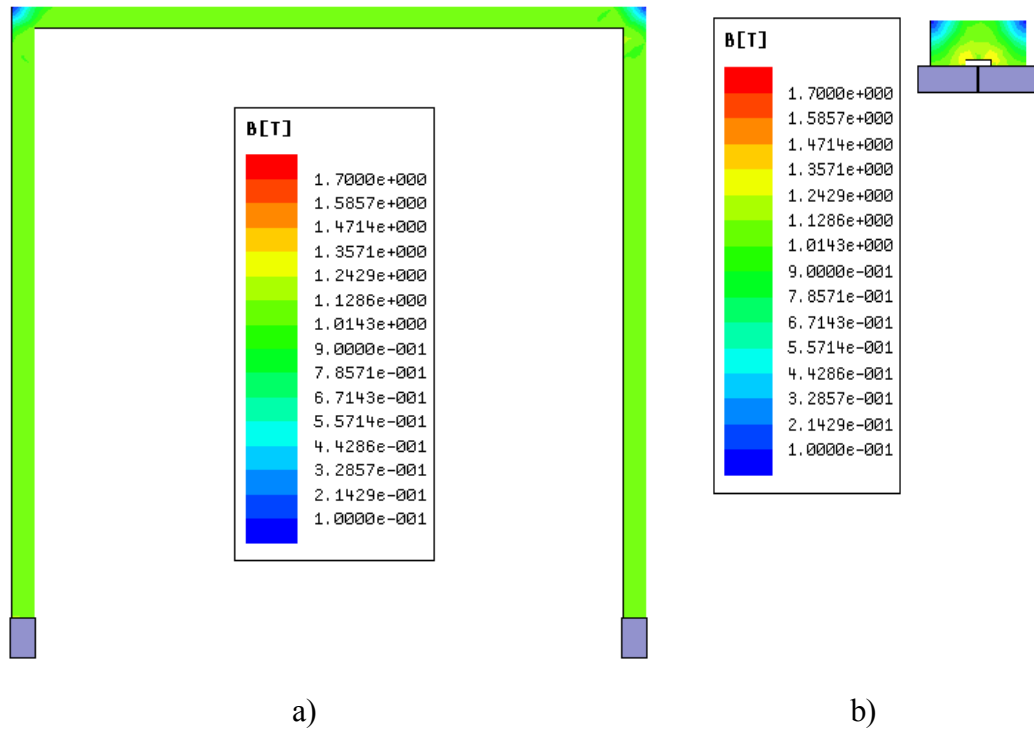


Figure 2.1 Upper halves of the two reactors having the same inductance value, a) no air-gap in the core, b) an air-gap in each limb

The dimensions and specifications of the two reactors are also illustrated in table 2.1. As can be seen from figure 2.1 and table 2.1, although both reactors have the same inductance value, the cross-sectional area of the core for the reactor without air-gaps is almost twice of the reactor with air-gaps. Mean path length of the reactor without air-gaps is about 32 meters whereas it is about 1 meter for the reactor with air-gaps. Since the permeability of the air ( $\mu_0 = 4.\pi.10^{-7}$ ) is much smaller than the permeability of any ferromagnetic core material ( $\mu_r$  equal to several thousand), a smaller reluctance therefore a higher inductance is obtained by using air-gaps in the core.

Table 2.1 Dimensions and specifications of the two reactors

Model	No gap	1 gap on each limb
Core cross-section (mm <sup>2</sup> )	306x180	197x116
Core width (mm)	5360	322
Limb height (mm)	10684	193
Winding height (mm)	684	153
Winding-yoke clearance (mm)	5000	20
Window width (mm)	5000	90
Gap length (mm)	0	16.2
N (turns)	50	116
L (mH)	29	29

Fig.2.2 shows an N-turn, single-phase shunt reactor with discretely distributed air-gaps. Its core is built up of non-grain-oriented (NGO) laminated steel. Equivalent magnetic circuit of the shunt reactor is as given in Fig.2.2.b where,  $\Phi_t$ ,  $\Phi_m$ ,  $\Phi_l$  are respectively total, magnetizing and leakage flux and  $R_c$ ,  $R_g$ ,  $R_l$  are respectively core, total air-gap and leakage reluctances. The NGO laminated core is to be operated on the linear portion of its B-H characteristic (see appendix A) in order to keep its self-inductance,  $L_s$  constant over the entire operating region. Therefore,  $R_c$ ,  $R_g$ ,  $R_l$  in Fig2.2.b would have constant values resulting in a linear magnetic circuit for an ideal shunt reactor.

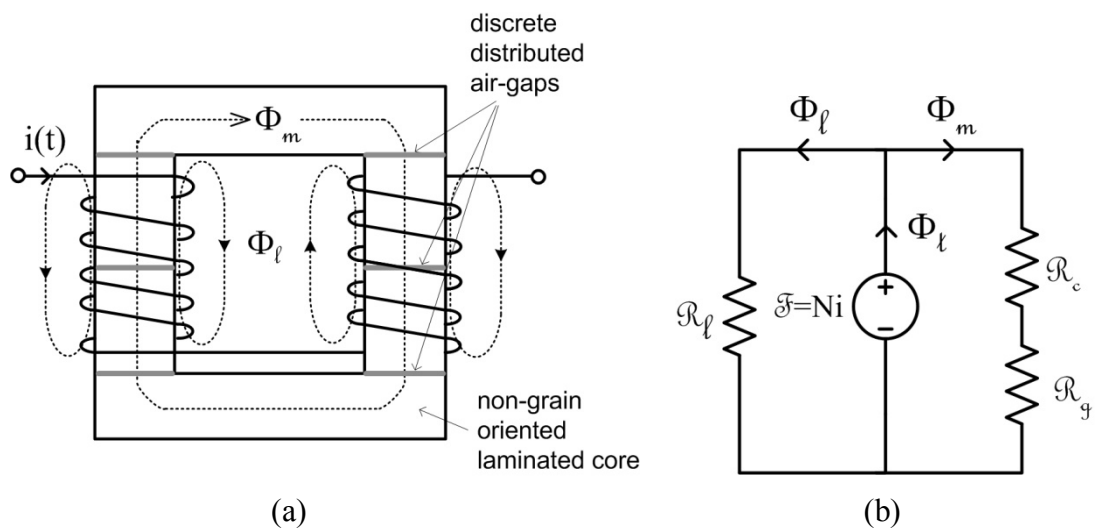


Figure 2.2 Single-phase shunt reactor having a laminated core with discretely distributed gaps. (a) Schematic diagram (b) Magnetic equivalent circuit

A conventional approach to defining the equivalent inductances of a reactor normally relies on a similar argument as for a transformer and relates the component inductances to different portions or paths of the magnetic flux [1, 5, 6, 10 and 41]. Unlike in a transformer, however, such paths are less clearly defined and the notions of ‘magnetizing’ or ‘leakage’ flux are subject to uncertainty as there is only one winding and thus mutual coupling cannot be used as the criterion [64, 71 and 72]. Moreover, in a gapped iron core design, the flux often leaves and then re-enters the core, thus the concept of which ‘flux tube’ forms the magnetizing and which the leakage portion is further confused [7, 46, 63 and 73]. Notwithstanding these difficulties, a definition based on magnetic flux is common as it provides clarity of the concept; this is illustrated by Fig. 2.2a where different flux paths are identified as a convenient approximation. This leads to various possible equivalent circuits with component inductances connected in series or parallel [8].

### 2.2.2 Parallel Equivalent Circuit Based on Magnetic Flux Distribution

The self-inductance of the shunt reactor in Fig.2.2 can be expressed as in (2.1),

$$L_s = \lambda/i \quad (2.1)$$

where,  $\lambda$  is the total flux linked by the N-turn coil.

Since  $\lambda = N(\Phi_m + \Phi_\ell)$ ,  $\Phi_\ell = F/\mathcal{R}_\ell$ ,  $\Phi_m = F/\mathcal{R}_m$  and  $\mathcal{R}_m = \mathcal{R}_c + \mathcal{R}_g$  then (2.1) can be rewritten as in (2.2).

$$L_s = N^2 \left[ \frac{1}{\mathcal{R}_\ell} + \frac{1}{\mathcal{R}_m} \right] \quad (2.2)$$

Since  $L = N^2/\mathcal{R}$  is a general self-inductance expression for linear magnetic circuits, (2.3) gives the expression of self-inductance,  $L_s$ ,

$$L_s = L_\ell + L_m \quad (2.3)$$

where,  $L_\ell$  is the leakage inductance and  $L_m$  is the magnetizing inductance of the NGO laminated core with discretely distributed air-gaps.

Since  $R_m$  is the series combination of  $R_c$  and  $R_g$ ,  $L_m$  can be determined from (2.4) in terms of core inductance  $L_c$  and gap inductance  $L_g$ .

$$\frac{1}{L_m} = \frac{1}{(N^2/\mathcal{R}_c)} + \frac{1}{(N^2/\mathcal{R}_g)} \quad (2.4)$$

$L_c$  and  $L_g$  can therefore be defined as in (2.5) and (2.6), respectively.

$$L_c = N^2/\mathcal{R}_c = N^2 \left( \frac{\mu_r \mu_0 A_c}{l_c} \right) \quad (2.5)$$

$$L_g = N^2/\mathcal{R}_g = N^2 \left( \frac{\mu_0 A_g}{l_g} \right) \quad (2.6)$$

where,  $\mu_r$  is the relative permeability of the chosen NGO laminated core material,  $\mu_0$  permeability of free space,  $A_c$  effective cross-sectional area of the core,  $l_c$  mean path length of the core,  $A_g$  effective cross-sectional area of each air-gap, and  $l_g$  the total length of the discretely distributed air-gaps.

As can be understood from (2.4), (2.5) and (2.6),  $L_m$  is the parallel combination of  $L_c$  and  $L_g$ , i.e.  $L_m = L_c // L_g$ . These derivations give the electric equivalent circuit in Fig.2.3 of a shunt reactor in which winding and core losses are neglected.

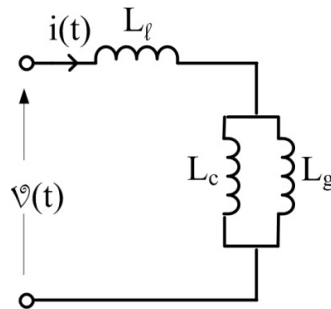


Figure 2.3 Electric equivalent circuit of a single-phase lossless reactor

On the other hand, winding losses owing to internal winding resistance ( $R_w$ ) for ac excitation, core losses ( $R_c$ ) and gap losses ( $R_g$ ) should also be included in the equivalent circuit of a practical reactor with distributed gaps in its laminated core, as shown in Fig.2.4.

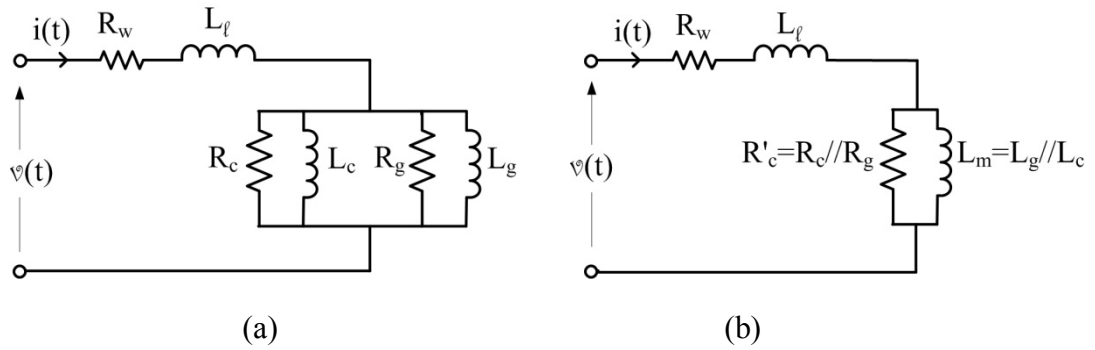


Figure 2.4 Equivalent circuit of a single-phase shunt reactor with distributed gaps in its laminated core.

Since operation takes place at power frequency (50/60 Hz), additional losses in high-frequency windings due to skin, proximity, fringing and other ac effects are neglected. Gap loss has been defined in [42] and [46] as additional eddy-current loss component in the core due to the fringing flux in the air-gap.

### 2.2.3 Series Equivalent Circuit Based on Energy Definition

The simplistic definitions based on Fig.2.2a are attractive but unfortunately also a source of difficulties in calculating the actual values. As mentioned already, the magnetic flux is unlikely to follow the strictly defined paths inside or outside the iron core and the analytical models in literature are often reliant on various empirical correction coefficients. The realistic field patterns are far more complicated as illustrated in Figs.2.5.a and 2.5.b.

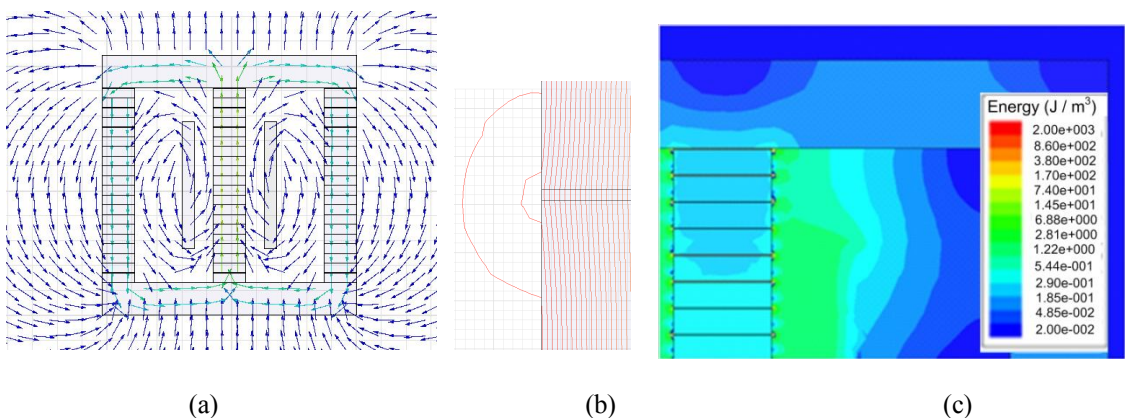


Figure 2.5 (a) Magnetic flux pattern in a three-limb reactor; (b) a detail showing fringing; (c) energy distribution.

The parallel/series connection of Fig.2.3 may not necessarily be the best representation; obviously a parallel connection of inductances may always be combined as a single equivalent inductance, as can the series connection, but the physical association with different magnetic flux paths may be lost in the process. As clearly demonstrated by Figs.2.5.a and 2.5.b, the magnetic flux paths cannot always be clearly identified as being purely leakage or magnetizing flux. Therefore, the physical meaning of component inductances of a reactor is subject to uncertainty and is open to different interpretations, leading to various equivalent circuits. Consequently, a definition based on flux distribution may not be reliable and calculations based on energy or co-energy are thus preferable. Resulting series equivalent circuit based on energy definition is given in Fig.2.6 where  $L_l$ ,  $L_{cs}$  and  $L_{gs}$  are leakage, core and gap inductances of the series equivalent circuit of the gapped iron core reactor, respectively.

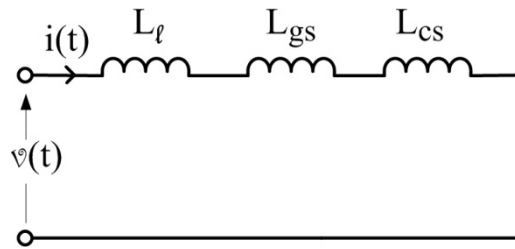


Figure 2.6 Series equivalent circuit of a lossless reactor

The self- inductance,  $L_s$  in Fig.2.6 of the shunt reactor is obviously the sum of the three inductances, i.e.  $L_s = L_l + L_{gs} + L_{cs}$ .

#### 2.2.4 Calculation of Equivalent Inductances Based on Energy Distribution

The difficulties associated with the analytical calculations are probably best illustrated by recalling the equations used for example in [7] based on the equivalent circuit of Fig.2.3:

$$L_g = \frac{\mu_0 N^2 A_c}{l_g k_g} \quad (2.7)$$

$$L_l = \frac{\mu_0 N^2 A_l k_l}{l_l} \quad (2.8)$$

where  $N$  is the number of turns,  $A_c$  the cross-section of the limb,  $A_l$  the cross-section of the leakage flux path,  $l_g$  the total length of the gaps,  $l_l$  the ‘length’ of the leakage path,  $k_g$  and  $k_l$  empirical correction coefficients (both less than 1). While  $L_g$  has a reasonable chance of being estimated correctly as dominated by the well defined gaps in the limbs, the calculation of the leakage inductance  $L_l$  is subject to all sorts of uncertainties and inevitable simplifications.

An alternative association can be made between the relevant component inductances and the energy (or co-energy) associated with different portions of the magnetic circuit. The total energy (which will be the same as co-energy if the magnetic circuit is unsaturated, which is normally the case in practical reactors) may be split into energy associated with the magnetic core, the gaps in the limbs and the rest of the volume surrounding the core (see an example in Fig. 2.5.c); this leads naturally to three component inductances connected in series (as illustrated in Fig. 2.6) with clear interpretation of the role and contribution of each element. There is no longer a need to be concerned about the actual flux paths. Therefore;

$$W = \frac{1}{2} L I^2 \quad (2.9)$$

$$W_t = W_g + W_c + W_l = \frac{1}{2} I^2 L_s = \frac{1}{2} I^2 (L_{gs} + L_{cs} + L_l) \quad (2.10)$$

where  $W_t$  is the total energy of the device,  $W_g$  is the energy associated with the volume filled by air-gaps in the limbs,  $W_c$  is the energy related to the volume filled by iron core, and  $W_l$  is the energy of the field in the rest of the system, respectively. Hence  $L_{gs}$ ,  $L_{cs}$  and  $L_l$  are the inductances calculated based on the energy corresponding to these volumes.

### 2.2.5 Conversion of Series Equivalent Circuit into Parallel Equivalent Circuit

The magnetic circuit of the gapped iron core may also be described in terms of magnetic fluxes and associated reluctances, namely by a series connection of two reluctances, one given by the gap and the other by the iron path of the flux, as shown in Fig. 2.2.b. Comparing the two equivalent circuit representations of the gapped iron core (Fig. 2.3 and Fig. 2.2.b) it can therefore be argued that there exists one unique



logical transformation of the series connection of inductances into a parallel connection, and vice versa. (A pure electrical circuit approach would obviously suggest that there is infinite number of possibilities of such a transformation, all resulting in identical total equivalent value of the inductance, which after all is what really matters.) As the leakage inductance,  $L_l$  is always likely to be connected in series with the rest, attention needs to be focused on  $L_g$  and  $L_c$  as – depending on the model used, energy or flux based – a series or parallel representation may be more appropriate, respectively.

The crux of the argument is therefore that the ratio of the energies corresponding to the two equivalent circuit representations should be preserved irrespectively of the connection. For the connection in series we can use inductances and associated current directly, whereas for the parallel connection work in terms of the flux and reluctances; thus

$$\frac{W_{gs}}{W_{cs}} = \frac{L_{gs} I^2}{L_{cs} I^2} = \frac{\Phi^2 R_g}{\Phi^2 R_c} \quad (2.11)$$

where  $R_g$  and  $R_c$  are the reluctances of the magnetic circuit of the reactor limb (these reluctances are connected in series as in Fig. 2.2.b). Therefore, the circuits in Figs. 2.3 and 2.2.b are equivalent in terms of associated energy. On the other hand, since inductance is inversely proportional to reluctance (obviously the square of the number of turns of the winding needs to be accommodated at some stage), the two reluctances connected in series can be expressed in terms of inductances as

$$R_g + R_c = \frac{l}{L_g} + \frac{l}{L_c} \quad (2.12)$$

which results in a parallel connection of the two equivalent inductances as depicted by Fig. 2.3, where  $L_g$  and  $L_c$  are the inductance of the air-gap and the iron core of the parallel equivalent circuit, respectively. This simple scheme provides a unique transformation of parallel into series connection of equivalent inductances, or the other way round, while preserving the proportions of component energies. The resultant inductance is of course the same:

$$L_{gs} + L_{cs} = \frac{l}{\frac{l}{L_g} + \frac{l}{L_c}} \quad (2.13)$$

Finally, the relationship between the inductances of the parallel equivalent circuit and the series equivalent circuit, as given by the energy ratio, may be written as

$$\frac{W_{gs}}{W_{cs}} = \frac{L_{gs}}{L_{cs}} = \frac{\frac{l}{L_g}}{\frac{l}{L_c}} \quad (2.14)$$

Consequently, equations (2.13) and (2.14) can be used to easily convert from one representation into the other as desired to calculate the equivalent inductances of the gapped iron core reactor.

## 2.2.6 Maxwell 3D FEA Software

Maxwell is one of the widely used Finite Element Analysis software produced by Ansoft Company. It is capable of performing 2D and 3D electromagnetic analysis with different solution types such as Electrostatic Solution, Magnetostatic Solution, Eddy-Current Solution and Transient Solution. Detailed information on Maxwell software is given in Appendix-E. In this thesis, Magnetostatic Analysis has been used to calculate inductance parameters of the reactors, to calculate and plot the flux density distributions in the reactor cores, to calculate the fringing fluxes around the air-gaps, etc. Transient Analysis has also been used to calculate the reactor losses.

### 2.2.6.1 Magnetostatic Solution

#### 2.2.6.1.1 Inductance Calculation

Definition and calculation of inductances is given below as defined in Maxwell technical notes [16].

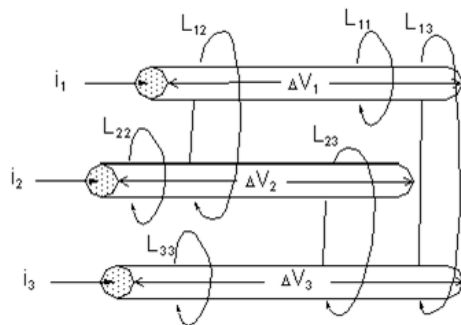
“Maxwell uses apparent inductance to calculate flux linkage as a function of the independent variables, since it changes with current as the material properties change. To obtain apparent inductances for nonlinear materials in Maxwell, a two-

step procedure is followed:

1. A nonlinear magnetostatic solution is generated with all sources at user specified values. This establishes a value of permeability that varies with each mesh element, since the degree of saturation varies throughout the device.
2. These self-consistent values are used in a linear solution for the inductance matrix, with each coil current set to one ampere. The resulting values are apparent inductances, which vary with each specified coil current operating point because the material properties change.

The apparent inductance calculated by Maxwell at the actual operating point due to all sources in the model (currents in the coils but also permanent magnets) is the base of all inductance calculations. It should be noted that the apparent value relates to the local frozen, current dependent absolute permeability as described above in the two step process.

An inductance matrix represents the magnetic flux linkage between the current loops in a system. Given the three current loops below, the relationship between induced flux and currents is as follows:



$$\lambda_1 = L_{11} i_1 + L_{12} i_2 + L_{13} i_3$$

$$\lambda_2 = L_{12} i_1 + L_{22} i_2 + L_{23} i_3$$

$$\lambda_3 = L_{13} i_1 + L_{23} i_2 + L_{33} i_3$$

This can be expressed in matrix form as:

$$\begin{bmatrix} \lambda_1 \\ \lambda_2 \\ \lambda_3 \end{bmatrix} = \begin{bmatrix} L_{11} & L_{12} & L_{13} \\ L_{12} & L_{22} & L_{23} \\ L_{13} & L_{23} & L_{33} \end{bmatrix} \begin{bmatrix} i_1 \\ i_2 \\ i_3 \end{bmatrix}$$

The inductance matrix above gives the relationship between  $\lambda$  and  $i$  for the three independent current loops. In a device with  $n$  current loops, this relationship would be expressed by an  $n \times n$  inductance matrix. Inductance matrix values are specified in henries.

If one ampere is applied to Current Loop 1 and zero amperes are applied to the other two loops, the inductance matrix becomes:

$$\begin{bmatrix} \lambda_1 \\ \lambda_2 \\ \lambda_3 \end{bmatrix} = [L] \begin{bmatrix} 1 \\ 0 \\ 0 \end{bmatrix} = \begin{bmatrix} L_{11} \\ L_{12} \\ L_{13} \end{bmatrix}$$

The diagonal terms in the matrix (such as  $L_{11}$ ) represent the self-inductance of each current loop. Self-inductance is numerically equal to the flux linkage in a current loop when one ampere is flowing in it, and no current is flowing in the other loops. For example,  $L_{11}$  is equal to the flux in Current Loop 1 when one ampere is flowing in that current loop, and no current is flowing in the other loops.

The off-diagonal terms (such as  $L_{12}$ ,  $L_{13}$ ) represent the mutual inductances between the current loops. Mutual inductance is numerically equal to the flux linkage in a current loop when one ampere is flowing through another loop, and no current is flowing anywhere else. For example,  $L_{12}$  is equal to the flux linkage in Loop 1 when one ampere is applied to Loop 2 and no current is flowing in the other loops.

Note that the inductance matrix is symmetric about the diagonal. This indicates that the mutual effects between any two loops are identical. For instance,  $L_{13}$ , the inductance between Current Loop 1 and Current Loop 3, is equal to the inductance between Current Loop 3 and Current Loop 1.

To compute an inductance matrix, the software performs a sequence of magnetostatic field simulations. In each field simulation, one ampere is allowed to flow in a single conductor. For an  $n$ -conductor system,  $n$  field simulations are automatically performed. The energy stored in the magnetic field that couples two conductors is:

$$W_{ij} = \frac{1}{2}LI^2 = \frac{1}{2} \int_{\Omega} B_i \cdot H_j d\Omega$$

where:

- $W_{ij}$  is the energy stored in the magnetic field linking conductor  $i$  with conductor  $j$ .
- $I$  is the current in conductor  $i$ .
- $B_i$  is the magnetic flux density where one ampere is allowed to flow through conductor  $i$ .
- $H_j$  is the magnetic field where one ampere is allowed to flow through conductor  $j$ .

The inductance coupling conductors  $i$  and  $j$  is therefore:

$$L_{ij} = \frac{2W_{ij}}{I^2} = \int_{\Omega} B_i \cdot H_j d\Omega$$

For multi-turn conductors, the net value of inductance is the value given by:

$$L_{net} = N^2 L_{matrix}$$

where  $N$  is the number of turns in the coil.”

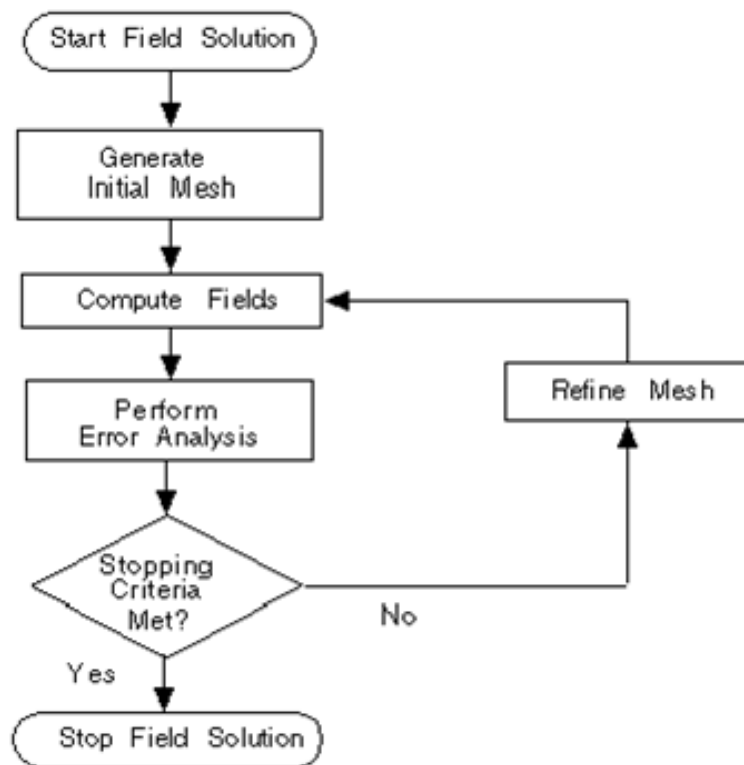
### 2.2.6.1.2 Analysis

Adaptive analysis is used in Magnetostatic Solution and it is defined in Maxwell technical notes as given below [16].

“During adaptive analysis the system iteratively refines the starting mesh in order to reduce the size of individual elements in areas of high error — thus improving the accuracy of the solution.

When an adaptive analysis is performed:

- Maxwell generates a field solution using the specified mesh.



- It then analyzes the accuracy of the solution by calculating an energy value based on the error in the solution. The exact mechanism for evaluating the error varies by solution type. For example, in magnetostatic it can use Curl H to find the current density and then subtract all input currents and other sources. For a perfect solution the result would be zero, for a real, finite mesh the result is some amount of residual current density. An energy value calculated from this residual current density is called the error energy. The “Energy Error %” is the error energy as a percentage of the total energy (calculated with the original sources).

- If more than 1 pass has been completed, the software also calculates the change in total energy from the previous pass. The percentage difference is the “Delta Energy (%)”. Adaptive refinement continues until both the “Energy Error %” and the “Delta Energy (%)” are below the target Percent Error specified by the user (or until it reaches the Maximum Number of Passes requested).

- When the error targets are not satisfied the mesh is refined. This is generally done by subdividing the elements with the highest error energy into smaller elements.

- The user can optionally request to “Use Output Variable Convergence”. This is an additional stopping criterion. The Energy Error % and the Delta Energy must still be below the target Percent Error, but the software will also compute the specified Output Variable for each adaptive pass and will calculate the percentage change in that value for each pass after the first (this is the “Output Var. Delta (%)”). The solution will continue until the energy error criteria are met and the Output Var. Delta is below the target “Max. Delta Per Pass” specified by the user for output variable convergence (or until Maximum Number of Passes).”

### 2.2.6.2 Transient Solution

“The transient solver in Maxwell supports the coil terminals and winding definitions. Thus it is possible to specify the number of turns of coils in models which is necessary for the calculation of global quantities with high engineering value such as flux linkage and back emf of coils. Thus for the 3D transient solver a number of quantities are automatically calculated and displayed as 2D plots (functions of time): voltage (current), flux linkage, back emf. Other global quantities can be also calculated by the 3D transient solver and displayed as 2D plots such as power loss, core loss, stranded loss, electromechanical quantities such as force/torque, speed and displacement” [16].

#### 2.2.6.2.1 Core Loss Coefficients for Electrical Steel

In order to calculate the core loss in Maxwell Transient Analysis, the loss curves of the core material obtained from the manufacturer have been defined in solution step. Calculation of the core loss coefficients for electrical steel from the loss curves is defined in Maxwell technical notes [16] as given below.

“Under sinusoidal flux conditions, core loss is computed in the frequency domain as the following:

$$P_v = P_h + P_c + P_e = K_h f (B_m)^2 + K_c (f B_m)^2 + K_e (f B_m)^{1.5}$$

When a DC component exists in the flux density, the core loss is modified to the following:

$$P_v = C_{dc} K_h f (B_m)^2 + K_c (f B_m)^2 + K_e (f B_m)^{1.5}$$

where

- $B_m$  is the amplitude of the AC flux component,
- $f$  is the frequency,
- $K_h$  is the hysteresis core loss coefficient,
- $K_c$  is the eddy-current core loss coefficient, and
- $K_e$  is the excess core loss coefficient.

$C_{dc}$  is computed from the following equation:

$$C_{dc} = \sqrt{K_{dc} |B_{dc}| / B_m + 1}$$

where

- $B_{dc}$  is the DC flux component, and
- $K_{dc}$  is the coefficient considering the DC flux bias effects.

The principles of the computation algorithm for  $K_h$ ,  $K_c$ , and  $K_e$  are summarized as below. Since the manufacturer-provided loss curve is obtained under sinusoidal flux conditions at a given frequency, these coefficients can be derived in the frequency domain.

The iron-core loss without DC flux bias is expressed as the following:

$$P_v = P_h + P_c + P_e = K_h f (B_m)^2 + K_c (f B_m)^2 + K_e (f B_m)^{1.5} = K_1 B_m^2 + K_2 B_m^{1.5}$$

where

$$K_1 = K_h f + K_c f^2$$



$$K_2 = K_2 f^{1.5}$$

The classical eddy-current loss coefficient is calculated directly as

$$K_e = \pi^2 \cdot \sigma \cdot \frac{d^2}{6}$$

where  $\sigma$  is the conductivity and  $d$  is the thickness of one lamination sheets.

Minimize the quadratic form to obtain  $K_1$  and  $K_2$ .

$$f(K_1, K_2) = \sum \left[ P_{vi} - \left( K_1 B_{mi}^2 + K_2 B_{mi}^{1.5} \right) \right]^2 = \min$$

where  $P_{vi}, B_{mi}$  – the  $i$ -th point of the data on the measured loss characteristics curve.

The other two loss coefficients are obtained as

$$K_h = \left( K_1 - K_e f_0^2 \right) l f_0$$

$$K_e = K_2 l f_0^{1.5}$$

where  $f_0$  is the testing frequency for **Loss Curve**.”

## 2.2.7 Numerical Investigation of the Proposed (Conversion and Calculation)

### Method using Finite Element Analysis

The behaviour of all components in both series and parallel representations of the inductance has been studied numerically using 3D finite element simulation for a wide range of currents encompassing both linear regime and extreme saturation.

The rated current of the gapped iron core reactor model used in simulations is 100 A; for illustrative purposes a particular design has been considered here but the actual values of inductance are of no consequence, only the relative proportions matter. The magnetic field of the reactor was simulated using Maxwell 3D software (as described in above section 2.2.6) for a series of values of the driving current from 1 A (1 percent of the rated current, hence magnetic circuit completely linear, well below saturation) to 100000 A (1000 times the rated current, thus magnetic circuit

extremely highly saturated). For each case the equivalent inductances of the series equivalent circuit were calculated based on the energy values as described in the previous section (equations 2.9 and 2.10). Finally, this series equivalent circuit was converted into a parallel equivalent circuit (using equations 2.11 – 2.14).

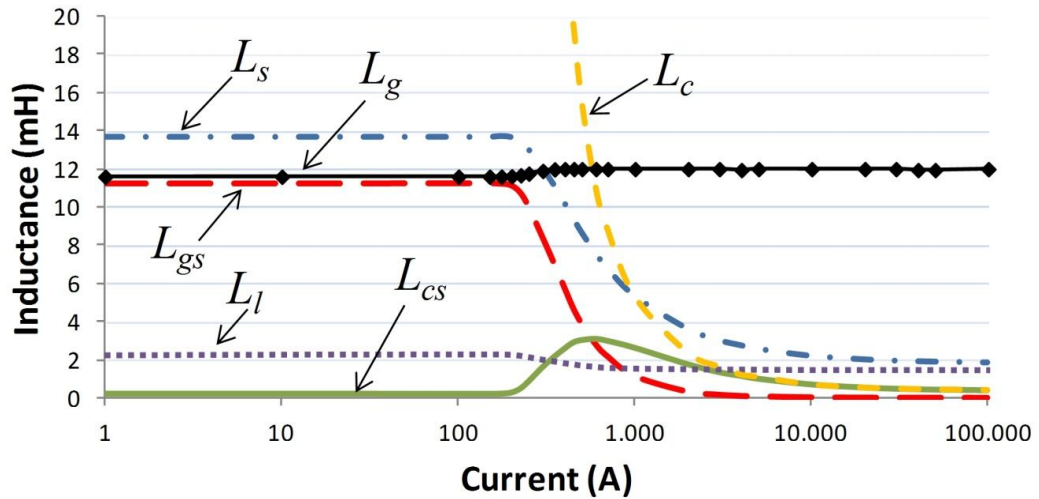


Figure 2.7 Variation of inductances of a gapped iron core reactor with increasing current from completely unsaturated to highly saturated magnetic circuit.

The results are presented in Figs.2.7 and 2.8, the former using a logarithmic scale to cover the full range of currents used (from unsaturated to highly saturated core), while the latter focusing on the range of currents of more practical interest using a linear scale but still allowing some saturation to be depicted as well. Up to about 150% of the rated current all inductances are effectively constant as expected in such designs. The more saturated region is perhaps of less practical importance but nevertheless shows interesting behaviour. Most notably, the leakage inductance (represented in the circuit as a series connection), and the inductance associated with the gaps in the limbs in the parallel circuit representation, both change very little throughout the whole range, whereas all other inductances (in either series or parallel representation) vary quite dramatically. As expected, the air-gap inductance totally dominates the ‘section’ responsible for the main flux (passing through the limbs and air gaps) below saturation and matches well the value calculated from (2.7). (It is also worth noting – which was to be expected – that the leakage inductance  $L_l$

calculated from the simplified model of (2.8) is in very poor agreement with the reality.)

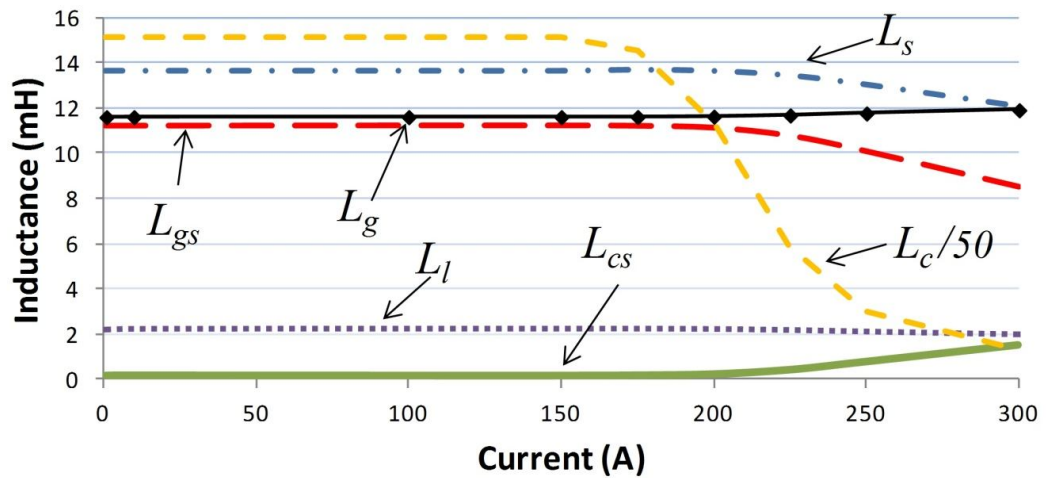


Figure 2.8 Variation of inductances of a gapped iron core reactor with increasing current in the magnetically linear region (as Fig. 2.7 but with linear scale and for smaller values of current).

For higher values of current the magnetic saturation results in the inductance representing the iron (in both series and parallel representation) becoming important so that it cannot be omitted (as a short or open circuit respectively), although in reality this inductance can never be neglected if core losses are of interest. Under extreme saturation the reactor behaves like an air-cored device and the leakage inductance takes over.

The somewhat strange behaviour of the iron inductance  $L_{cs}$  (in the series circuit) at high saturation is perhaps difficult to explain, as first the value rises, then reaches a peak and finally starts to decrease, but this is simply a reflection of the fact that highly saturated iron acts like air and the final proportions of the ‘gap’ and ‘iron’ inductances will be related more to geometry rather than to magnetic properties.

The main purpose of the above numerical investigation was to demonstrate how the energy criterion allows for simple and unique transformation between parallel and series representations of the gapped limb of the reactor. In view of the recognised difficulties of defining the different components of flux (magnetizing, leakage, gap)

it is therefore recommended that energy/co-energy is used throughout while relevant equivalent circuits naturally linked with such fluxes may be established ‘retrospectively’ by applying the transformation suggested in this chapter.

### **2.3 Effects of Distributing Air-Gap into Several Discrete Air-Gaps on Inductance Parameters**

In this section, effects of discretely distributed gaps on equivalent inductances of a shunt reactor are investigated by using the results of FEM analyses (Maxwell 3D models). The results are then verified by analytical calculations and experimental work carried out on an optimized 50 Hz, 73 A, 28 mH single-phase shunt reactor, three of which form a 1 kV Y-connected three-phase reactor bank.

Whenever an air-gap is inserted into the magnetic circuit, fringing effect at the air-gap causes additional winding losses [73], [50] and additional eddy-current losses in the magnetic core which is called ‘gap loss’ in [42], [46]. Another undesirable effect of fringing flux is the increase in the inductance by decreasing the total reluctance of the magnetic path [42]. To solve these problems in various application areas, the use of several discretely or uniformly distributed gaps in the magnetic cores are recommended in [42, 46, 50, 62 and 73]. However, the effects of the number of discrete gaps on the inductance parameters of iron-core shunt reactor, gap loss component have not been quantified and the effects on leakage inductance have not been discussed in the literature.

Since FEM analyses give the series equivalent inductances  $L_{gs}$  and  $L_{cs}$ , (Fig.2.6) the parameters of this series equivalent circuit can be related to the equivalent circuit parameters in Fig.2.3 by using the energy calculations described in section 2.2.5.

The results presented in this section are obtained for the shunt reactor given in Fig.2.9 and table 2.2. This reactor has been optimized for a cost function consisting of initial cost of the reactor and present value of reactor losses for 20 years of economic life.

$L_1$ ,  $L_{cs}$  and  $L_{gs}$  in Fig.2.6 are calculated for the reactor in Fig.2.9 and table 2.2 against different number of discretely distributed air-gaps,  $G$  by using Maxwell 3D analysis tool. It is worth to note that the total air-gap length,  $l_g=22.4$  mm is kept constant while subdividing it into several equal (identical) air-gap portions from  $G=2$  to 160. The variations in  $L_1$ ,  $L_{cs}$  and  $L_{gs}$  against  $G$  are plotted in Fig.2.10. The self-inductance,  $L_s$  in Fig.2.10 of the shunt reactor is obviously the sum of the three inductances, i.e.  $L_s = L_1 + L_{gs} + L_{cs}$ .

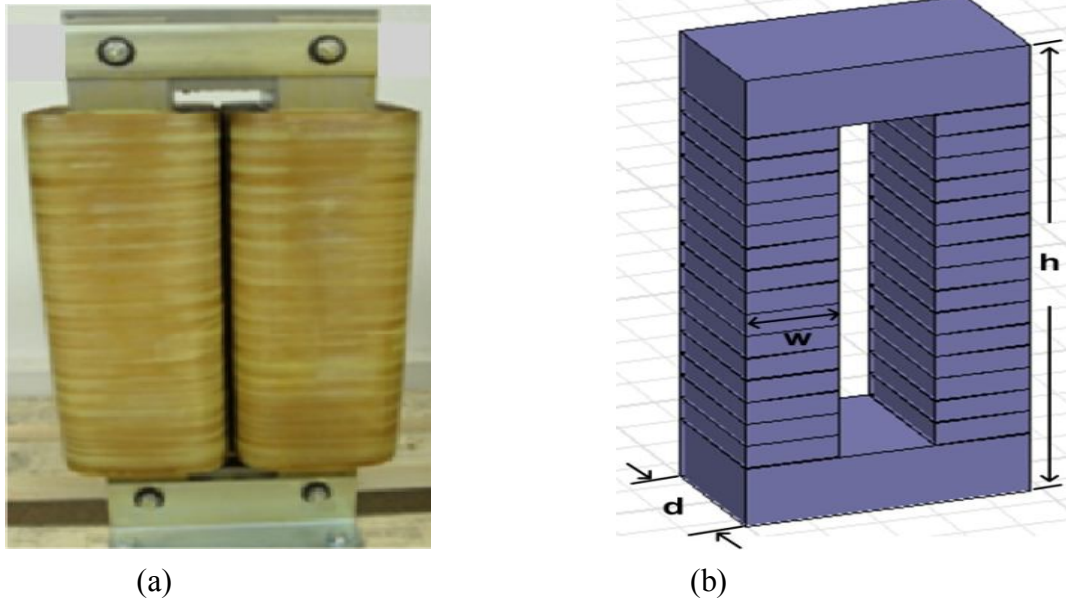


Figure 2.9 Single-phase shunt reactor as specified in Table 2.2.

Table 2.2 Technical Specifications of the Optimized Single-Phase Shunt Reactor

Self Inductance, $L_s$	28 mH
No of phases	1
Rated Voltage, V	$1/\sqrt{3}$ kV
Rated Current, I	73 Amps
Operating Frequency, f	50 Hz
Winding Type	Aluminum Foil 400*0.15 in mm
Winding Resistance (dc)	82 m $\Omega$
Core Material	M330-35AP (See Appendix-A for the B-H ch.)
Relative permeability, $\mu_r$	5550
Maximum Flux Density, $B_m$	1.1 Wb/m <sup>2</sup>
w*d*h	80*137*620 mm
Total Gap Length	22.4 mm
No of distributed gaps, G	32

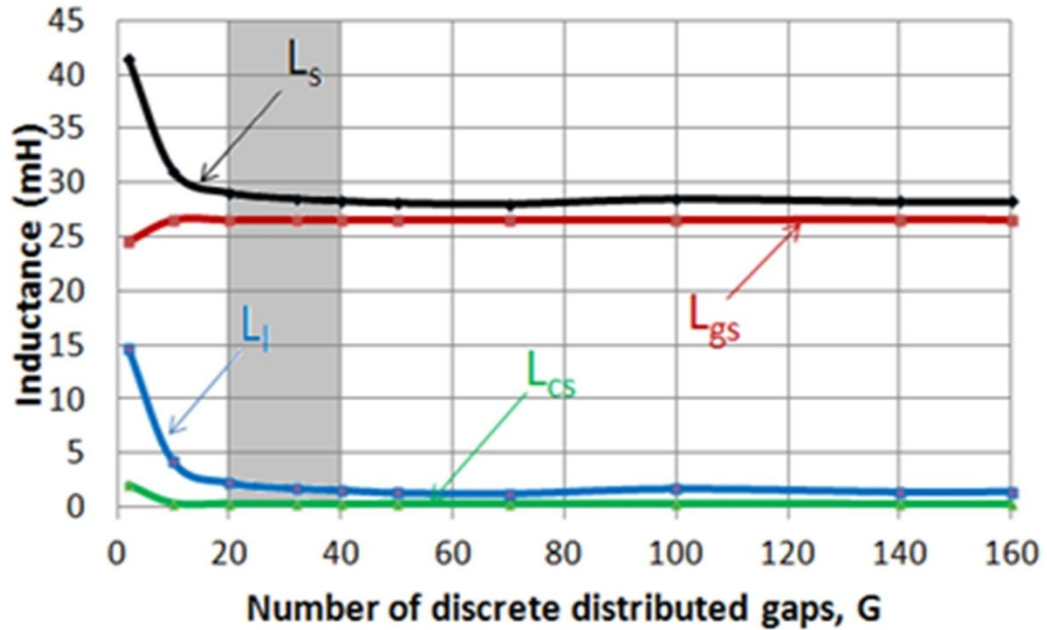


Figure 2.10 Variations in inductance parameters in Fig.2.6 against G

Following conclusions can be drawn from the results in Fig.2.10:

- Leakage inductance,  $L_1$  drastically drops to a minimum value as the number of distributed gaps is increased. This is because as the length of each individual air-gap is significantly reduced, fringing effect will be too small which may permit design of the reactor even by analytical calculations. The increase in inductance due to fringing flux has been defined as ‘Fringing Factor’ in [10] and [42].
- The drastic drop in  $L_1$  causes a rapid decay of  $L_s$  and hence  $L_s$  settles down to a constant value as a sufficiently large number of discrete gaps is used. This property makes self-inductance of the shunt reactor more deterministic thus permitting the use of analytical techniques in design work.
- Optimum number of discrete gaps is between  $G=20$  and  $40$  which corresponds to gray colored area in Fig.2.10. Further increase in  $G$  makes the shunt reactor impractical, more costly and maybe unimplementable.

In the design and implementation of the shunt reactor in Fig.2.9 and table 2.2,  $G$  is chosen to be 32 in view not only of Fig.2.10 but also of reactor losses. Equivalent

circuit parameters found by FEM analyses of the optimized shunt reactor are compared with parameters obtained by analytical calculations and self-inductance measured on the implemented reactor in table 2.3. Since analytical calculations give  $L_c$  and  $L_g$  in Fig.2.3 while FEM analyses give  $L_l$ ,  $L_{cs}$  and  $L_{gs}$  in Fig.2.6,  $L_{cs}$  and  $L_{gs}$  are converted to their shunt equivalents,  $L_c$  and  $L_g$  by using the method recommended in [8] and marked on table 2.3 for comparison purposes. Following conclusions can be drawn from the results given in table 2.3.

- $L_c$  and  $L_g$  values calculated analytically are nearly the same with the values deduced from the results of FEM analyses.
- Leakage inductance  $L_l$  could not be calculated analytically as simple as those of  $L_c$ ,  $L_g$  and  $L_m$ . However, the aluminum foil coils of the sample reactor winding is tightly wound around left- and right-hand legs of the discretely distributed reactor core in the form of two series coil parts (Fig.2.9). Each foil layer is separated from the neighboring layers by an insulating material of 0.15 mm thickness. The leakage inductance,  $L_l$  is primarily dictated by the winding arrangement and secondarily by the length,  $l_g$  and the number of distributed gaps,  $G$ . In the sample reactor since there is very low non-magnetic space between foil layers and inner foil layer and the core, relative magnitude of leakage inductance is largely dictated by the number of distributed gaps. Therefore, it can only be assumed to be in a relatively low range around 5 % of  $L_s$  for the winding of shunt reactor with 32 gaps in its design phase by analytical techniques.
- $L_c$  and  $L_{cs}$  can be neglected in comparison respectively with  $L_g$  and  $L_{gs}$  in simple analytical calculations for a shunt reactor having sufficiently large number of distributed air-gaps.
- Magnetostatic and transient solution tools of FEM give very close results for  $L_s$ .
- The tolerance for shunt reactor impedance at rated voltage and frequency shall be  $\pm 5$  % of the specified value according to IEC 289 [74] and IEC 60076-6 [75],  $\pm 2.5$  % according to IEEE Std. C57.120-1991 [76]. It is seen from table 2.3 that

both the theoretical and the measured value of  $L_s$  lie in the recommended tolerance range for the optimized 28 mH shunt reactor.

Table 2.3 Equivalent Inductance Parameters of a  $1/\sqrt{3}$  kV, 73 A, 50 Hz, 28 mH Single-Phase Shunt Reactor with G=32 Gaps

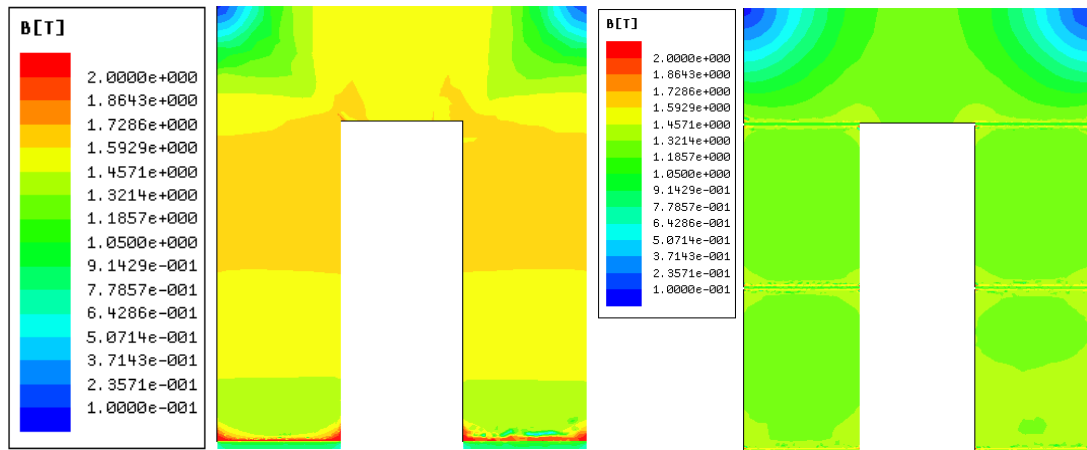
Inductance Components	Calculated (mH)			Measured (mH)
	Analytical from (2.5) and (2.6)	FEM Analysis		
		Magnetostatic Solution	Transient Solution	
$L_c$ and $L_g$ in Fig.2.3 $L_{cs}$ and $L_{gs}$ in Fig.2.6				
Self, $L_s$	–	28.5	27.6	27.3
Leakage, $L_l$	–	1.6	–	–
Core, $L_c$	2407.0	2412.0	–	–
Gap, $L_g$	27.1	27.2	–	–
Magnetizing, $L_m$ $L_m=L_g/L_c$	26.8	26.9	–	–
$L_{cs}$	–	0.3	–	–
$L_{gs}$	–	26.6	–	–

#### 2.4 Effects of Distributing Air-Gap into Several Discrete Air-Gaps on Reactor Losses

Power dissipation in gapped reactors operating at low frequencies is composed of  $I^2R$  loss due to the ac resistance of windings and core losses due to the magnetizing flux and the fringing flux. Eddy-current loss due to fringing flux around the air-gaps is called the Gap-loss in [42], [46].

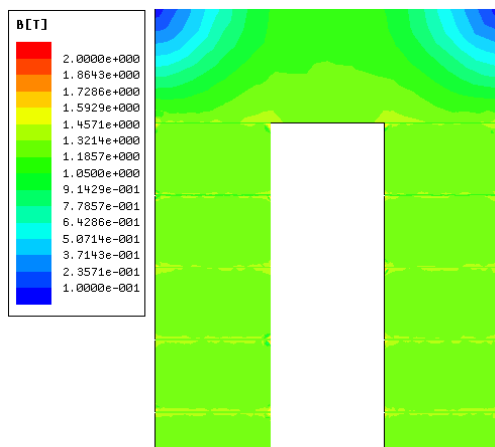
In this section, for the single-phase shunt reactor defined in Fig.2.9 and table 2.2, winding loss ( $I^2R$  loss) and core loss due to magnetizing flux are obtained by analytical calculations. Gap-loss is estimated for different number of gaps by using the empirical expression given in [42] and [46] together with the results of a novel usage of Maxwell 3D model outputs. The total core loss is directly obtained from the results of Maxwell 3D transient analyses.



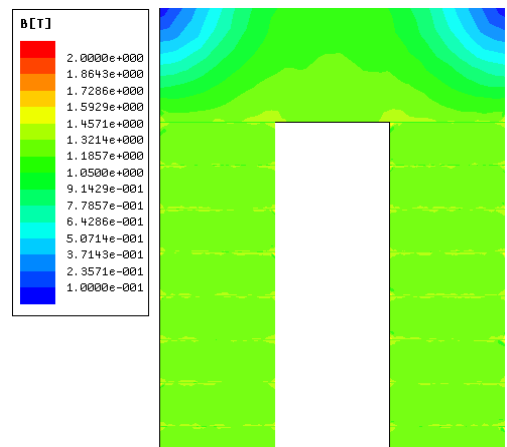


1 gap on each leg

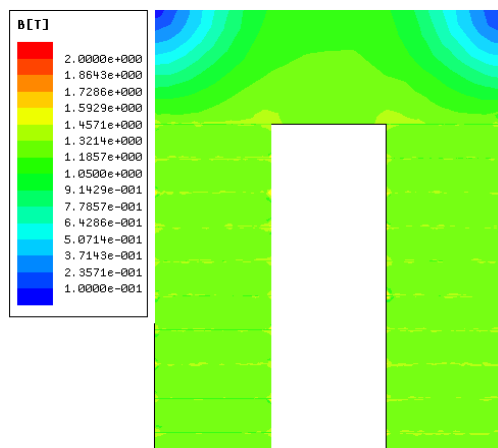
5 gaps on each leg



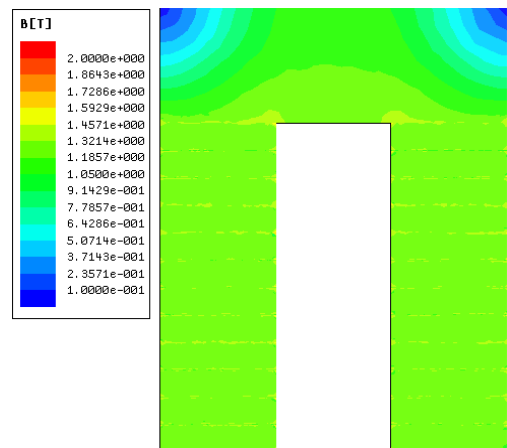
10 gaps on each leg



16 gaps on each leg



20 gaps on each leg



35 gaps on each leg

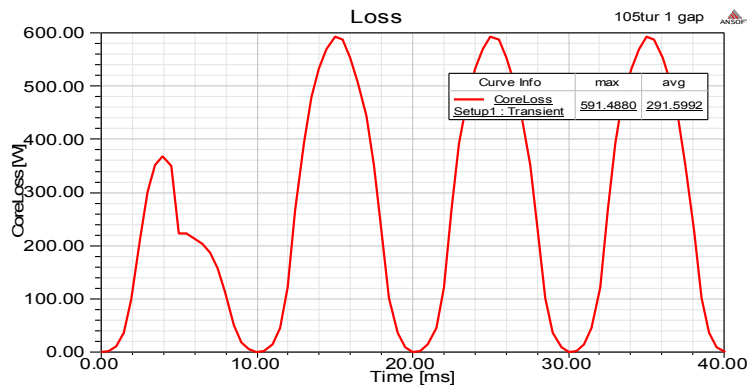
(Upper halves of the reactors are illustrated and B scale for all figures are the same as in the first one, i.e, max 2.0 T and min 0.1 T)

Figure 2.11 Magnetic flux density distributions of the reactor along the core for different number of distributed gaps for single-phase shunt reactor (FEM results)

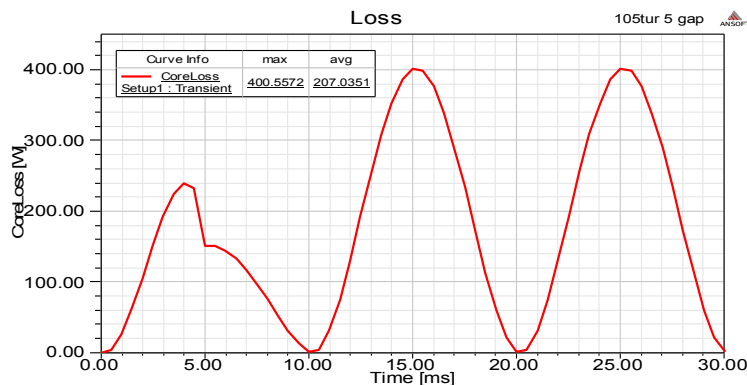
Fig.2.11 shows magnetic flux density distribution within the volume of magnetic core (obtained by Maxwell 3D magnetostatic analyses) for different number of distributed gaps (for G=2, 10, 20, 32, 40 and 50). The average flux density in the core for G=2 is about 1.4-1.6 T, for G=10, 20, 32, 40 and 50 it is 0.9-1.2 T. It is also clear that peak value of the magnetic flux density in the core decreases as the number of gaps, G increases. By discretely distributing the air-gaps fringing flux around the air-gaps also decreases. Therefore, leakage inductance,  $L_1$  and thus total inductance of the reactor,  $L_s$  decreases as described in the previous section.

Another important effect of discretely distributing the air-gap is the decrease in core loss of the reactor. Since core loss is directly proportional to peak flux density value in the core, as the number of discretely distributed air-gaps increases the core loss of the reactor decreases.

Fig.2.12 shows the core losses and mesh plots of the reactor models calculated by Maxwell 3D Transient Analyses for different number of distributed gaps.

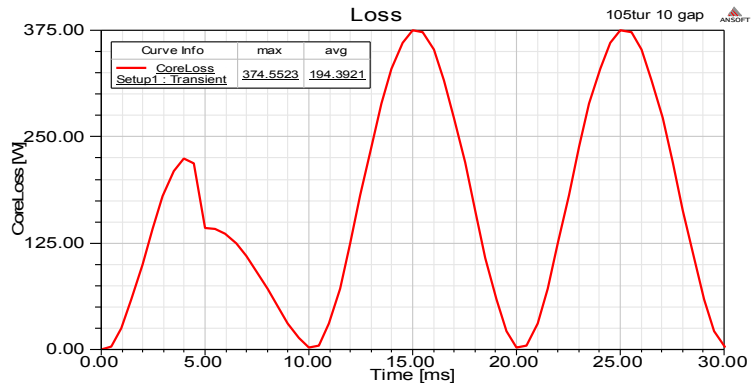


a) Core Loss Variation Against Time for G=2

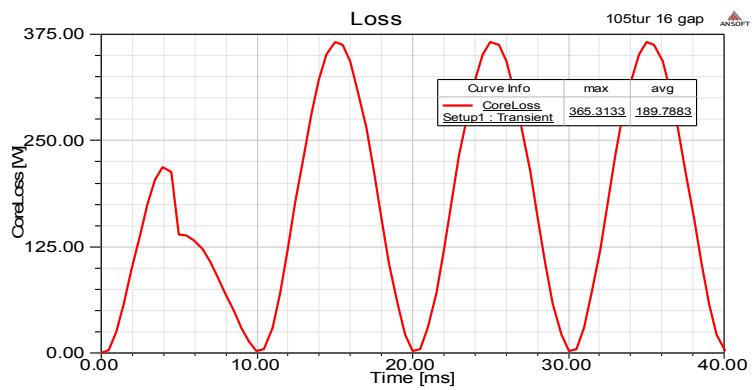


b) Core Loss Variation Against Time for G=10

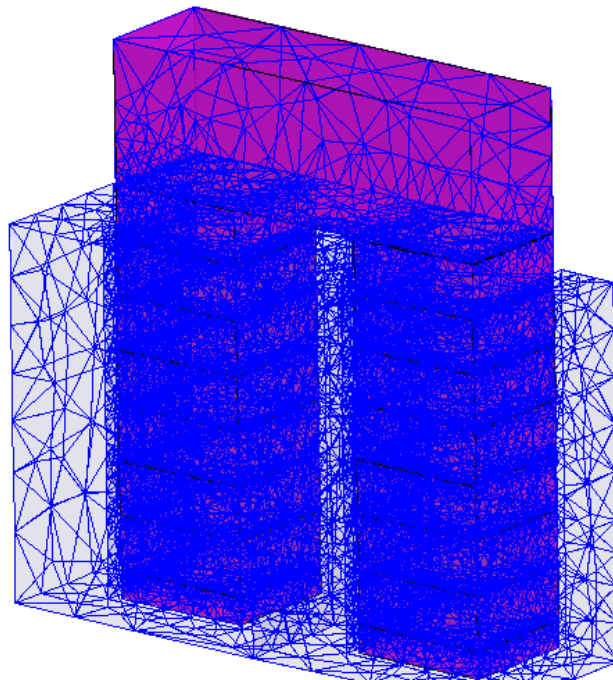
Figure 2.12 Variation of core loss for different number of distributed gaps for single-phase shunt reactor (Calculated by Maxwell Transient Analyses)



c) Core Loss Variation Against Time for G=20

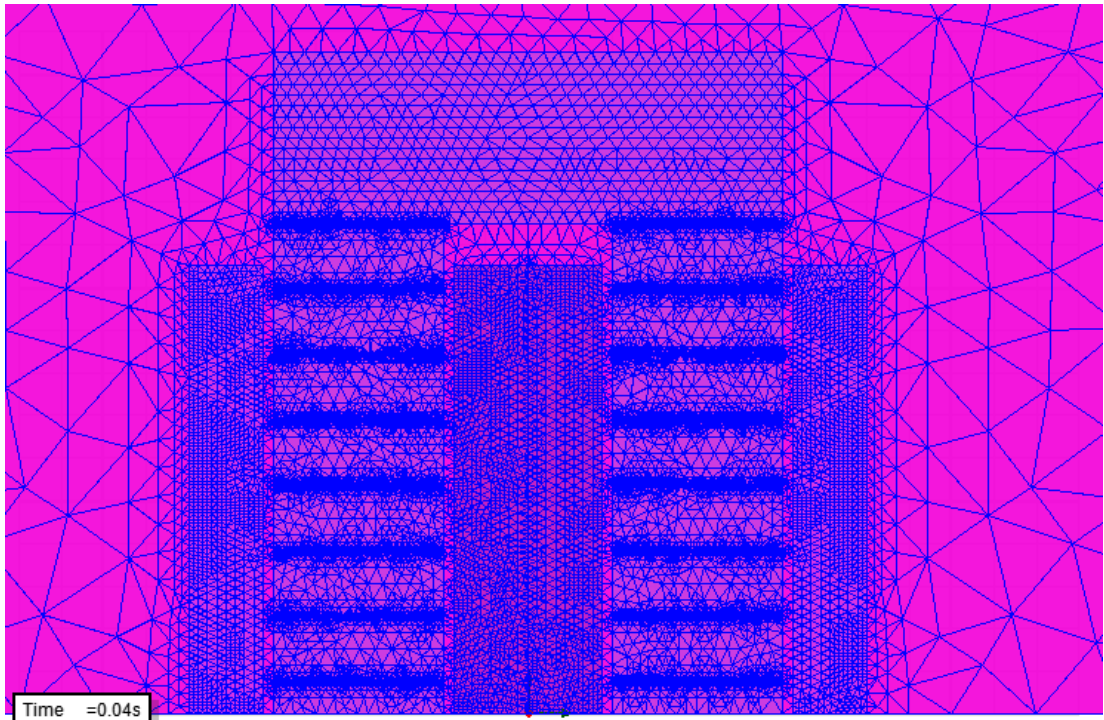


d) Core Loss Variation Against Time for G=32



e) Mesh Plot of the 3D Model Used in Magnetostatic Analysis (Upper half, G=32)

Figure 2.12 (Cont'd) Variation of core loss for different number of distributed gaps for single-phase shunt reactor (Calculated by Maxwell Transient Analyses)



f) Mesh Plot of the 2D Model Used in Transient Analysis (Upper half, G=32)

Figure 2.12 (Cont'd) Variation of core loss for different number of distributed gaps for single-phase shunt reactor (Calculated by Maxwell Transient Analyses)

As it is seen from Fig.2.12, core loss of the reactor decreases as the number of discretely distributed air-gaps in the core increases.

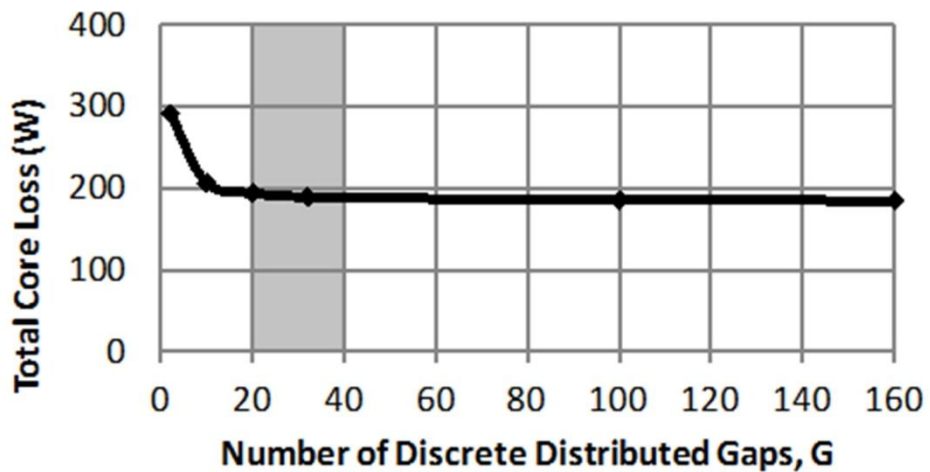


Figure 2.13 Variation of total core loss against number of distributed gaps for single phase shunt reactor (FEM results)

Fig.2.13 shows the variations in total core loss within the volume of magnetic core as a function of different number of distributed gaps. Fig.2.13 shows that;

- Total core loss drastically decreases from 292 W to 190 W as G is increased from 2 to 20. Further increase in G above 20 makes only minor reduction in the total core loss and above 40 makes no contribution to core loss reduction. Therefore, optimum G can be chosen on the curve section within gray shaded area in Fig.2.13.

Fringing flux causes additional eddy-current loss by leaving and re-entering the laminations near to the air-gap. That is, only the flux lines perpendicular to laminations in x-direction (Fig.2.14) will be the cause of gap-loss in gapped iron-core reactors. [42] and [46] proposes the empirical formula given in (2.15) to calculate the gap-loss.

$$P_g = G \cdot l_g \cdot d \cdot f \cdot B_m^2 \quad \text{Watts} \quad (2.15)$$

where,  $P_g$  is the gap-loss, G a numerical constant ( $0.155 \times 10^{-8}$ ),  $l_g$  the gap length in cm, d the core width in cm, f the frequency and  $B_m$  the maximum value of flux density in Gauss. (1Gauss= $10^{-4}$  Tesla)

Unfortunately, this formula has only been tested for iron cores having relatively large air-gaps. It means that when the total air-gap for the reactor in Fig.2.9 and table 2.2 is divided into several segments the validity of (2.15) is not known. Therefore a novel approach is needed to estimate the gap-loss component.

For G=2,  $P_{g2}$  will be calculated from (2.15) and  $P_{g32}$  for G=32 will be estimated relative to  $P_{g2}$  by using FEM analyses results.

Relative magnitudes of gap loss for different number of discretely distributed gaps, G are estimated by considering an incremental area on the core surface yz near to each air-gap and moving it in z-direction as illustrated in Fig.2.14. By this way the variations in x-component of flux density,  $B_x$  are obtained in z-direction by using the results of FEM analyses. This method will be called ‘The Moving Strip Method’ in this work. Here, fringing flux component in y-direction,  $B_y$  causes negligibly small gap loss is the main assumption because xz-plane of the iron core is composed of thin laminations.

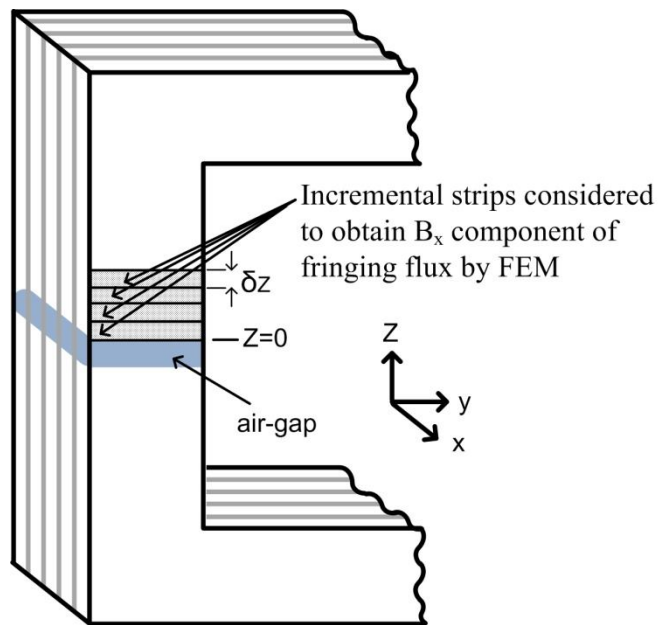


Figure 2.14 Illustration of moving strip method

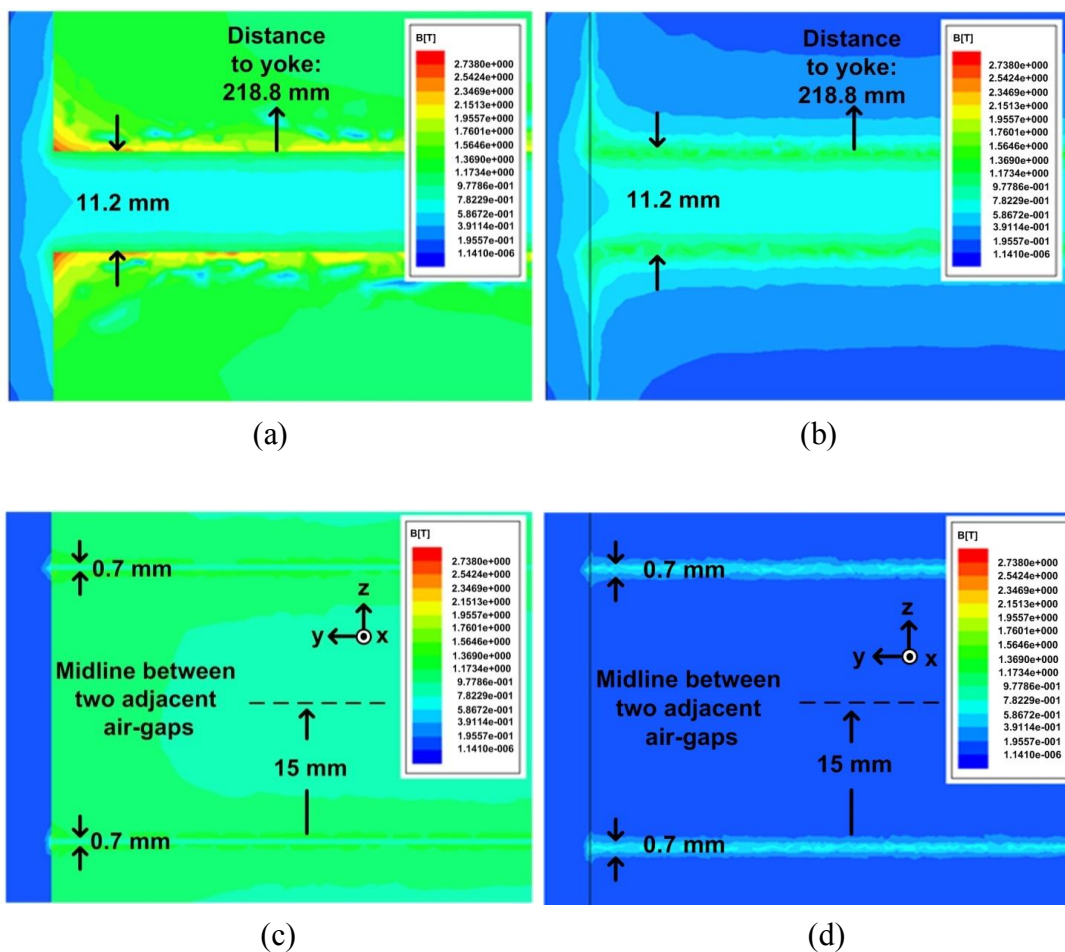


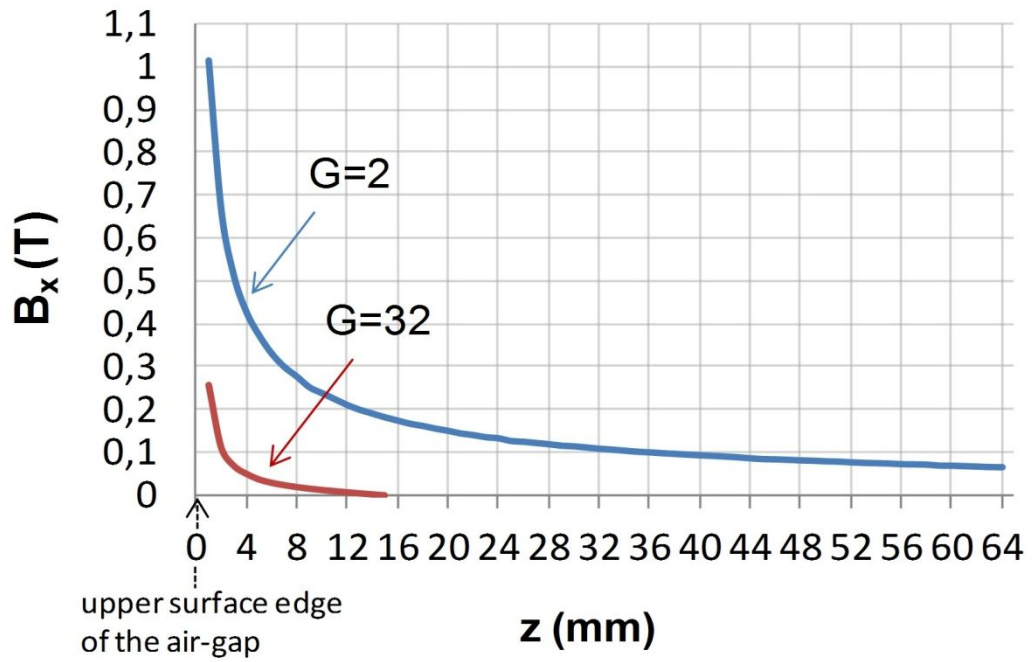
Figure 2.15 Flux density distribution, (a) in the core for  $G=2$ , (b) in the air-layer for  $G=2$ , (c) in the core for  $G=32$  and (d) in the air-layer for  $G=32$

Flux density distributions near to the air-gaps obtained by FEM analyses are as given in Fig.2.15. Fig. 2.15.a and Fig.2.15.c show the flux density distribution in the core on yz-plane. However, Fig.2.15.b and Fig.2.15.d show the flux density distribution in air layer on yz-plane. It is worth to note that yz air plane is chosen in parallel to and displaced 0.1 mm from the core surface. On the other hand flux distributions in Fig.2.15.a and Fig.2.15.b are obtained for the core structure with  $G=2$  while those of Fig.2.15.c and Fig.2.15.d for the core structure with  $G=32$ . Plots in Fig.2.15 are 3D drawings of flux density distribution.

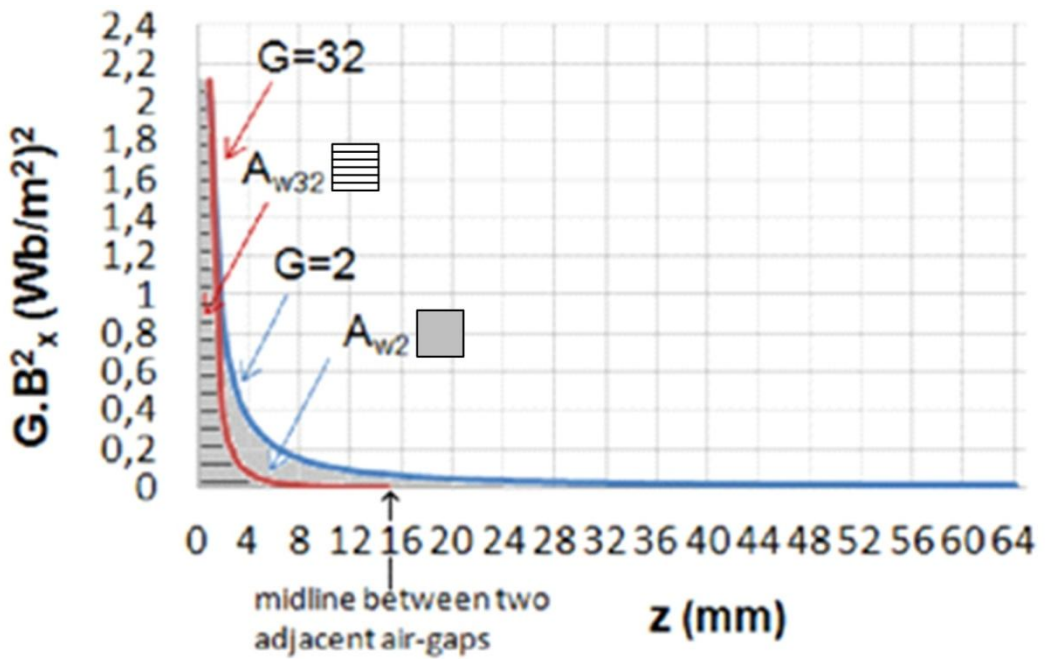
Since the air layer on yz-plane for Fig. 2.15.b and Fig. 2.15.d is defined as a sheet of 1 mm thick, the associated flux density distribution can be taken as  $B_x$  component of the fringing flux leaving and entering the core surface on yz-plane. As can be seen from Fig. 2.15.a and Fig. 2.15.b, flux density distributions in the previously chosen air-layer, as well as in the magnetic core, are not uniform for large air-gaps ( $G=2$ ), that is, flux lines are more dense at the corners and sharp edges of the structure. However, by dividing the large air-gap into several discrete gaps which corresponds to  $G=32$  in Fig.2.15.c and Fig.2.15.d, flux density distributions become nearly uniform. By comparing the flux density distributions in Fig.2.15.d and Fig. 2.15.b magnitudewise, it can be concluded that the use of several discretely distributed air-gaps reduce the fringing flux significantly.

As described in the foregoing section and in Fig.2.14 the incremental strips are defined on yz-plane in y-direction and then moved up in z-direction. By this way, flux density distributions will be quantified strip by strip. Although the flux density on the surface of each strip is not perfectly uniform, especially for Fig.2.15.b, it will be assumed to be uniform in the calculation of gap losses.

The variations in  $B_x$  against  $z$  are given in Fig.2.16 for  $G=2$  and  $G=32$  cases. Displacement  $z$  has been defined as zero just on the upper surface edge of each air-gap. Each strip has been moved from  $z=0$  position to the yoke for  $G=2$ . However, for  $G=32$  each strip has been moved from  $z=0$  to the midline between two adjacent air-gaps defined in Fig.2.15. Fig.2.16 shows that  $B_x$  component of fringing flux for  $G=2$  is higher than that of  $G=32$  and becomes effective over a larger surface area.



(a)



(b)

Figure 2.16 Estimation of additional eddy-current loss arising from fringing flux around air-gaps for  $G=2$  and  $G=32$ , (a) Variations in fringing flux determined by moving strip method, (b) Illustration of areas corresponding to gap-losses

Since the eddy-current loss due to fringing flux in x-direction which is termed the gap loss component, is directly proportional to  $B_x^2$  [42], [46],  $B_x$  values on the curve marked by  $G=2$  in Fig.2.16.a are first squared and then multiplied by  $G=2$  while



those of curve marked as G=32 are multiplied by 32 after finding their squares. These calculations give us variations in density of eddy-current loss in z- direction as given in Fig.2.16.b. Gap loss is found to be 168 Watts from (2.15) for the core with G=2. Since the areas under the curves ( $A_{w2}$  and  $A_{w32}$ ) in Fig.2.16.b are directly proportional to corresponding gap losses for core structures with G=2 and 32, the total gap loss of the core with G=32 ( $P_{g32}$ ) can be expressed in terms of the gap loss of the core with G=2 ( $P_{g2}$ ). That is,

$$P_{g32} = (A_{w32}/A_{w2}) P_{g2} \text{ Watts} \quad (2.16)$$

where  $A_{w32}$  and  $A_{w2}$  are the areas under the curves in Fig.2.16.b marked respectively by G=32 and G=2, and  $P_{g2}$  is the gap loss calculated from (2.16) of the core with G=2.

Since  $A_{w32} / A_{w2}$  ratio is 1/2.5 in Fig.2.16.b then  $P_{g32}$  is calculated to be 67 Watts from (2.16). Theoretical and experimental power loss components of the core structures with G=2 and 32 are given in Table 2.4.

Table 2.4 Power Loss Components of Optimized  $1/\sqrt{3}$  kV, 73 A, 50 Hz, 28 mH Single-Phase Shunt Reactor with G=32 Gaps

Number of air-gaps (G)	Winding Loss <sup>‡</sup> (W)	Core Loss (W)			Gap Loss (W)			Total Loss (W)		
		Analytical <sup>‡</sup>	FEM <sup>◊</sup>	Exp.	Analytical	FEM	Exp.	Analytical	FEM	Exp.
2	472	156	292	–	168 <sup>†</sup>	–	–	796	764	–
32	472	156	190	200 <sup>*</sup>	67 <sup>Δ</sup>	–	–	695	662	672

‡ Calculated from (2.17)  
+ Calculated from (2.18) for  $B_m = 1.1$  T, takes into account only the flux lines along mean path length and assumes uniform flux density distribution  
◊ Calculated from (2.19) [45], [70]  
† Calculated from (2.15) given in [42], [46]  
\* Obtained by subtracting winding loss from measured total loss  
Δ Estimated from  $A_2 / A_{32} = 2.5$  ratio of the areas under the curves in Fig.2.16.b

Following points should be stressed for the analytical calculations of power loss components and interpretation of FEM analyses results.

1. Winding loss,  $P_w$  is calculated from (2.17)

$$P_w = I^2 k R_{dc} \quad \text{Watts} \quad (2.17)$$

where  $I$  is the rated current in rms Amps,  $k=1.08$  is the skin effect factor at 50 Hz for the given aluminum foil conductor and  $R_{dc}$  is the dc resistance of the windings and is measured to be 82 m $\Omega$ .

2. Analytical calculation of core loss utilizes core loss versus  $B_m$  curves in Appendix-A provided by the manufacturer of NGO laminations. For 50 Hz operation the curve in (2.18) has been fitted and used throughout the calculations. Analytical calculation of core loss assumes a uniform flux density distribution within the core and takes into account only the flux lines along mean path length. Therefore the core loss in Table 2.4 is calculated from (2.18) for the design value of peak flux density ( $B_m=1.1$  T) and excludes gap loss.

$$P_c = 1.14 B_m^{1.75} \quad \text{W/kg} \quad (2.18)$$

3. Analytical calculation of gap-loss has been carried out relative to (2.15) as described in the previous part of this section.
4. Core loss found from 3D FEM analyses results take into account flux density distribution within the core in all directions and based upon (2.19) [45], [70]. Therefore it is decided that gap-loss component is already included in (11).

$$P_c = k_h f B_m^2 + k_c f^2 B_m^2 + k_e f^{1.5} B_m^{1.5} \quad (2.19)$$

where  $k_h$ ,  $k_c$  and  $k_e$  are hysteresis, eddy-current and excess loss coefficients, respectively,  $f$  is the operating frequency (50 Hz),  $B_m$  is the peak flux density in the core.

From the results in table 2.4 following conclusions can be drawn:

- Analytical calculations and FEM analyses give very close results.

- Gap-loss is reduced significantly and hence the total core loss of the shunt reactor is reduced considerably by separating the total air-gap length into an optimum number of discrete gaps. The reduction in total reactor loss amounts nearly to 15 % by increasing the number of gaps from  $G=2$  to 32 for the reactor presented in this section.

## 2.5 Conclusions

Following conclusions are drawn from the results presented in this chapter;

- The physical meaning of component inductances of a reactor is subject to uncertainty and it is open to different interpretations, leading to various equivalent circuits. Therefore a definition based on flux distribution may not be reliable and calculations based on energy or co-energy are thus preferable.
- The use of several discretely distributed small air-gaps in the design and implementation of a shunt reactor yields more uniform flux density distribution in the core in comparison with that of an equivalent core having only a few air-gaps. This will cause a significant reduction in gap-loss component and a considerable reduction in the total reactor losses.
- The Moving Strip Method proposed in this chapter permits the estimation of gap-loss owing to the fringing flux in iron cores having discretely distributed small air-gaps. This method is based on FEM analyses and estimates the gap-loss relative to empirical gap-loss calculation for large air-gaps.
- Several discrete air-gaps also cause a significant reduction in the percentage of leakage inductance,  $L_l$  as compared to magnetizing inductance,  $L_m$  and makes core inductance,  $L_c$  much greater than gap inductance,  $L_g$ . Therefore,  $L_c$  and  $R_g$  for a shunt reactor having several discretely distributed small air-gaps can be neglected thus permitting practical hand-calculations in the design of such reactors.

## CHAPTER 3

### REACTOR DESIGN BY THE AID OF FINITE ELEMENT ANALYSIS

#### 3.1. Introduction

In this chapter Finite Element Analysis (FEA) aided reactor design is described. FEA tools are needed in the design of shunt reactors because a simple analytical expression for the percentage value of the leakage inductance of the equivalent circuit in Fig.2.3 is not available in the literature. Following analysis and computational tools of Maxwell FEA Software can be used for the design of iron-core shunt reactors with discretely distributed gaps:

- a. Magnetostatic Analysis Tool: 3D optimization work is carried out in order to obtain magnetic field distribution in the magnetic circuit and to calculate inductance components ( $L_l$ ,  $L_c$ ,  $L_g$  and  $L_s$ ). The excitation model in this work is as shown in Fig.3.1.a where  $\hat{I}$  is the peak value of the sinusoidal current that will pass through the target inductance in the steady-state.
- b. Transient Analysis Tool: This tool permits the 2D or 3D analysis of the magnetic circuit in the time-domain. The magnetic circuit of the target shunt reactor may be excited either by current (Fig.3.1.b) or voltage (Fig.3.1.c). As in the case of magnetostatic analysis, the excitation current in Fig.3.1.b is the purely sinusoidal current in the steady-state. Sinusoidal current excitation of the model makes the use of both 2D and 3D models practicable.

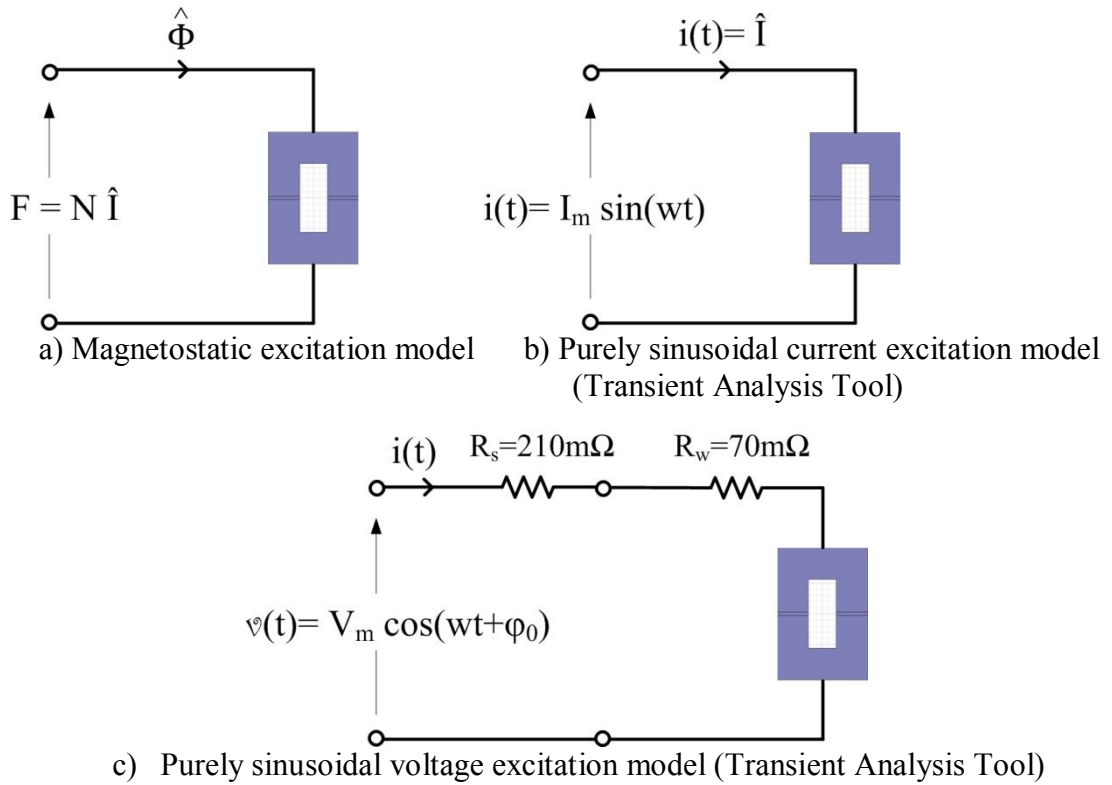


Figure 3.1 Excitation models of the target shunt reactor for Magnetostatic and Transient Analysis Tools

Unfortunately, 3D analysis requires a very powerful computing infrastructure. In this research work, core losses of the target shunt reactor are computed by using 2D transient analysis tools. It also gives us magnetic field distribution as a function of time and induced emf which may be used in the alternative calculation of self-inductance. As an alternative to purely sinusoidal current excitation, the target shunt reactor and its power supply can be excited from a purely sinusoidal voltage source as shown in Fig.3.1.c.

The practicability and hence applicability of the sinusoidal current excitation and sinusoidal voltage excitation approaches in the design of shunt reactors will be compared in the next subsection.

### 3.2 Comparison of Sinusoidal Current and Voltage Excitation Methods

A 46 kVAr, 1.1 kV, 28 mH, 73 A shunt reactor with two air-gaps has been designed and optimized for minimum Present Value Cost (min PVC) design criterion. The optimum design procedure has been repeated for different peak flux density values:

$B_m=1$  T, 1.4 T and 1.6 T. each optimum design is excited by both purely sinusoidal current as in Fig.3.1.b and purely sinusoidal voltage as in Fig.3.1.c by using Maxwell 2D Transient Analysis Tool. These analysis yield magnetic field distribution in the core in the steady-state and permit the calculation of self-inductances and comparison of execution times. When sinusoidal voltage excitation approach is used, Maxwell 2D Transient Analysis Tool give the waveform of the current passing through the shunt reactor and its THD and harmonic components as a function of  $B_m$  in the steady-state.

Magnetic field distributions in the magnetic cores of optimized designs are given in Figs. 3.2, 3.3 and 3.4 for  $B_m=1$  T, 1.4 T and 1.6 T, respectively.

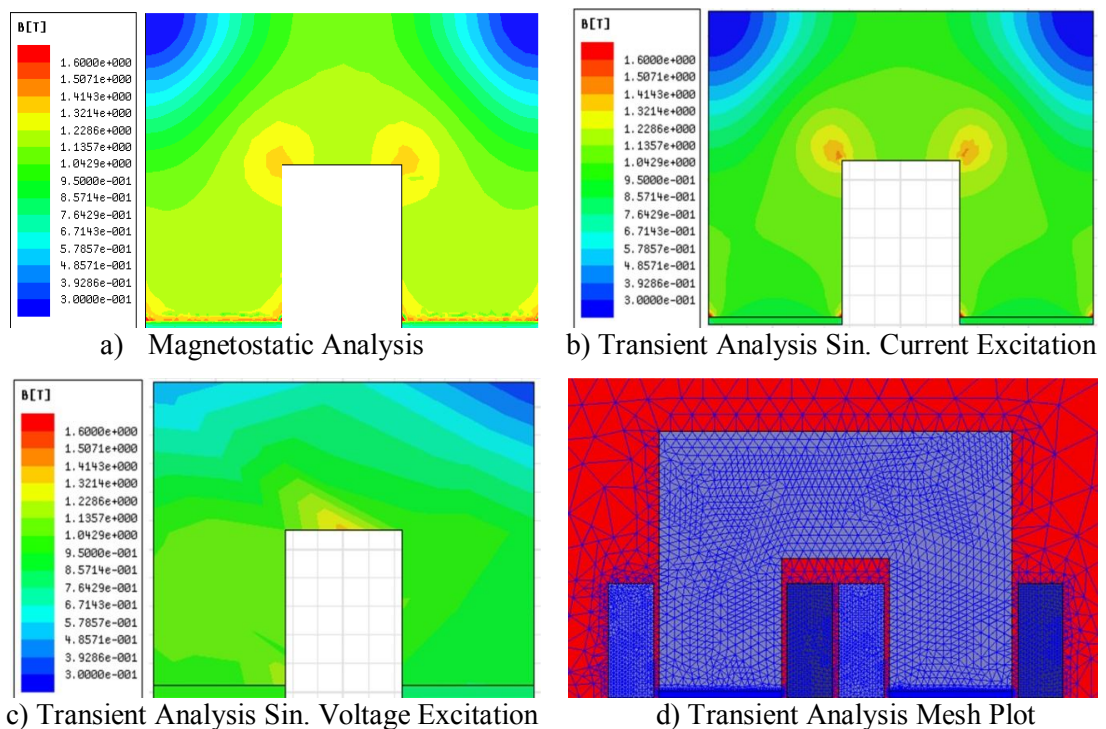


Figure 3.2 Magnetic field distributions in the magnetic cores for  $B_m=1$  T

The results of magnetostatic analysis, transient analysis with purely sinusoidal current excitation and transient analysis with purely sinusoidal voltage excitation in Fig.3.2 are very close to each other, as expected. This is because  $B_m=1$  T is on the linear portion of the B-H characteristic given in Appendix-A. However, there are some minor differences between magnetic field distributions in Fig.3.3. This is because  $B_m=1.4$  T is on the slightly saturated region of the B-H characteristic. The

reactor current is no longer purely sinusoidal as will be illustrated in the foregoing section when the core saturates.

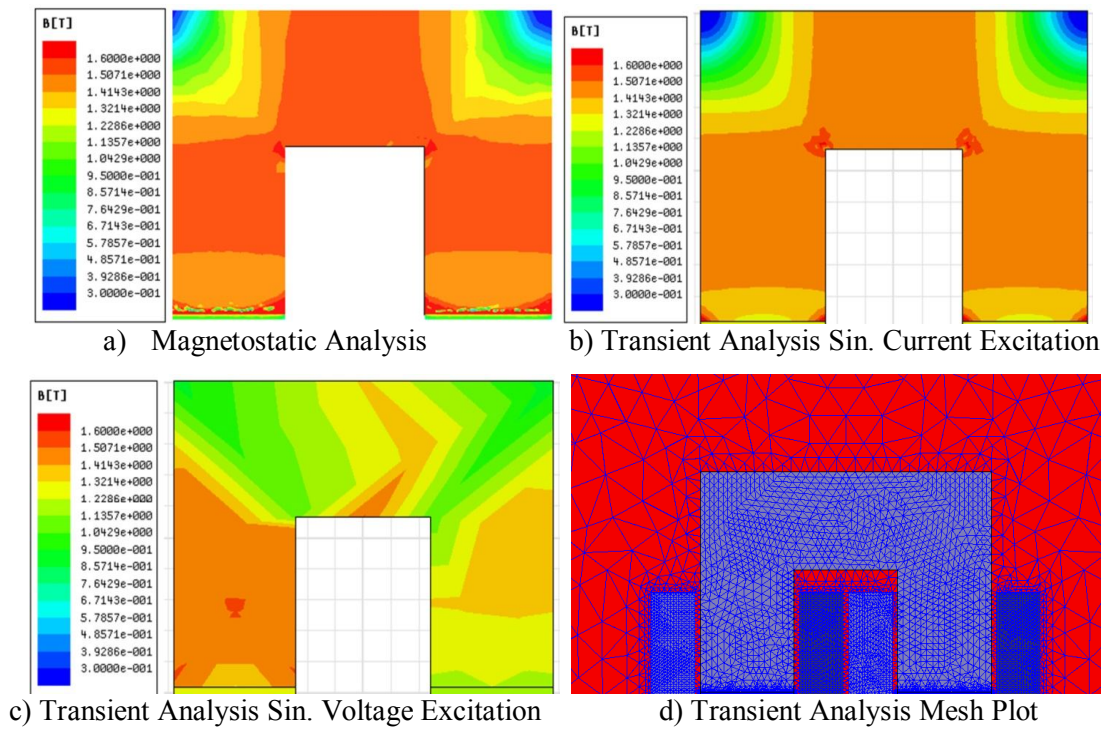


Figure 3.3 Magnetic field distributions in the magnetic cores for  $B_m=1.4$  T

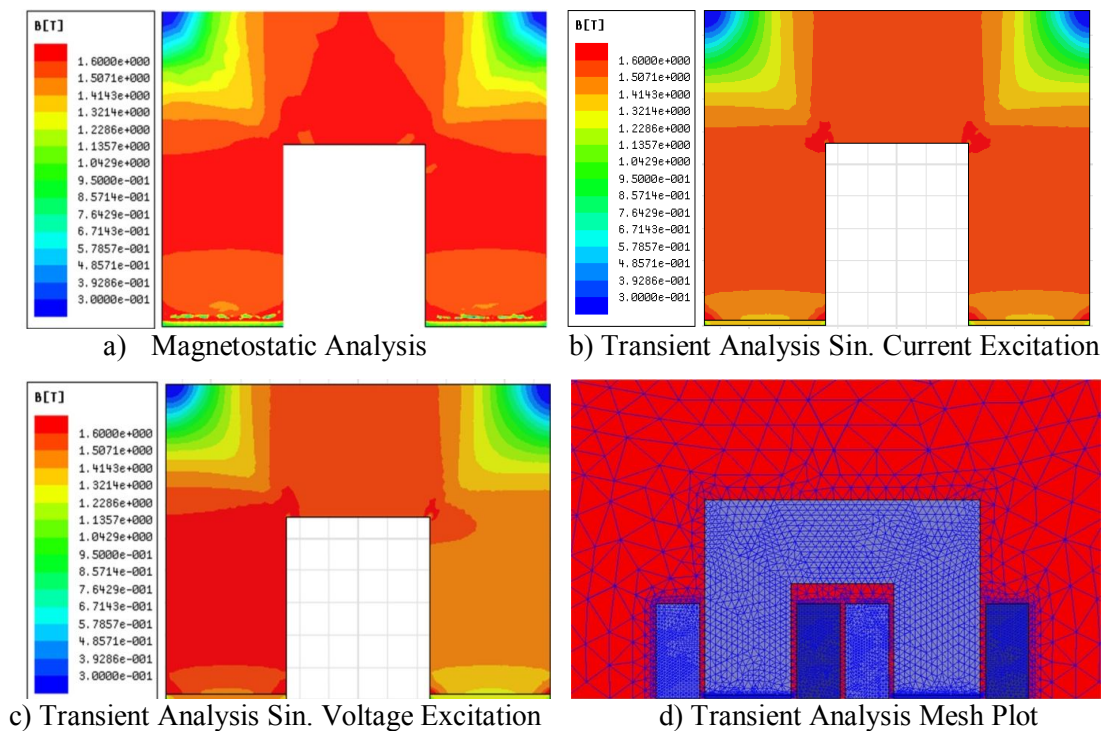


Figure 3.4 Magnetic field distributions in the magnetic cores for  $B_m=1.6$  T

The differences between magnetic field distributions in Fig.3.4 are more prominent because for the design value of  $B_m=1.6$  T reactor current waveform in the steady-state is more distorted than that of  $B_m=1.4$  T.

Further differences between magnetic field plots, especially in Figs.3.3 and 3.4, are attributed to the fact that magnetostatic analysis and transient analysis with sinusoidal current excitation are based on a model of two equal reactor coils while the transient analysis with sinusoidal voltage excitation employs the coil in one part on the left hand leg of the reactor core.

Harmonic current components and THD of the reactor current obtained from transient analysis tool with sinusoidal voltage excitation as a function of design values of  $B_m$  are given in Table 3.1. It is seen from these results that when the design value of  $B_m$  is placed on the linear portion of B-H characteristic in Appendix-A, reactor current becomes purely sinusoidal. However,  $B_m=1.4$  T yields slightly distorted reactor current and  $B_m=1.6$  T yields considerable distortion. Therefore,  $B_m$  should be set to a value in the range from 1 T to 1.2 T in order to fulfill technical specs of a shunt reactor. That is, the inductance of the shunt reactor should remain constant up to 1.2 times the rated operating voltage.

Table 3.1 Harmonic current components and THD of the reactor current

harmonic no	frequency (Hz)	Current (A <sub>peak</sub> )		
		1.0 T	1.4 T	1.6 T
DC	0	0.1350	0.1286	0.1303
1	50	108.3491	100.8137	96.4963
2	100	0.0907	0.0754	0.0500
3	150	0.0329	1.2627	4.5583
4	200	0.0187	0.0145	0.0090
5	250	0.0271	0.7591	2.6936
6	300	0.0087	0.0091	0.0161
7	350	0.0068	0.3684	1.1429
8	400	0.0050	0.0074	0.0185
9	450	0.0060	0.1721	0.2699
10	500	0.0034	0.0064	0.0147
11	550	0.0004	0.0544	0.0795
12	600	0.0026	0.0051	0.0086
13	650	0.0024	0.0016	0.1118
14	700	0.0020	0.0037	0.0041
15	750	0.0023	0.0075	0.0369
16	800	0.0017	0.0028	0.0028
17	850	0.0014	0.0095	0.0090
THD %		0.10	1.52	5.62



Although the transient analysis with purely sinusoidal voltage excitation is a more powerful design tool than the transient analysis with purely sinusoidal current excitation, the latter will be preferred as a basic approach in the Finite Element Aided design of shunt reactors with discretely distributed air-gaps. This is because purely sinusoidal current excitation approach needs less labor and saves time when the design value of  $B_m$  is placed on the linear portion of the B-H characteristic. For the same reactor, the execution times of the magnetostatic analysis, transient analysis with purely sinusoidal current excitation and transient analysis with purely sinusoidal voltage excitation on a computer with Intel Core2Duo P8700 2.53 GHz processor and 4 GB of RAM are given in Table 3.2 for comparison purposes.

Table 3.2 Execution times of the Magnetostatic and Transient Analysis tools

Maxwell Analysis Tool	Execution Time
Magnetostatic (3D)	3 hours
Transient analysis with purely sinusoidal current excitation (2D)	1½ hours
Transient analysis with purely sinusoidal voltage excitation (2D)	36 hours

### 3.3 Design Procedure

In this work a single-phase, 46 kVAr, 1.1 kV, 28 mH, 73 A shunt reactor has been designed and optimized for three different design criteria, i.e., minimum Initial Cost (min IC), minimum Total Loss (min  $P_t$ ) and minimum Present Value Cost (min PVC), respectively. Each individual design case has also been repeated for four different peak flux densities,  $B_m = 0.8$  T, 1 T, 1.2 T and 1.4 T in the core. Inductance parameters and core losses have been calculated by using Maxwell 3D optimization work. Finally, the results of these three different design criteria obtained from FEA have been compared. A further objective of this work is to investigate the effects of number of discretely distributed air-gaps,  $G$  on the IC,  $P_t$  and PVC of the optimum reactors. For this purpose, each design work is carried out for two different number of air-gaps i.e.,  $G=2$  and  $G=20$ .

Initial Cost (IC) is the manufacturing cost of the reactor and calculated as;

$$IC = (C \times A + W \times B) \times 1.75 \times 1.2 \times 1.18 \quad (3.1)$$

where;

C :core weight (kg)

A :steel price (2 Euros /kg)

W :aluminum weight (kg)

B :aluminum price (4.2 Euros/kg)

1.75 :labor, fixed and insulating material costs

1.2 :profit

1.18 :VAT (KDV)

Operating Cost (OC) is the cost due to reactor losses throughout its life cycle;

$$OC = \text{Total Loss in kWh} \times 0.1 \text{ Euro Cent} \times 24 \times 300 \times 20 \quad (3.2)$$

Reactor is assumed to operate 300 days per annum for 20 years and electricity price is assumed to be 0.1 Euro-cent/kWh.

Present value of the operation cost has been calculated by using equation (3.3) [15, 75, and 76].

$$PV = \frac{(1+i)^n - 1}{i(1+i)^n} OC \quad (3.3)$$

where;  $i$  is discount factor (assumed to be 10 %) ,  $n$  = number of years (in this case  $n=20$  since the life cycle of the reactor is assumed to be 20 years). PV can also be calculated using the definition given in IEEE Standard C.57-120 (both method give close results).

Present Value Cost (PVC) is the sum of the present value of OC and IC (in Euros).

$$PVC = PV + IC \quad (3.4)$$

### 3.3.1 Assumptions

1. The insulation classes of dry type transformers and reactors are defined in IEC 60076-3. The maximum allowable winding temperature values for these insulation classes (for maximum ambient temperature of 40 °C) are;

Class B        130 °C

Class F        155 °C

Class H        180 °C

In design phase of this chapter, the insulation class is decided to be Class B and for 40 °C ambient temperature, maximum temperature rise is allowed to be 65 K  $\pm$  3% by using a safety margin of 15 K. Temperature rise above the ambient is denoted by  $\Delta T$  in this work.

2. In transformer and reactor design works, the thickness of the winding material is chosen to be smaller than twice the skin depth of the material at the operating frequency. In this work, the winding material is aluminum foil and the operating frequency is 50 Hz. Therefore, in the optimization work the thickness of the foil ( $t$ ) is varied between 0.1 mm ( $t_1$ ) and 1 mm ( $t_{\max}$ ) in steps of 0.1 mm, by considering the commercially available thickness of the aluminum foil.
3. Core material used in design and optimization work is M330-35AP non-oriented steel (see Appendix-A for B-H and loss curves). The laminated core has been modeled as a solid core in Maxwell software. Modeling a laminated core requires a powerful computer and very long optimization work time. Solid core had been used in many studies in the literature [56, 57, 67, and 68] and it had been proved that this type of modeling gives accurate results.
4. The current density,  $J$  is varied between 1.1 A/mm<sup>2</sup> ( $J_1$ ) and 2 A/mm<sup>2</sup> ( $J_{\max}$ ) in steps of 0.1 A/mm<sup>2</sup>.

5. Number of turns,  $N$  is varied between 50 ( $N_1$ ) turns and 500 ( $N_{\max}$ ) turns in steps of 50 turns.
6. Three design criteria used in reactor design. The design problem has been treated as a general optimization problem. The optimization problem for these criteria can be defined as given in (3.5), in (3.6) and in (3.7), respectively for min IC, min  $P_t$  and for min PVC.

min IC ( $N, J, t$ )

$$\begin{aligned}
N_1 &\leq N \leq N_{\max} \\
J_1 &\leq J \leq J_{\max} \\
t_1 &\leq t \leq t_{\max} \\
\text{subjected to } \Delta T(N, J, t) &\leq 65 \text{ K} \pm 3\% \\
\text{subjected to } L_s &= 28 \text{ mH} \pm 3\%
\end{aligned} \tag{3.5}$$

min  $P_t$  ( $N, J, t$ )

$$\begin{aligned}
N_1 &\leq N \leq N_{\max} \\
J_1 &\leq J \leq J_{\max} \\
t_1 &\leq t \leq t_{\max} \\
\text{subjected to } \Delta T(N, J, t) &\leq 65 \text{ K} \pm 3\% \\
\text{subjected to } L_s &= 28 \text{ mH} \pm 3\%
\end{aligned} \tag{3.6}$$

min PVC ( $N, J, t$ )

$$\begin{aligned}
N_1 &\leq N \leq N_{\max} \\
J_1 &\leq J \leq J_{\max} \\
t_1 &\leq t \leq t_{\max} \\
\text{subjected to } \Delta T(N, J, t) &\leq 65 \text{ K} \pm 3\% \\
\text{subjected to } L_s &= 28 \text{ mH} \pm 3\%
\end{aligned} \tag{3.7}$$

where IC,  $P_t$  and PVC are the objective functions to be minimized,  $N, J$  and  $t$  are the variables of the optimization problem.  $\Delta T$  is called the constraint of the optimization problem.

7. For each peak flux density value, design and optimization work have been performed for two different initial estimations of leakage inductance for

comparison purposes as given in Table 3.3. The effects of percentage leakage inductance on IC,  $P_t$  and PVC are discussed in section 3.6.

Table 3.3 Leakage inductance percentage estimations used in design procedure

$B_m$	0.8 T	1 T	1.2 T	1.4 T
Initial estimate of leakage inductance %	5 and 15	5 and 15	5 and 20	5 and 18

8. Inductance components of the shunt reactor have been calculated by Maxwell 3D Magnetostatic Analysis and core losses by Transient Analysis tools.
9. Winding losses ( $I^2R$  losses) have been calculated by using the physical dimensions of the reactor obtained in design phase.
10. Total reactor loss given in the results section of each design criterion is the sum of the core loss calculated by Maxwell Transient Analyses and the winding loss calculated by Matlab.

$$P_t = P_c + P_w \quad (3.8)$$

11. Temperature rise,  $\Delta T$  was calculated by the empirical equation given in (3.9) [40] and limited to  $65 \text{ K} \pm 3\%$  since the insulation class has been decided to be class B.

$$\psi = P_t / A_s \quad (3.9)$$

$$\Delta T = 450 (\psi)^{0.826}$$

where;  $\psi$  is watt density,  $P_t$  is total loss and  $A_s$  is total surface area of the core. 450 and 0.826 are constants for laminated steel cores to calculate the temperature rise.

12. The symbols indicating the reactor dimensions are given in Fig.3.5 for both windings and core in detail.

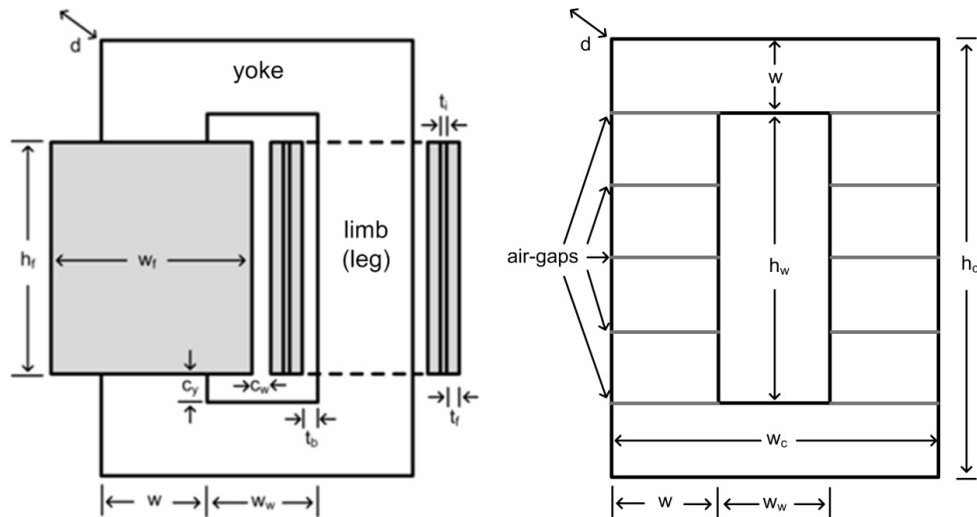


Figure 3.5 Illustration of core and winding dimensions

The explanations of the symbols used in Fig.3.5 are as follows;

- $c_y$  clearance between winding and yoke
- $c_w$  clearance between two windings
- $d$  depth of the core
- $h_c$  total height of the core
- $h_f$  height of the coil
- $h_w$  height of the window
- $t_b$  thickness of the tube
- $t_f$  thickness of the aluminum foil (each turn)
- $t_i$  thickness of the insulation material between each turn
- $w$  width of the limb and the yoke
- $w_c$  total width of the core
- $w_w$  width of the window

13. The operating line-to-line voltage of the shunt reactor is 1.1 kV, clearances used in design phase are given in Table 3.4.

Table 3.4 Clearances used in design procedure

Clearance to yokes, $c_y$	20 mm
Clearance between windings, $c_w$	5 mm
Insulation thickness between each turn, $t_i$	0.15 mm
Tube thickness, $t_b$	5 mm

14. As mentioned before, each optimization work has been performed for four different peak flux density values (0.8 T, 1 T, 1.2 T and 1.4 T), therefore several iterations were needed to be performed to obtain the target inductance. If the target inductance has not been satisfied in the first iteration, next iteration has been performed by increasing the number of turns or decreasing the total length of the air-gap sections in the core or vice versa. Iterations continued until the target inductance value has been obtained from Maxwell 3D optimization work. In this chapter, in order to focus on the most relevant results, only the results of the iterations which satisfy the target inductance value are discussed, however results of all iterations are given in detail in Appendix-B.

### 3.3.2 Flowchart of the Design Procedure

The parameters of each design (number of turns, total air-gap length, physical dimensions of the core and winding etc.) have been obtained from the calculations in Matlab as described in Fig.3.6 and these parameters have been used to create the models for Maxwell 3D optimization work (Fig3.7). Each optimization work has been iterated several times until the target self inductance ( $28 \text{ mH} \pm 3\%$ ) obtained and after it has been met, the equivalent inductances, core losses and flux density distributions in the core of the reactor have been calculated by Maxwell 3D software as described in chapter 2.

For each reactor which is specified by  $k\text{VAr}$ ,  $V_r$ ,  $\Delta T$ ,  $f$ ,  $B_m$ ,  $H_{\text{year}}$  and the initial estimate of the percentage leakage inductance (5% and 15%), the core dimensions, the values of  $IC$ ,  $P_t$  and  $PVC$  are determined analytically by using Matlab tools by varying  $N$ ,  $J$  and  $t$ . Among several trials those satisfying min  $IC$ , min  $P_t$  and min  $PVC$  are chosen separately for both initial estimates of percentage leakage inductance. The associated flowchart is given in Fig.3.6. In summary, the same reactor is optimized analytically according to design objectives of min  $IC$ , min  $P_t$  and min  $PVC$  in the first phase of the design procedure.

In order to verify the success of the design, FEA method will be used in the second phase of the design procedure. The associated flowchart is given in Fig.3.7. The objective of FEA method can be summarized as follows;

1. In order to investigate the number of discretely distributed air-gaps, i.e.,  $G=2$  and  $G=20$ , on the flux density distribution in the magnetic core. This analysis also shows whether the chosen peak flux density value is convenient for the chosen core material or not.
2. FEA (Maxwell 3D Magnetostatic Analysis Tool) also gives the optimum value of  $B_m$  for the chosen core material and reactor cores with several discretely distributed air-gaps.
3. Fine adjustment is needed in order to meet the target inductance in Henry with a  $\pm 5$  % tolerance according to IEC 289 and IEC 60076-6 Standards. If the analytical calculations yield a self-inductance value beyond the permissible tolerances, some minor modifications in number of turns and/or total air-gap length in an iterative manner by FEA (Maxwell 3D Magnetostatic Analysis Tool) until a self inductance value within the permissible tolerance limits is reached.
4. More precise calculations for core loss including the gap-loss component are achieved by using FEA tools (Maxwell 3D Transient Analysis Tool).



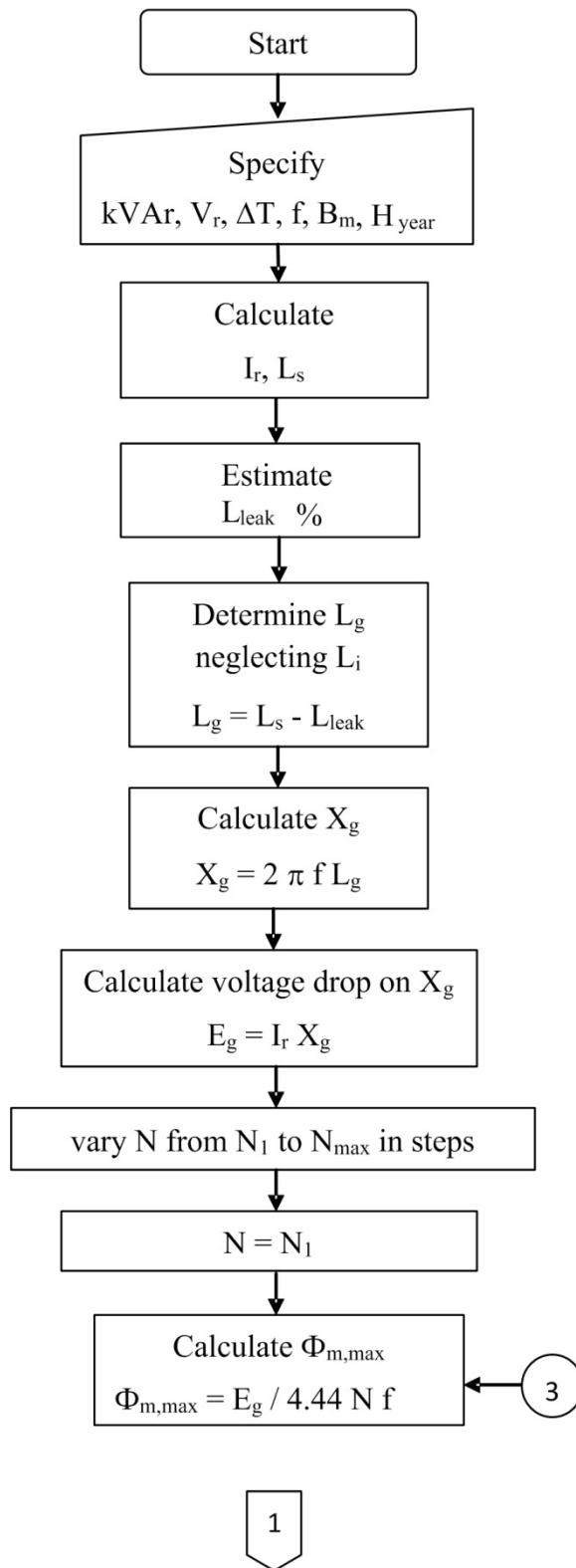


Figure 3.6 Flowchart of the design procedure (Matlab)

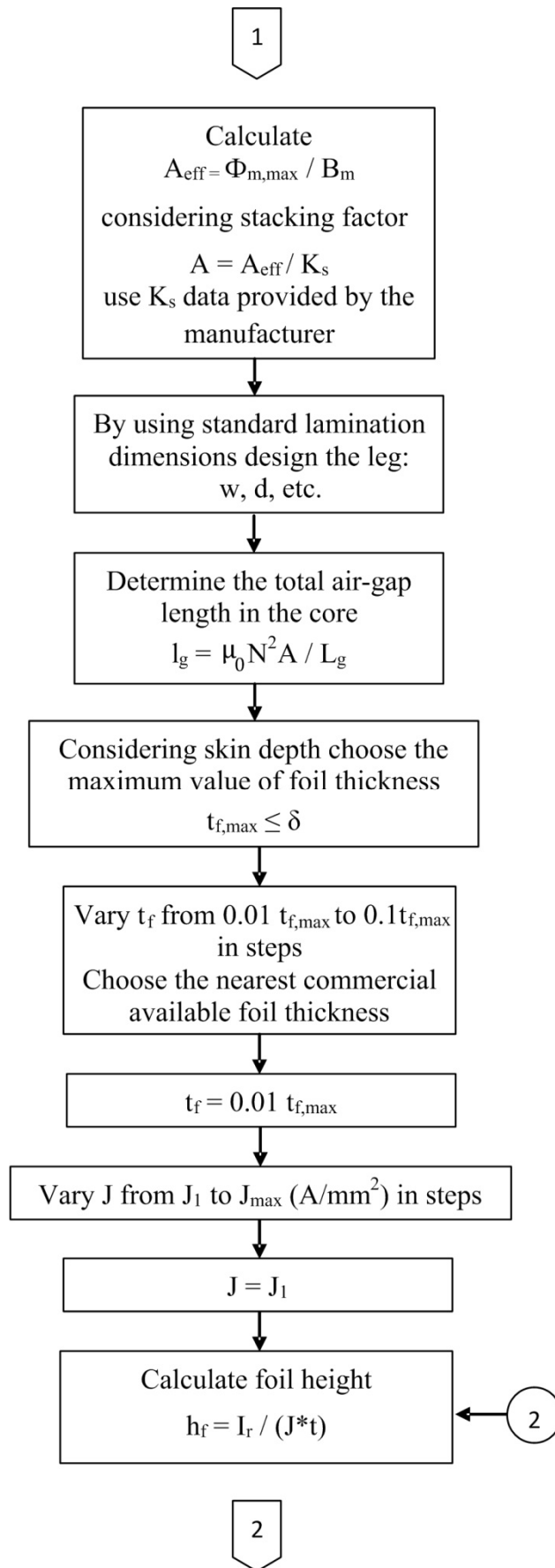


Figure 3.6 (Cont'd) Flowchart of the design procedure (Matlab)

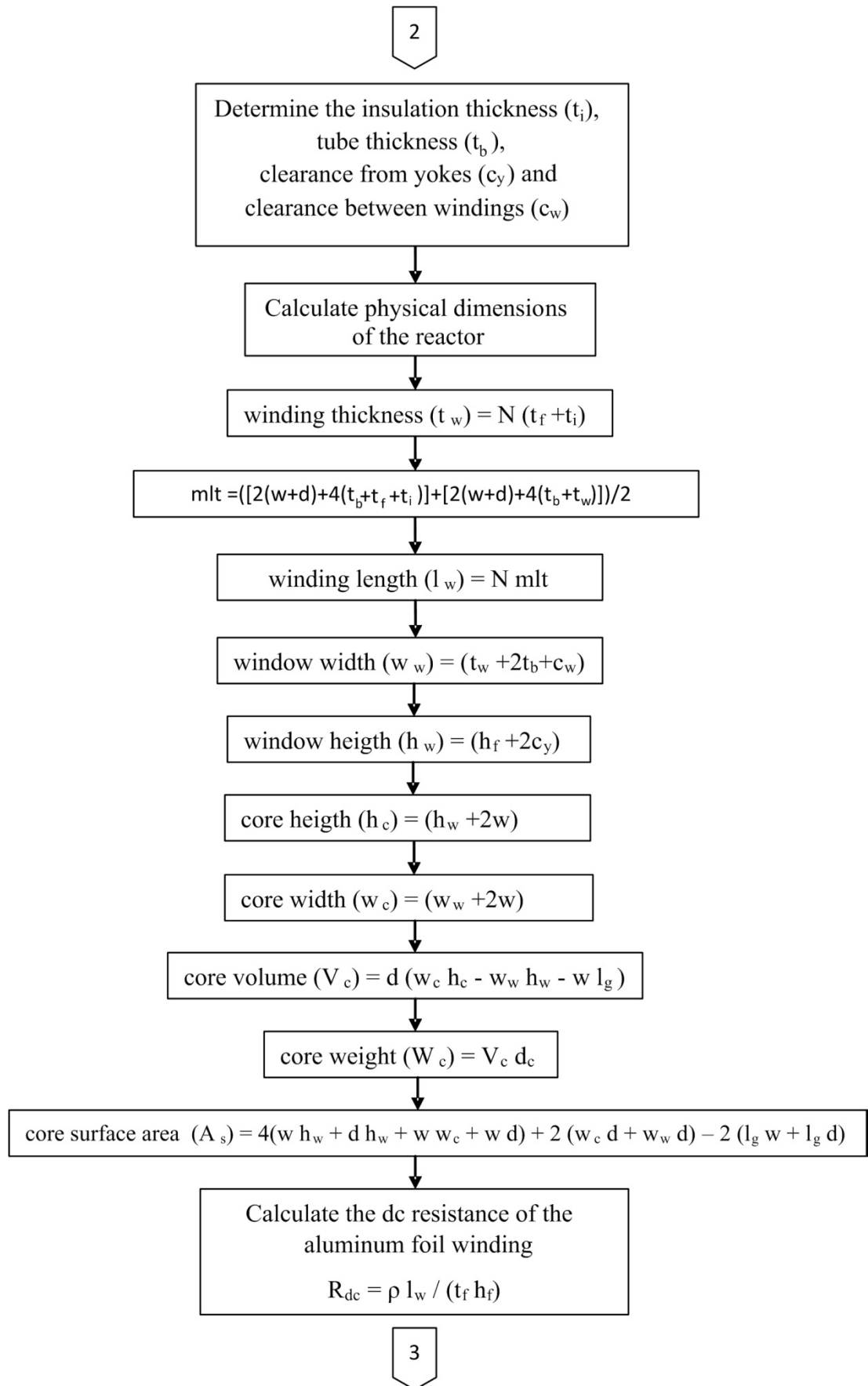


Figure 3.6 (Cont'd) Flowchart of the design procedure (Matlab)

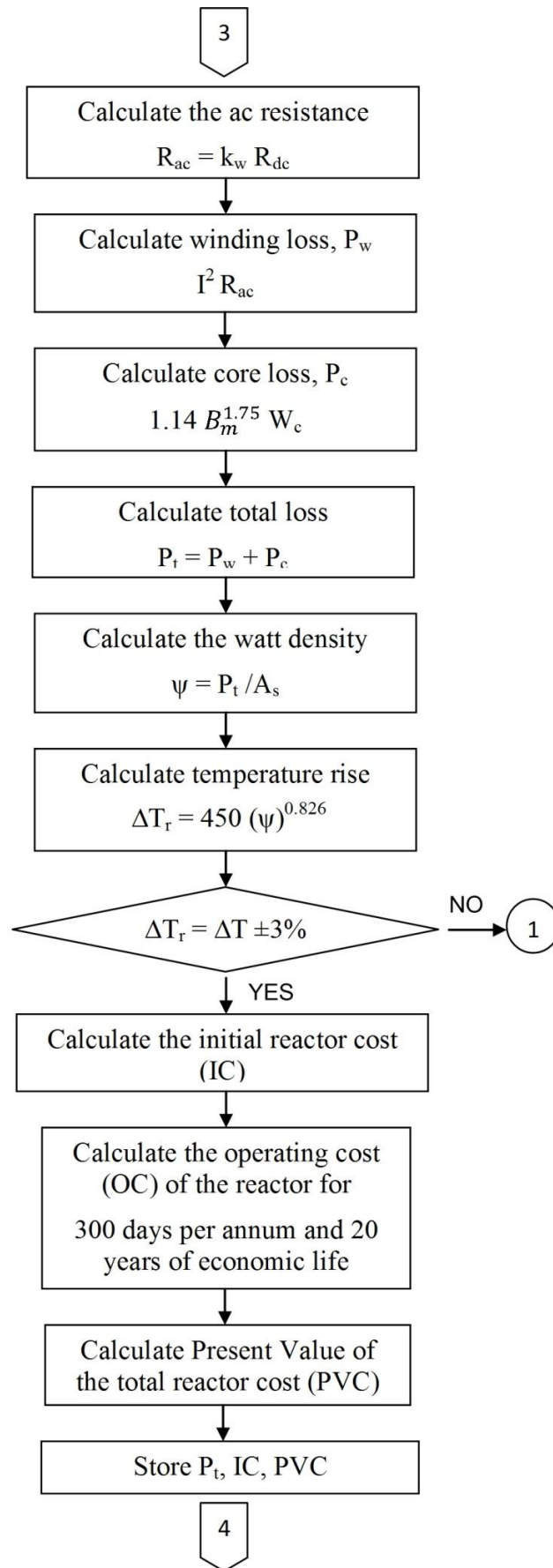


Figure 3.6 (Cont'd) Flowchart of the design procedure (Matlab)

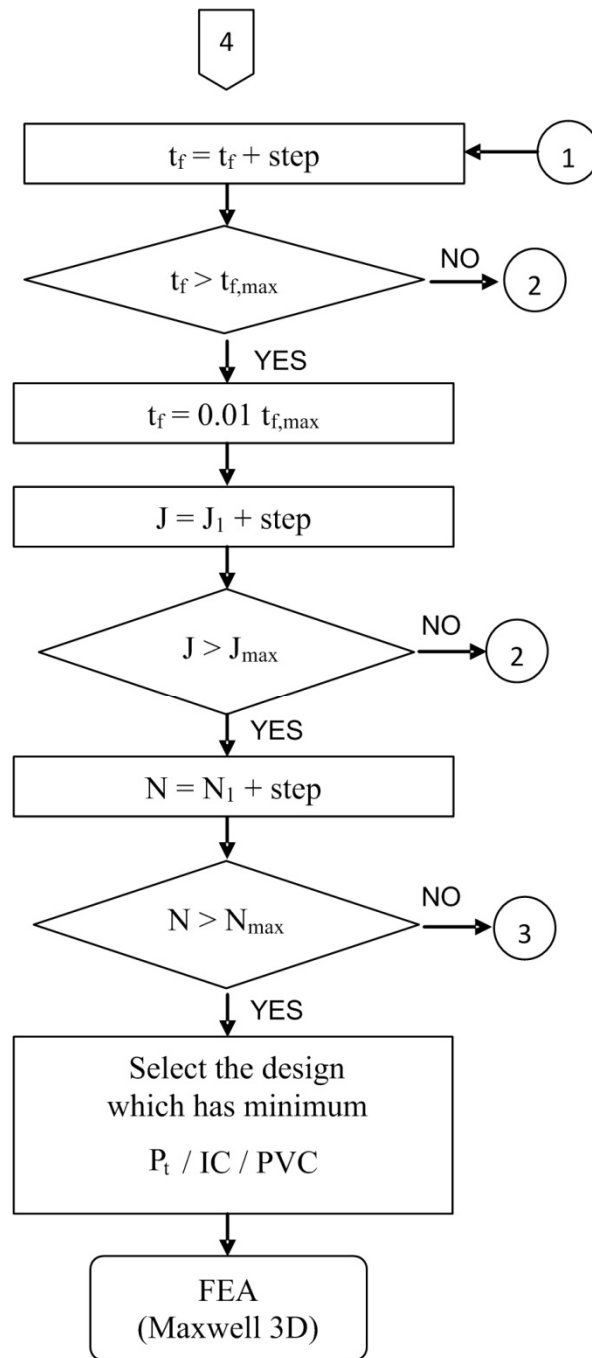


Figure 3.6 (Cont'd) Flowchart of the design procedure (Matlab)

The flowchart in Fig.3.6 shows the calculation steps performed in Matlab to find the optimum design parameters, such as physical dimensions of the reactor, number of turns, thickness of the winding etc. which are necessary to create the model for Maxwell optimization work.

This step has been followed by the FEA iterations to obtain the optimum reactor model which satisfies the target self inductance ( $28 \text{ mH} \pm 3\%$ ) value of the single-phase shunt reactor. The flowchart of the FEA iterations is given in Figure 3.7.

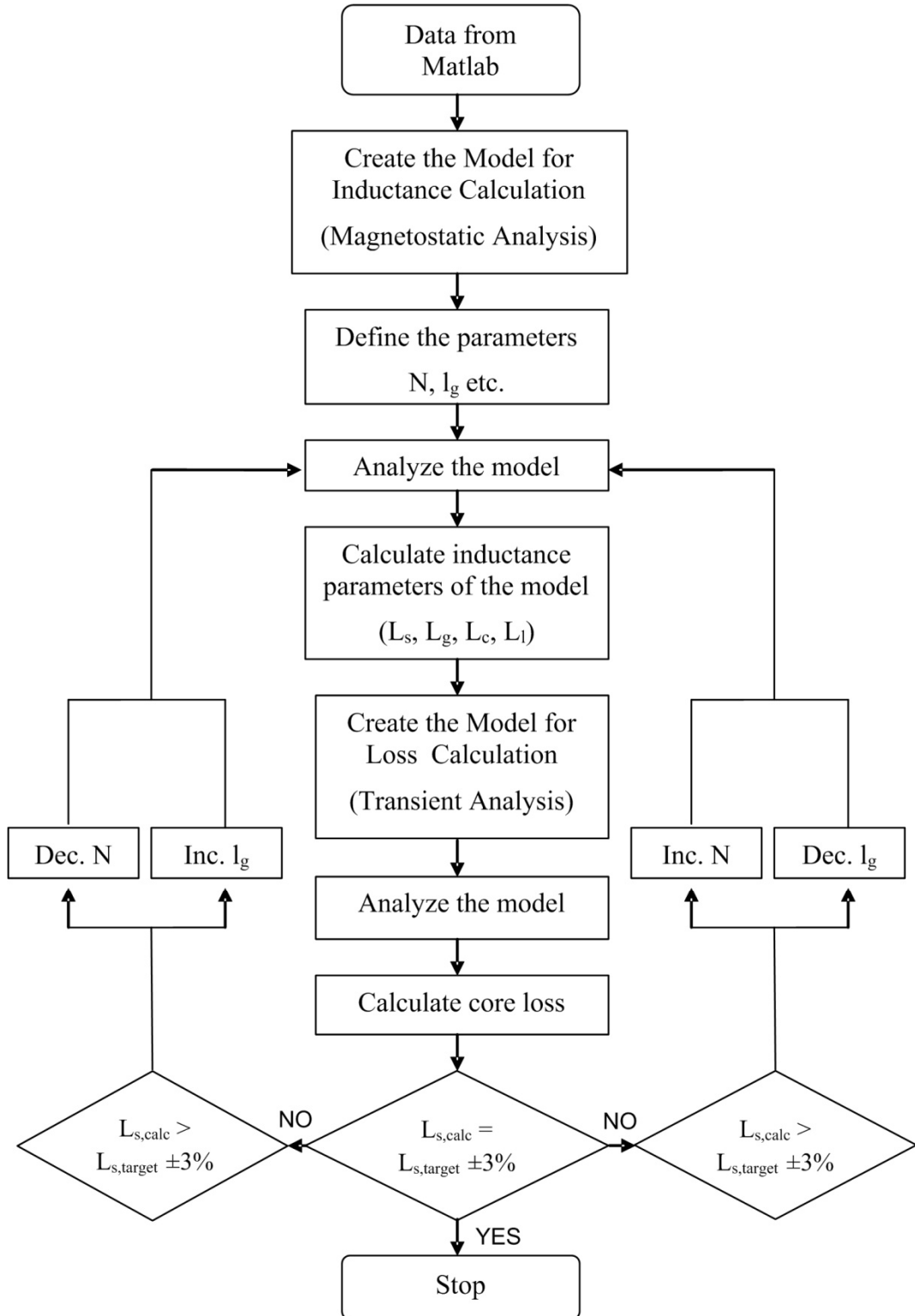


Figure 3.7 Flowchart of the design procedure (FEA)

### 3.4 Results of FEA Aided Design Work

Optimizations have been performed firstly by Matlab and then by Maxwell 3D software for three different design criteria, min IC, min  $P_t$  and min PVC. For each design criteria, the reactor has been designed at four peak flux densities, 0.8 T, 1 T, 1.2 T and 1.4 T, respectively. The total air-gap length in the core has been first placed as a single air-gap in each limb of the reactor ( $G=2$ ) and then discretely distributed along the limb ( $G=20$ ). Optimizations have been performed for both cases using the procedure shown in Fig.3.7.

#### 3.4.1 Design Work According to Minimum Initial Cost Criterion

The results of the optimization work performed for minimum initial cost criterion are given in Fig.3.8, Fig.3.9 and Fig.3.10.

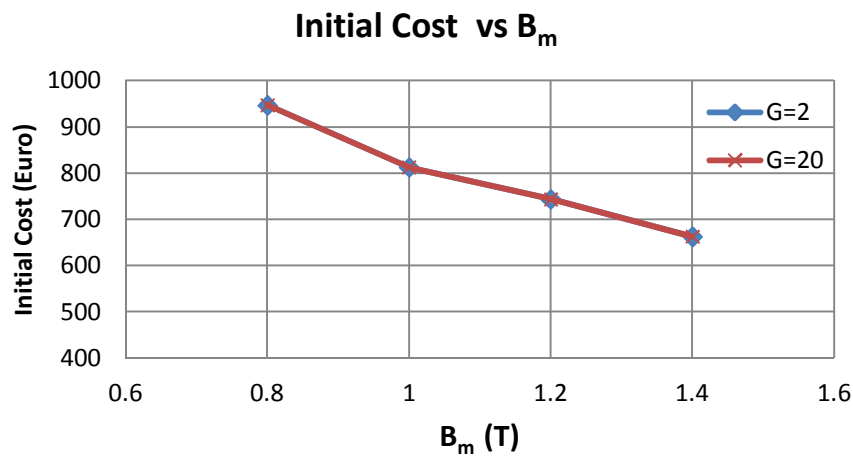
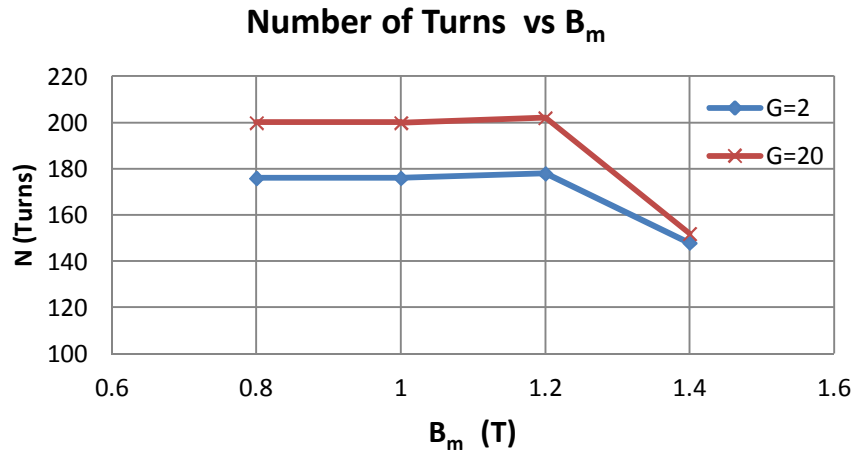
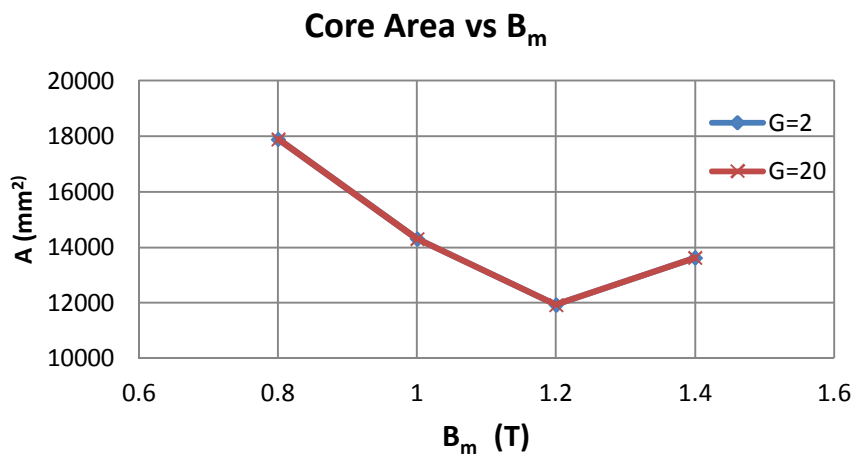


Figure 3.8 Variations in initial cost of the optimum reactor against design value of  $B_m$  (min IC (N, J, t))

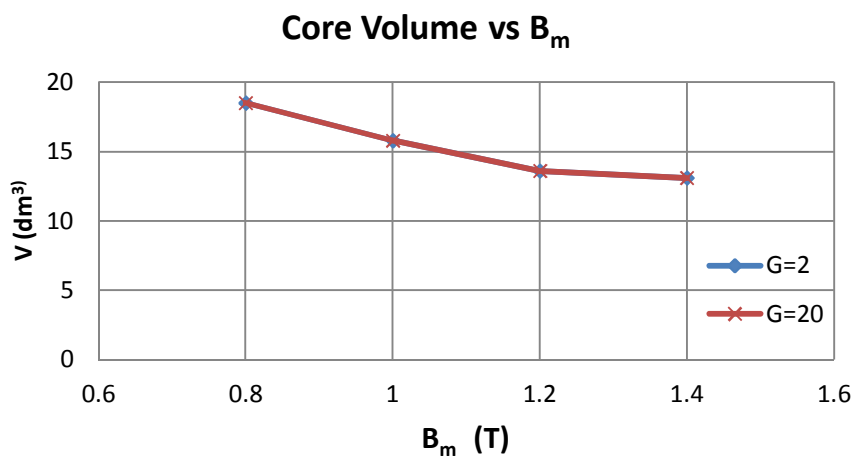
Fig.3.8 shows the variations in initial cost against  $B_m$  for min IC cost criterion. IC decreases while  $B_m$  increases as expected since the reactor volume decreases and hence the cost of producing the final reactor decreases. IC values are the same for both  $G=2$  and  $G=20$  because the only difference between two reactors is having only one or 10 air-gap portions in each limb.



a) Variations in number of turns against  $B_m$  for the optimized reactor in Fig.3.8



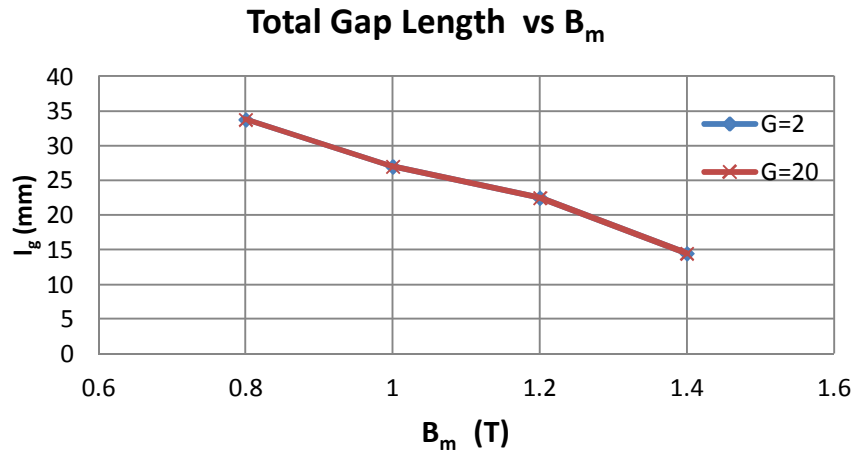
b) Variations in core area against  $B_m$  for the optimized reactor in Fig.3.8



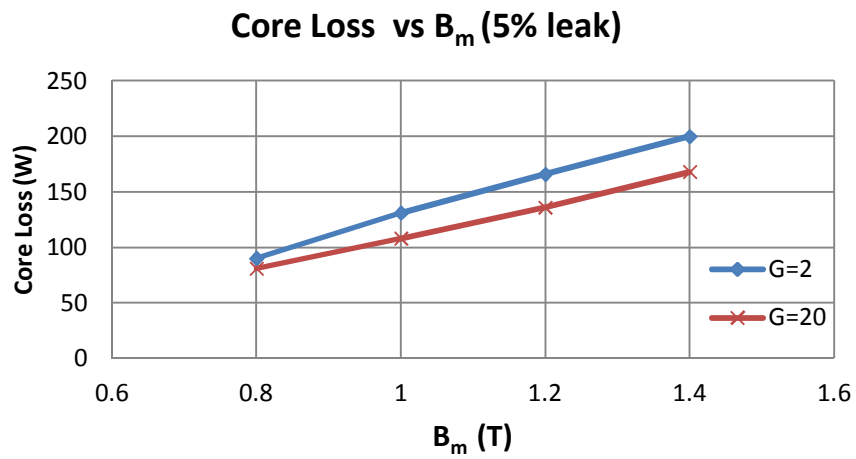
c) Variations in core volume against  $B_m$  for the optimized reactor in Fig.3.8

Figure 3.9 Variations in design parameters against  $B_m$  for the optimized reactor in Fig.3.8 (min IC (N, J, t))

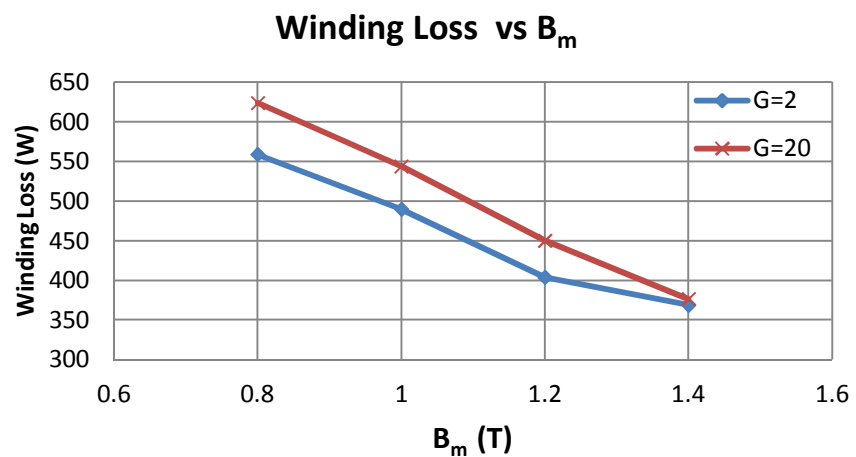




d) Variations in total gap length against  $B_m$  for the optimized reactor in Fig.3.8

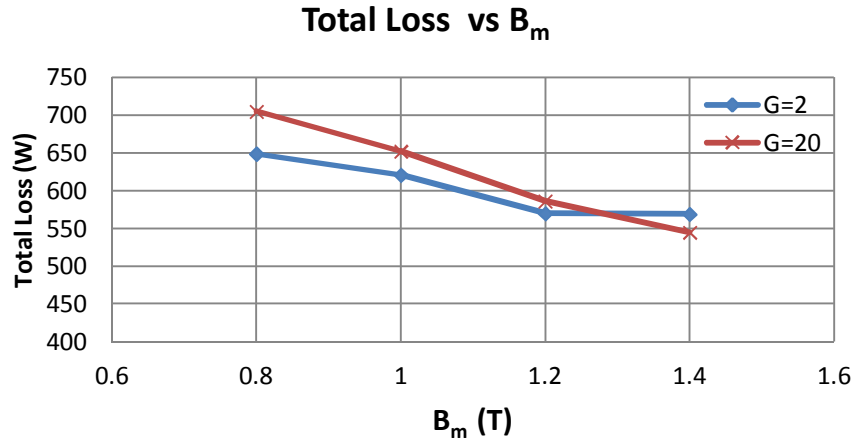


e) Variations in core loss against  $B_m$  for the optimized reactor in Fig.3.8



f) Variations in winding loss against  $B_m$  for the optimized reactor in Fig.3.8

Figure 3.9 (Cont'd) Variations in design parameters against  $B_m$  for the optimized reactor in Fig.3.8 (min IC (N, J, t))



g) Variations in total loss against  $B_m$  for the optimized reactor in Fig.3.8

Figure 3.9 (Cont'd) Variations in design parameters against  $B_m$  for the optimized reactor in Fig.3.8 (min IC (N, J, t))

Fig.3.9 shows the variations in number of turns, core area, core volume, total air-gap length, core loss, winding loss and total loss of the optimized reactor against  $B_m$  for min IC cost criterion, both for  $G=2$  and  $G=20$ . Following conclusions can be drawn from the results of Fig.3.9;

- Number of turns of the optimized reactors for  $G=2$  are smaller than those of  $G=20$  as shown in Fig.3.9.a, this causes winding loss of the optimized reactor for  $G=2$  to be smaller than those of  $G=20$  as can be seen in Fig.3.9.f.
- Core loss of the optimized reactor increases as the design value of  $B_m$  is increased as expected.
- Core area of the optimized reactor decreases in the range of  $B_m = 0.8$  T to 1.2 T, however it increases for the design value of  $B_m = 1.4$  T.
- Core volume of the optimized reactor decreases as the design value of  $B_m$  is increased.
- Total loss which is sum of the core loss and the winding loss of the optimized reactor decreases as the design value of  $B_m$  is increased. The total loss for  $G=20$  is higher than those of  $G=2$  in the range of  $B_m = 0.8$  T to 1.2 T, whereas

it is less than those of for  $G=2$  at 1.4 T. This is because of the differences in core loss and winding loss values as shown in Figs.3.9.e and f.

Since Present Value Cost (PVC) of the optimized reactor is sum of the Initial Cost (IC) and the present value of Operating Cost (OC) due to the total losses of the reactor throughout its life cycle, PVC decreases as the design value of  $B_m$  is increased as shown in Fig.3.10.

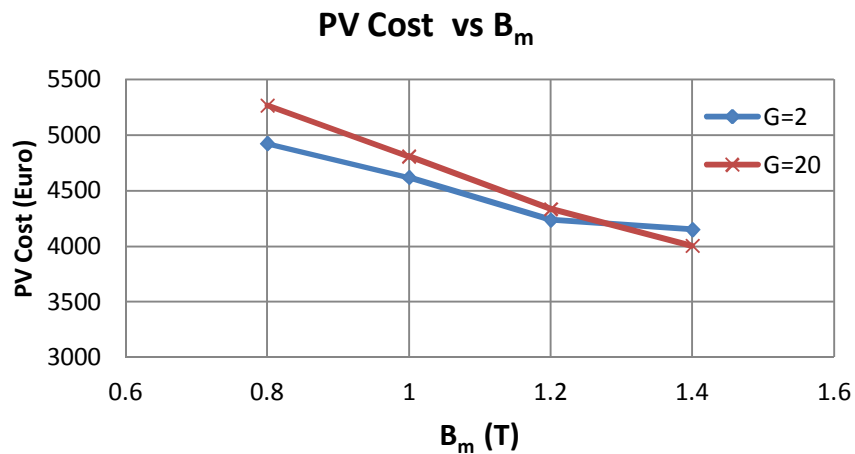


Figure 3.10 Variations in PVC against  $B_m$  for the optimized reactor in Fig.3.8

Flux density distributions in the core of the optimized reactors are obtained by using Maxwell 3D software for both  $G=2$  and  $G=20$  and are given in Fig.3.11 using the same flux-density scale. That is, enlarged scale showing the flux density values in Fig.3.11.a is applicable to all plots given in Fig.3.11. It is worth to note that Fig.3.11 shows;

- a) only the upper half of the overall structure,
- b) the core depths,  $d$ , are different and they are not shown in this figure (see Appendix-B),
- c) the core structures are drawn in scale.

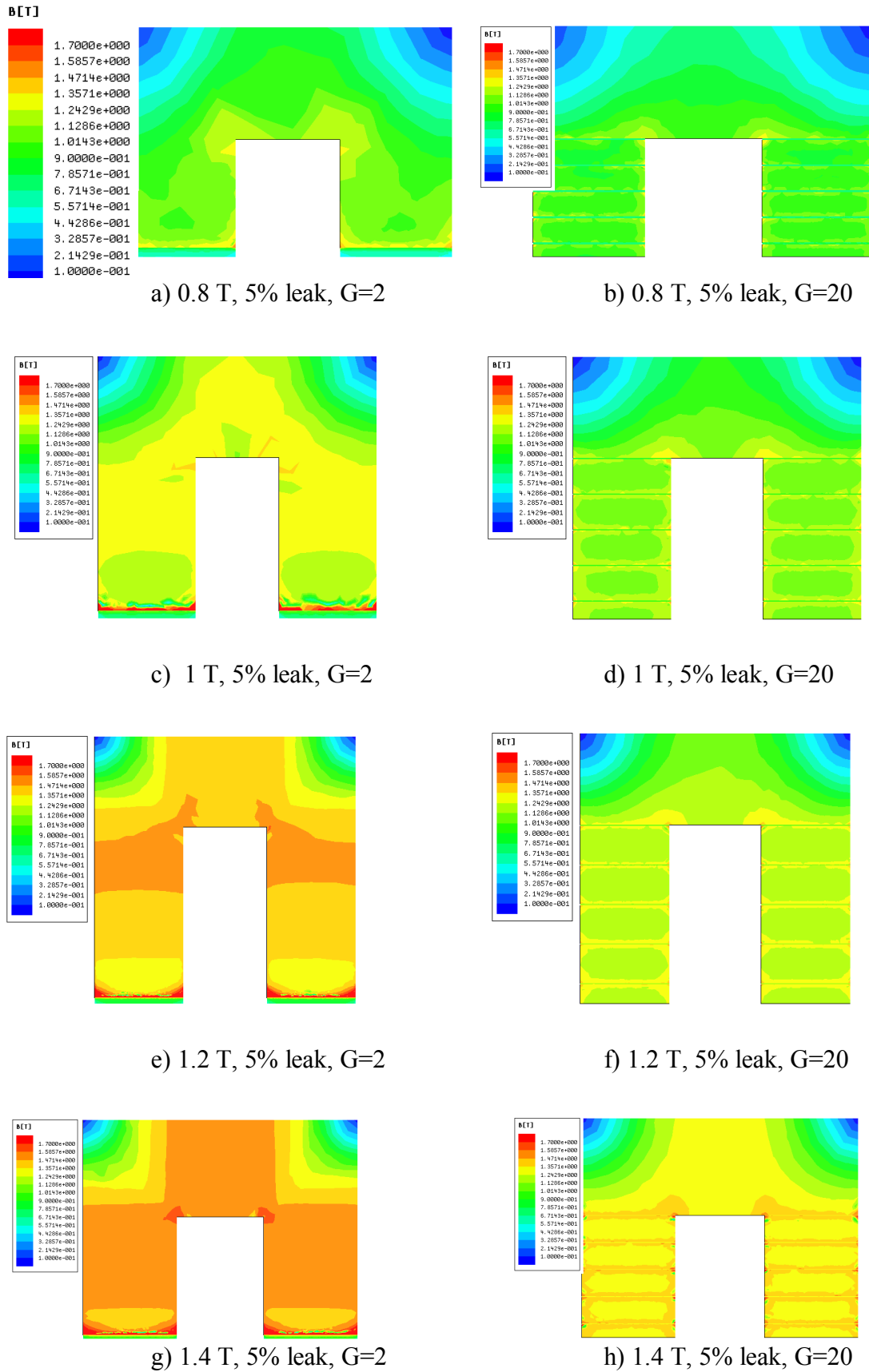


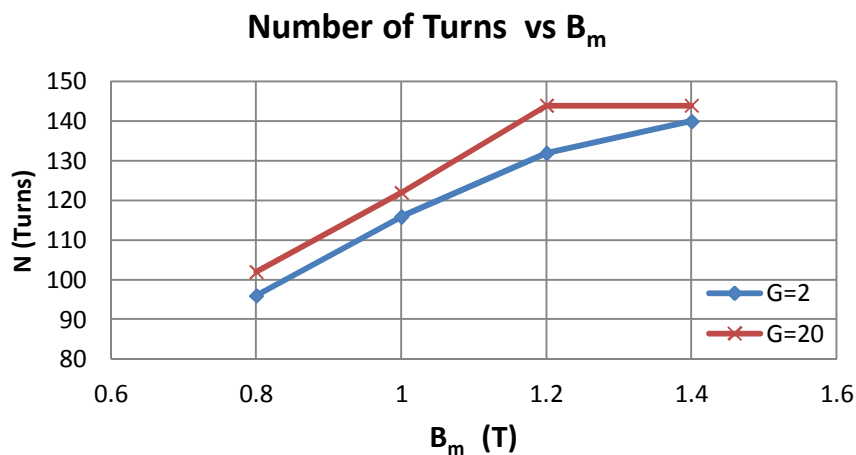
Figure 3.11 Flux density distributions in the core of the optimized reactors for different peak flux densities both for G=2 and G=20 (min IC (N, J, t))

Following conclusions can be drawn from these plots of flux density distribution;

- Having several discretely distributed air-gaps in the core ( $G=20$ ) gives more uniform flux density distribution regardless of the chosen  $B_m$  value in comparison with those of the core with  $G=2$ .
- The use of only two air-gap portions in the core ( $G=2$ ) may give higher flux densities than the design value of  $B_m$  in some parts of the magnetic core, e.g., Fig.3.11.g and Fig.3.11.e.
- For the chosen material, if one sets  $B_m$  to 1.4 T, as can be observed from Fig.3.11.g local saturation may occur at the corners of the structure. Since this is not desirable for the designer,  $B_m = 1.4$  T should be eliminated among the options in the design of the reactor for the chosen core material.
- The core size reduces as the design value of  $B_m$  is increased as expected. Further information is given in Appendix-B.

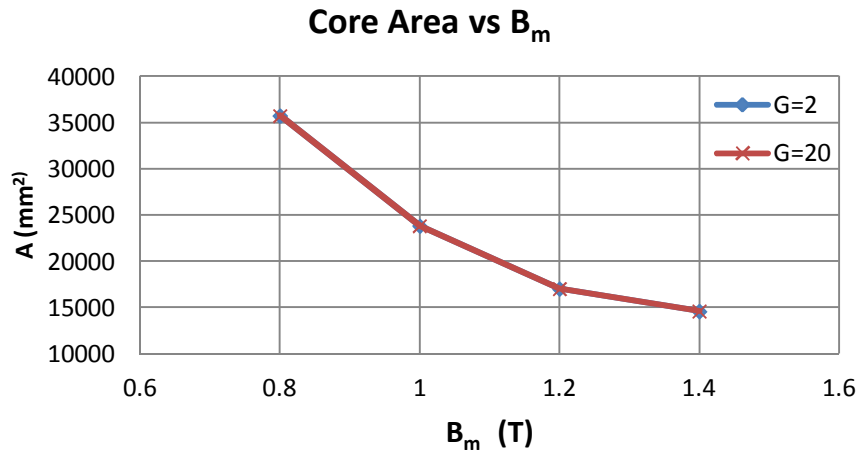
### 3.4.2 Design Work According to Minimum Total Loss Criterion

Results of the optimization work performed for the minimum total loss criterion are illustrated in Fig.3.12, Fig.3.13 and Fig.3.14.

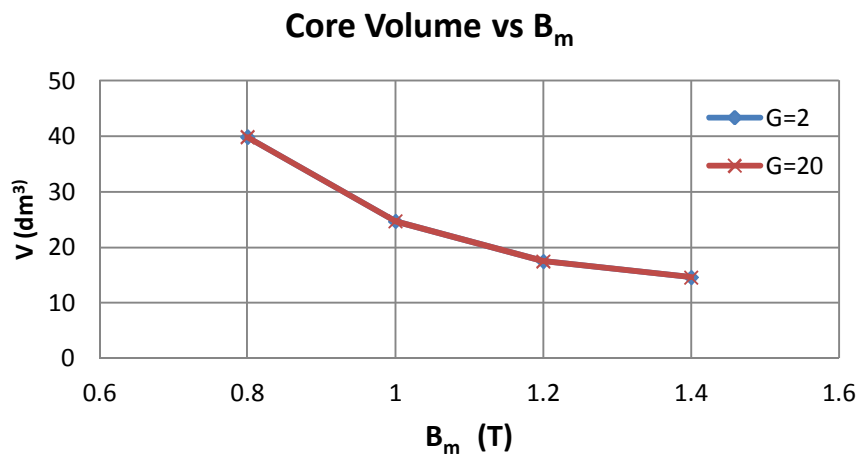


a) Variations in number of turns of the optimum reactor against design value of  $B_m$

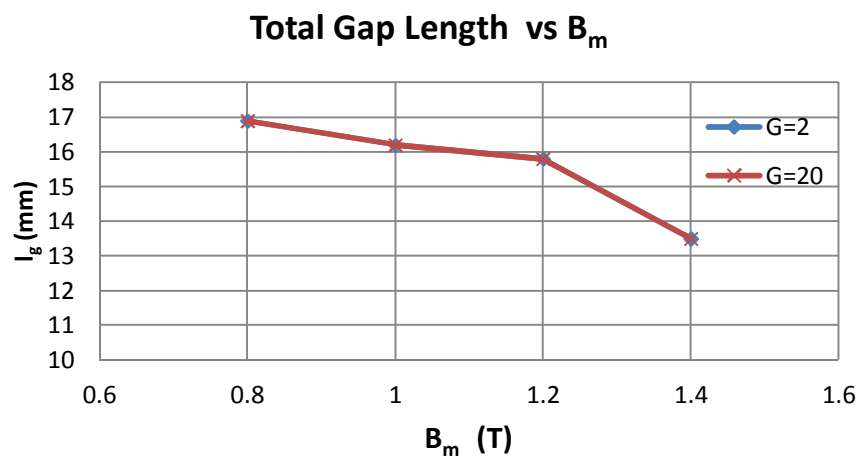
Figure 3.12 Variations in design parameters of the optimum reactor against design value of  $B_m$  (min  $P_t$  (N, J, t))



b) Variations in core area of the optimum reactor against design value of  $B_m$

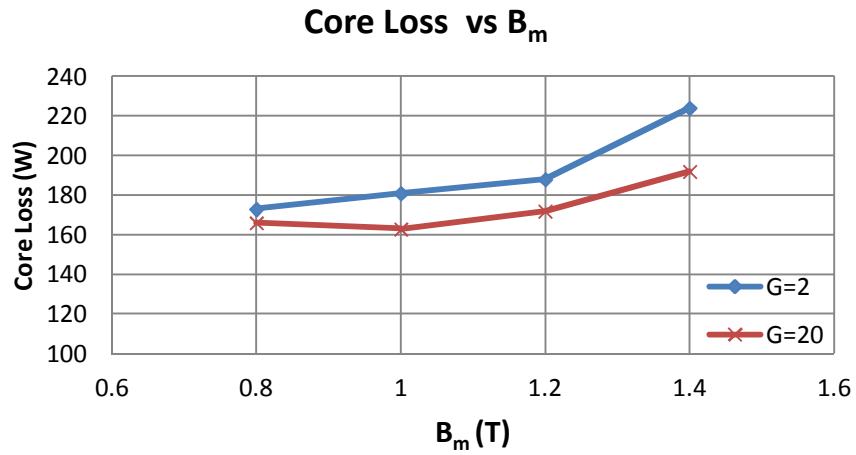


c) Variations in core volume of the optimum reactor against design value of  $B_m$

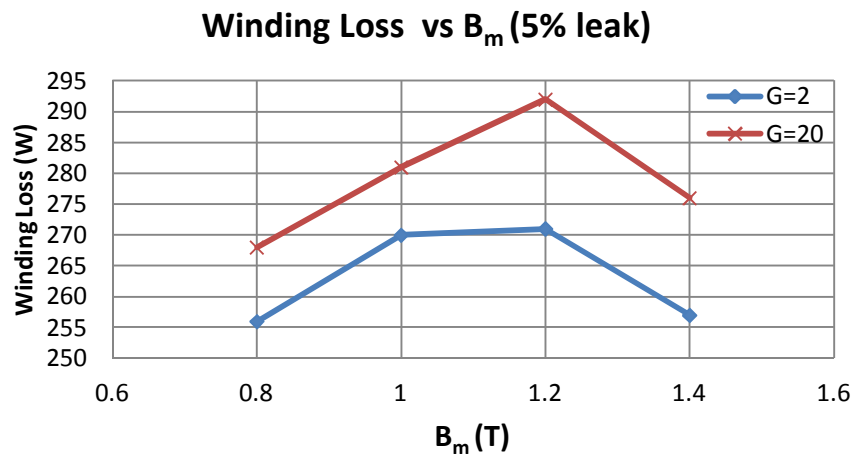


d) Variations in total gap length of the optimum reactor against design value of  $B_m$

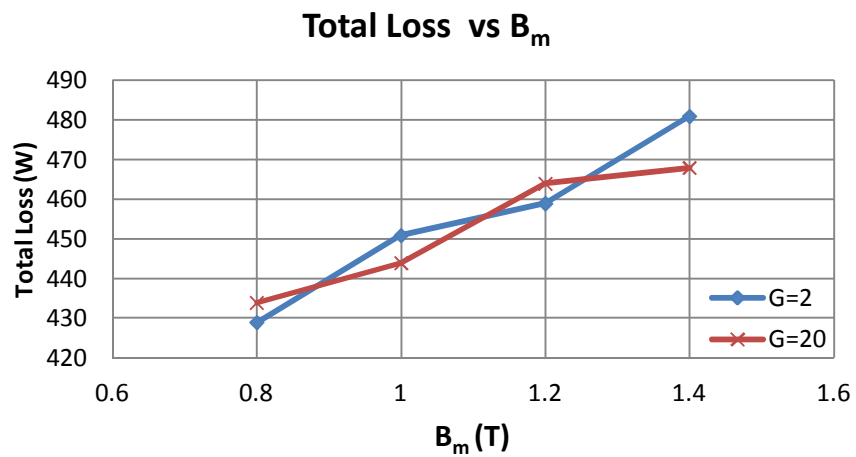
Figure 3.12 (Cont'd) Variations in design parameters of the optimum reactor against design value of  $B_m$  (min  $P_t$  (N, J, t))



e) Variations in core loss of the optimum reactor against design value of  $B_m$



f) Variations in winding loss of the optimum reactor against design value of  $B_m$



g) Variations in total loss of the optimum reactor against design value of  $B_m$

Figure 3.12 (Cont'd) Variations in design parameters of the optimum reactor against design value of  $B_m$  (min  $P_t$  (N, J, t))

Fig.3.12 shows the variations in number of turns, core area, core volume, total air-gap length, core loss, winding loss and total loss of the optimized reactor against  $B_m$  for min  $P_t$  criterion, both for  $G=2$  and  $G=20$ . Following conclusions can be drawn from the results of Fig.3.12;

- Number of turns of the optimized reactors increases as the design value of  $B_m$  is increased and for  $G=2$  it is smaller than those of  $G=20$  as shown in Fig.3.12.a. Therefore, winding loss of the optimized reactor for  $G=2$  have smaller values in comparison with those of  $G=20$  as can be seen in Fig.3.12.f.
- Core loss of the optimized reactor increases as the design value of  $B_m$  is increased as illustrated in Fig.3.12.e.
- Core area and core volume of the optimized reactor decrease as the design value of  $B_m$  is increased.
- Total loss which is sum of the core loss and the winding loss of the optimized reactor increases as the design value of  $B_m$  is increased. The total loss for  $G=2$  and  $G=20$  are very close for all  $B_m$  values.

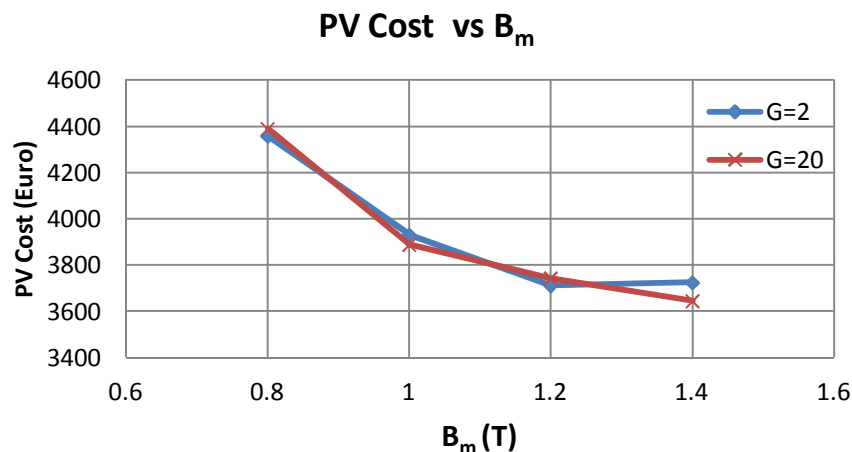


Figure 3.13 Variations in Present Value Cost of the optimum reactor against design value of  $B_m$  (min  $P_t$  (N, J, t))



Fig.3.13 and Fig.3.14 show the variations in PVC and IC of the optimized reactor against  $B_m$  for min  $P_t$  design criterion, respectively. Both PVC and IC decrease as the design value of  $B_m$  is increased. Although the total loss of the optimized reactor increases as the design value of  $B_m$  is increased, PVC of the optimized reactor decreases. Because, the difference between minimum and maximum values of the total loss is almost 50 Watts whereas it is almost 1000 Euros in IC values as illustrated in Fig.3.14. Since the total loss and initial cost values of the optimized reactor are nearly same for  $G=2$  and  $G=20$ , PVC values are also very close to each other.

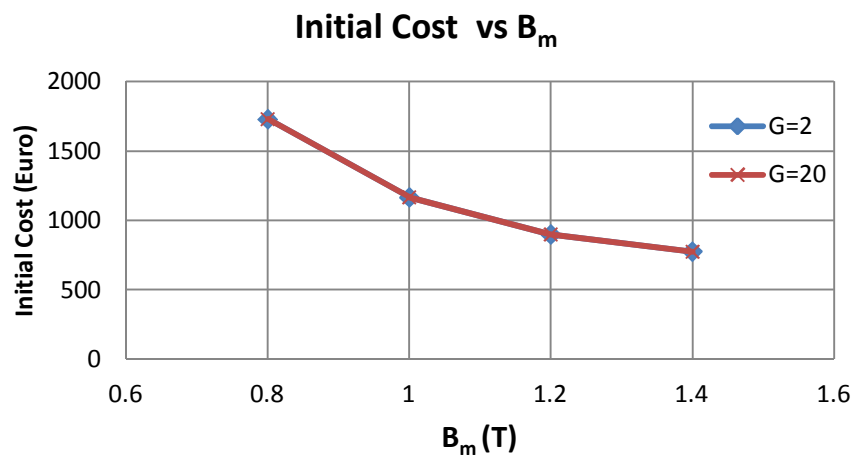


Figure 3.14 Variations in Initial Cost of the optimum reactor against design value of  $B_m$  (min  $P_t$  (N, J, t))

Flux density distributions in the core of the optimized reactors are obtained by using Maxwell 3D software for both  $G=2$  and  $G=20$  and are given in Fig.3.15 using the same flux-density scale. That is, enlarged scale showing the flux density values in Fig.3.15.a is applicable to all plots given in Fig.3.15. It is worth to note that Fig.3.15 shows;

- a) only the upper half of the overall structure,
- b) the core depths,  $d$ , are different and they are not shown in this figure (see Appendix-B),
- c) the core structures are drawn in scale.

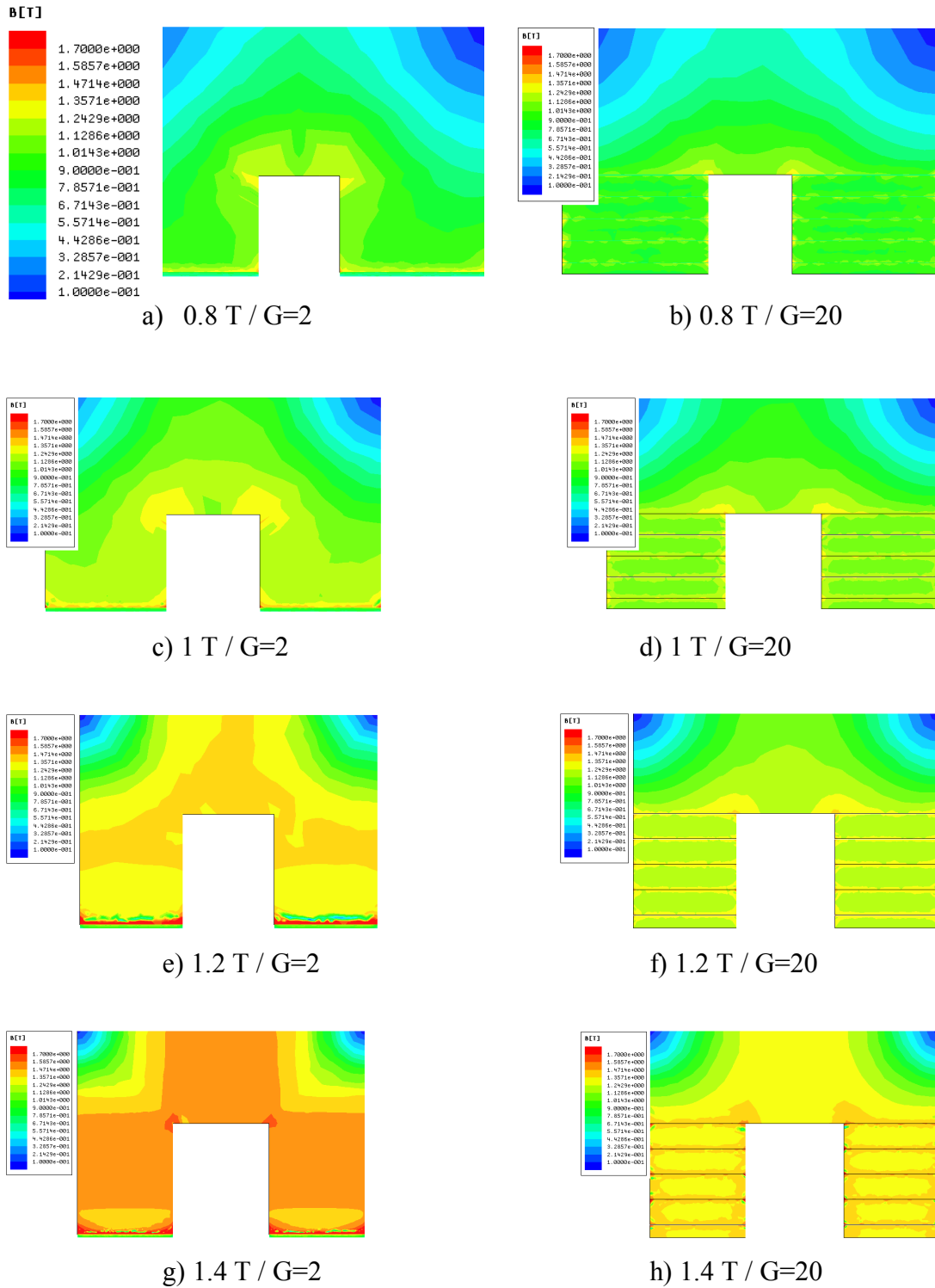


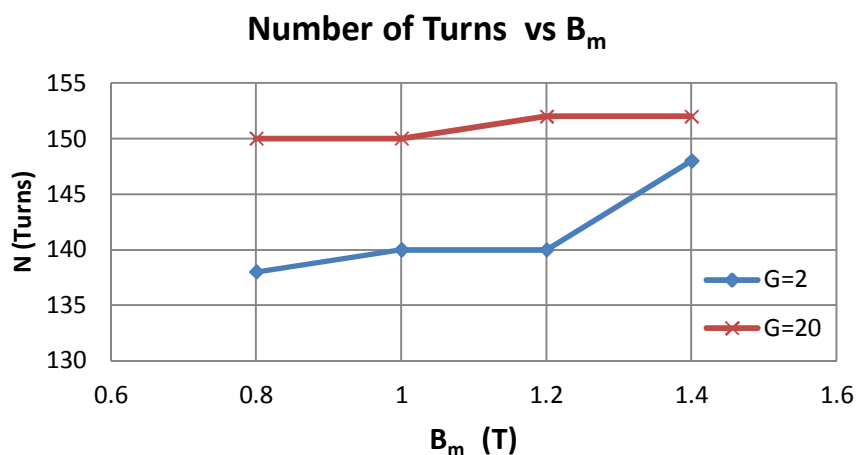
Figure 3.15 Flux density distributions in the core of the optimized reactors for different peak flux densities both for G=2 and G=20 (min  $P_t$  (N, J, t))

Following conclusions can be drawn from these plots of flux density distribution;

- Having several discretely distributed air-gaps in the core ( $G=20$ ) gives more uniform flux density distribution regardless of the chosen  $B_m$  value in comparison with those of the core with  $G=2$ .
- The use of only two air-gap portions in the core ( $G=2$ ) may give higher flux densities than the design value of  $B_m$  in some parts of the magnetic core, e.g., Fig.3.15.e and Fig.3.15.g.
- For the chosen material if one sets  $B_m$  to 1.4 T, as can be observed from Fig.3.15.g local saturation may occur at the corners of the structure. Since this is not desirable for the designer,  $B_m = 1.4$  T should be eliminated among the options in the design of the reactor for the chosen core material.
- The core size reduces as the design value of  $B_m$  is increased as expected. Further information is given in Appendix-B.

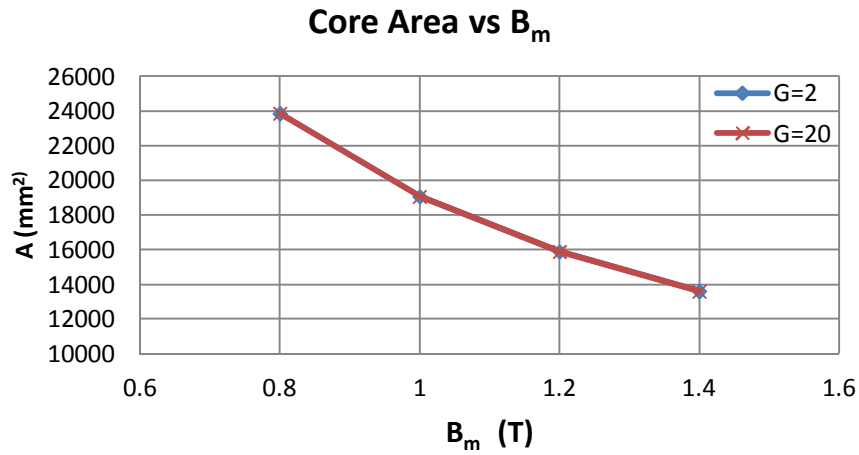
### 3.4.3 Design Work According to Minimum Present Value Cost Criterion

Results of the optimization work performed for the min PVC criterion are illustrated in Fig.3.16.

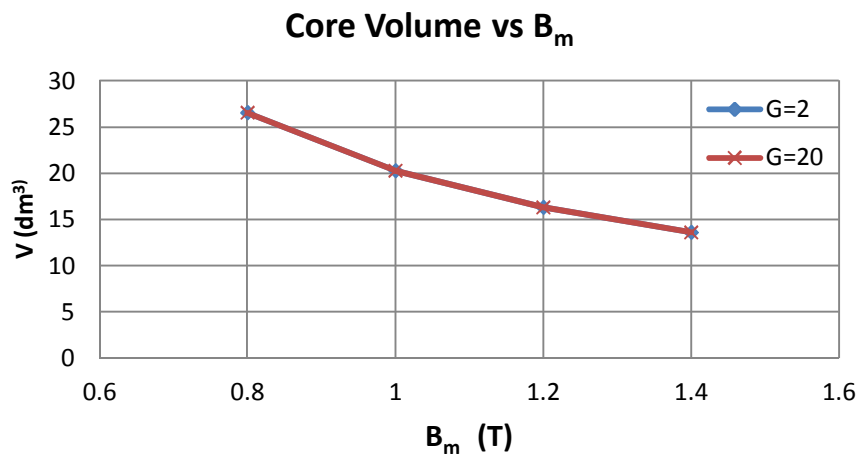


a) Variations in number of turns of the optimum reactor against design value of  $B_m$

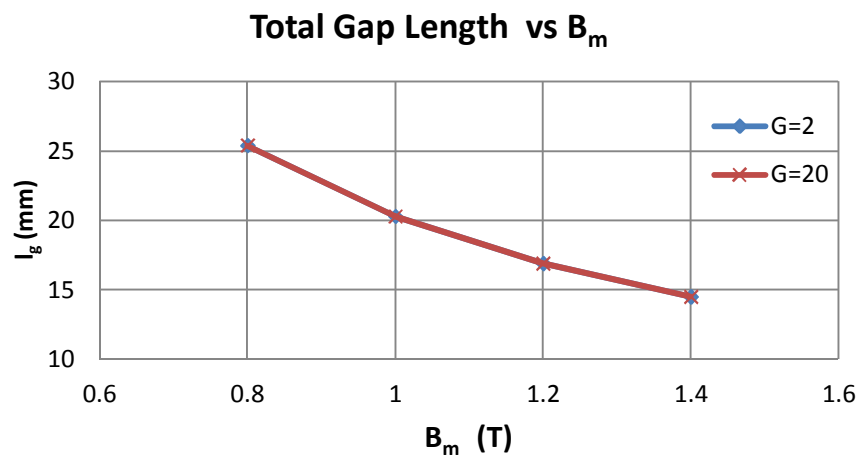
Figure.3.16 Variations in design parameters of the optimum reactor against design value of  $B_m$  (min PVC ( $N, J, t$ ))



b) Variations in core area of the optimum reactor against design value of  $B_m$

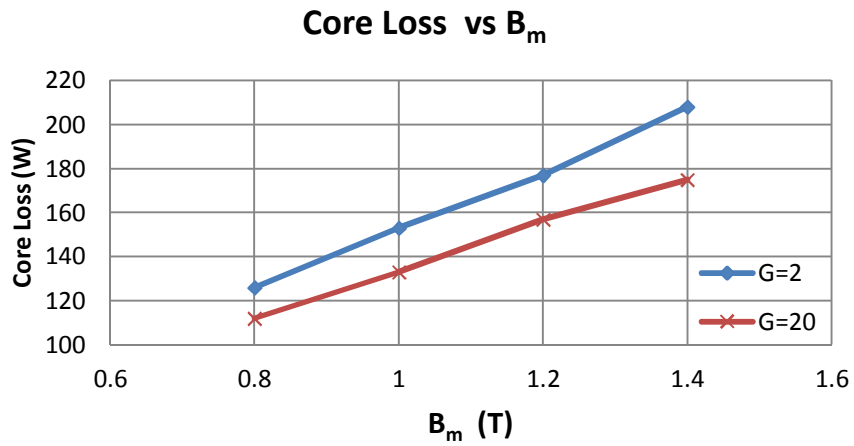


c) Variations in core volume of the optimum reactor against design value of  $B_m$

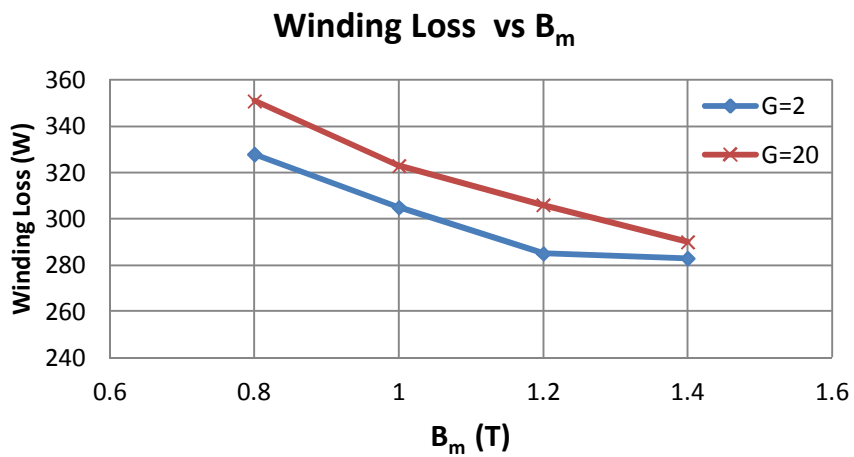


d) Variations in total gap length of the optimum reactor against design value of  $B_m$

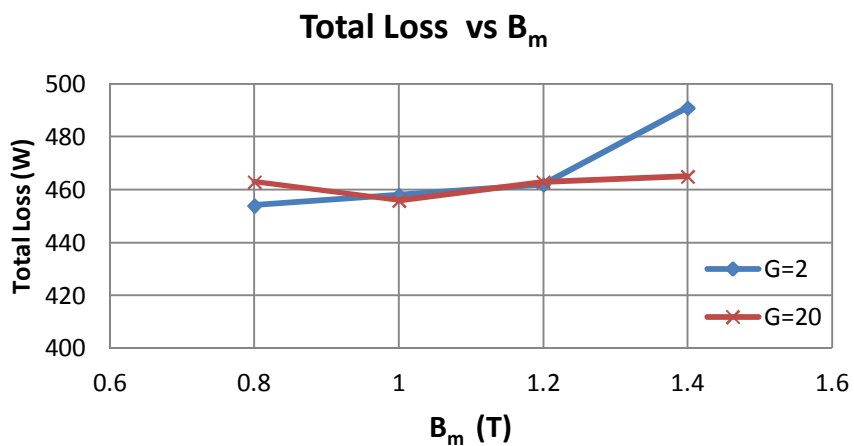
Figure.3.16 (Cont'd) Variations in design parameters of the optimum reactor against design value of  $B_m$  (min PVC (N, J, t))



e) Variations in core loss of the optimum reactor against design value of B<sub>m</sub>

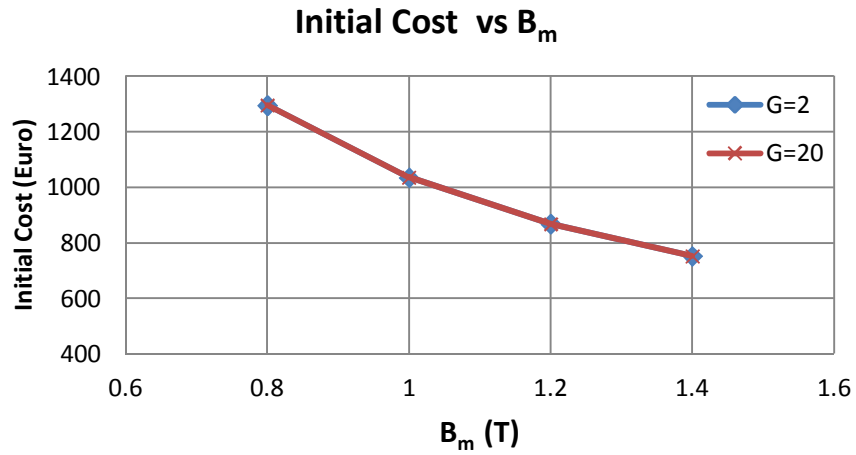


f) Variations in winding loss of the optimum reactor against design value of B<sub>m</sub>

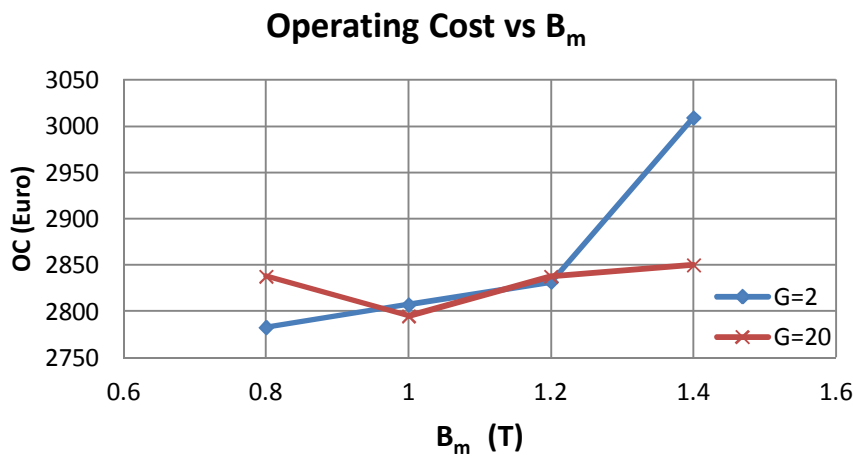


g) Variations in total loss of the optimum reactor against design value of B<sub>m</sub>

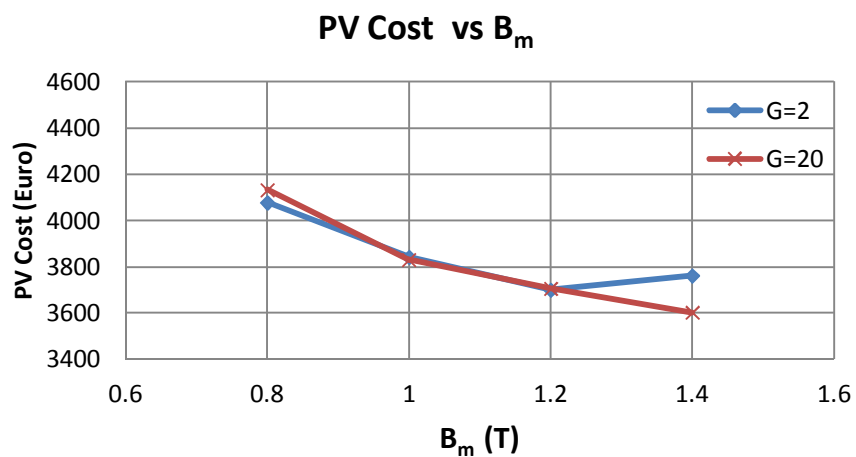
Figure.3.16 (Cont'd) Variations in design parameters of the optimum reactor against design value of B<sub>m</sub> (min PVC (N, J, t))



h) Variations in initial cost of the optimum reactor against design value of  $B_m$



i) Variations in operating cost of the optimum reactor against design value of  $B_m$



j) Variations in present value cost of the optimum reactor against design value of  $B_m$

Figure.3.16 (Cont'd) Variations in design parameters of the optimum reactor against design value of  $B_m$  (min PVC (N, J, t))

Fig.3.16 shows the variations in number of turns, core area, core volume, total air-gap length, core loss, winding loss, total loss, initial cost, operating cost and present value cost of the optimized reactor against  $B_m$  for min PVC criterion, both for  $G=2$  and  $G=20$ . Following conclusions can be drawn from the results of Fig.3.16;

- Number of turns of the optimized reactors increases as the design value of  $B_m$  is increased and for  $G=2$  it is smaller than those of  $G=20$  as shown in Fig.3.16.a. Therefore, winding loss of the optimized reactor for  $G=2$  have smaller values than those of  $G=20$  as can be seen in Fig.3.16.f.
- Core loss of the optimized reactor increases as the design value of  $B_m$  is increased as illustrated in Fig.3.16.e.
- Core area and core volume of the optimized reactor decrease as the design value of  $B_m$  is increased.
- Total loss which is sum of the core loss and the winding loss of the optimized reactor increases for  $G=2$  as the design value of  $B_m$  is increased. The change in the total loss of the optimized reactor for  $G=20$  is not significant. Total loss values are very close for  $G=2$  and  $G=20$  in the range of operating flux density from  $B_m = 0.8$  T to 1.2 T, however for  $B_m = 1.4$  T, total loss for  $G=2$  is higher than that of for  $G=20$ . This leads to the variations in the operating cost shown in Fig.3.16.i to be in the same manner as variations in total loss.
- Initial cost of the optimized reactor decreases as the design value of  $B_m$  is increased as illustrated in Fig.3.16.h. Therefore, present value cost of the optimized reactor shown in Fig.3.16.j decreases as the design value of  $B_m$  is increased.

Flux density distributions in the core of the optimized reactors are obtained by using Maxwell 3D software for both  $G=2$  and  $G=20$  and are given in Fig.3.17 using the same flux-density scale. That is, the enlarged scale showing the flux density values in

Fig.3.17.a is applicable to all plots given in Fig.3.17. It is worth to note that Fig.3.17 shows;

- a) only the upper half of the overall structure,
- b) the core depths,  $d$ , are different and they are not shown in this figure (see Appendix-B),
- c) the core structures are drawn in scale.

Following conclusions can be drawn from these plots of flux density distribution;

- Having several discretely distributed air-gaps in the core ( $G=20$ ) gives more uniform flux density distribution regardless of the chosen  $B_m$  value in comparison with those of the core with  $G=2$ .
- The use of only two air-gap portions in the core ( $G=2$ ) may give higher flux densities than the design value of  $B_m$  in some parts of the magnetic core, e.g., Fig.3.17.g and Fig.3.17.e.
- For the chosen material if one sets  $B_m$  to 1.4 T, as can be observed from Fig.3.17.g local saturation may occur at the corners of the structure. Since this is not desirable for the designer,  $B_m=1.4$  T should be eliminated among the options in the design of the reactor for the chosen core material.
- The core size reduces as the design value of  $B_m$  is increased as expected. Further information is given in Appendix-B.



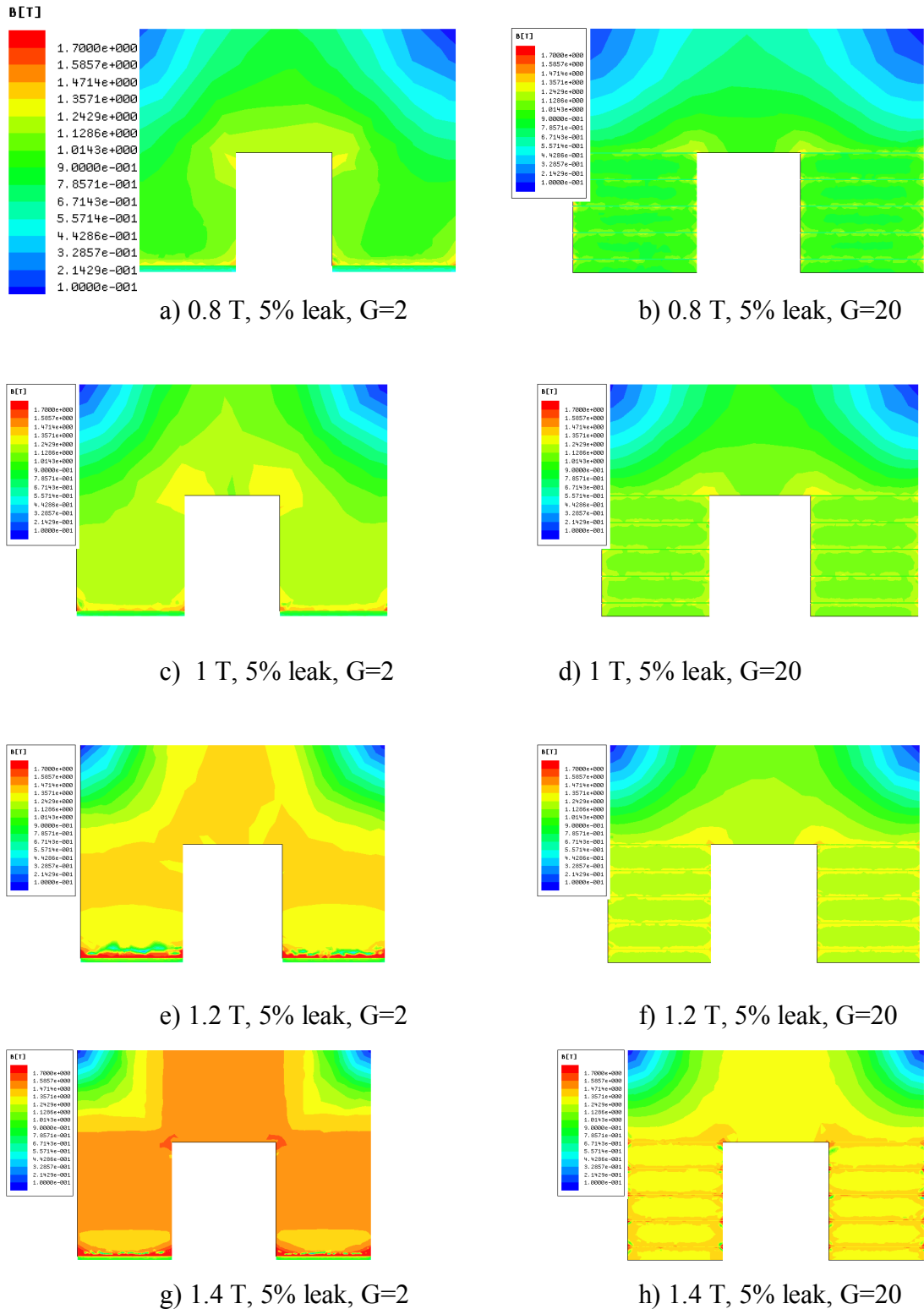


Figure 3.17 Flux density distributions in the core of the optimized reactors for different peak flux densities both for G=2 and G=20 (min PVC (N, J, t))

### 3.5 Comparison of Three Design Criteria

The variations in the initial cost of the same reactor which is designed according to different design objectives (min IC, min  $P_t$  and min PVC) and at different operating flux densities ( $B_m = 0.8, 1, 1.2$  and  $1.4$  T) are given in Fig.3.18 for  $G=2$  and in Fig.3.19 for  $G=20$ . As expected, when the same reactor is designed according to min IC design objective, its initial cost is considerably lower than those of the same reactor designed according to min  $P_t$  and min PVC objectives. That is the main reason why some of the reactor manufacturers prefer min IC criterion in their designs. By this way, they may reduce the selling prices of their reactors and thus increasing their market share. However, this is not the best approach to the reactor design from the viewpoint of macroeconomics and also of consumer economy.

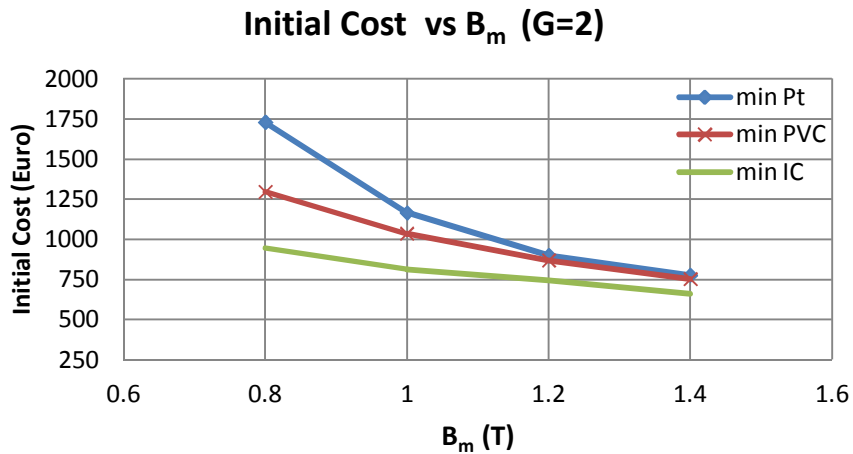


Figure 3.18 Variations in Initial Cost against  $B_m$  for three design criteria ( $G=2$ )

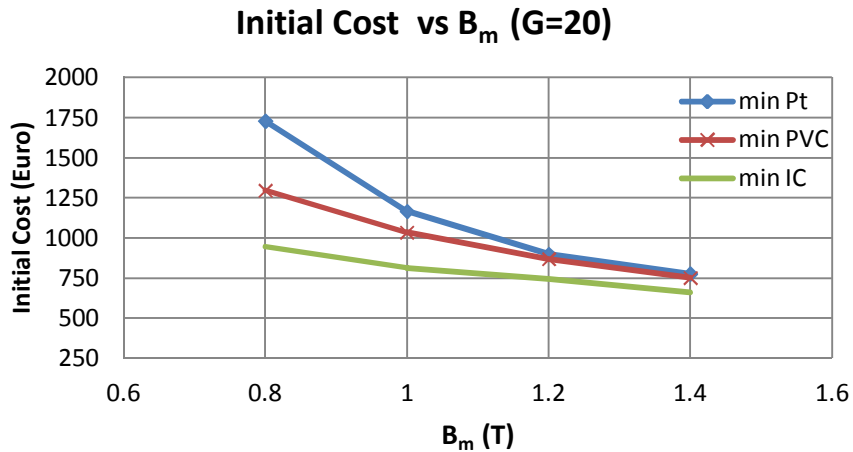


Figure 3.19 Variations in Initial Cost against  $B_m$  for three design criteria ( $G=20$ )

The variations in total reactor loss against  $B_m$  for the same reactor designed according to three different design criteria are given in Fig.3.20 for  $G=2$  and in Fig.3.21 for  $G=20$ . The variations in PVC against  $B_m$  for the same reactor designed according to three different design criteria are also given in Fig.3.22 for  $G=2$  and in Fig. 3.23 for  $G=20$ .

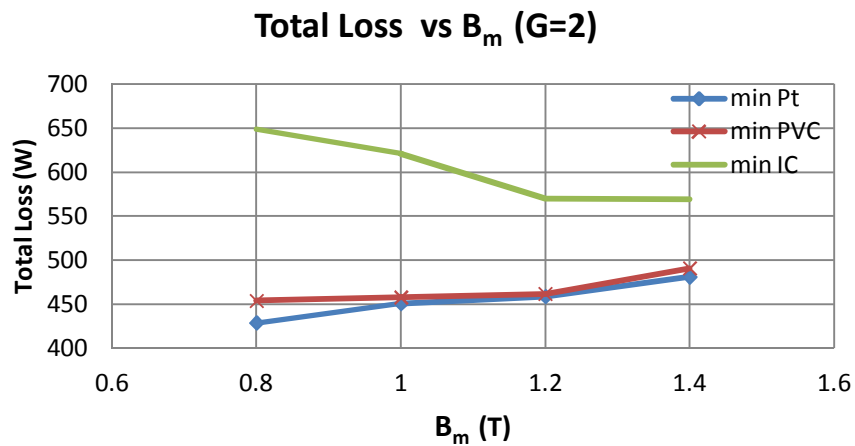


Figure 3.20 Variations in total loss against  $B_m$  for three design criteria ( $G=2$ )

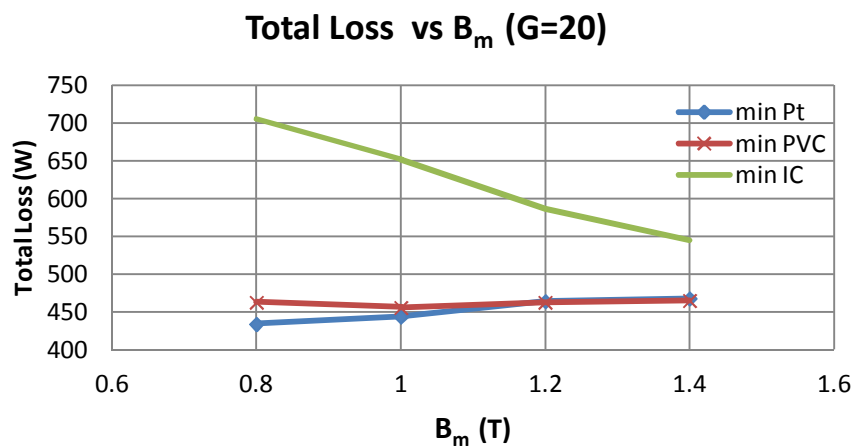


Figure 3.21 Variations in total loss against  $B_m$  for three design criteria ( $G=20$ )

From these figures following conclusions can be drawn;

- When the same reactor is designed according to min  $P_t$  design objective, minimum reactor loss is obtained. Total loss of this reactor is much lower

than total loss of the same reactor designed according to min IC design objective.

- The reactor designed according to min  $P_t$  criterion has the minimum total loss as expected. In a similar way, as illustrated in Figs.3.22 and 3.23, the reactor designed according to min PVC criterion has the minimum PVC as expected.

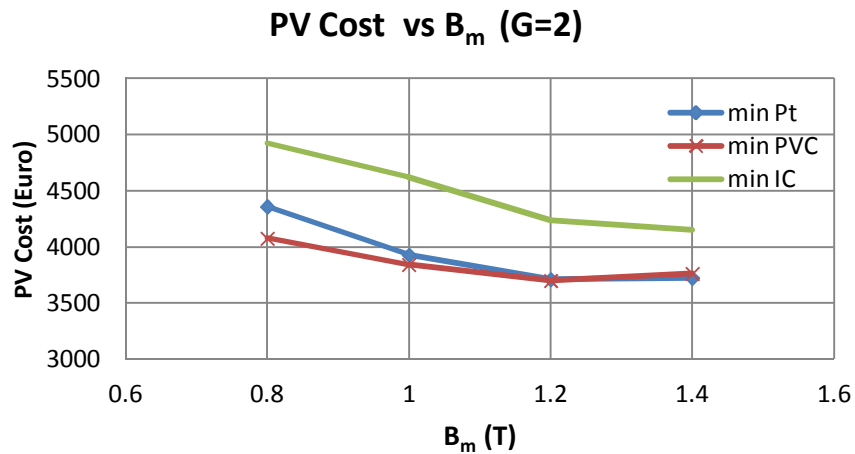


Figure 3.22 Variations in present value cost against  $B_m$  for three design criteria (G=2)

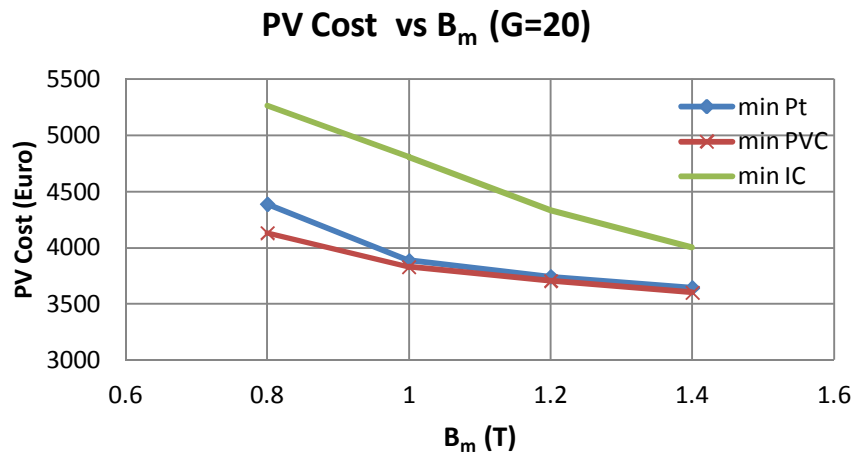


Figure 3.23 Variations in present value cost against  $B_m$  for three design criteria (G=20)

- Min  $P_t$  and min PVC design criteria give nearly the same results.
- Having G=2 and G=20 air-gaps in the magnetic core of the same reactor give nearly the same results.

- The flux density range from  $B_m = 0.8$  to  $1.2$  T yield nearly the same total reactor loss when the same reactor is designed according to min  $P_t$  or min PVC design objective. However, in the flux density range from  $B_m = 0.8$  to  $1.0$  T, PVC is higher than that of  $B_m$  range from  $1.0$  to  $1.2$  T. Therefore, for the core material M330-35 AP,  $B_m = 1.1$  T is chosen as the optimum value and will be used as the design value of the flux density in Chapter 4.
- In view of the above considerations and since several discretely distributed air-gaps for the same reactor gives more uniform flux density distribution in the reactor core as proven in subsections 3.1, 3.2 and 3.3, a practical approach to the reactor design in Chapter 4 will be developed for shunt reactors having several discretely distributed air-gaps.

In view of the above findings, it is recommended in this research work that, shunt reactors with several discretely distributed air-gaps should be designed according to min  $P_t$  or min PVC design objective. On this occasion, the graphical constructions for percentage leakage inductance, which are obtained according to min PVC design criterion and given in Chapter 4, should be used as an inevitable tool for the practical shunt reactor design approach.

### **3.6 Effects of Leakage Inductance Percentage on Reactor Cost and Losses**

The leakage flux component and hence the percentage leakage inductance depend on the shape and dimensions of the magnetic core, winding arrangement and its number of series turns and the number of discretely distributed air-gaps. In most of the industry applications, shunt reactors with low leakage flux component are more desirable. This is because, if the leakage flux component is significant and scattered in a wider area around the reactor structure, part of these leakage flux lines may close their paths through iron based materials existing around the shunt reactor thus causing additional power dissipation in the form of eddy-current losses and affecting the self inductance of the shunt reactor. Especially for shunt reactors placed into oil filled metallic tanks, special attention should be paid to leakage flux component. High leakage flux in natural air cooled reactors requires larger clearances around the reactor. On the other hand, higher percentage leakage reactance reduces the volume

and hence the initial cost of the shunt reactor and also may reduce the present value cost as will be illustrated in this subsection.

It should be noted that having several discretely distributed gaps in the core, effectively reduces the leakage flux component as proven previously in Chapter 2. Therefore, in this subsection the effects of percentage leakage inductance will be investigated for 1.1 kV, 28 mH shunt reactor with two air-gaps ( $G=2$ ). The FEA aided reactor design is carried out according to min PVC design objective for two different values of leakage inductance (5% and 15%). The variations in initial cost, total reactor loss and PVC against  $B_m$  are given respectively in Figs.3.24, 3.25 and 3.26 for the two different values of percentage leakage inductance.

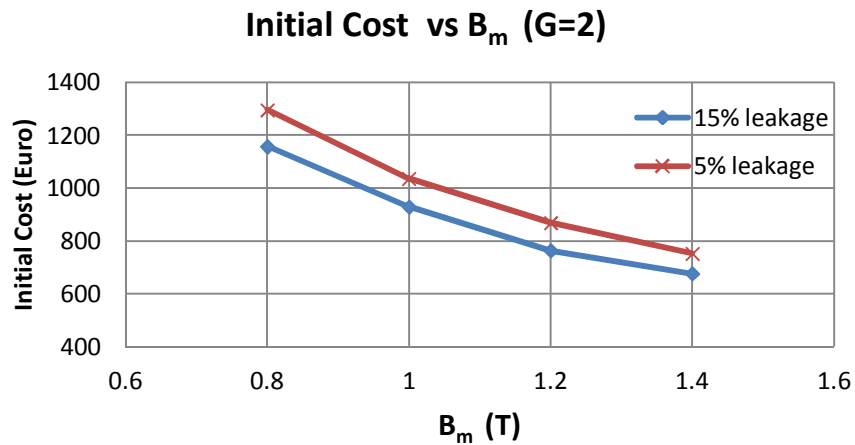


Figure 3.24 Variations in Initial Cost against  $B_m$  for 5% and 15% leakage inductance ( $G=2$ )

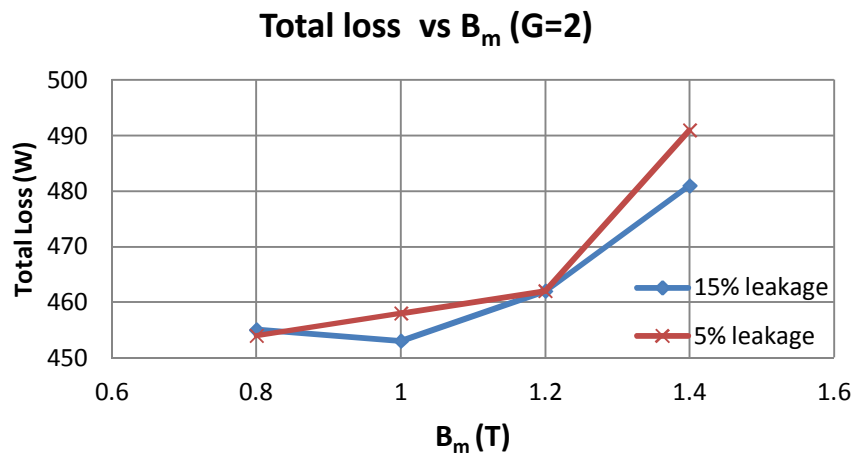


Figure 3.25 Variations in Total Loss against  $B_m$  for 5% and 15% leakage inductance ( $G=2$ )

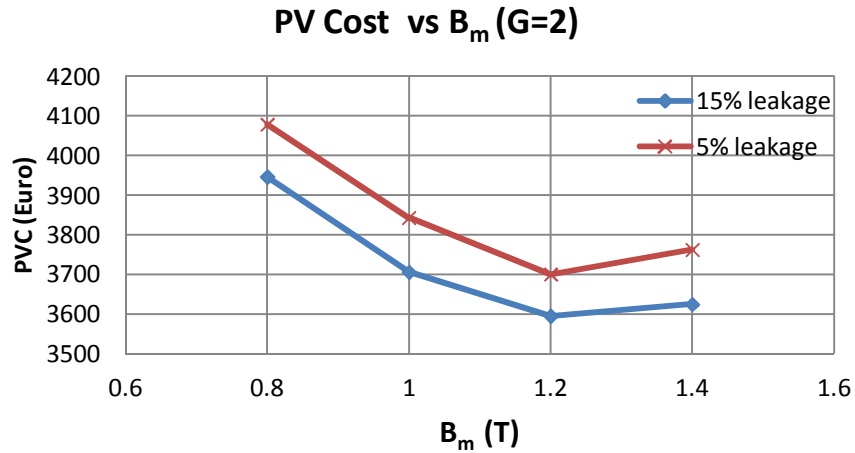


Figure 3.26 Variations in Present Value Cost against B<sub>m</sub> for 5% and 15% leakage inductance (G=2)

As can be observed from these figures higher leakage reactance for the same reactor makes marginal contributions in reducing initial cost, total reactor loss and present value cost. Core dimensions and number of series turns are given in Table 3.5 for comparison purpose.

Table 3.5 Core dimensions of the optimized shunt reactor for 5% and 15% leakage inductance (G=2)

	5% leakage inductance				15% leakage inductance			
	0.8	1.0	1.2	1.4	0.8	1.0	1.2	1.4
B <sub>m</sub> (T)	0.8	1.0	1.2	1.4	0.8	1.0	1.2	1.4
N (turns)	138	140	140	148	146	146	144	150
A (mm <sup>2</sup> )	23861	19084	15910	13621	21342	17072	14344	12607
t (mm)	0.4	0.4	0.4	0.4	0.4	0.4	0.4	0.4
l <sub>g</sub> (mm)	25.4	20.3	16.9	14.5	25.4	20.3	15.8	13.5
w (mm)	116.1	103.8	94.8	87.7	109.8	98.2	90	84.4
d (mm)	197.3	176.5	161.1	149.1	186.6	166.9	153	143.4
L <sub>s</sub> (mH)	28.13	28.75	28.65	28.39	28.46	28.16	27.49	27.45

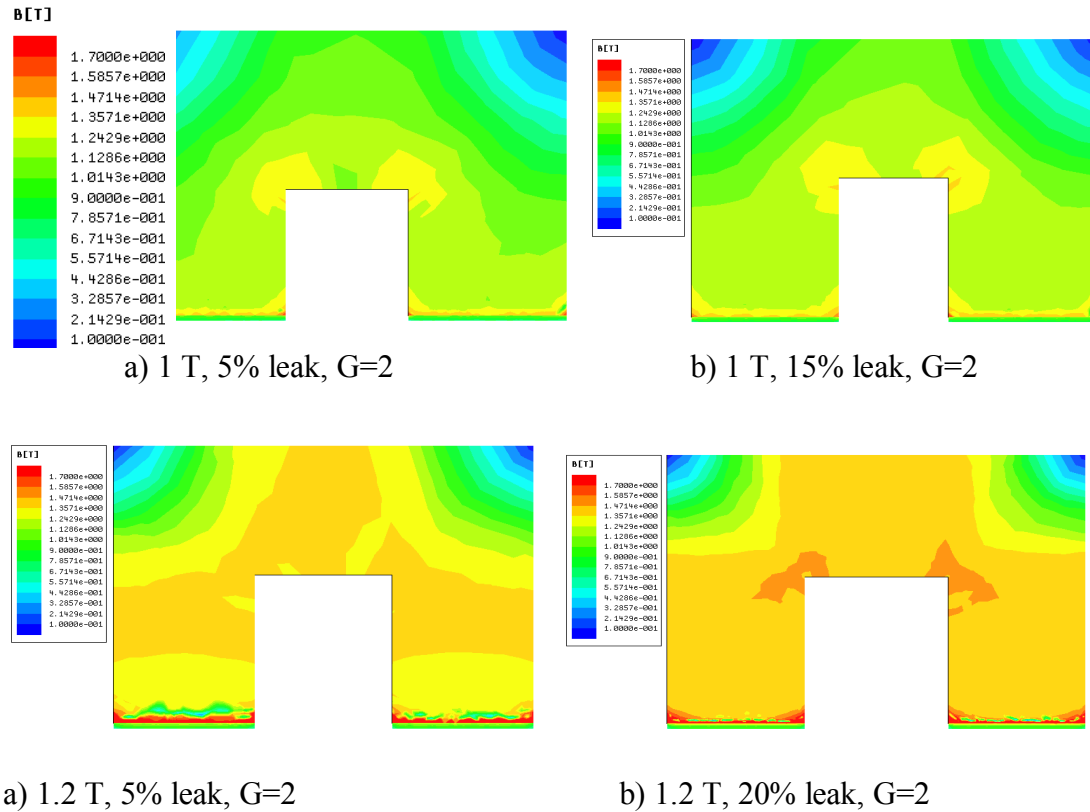


Figure 3.27 Flux density distributions in the core of the reactors designed for different leakage inductance percentages (G=2)

In order to investigate the effects of percentage leakage inductance on flux density distribution on the core, the flux density plots for 1.0 and 1.2 T are given in Fig.3.27. It is seen from these plots that the shunt reactor having a low percentage leakage inductance has better flux density distribution. In view of the above considerations and findings, it is therefore recommended in this research work that the percentage leakage inductance in the optimum shunt reactor design should be kept at a reasonably low value, if possible.

### 3.7 Discussions

In this chapter, a single-phase shunt reactor with pre-specified technical specifications are designed according to a) min IC, b) min  $P_t$ , c) min PVC design objectives by the aid of FEA. The optimized designs are repeated for G=2 and G=20 air-gaps. Since a clear-cut analytical expression for the calculation of percentage



leakage inductance of shunt reactors is not available in the literature, FEA is an inevitable part of the design procedure. The results of the design work presented in this chapter show that;

- Reactor cores with several discretely distributed air-gaps yield more uniform flux density distribution in the core in comparison with the equivalent core having only one or two air-gap portions.
- The optimum value of time maximum (peak) flux density in the core is found to be  $B_m = 1.1 \text{ T}$ .
- Min IC design criterion is beneficial only for the reactor manufacturers. Because, the resulting reactor costs more to the user in the long-term (economic life of the reactor).
- Min  $P_t$  design criterion minimizes reactor losses and hence the operating cost of the reactor during its life time.
- Min PVC design criterion minimizes the sum of initial cost and operating cost of the shunt reactor. Although this criterion gives nearly the same economic results with the min  $P_t$  design criterion, it is considered to be the best approach to the reactor design from the viewpoint of macroeconomics and user benefits.

Therefore, the practical approach to reactor design which will be described in Chapter 4 is based on min PVC design objective.

## CHAPTER 4

### A PRACTICAL APPROACH TO THE REACTOR DESIGN

#### 4.1 Introduction

The objective of this chapter is to develop a practical approach to the design of shunt reactors with discretely distributed air-gaps. Graphical constructions for percentage leakage inductance, which have been obtained according to min PVC design criterion (described in Chapter 3) by using FEA optimizations, has been defined for the practical shunt reactor design approach.

#### 4.2 Design Procedure and Assumptions

##### 4.2.1 Definition of the Optimized Reactor

Design procedure is based on the electrical equivalent circuit of the reactor shown in Fig.4.1. Detailed derivation of this electrical equivalent circuit is already given in Chapter 2. All parameters of this equivalent circuit can be calculated analytically except the leakage inductance,  $L_l$ .

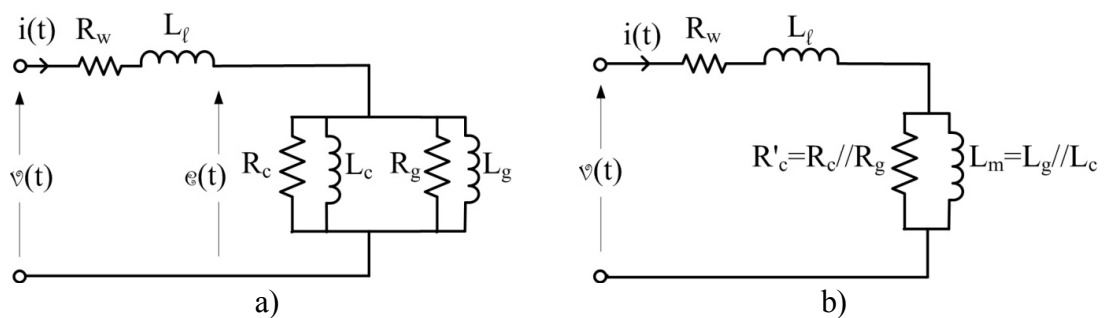


Figure 4.1 Equivalent circuit of a single-phase shunt reactor with distributed gaps in its laminated core

The shunt reactor that will be designed can be specified by either of the followings:

- 1) Self inductance,  $L_s$  in Henry, rated current,  $I_r$  in Amps, frequency,  $f$  in Hz, time maximum value of flux density in the core,  $B_m$  in  $\text{Wb/m}^2$  and temperature rise above ambient,  $\Delta T$  in K.
- 2) Rated power,  $Q_r$  in VAR, operating voltage,  $V_r$  in Volts, frequency,  $f$  in Hz, time maximum value of flux density in the core,  $B_m$  in  $\text{Wb/m}^2$  and temperature rise above ambient,  $\Delta T$  in K.

The relationships between the two sets of shunt reactor specifications are as given in (4.1) and (4.2).

$$V_r = w L_s I_r \quad (4.1)$$

$$Q_r = w L_s I_r^2 \quad (4.2)$$

where,  $w=2\pi f$  is the rated angular frequency of the grid in electrical rad/s.

An optimum shunt reactor can be designed by using the Practical Approach that will be described in this chapter. By optimum shunt reactor it is meant that;

$$\begin{aligned} &\min \text{PVC}(N, J, t) \\ &N_1 \leq N \leq N_{\max} \\ &J_1 \leq J \leq J_{\max} \\ &t_1 \leq t \leq t_{\max} \\ &\text{subjected to } \Delta T(N, J, t) = 60 \pm 2 \text{ K} \\ &\text{subjected to } \Delta T(N, J, t) = 80 \pm 2 \text{ K} \\ &\text{subjected to } \Delta T(N, J, t) = 100 \pm 2 \text{ K} \end{aligned} \quad (4.3)$$

where; PVC is the Present Value Cost of the reactor.

In this work, a Practical Design Approach has been developed to minimize the Present Value Cost of the shunt reactor. The PVC of the shunt reactor (as described in Chapter 3) is the sum of the Initial Cost (IC) and the present value of the Operating Cost (OC) of the reactor due to the reactor losses throughout its life cycle

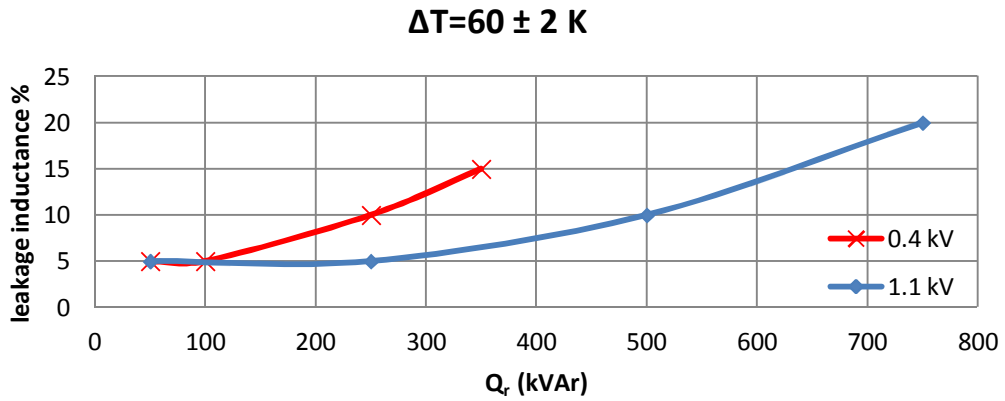
(in Euros). Present value of the OC can be defined as in equation (4.4) [15, 75]. IEEE Std. C57.120-1991 Appendix-B illustrates an example of predicting the future energy costs of transformers by using present value definitions [76].

$$PV = \frac{(1+i)^n - 1}{i(1+i)^n} OC \quad (4.4)$$

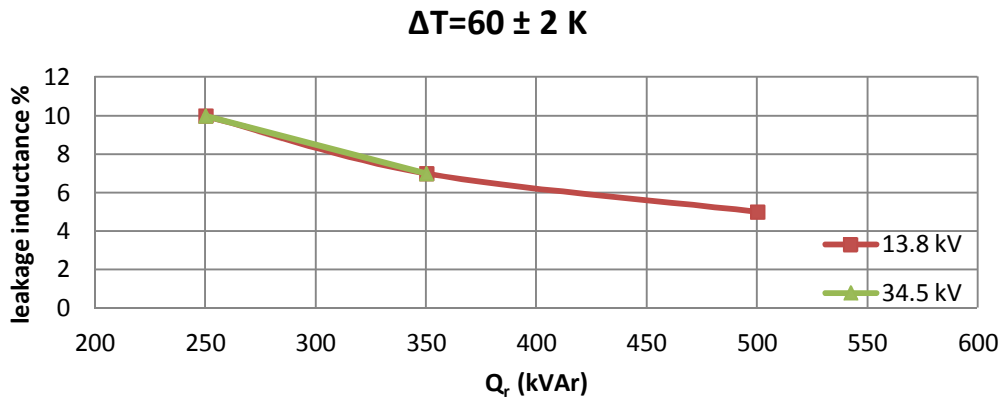
where;  $i$  is the discount factor (assumed to be 10%) ,  $n$  = life cycle of the reactor, in this case  $n=20$  years as an assumption. The variations in initial cost and present value cost of the reactors which met design objectives are given in Appendix-C.

#### **4.2.2 Graphical Tools Required For Practical Design Approach**

Since only  $L_1$  in the electrical equivalent circuit of the shunt reactor cannot be expressed analytically, a few hundreds of optimization study have been carried out by the aid of FEM analysis (Maxwell 3D) as described in Chapter 3 according to min PVC design objective. By this way, percentage value of  $L_1$  with respect to hundred percent self inductance for various technical specifications of the reactor ( $L_s$ ,  $I_r$ ,  $f$ ,  $B_m$ ,  $\Delta T$  or  $Q_r$ ,  $V_r$ ,  $f$ ,  $B_m$ ,  $\Delta T$ ) have been obtained for use in Practical Design Approach. Percentage leakage inductance is defined as the ratio of leakage inductance in Henry to self inductance in Henry and then multiplied by hundred. The resulting percentage leakage inductance variations against kVAr rating of the reactor under design and in terms of standard line-to-line operating voltages and three different temperature rise values above the ambient are given in Figs.4.2-4.8. In obtaining these percentage leakage inductance characteristics, reasonable variation ranges of installed reactor capacity ( $Q_r$ ) are assumed by considering standard kVA ratings of power and distribution transformers. The most common standard transformer ratings with low voltage and medium voltage secondary windings are given in Appendix-D. Further design details of the optimum reactors, such as; variations in number of turns foil thickness, current density, PVC, PVC/kVAr and IC against power rating of the reactors are given in Appendix-C.

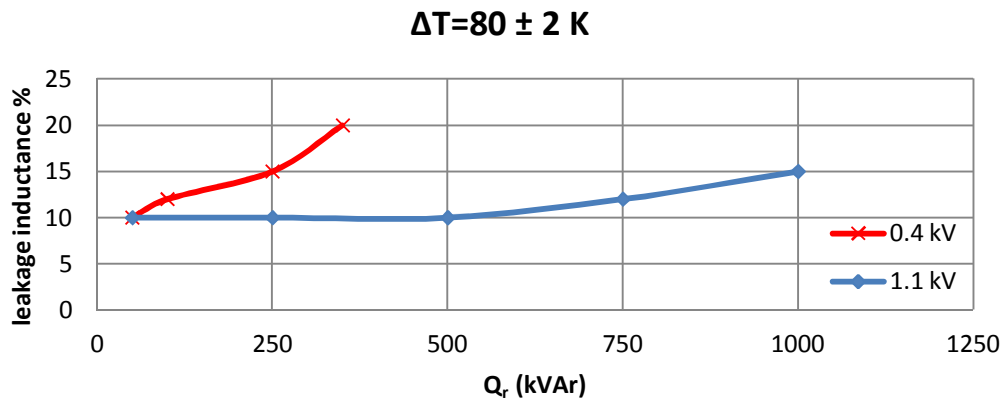


a) Leakage inductance percentage variations against kVAr rating of the reactor for 60 K temperature rise above the ambient (low voltage)



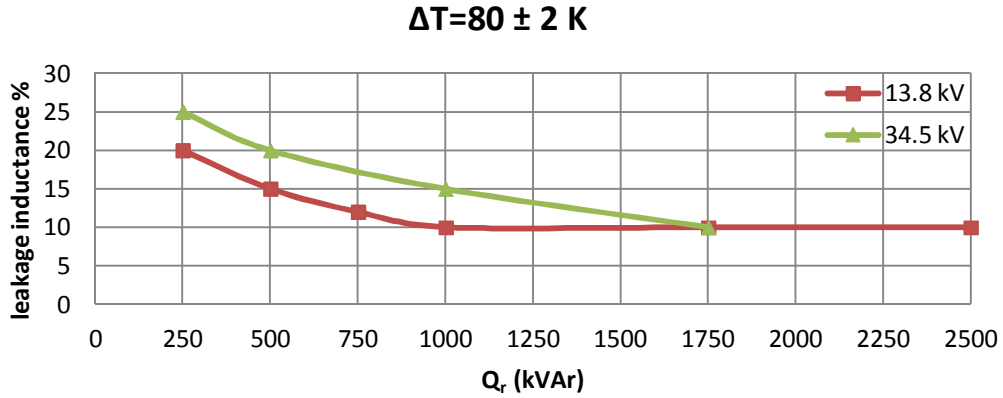
b) Leakage inductance percentage variations against kVAr rating of the reactor for 60 K temperature rise above the ambient (medium voltage)

Figure 4.2 Leakage inductance percentage variations against kVAr rating of the reactor for 60 K temperature rise above the ambient



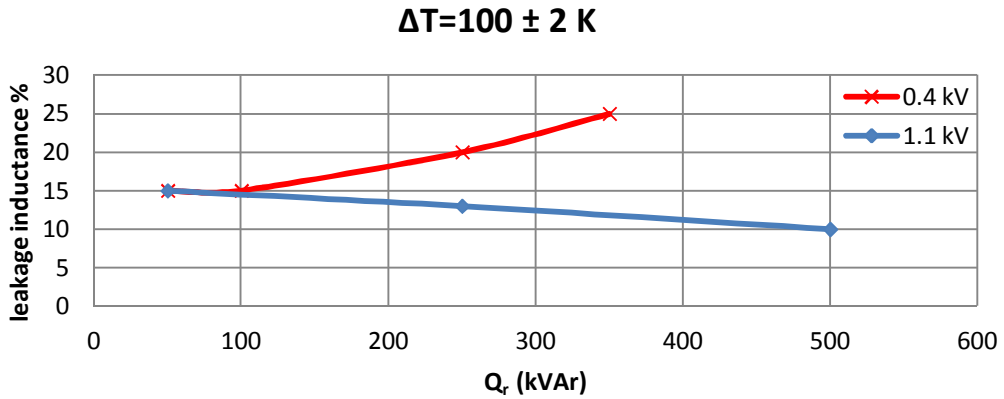
a) Leakage inductance percentage variations against kVAr rating of the reactor for 80 K temperature rise above the ambient (low voltage)

Figure 4.3 Leakage inductance percentage variations against kVAr rating of the reactor for 80 K temperature rise above the ambient

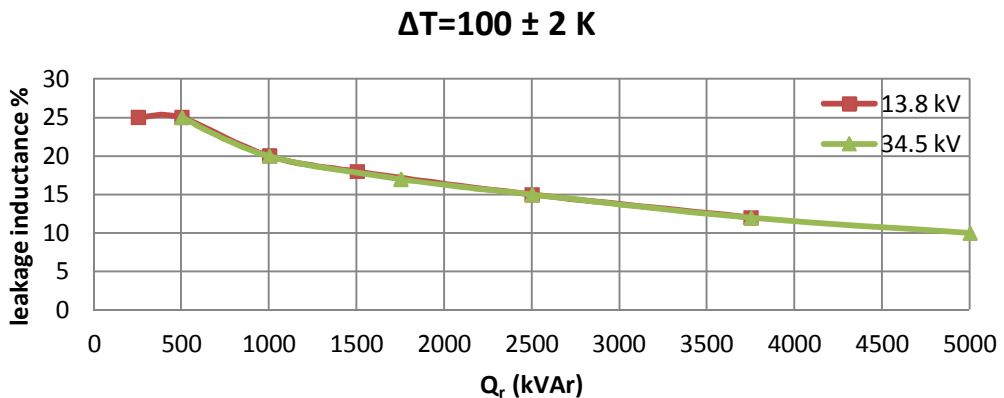


b) Leakage inductance percentage variations against kVAr rating of the reactor for 80 K temperature rise above the ambient (medium voltage)

Figure 4.3 (Cont'd) Leakage inductance percentage variations against kVAr rating of the reactor for 80 K temperature rise above the ambient



a) Leakage inductance percentage variations against kVAr rating of the reactor for 100 K temperature rise above the ambient (low voltage)



b) Leakage inductance percentage variations against kVAr rating of the reactor for 100 K temperature rise above the ambient (medium voltage)

Figure 4.4 Leakage inductance percentage variations against kVAr rating of the reactor for 100 K temperature rise above the ambient

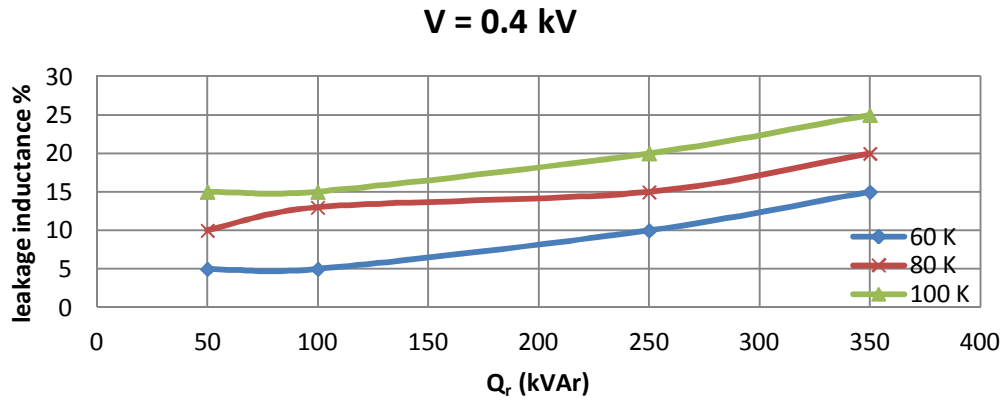


Figure 4.5 Leakage inductance percentage variations against kVAr rating of the reactor for 0.4 kV operating voltage

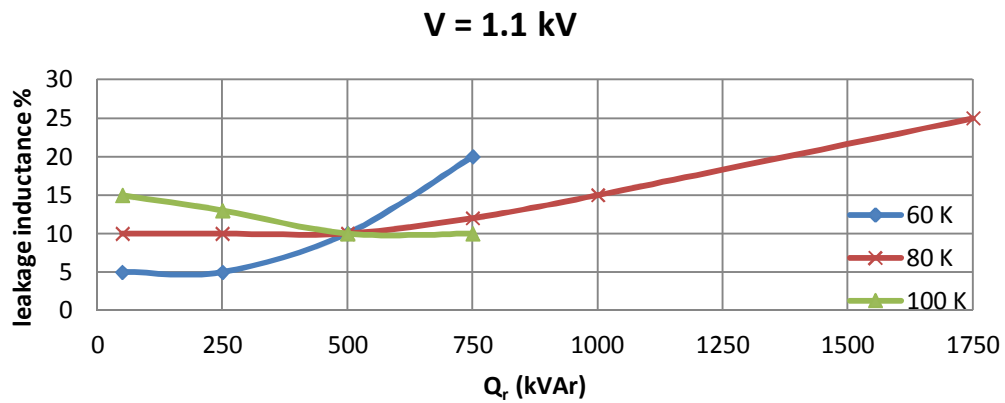


Figure 4.6 Leakage inductance percentage variations against kVAr rating of the reactor for 1.1 kV operating voltage

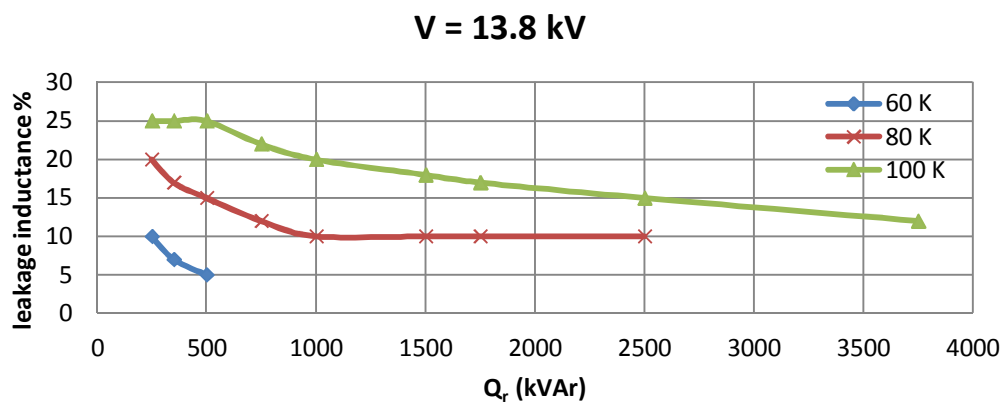


Figure 4.7 Leakage inductance percentage variations against kVAr rating of the reactor for 13.8 kV operating voltage

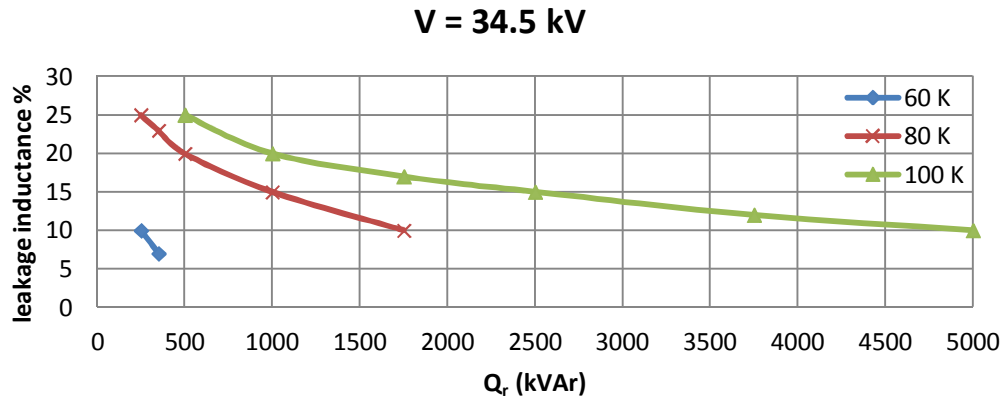


Figure 4.8 Leakage inductance percentage variations against kVAr rating of the reactor for 34.5 kV operating voltage

These characteristics have been obtained by using the Finite Element Analysis based design method described in Chapter 3 under the following assumptions;

- The core material is M330-35 AP non-oriented electrical steel (Appendix A);
- Winding material is aluminum foil;
- The optimum operating peak flux density is  $B_m = 1.1$  T. It is proven in Chapter 3 that 1.1 T is the optimum peak flux density for the core material chosen and the core structure with several discretely distributed air-gaps;
- The design objective is min PVC.

In summary, in designing a shunt reactor with several discretely distributed air-gaps, the previously constructed characteristics in Figs. 4.2-4.8 are to be used inevitably. For a different core material and/or a different  $B_m$  value a new family of percentage leakage inductance characteristics are obviously needed.

### 4.3 Proposed Practical Design Approach

After specifying the technical specs of the shunt reactor that will be designed, the designer will read the percent value of the leakage inductance on the vertical percentage leakage inductance axis of the appropriate graphical construction in one of the Figs. 4.2-4.8.



After determining percentage leakage inductance of the target reactor from one of the previously developed graphical constructions following assumptions are used;

- a)  $R_w$  in Fig.4.1 is much lower than  $x_l = \omega.L_l$  and in a similar way  $R'_c$  in Fig.4.1 is much larger than  $x_m = \omega.L_m$ , where,  $\omega=2\pi f$  is the rated angular frequency of the grid in electrical rad/s. Therefore, their effects can be neglected at the initial calculation steps of the Practical Design Approach.
- b) As proven in Chapter 2,  $L_c$  is much larger than  $L_g$  in Fig.4.1 for shunt reactors with several discretely distributed air-gaps. Therefore,  $L_c$  is ignored throughout the practical design procedure.

These assumptions lead to the simplified electrical equivalent circuit in Fig.4.9. All design steps except those of winding loss, core and gap loss calculations are based on the simplified circuit in Fig.4.9.

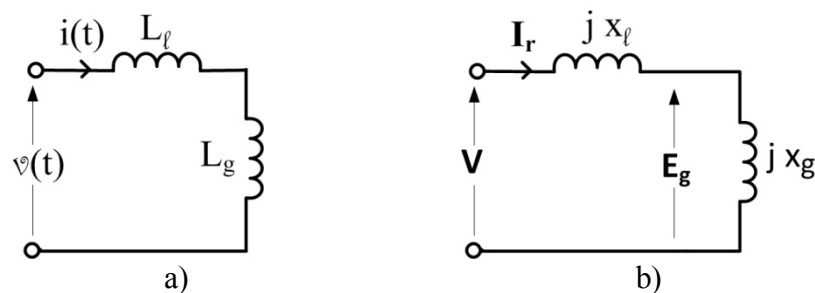


Figure 4.9 Simplified electrical equivalent circuit of a single-phase shunt reactor with several discretely distributed air-gaps.

The design work according to the technical specs of the reactor is then carried out by making several iterations (further information on iteration results are given in Appendix-C) for different number of series turns of the coil ( $20 \leq N \leq 2500$  Turns), current density in the aluminum foil conductor ( $1.1 \leq J \leq 2$  A/mm<sup>2</sup>) and thickness of the foil conductor ( $0.1 \leq t \leq 1$  mm) until minimum PVC (N, J, t) objective is met. These iterations can be achieved on a personal computer by using some package programs such as the computational tools of Matlab in a few hours time including the development of the necessary Matlab codes. The Practical Design Approach recommended in this chapter can also be carried out by hand calculations. For this case the researcher or the engineer who is going to design his / her shunt reactor will

spend a few days time. It is seen that this Practical Design Approach eliminates entirely the need to a proper FEA package program and to a powerful digital computer.

After neglecting winding resistance  $R_w$  in Fig.1a and all voltage and current harmonics, the rms value of the induced emf  $E$  at power frequency (50/60 Hz) that will appear across the exciting branch can be expressed as in equation (4.5).

$$E \cong V - j I_r x_l \quad (4.5)$$

where;  $x_l = 2.\pi.f.L_l$  is the leakage reactance of the shunt reactor,  $I_r$  is the rms value of the rated reactor current.

Alternatively,  $E$  is the potential drop on the gap reactance  $X_g$  in Fig.4.9b owing to reactor current,  $I_r$ , i.e.,

$$E = E_g \cong I_r X_g \quad (4.6)$$

$E$  is given by (4.7),  $f=50$  or  $60$  Hz and  $B_m$  is pre-specified by the designer.

$$E = 4.44 N f A B_m \quad (4.7)$$

Therefore, in the initial iteration phase of the Practical Reactor Design Approach, effective cross-sectional area of the core,  $A$ , will be calculated from (4.7) for different number of turns,  $N$ , of the reactor.

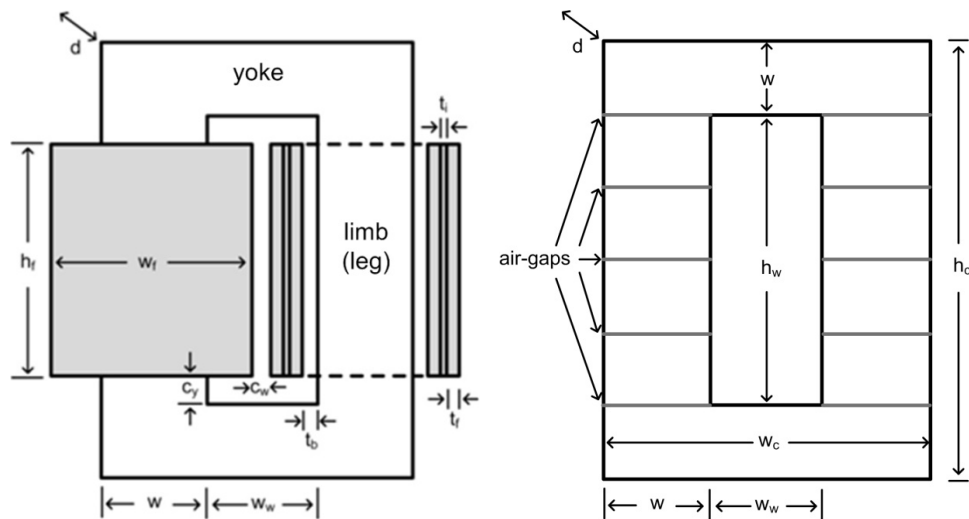


Figure 4.10 Illustration of core and winding dimensions

The shape and dimensions of the shunt reactor under design are as given in Fig.4.10.

The explanations of the symbols used in Fig.4.10 are as follows;

$c_y$	clearance between winding and yoke
$c_w$	clearance between two windings
$d$	depth of the core
$h_c$	total height of the core
$h_f$	height of the coil
$h_w$	height of the window
$t_b$	thickness of the tube
$t_f$	thickness of the aluminum foil (each turn)
$t_i$	thickness of the insulation material between each turn
$w$	width of the limb and the yoke
$w_c$	total width of the core
$w_w$	width of the window

The flowchart of the Practical Design Approach recommended in this work is given in Fig.4.11. In the application of the Practical Design Approach, following assumptions are used.

- a) Number of discretely distributed gaps is  $G=40$
- b) Permissible deviation from target inductance is  $\pm 5\%$  [IEC 289 and IEC 60076-6]
- c) Winding loss is calculated from (4.8)

$$P_w = I_r^2 k R_{dc} \quad \text{Watts} \quad (4.8)$$

where,  $I_r$  is the rms value of the rated reactor current,  $k$  is the skin effect factor and  $R_{dc}$  is the dc resistance of the winding.

- d) Power dissipation in the core is calculated from (4.9) which is obtained by fitting the curve to power loss curve provided by the core manufacturer (Appendix-A / ThyssenKrupp).

$$P_c = 1.14 B_m^{1.75} \quad \text{W/kg} \quad (4.9)$$

where,  $B_m$  is the time maximum value of the flux density in the core. Flux density in the core is assumed to be nearly uniform in these calculations owing to the presence of several discretely distributed air-gaps as described in Chapter 2.

- e) Temperature rise,  $\Delta T$  is calculated by the empirical equation given in (4.10) [40].

$$\psi = P_t / A_s \quad (4.10)$$

$$\Delta T = 450 (\psi)^{0.826}$$

where;  $\psi$  is watt density,  $P_t$  is total loss and  $A_s$  is total surface area of the core. 450 and 0.826 are constants for laminated steel cores to calculate the temperature rise.

- f) The clearances, tube thickness and other parameters can be determined from Table 4.1.

Table 4.1 Specifications used in design phase

Voltage Level (kV)	0.4&1.1	13.8	34.5
Clearance to yokes (mm), $c_y$	20	120	200
Clearance between windings (mm), $c_w$	5	25	50
Clearance between tube and winding (mm), $c_{tw}$	0	50	50
Insulation thickness between each turn (mm), $t_i$	0.15	0.3	0.5
Tube thickness (mm), $t_b$	5	10	10

- g) Current density in the core is varied in the range of  $1.1 \leq J \leq 2 \text{ A/mm}^2$  from the field experience.

- h) Thickness of the aluminum foil is varied in the range of  $0.1 \leq t \leq 1$  mm in order to make skin effect negligibly small for aluminum foil conductors at power frequency.
- i) Economic life of the shunt reactor is taken to be 20 years and its utilization is assumed to be 300 days per annum.
- j) Unit price of the electricity is taken to be 0.1 Euro cent per kWh.
- k) The price of the steel is taken to be 2 Euros/kg and the price of the aluminum to be 4.2 Euros/kg (these data have been obtained from manufacturers by the end of February 2012). Fixed manufacturing costs, insulation material cost and profit are also included in the calculation of reactor initial cost.
- l) Unit prices of B-, F- and H-type insulating materials are not discriminated in the design procedure because their prices are varying in a wide range from one manufacturer to another.
- m) In order to decrease the gap-losses, d/w ratio in Fig.4.10 is taken to be 1.7. Cross-sectional area of the yoke is taken to be equal to the limb cross-sectional area of the core.

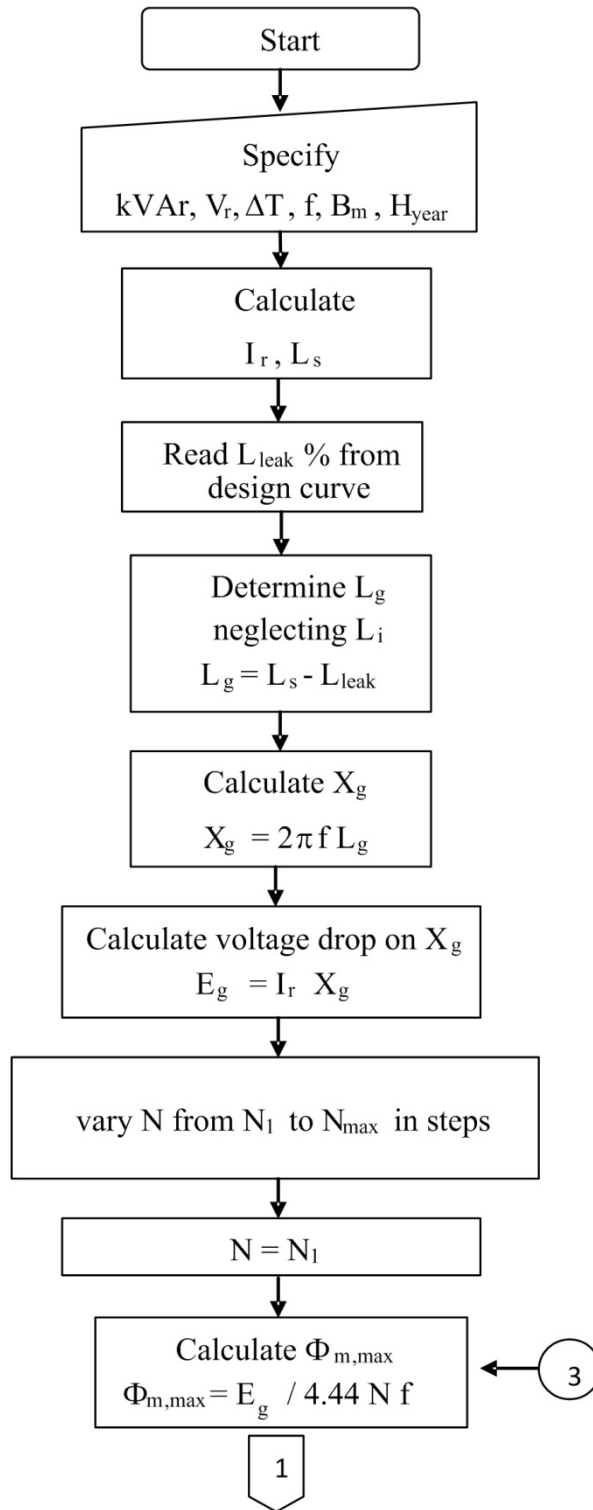


Figure 4.11 Flowchart of the proposed Practical Design Approach

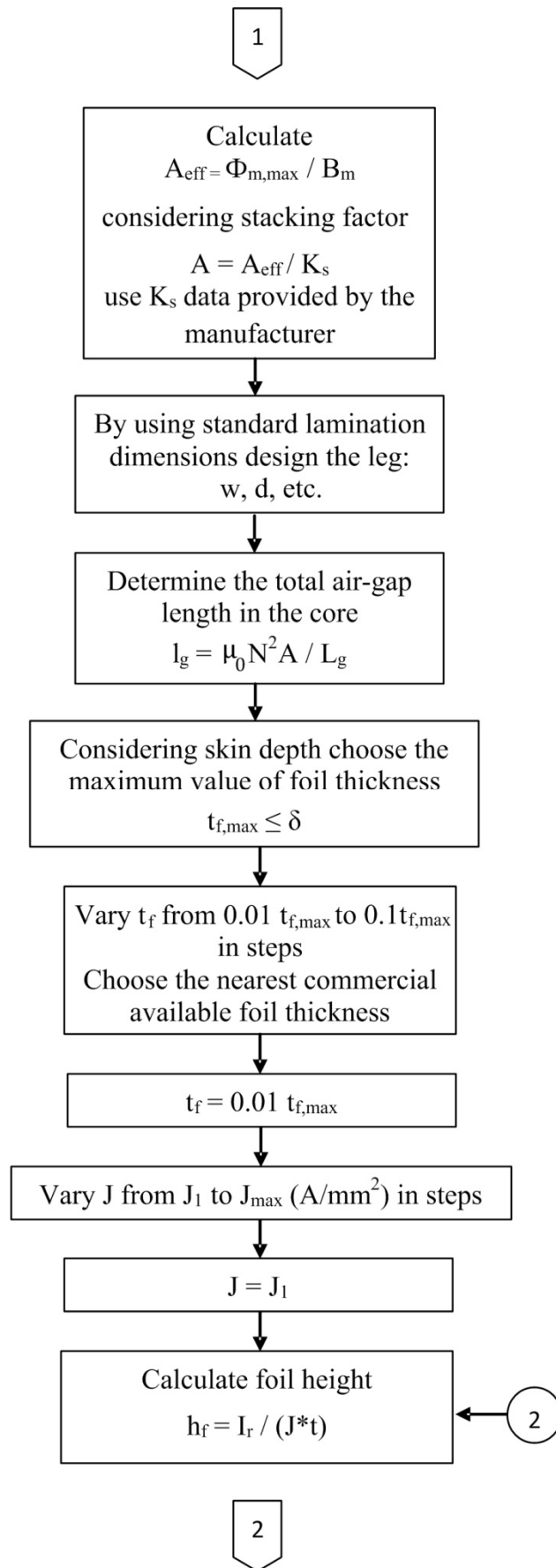


Figure 4.11 (Cont'd) Flowchart of the proposed Practical Design Approach

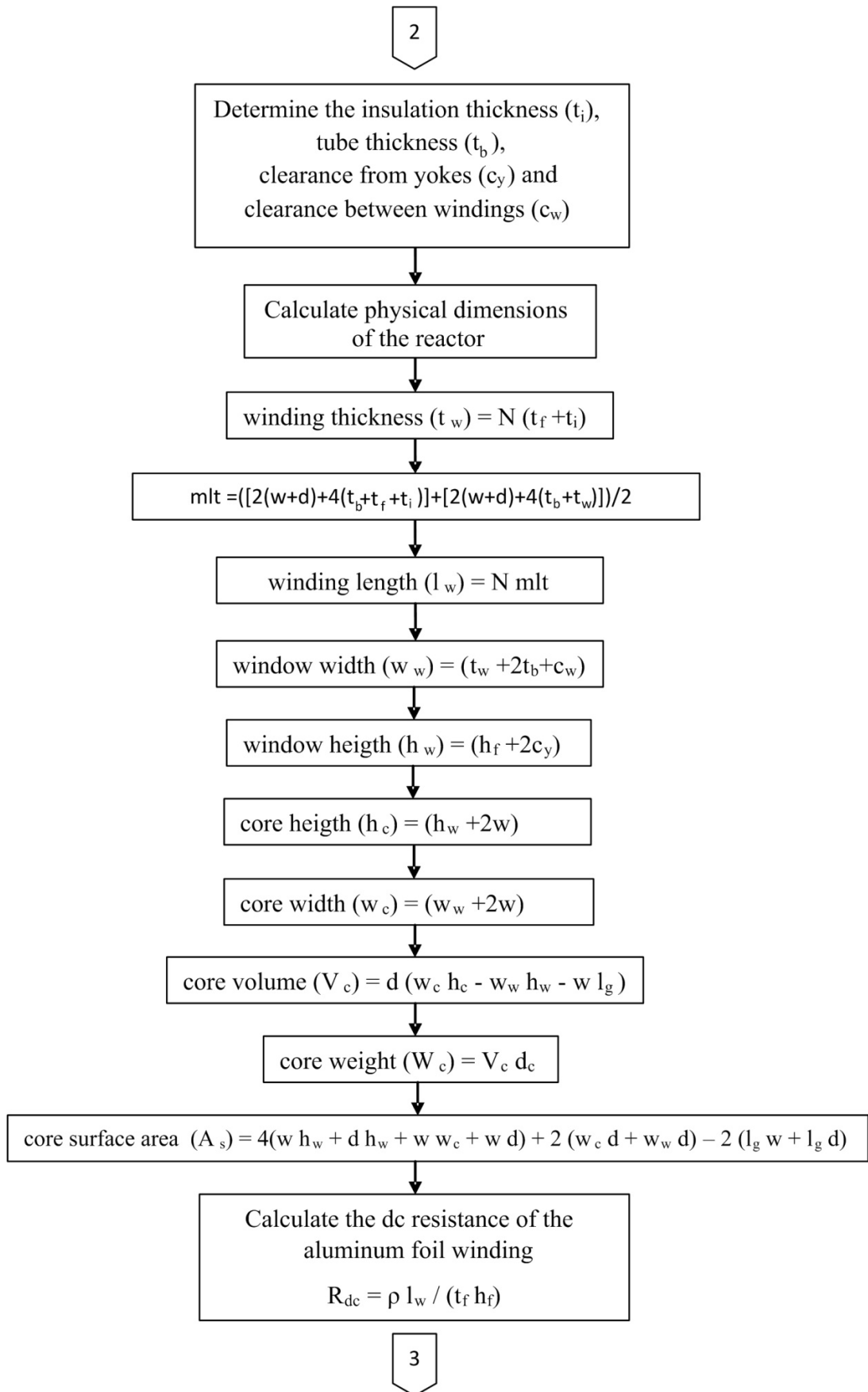


Figure 4.11 (Cont'd) Flowchart of the proposed Practical Design Approach



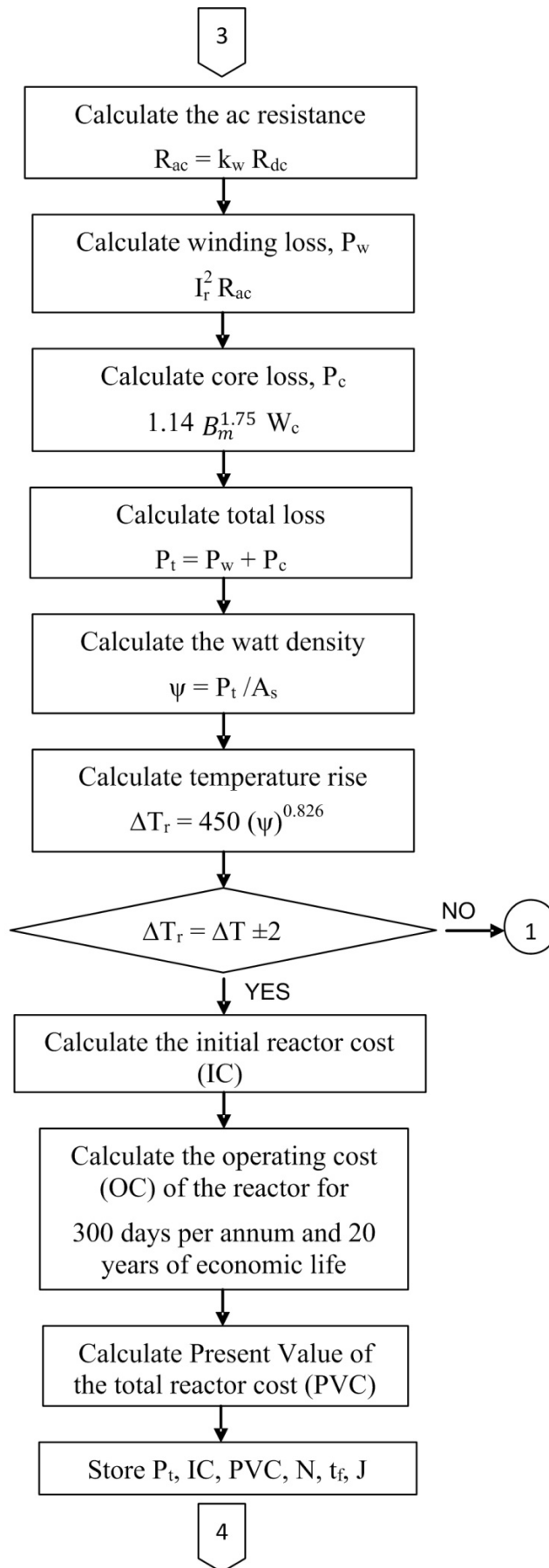


Figure 4.11 (Cont'd) Flowchart of the proposed Practical Design Approach

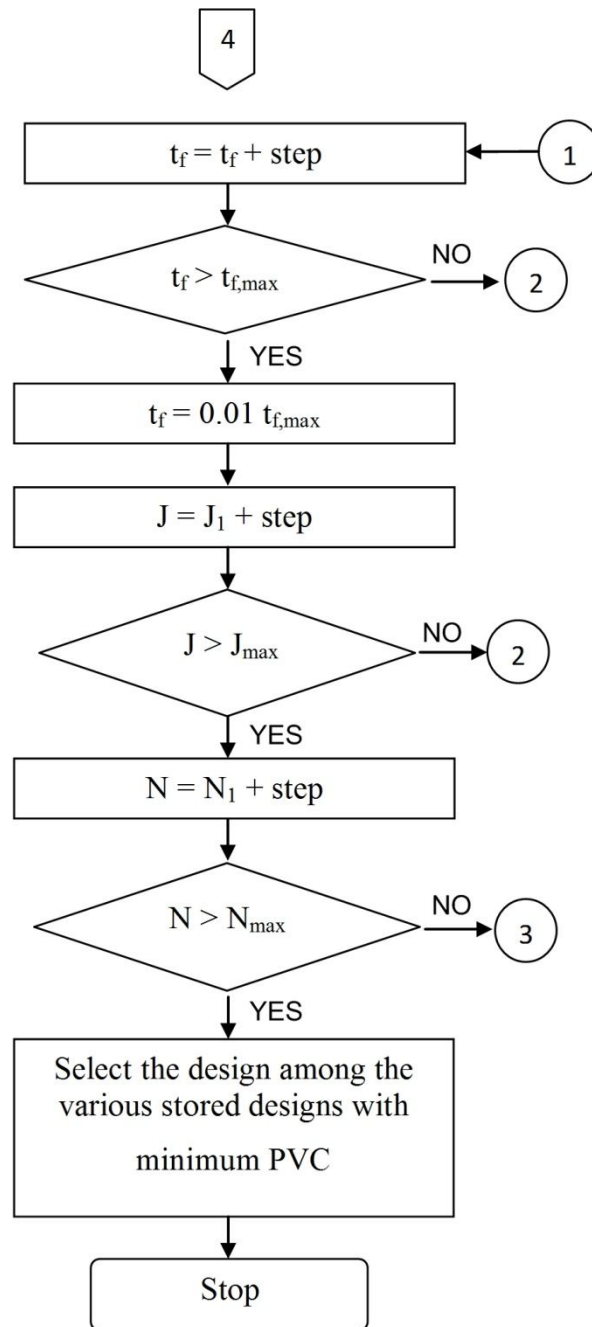


Figure 4.11 (Cont'd) Flowchart of the proposed Practical Design Approach

An alternative method based on energy definition can be used to calculate the reactor dimensions in the design phase. Volume of the air-gap in the core is the ratio of the stored energy to the energy density of the air-gap. By using the gap inductance definition in terms of air-gap volume, for different number of turns, total air-gap of the reactor is obtained. On the other hand, gap volume is the product of the total air-gap length and the cross-sectional area of the air-gap. Once the area of the gap is obtained, reactor dimensions can be calculated. The flowchart of this alternative calculation method is given in Fig.4.12.

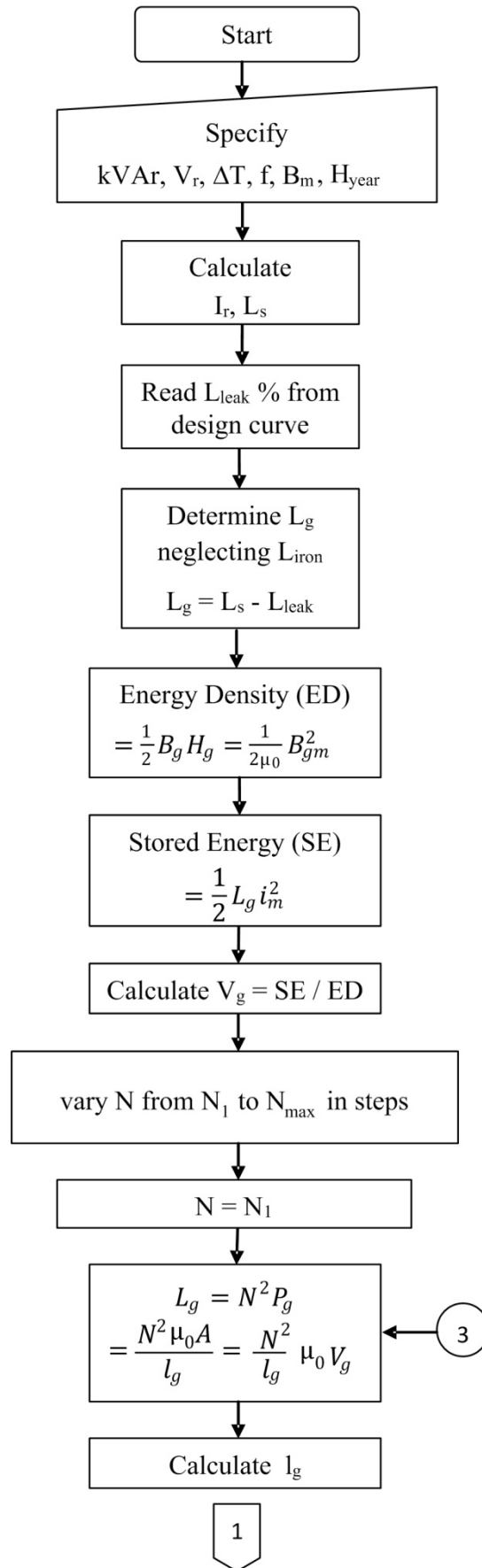


Figure 4.12 Flowchart of the proposed Practical Design Approach by energy method

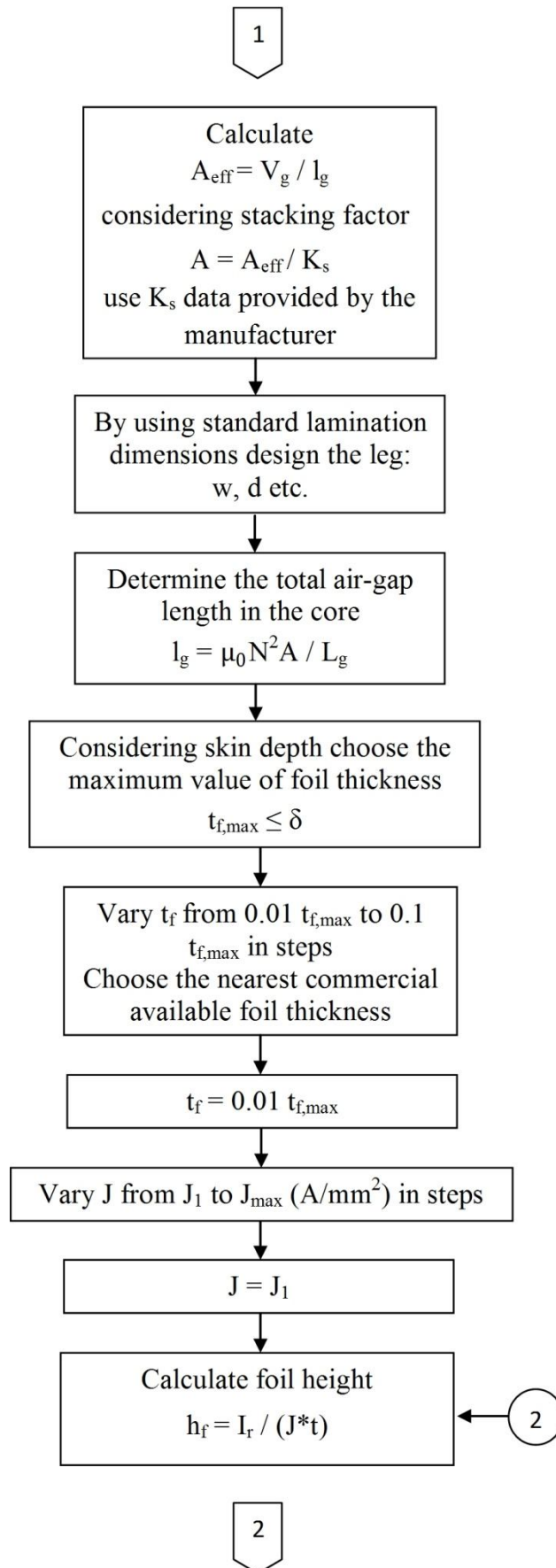


Figure 4.12 (Cont'd) Flowchart of the proposed Practical Design Approach by energy method

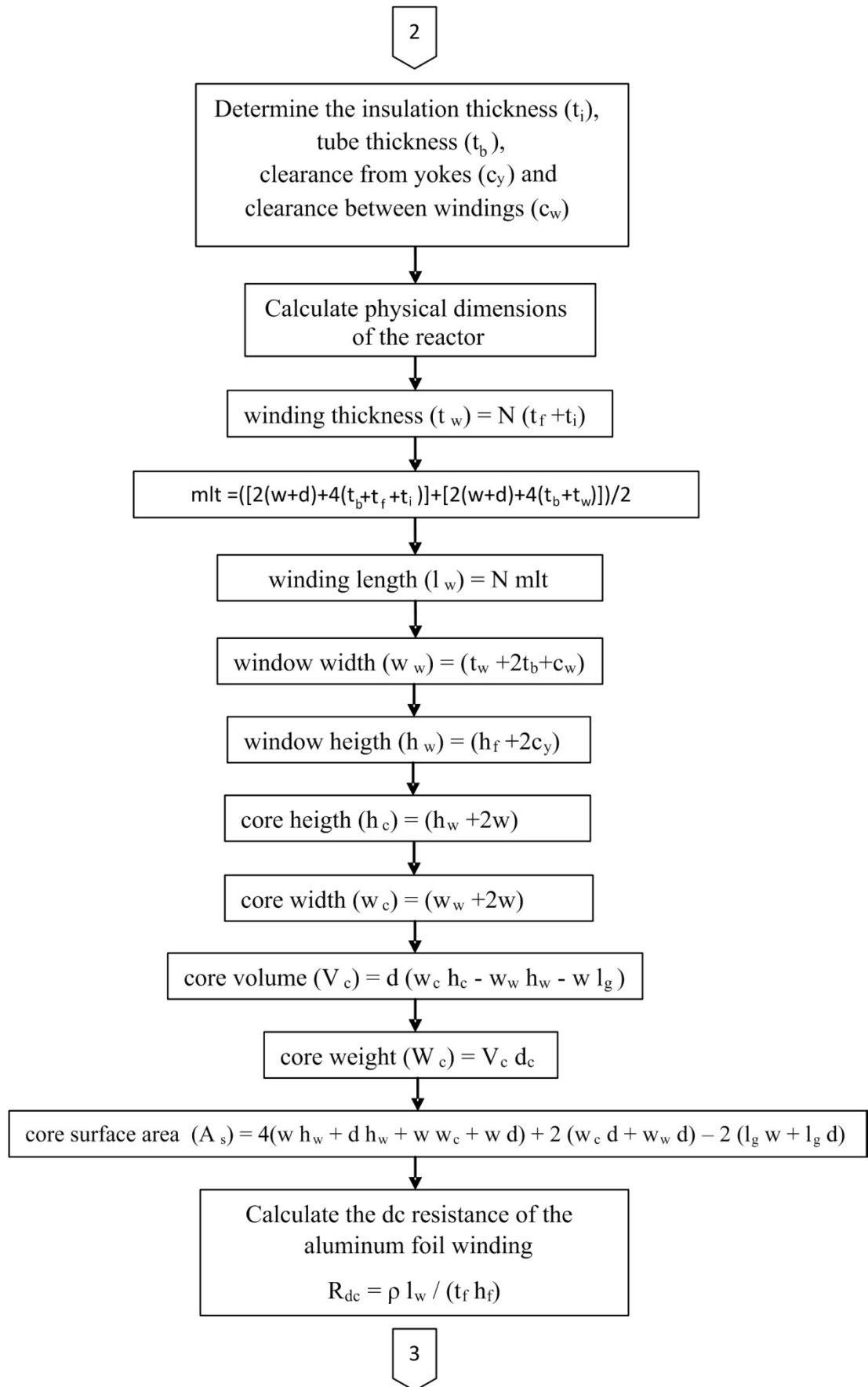


Figure 4.12 (Cont'd) Flowchart of the proposed Practical Design Approach by energy method

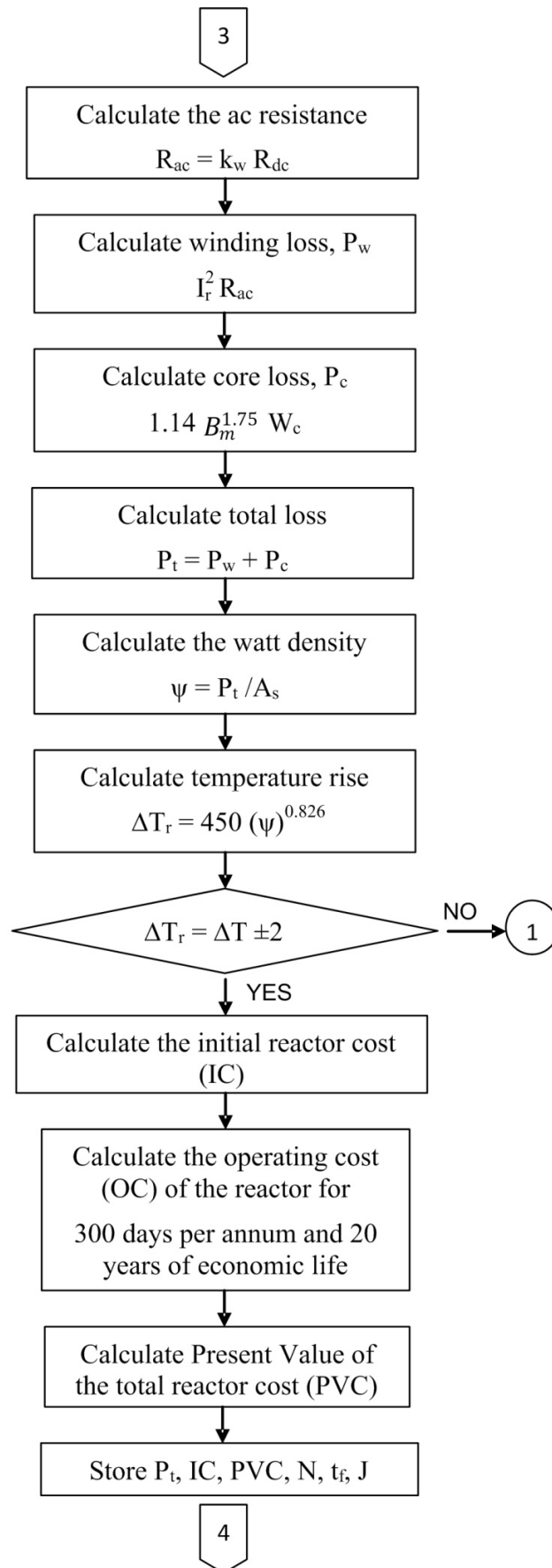


Figure 4.12 (Cont'd) Flowchart of the proposed Practical Design Approach by energy method

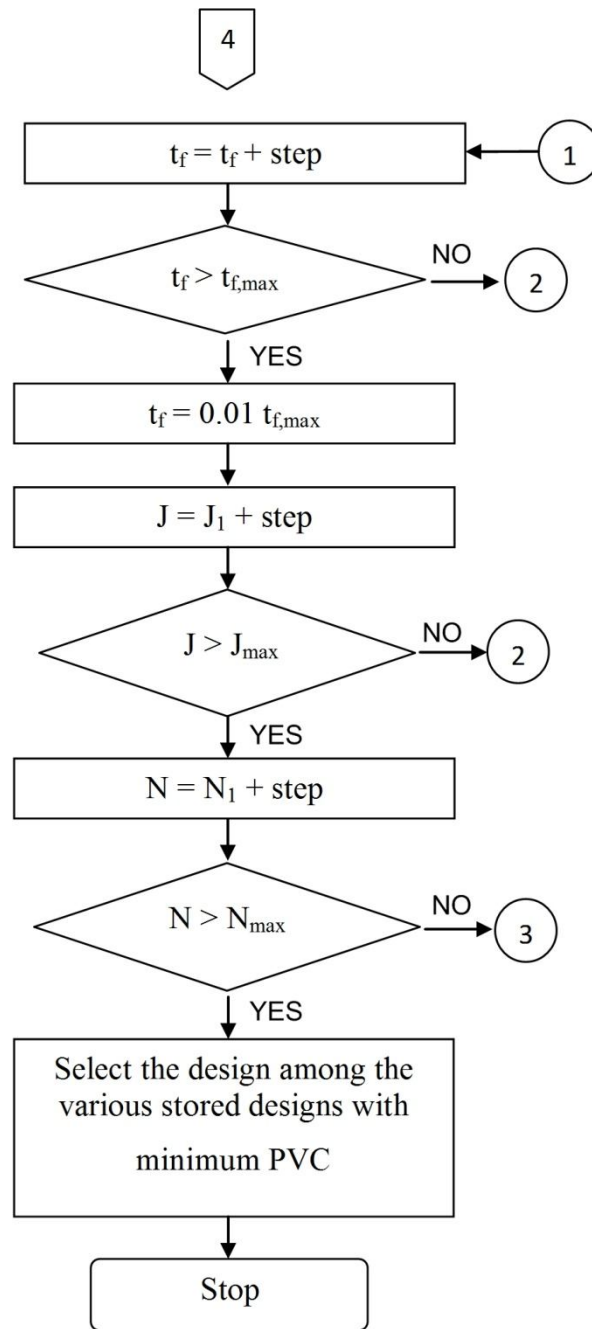


Figure 4.12 (Cont'd) Flowchart of the proposed Practical Design Approach by energy method

#### 4.4 Verification of the Practical Design Approach

The correctness of the reactor designs obtained from the Practical Design Approach will be tested for two different shunt reactors having 40 discretely distributed air-gaps by using FEA tools. These reactors are specified as follows;

Shunt reactor 1: 1-phase to form a 3-phase wye-connected reactor bank, 600-kVAr/phase, 1.1 kV l-to-l and  $\Delta T=60$  K.

Shunt reactor 2: 1-phase to form a 3-phase wye-connected reactor bank, 1500-kVAr/phase, 10 kV l-to-l and  $\Delta T=80$  K.

It is worth to note that, for the first reactor, percentage leakage inductance curve is available (Fig.4.2a) but the associated leakage inductance point appears on the curve fitting part. However, for the second shunt reactor, percentage leakage inductance characteristic for 10 kV operating voltage is not available. Therefore, the percentage leakage inductance of the second reactor should be estimated to be somewhere between 10% and 15% from Fig.4.3b.

First reactor is then designed according to Practical Design Approach. The results are given in the first column of Table 4.2. After calculating core and winding dimensions according to min PVC design criterion, reactor parameters are calculated by FEA tools and performance of the design procedure by Matlab tools. These are also given in the first column of Table 4.2. An examination of these results show that the actual value of percentage leakage inductance is found to be 10.8% in comparison with 14% read on the Fig.4.2a. More important than this, self inductance deviation of the design which is carried out according to the Practical Design Approach is -0.5% of the target self inductance value of 2.14 mH.

For the second shunt reactor, first the reactor is designed according to the Practical Design Approach by considering 10% leakage inductance. Its parameters and performance of the design procedure are calculated in the usual manner respectively by FEA and Matlab tools. These values are given in the second column of Table 4.2. Percentage leakage inductance of 9.4% is very close to 10% estimated value.



Furthermore, the deviation in self-inductance is found to be -0.99% of the 70.8 mH target self-inductance.

Table 4.2 Technical specs, reactor parameters and performance figures of the optimized shunt reactors designed according to the FEA and Practical Approaches

Technical Specs, Reactor Parameters and Performance Figures		According to Practical Design Approach		According to FEA Design Approach
Reactor Specs	# Distributed gaps	G=40	G=40	G=40
	Q <sub>r</sub> (kVAR)	600	1500	1500
	V <sub>r</sub> (l-to-l) (kV)	1.10	10.00	10.00
	I <sub>r</sub> (A)	945	260	260
	L <sub>s</sub> (mH)	2.14	70.80	70.80
	Leakage inductance%	14%	10%	15%
	B <sub>m</sub> (T)	1.10	1.10	1.10
	Temperature rise, ΔT (K)	60	80	80
Parameters Calculated by FEA Tools	L <sub>s</sub> (mH)	2.13	70.10	70
	L <sub>gap</sub> (mH)	1.90	63	62.70
	L <sub>iron</sub> (mH)	0.02	0.50	0.50
	L <sub>leakage</sub> (mH)	0.23	6.60	6.80
	Leakage inductance%	10.80%	9.40%	9.70%
Performance of the design procedure	PV Cost (Euro)	31030	68640	64620
	Initial Cost (Euro)	8820	19480	17960
	Operating Cost (Euro)	22210	49160	46660
	Self-Inductance Deviation%	-0.50%	-0.99%	-1.13%
	Temperature rise, ΔT (K)	62	82	82
Dimensions of the reactors	Total gap length (mm)	61.1	63	63
	Number of turns	40	150	154
	w (mm)	181.4	289.5	281.4
	d (mm)	308.4	492.2	478.3
	Winding height (mm)	1227	338	358
	Limb height (mm)	1267	598	598
	Core height (mm)	1629.8	1177	1160.8
	Core width (mm)	411.8	874	861.8

The second shunt reactor is also optimized according to the FEA Design Approach (Chapter 3) for  $\Delta T=80$  K and 15% leakage inductance. The results are given in the last column of Table 4.2. For this case, 9.7% leakage inductance is obtained in comparison with 9.4% arising from the Practical Design Approach. These values are very close to each other. Furthermore, -1.13% self-inductance deviation is obtained in comparison with -0.99% deviation obtained from the Practical Design Approach.

When the design of the second shunt reactor is carried out according to the Practical Approach, its PVC is found to be higher than that of the time consuming FEA Design Approach. Since the rise in PVC does not exceed 6%, it is considered to be tolerable for a practical design approach.

The case studies and the associated results presented in Table 4.2 show that, the Practical Design Approach recommended in this research work can be used as a short-cut and simple design method for shunt reactors provided that percentage leakage variations for different reactor sizes, operating voltages and temperature rises above the ambient are available in the form of look-up tables or graphical tools.

#### **4.5 Discussions**

In this chapter, a practical approach to the design of shunt reactors with discretely distributed air-gaps is developed. Graphical constructions for percentage leakage inductance, which have been obtained according to min PVC design criterion by using FEA optimizations, are defined for the Practical Design Approach. The correctness of the proposed design approach is tested for two different shunt reactors by using FEA tools. The results of the research work presented in this chapter show that;

- The target self-inductance values are obtained with about 1% deviations by using the proposed Practical Design Approach,
- The graphical tools constructed for leakage inductance percentage estimations give accurate results for both shunt reactor design approaches, i.e., the Practical Design Approach and FEA Design Approach.

- The Present Value Cost of the shunt reactor designed according to the Practical Design Approach is slightly higher than that of the FEA Design Approach. It can be considered to be tolerable since the Practical Design Approach has the advantage of being simple and fast.

Therefore, the Practical Design Approach proposed in this chapter can be used as a short-cut and simple design method for shunt reactors with discretely distributed air-gaps.

## CHAPTER 5

### CONCLUSIONS

In this research work, the fundamental definitions and the computational alternatives of equivalent inductances of discretely distributed-gapped iron-core shunt reactors are described in Chapter 2. It is argued that a definition based on flux distribution may not be reliable and calculations based on energy or co-energy are preferable. The behavior of all inductance components in both series and parallel equivalent circuit representations of the reactor is studied numerically using 3D finite element simulation for a wide range of currents encompassing both linear regime and extreme saturation. Effects of dividing the air-gap in the iron-core of shunt reactors into several discrete gaps on inductance parameters of the equivalent circuit, core losses and gap losses are also investigated both quantitatively and qualitatively. An optimum range for the number of discrete gaps is defined which minimizes fringing flux and hence leakage inductance. A new method called Moving Strip Method is also introduced to estimate the gap-loss in the iron-core of shunt reactors having discretely distributed small air-gaps relative to those with large air-gaps. For an optimized shunt reactor, parameters of the equivalent electric circuit are obtained by both analytical calculations and FEM analyses and then verified by measurements on the implemented reactor.

In Chapter 3, a single-phase shunt reactor with pre-specified technical specifications is designed according to a) min IC, b) min  $P_t$ , c) min PVC design objectives by the aid of FEA. The optimized designs are repeated for  $G=2$  and  $G=20$  air-gaps. Since a clear-cut analytical expression for the calculation of percentage leakage inductance of shunt reactors is not available in the literature, FEA is an inevitable part of the design procedure.

In Chapter 4, a practical approach to the design of shunt reactors with discretely distributed air-gaps is developed. Graphical constructions for percentage leakage inductance, which have been obtained according to min PVC design criterion by using FEA optimizations, are defined for the Practical Design Approach. The correctness of the proposed design approach is tested for two different shunt reactors by using FEA tools.

Following conclusions are drawn from the results presented in this research work;

- The physical meaning of component inductances of a reactor is subject to uncertainty and it is open to different interpretations, leading to various equivalent circuits. Therefore a definition based on flux distribution may not be reliable and calculations based on energy or co-energy are thus preferable.
- The use of several discretely distributed small air-gaps in the design and implementation of a shunt reactor yields more uniform flux density distribution in the core in comparison with that of an equivalent core having only a few air-gaps. This will cause a significant reduction in gap-loss component and a considerable reduction in the total reactor losses.
- The Moving Strip Method proposed in this research work permits the estimation of gap-loss owing to the fringing flux in iron cores having discretely distributed small air-gaps. This method is based on FEM analyses and estimates the gap-loss relative to empirical gap-loss calculation for large air-gaps.
- Several discrete air-gaps also cause a significant reduction in the percentage of leakage inductance,  $L_l$  as compared to magnetizing inductance,  $L_m$  and makes core inductance,  $L_c$  much greater than gap inductance,  $L_g$ . Therefore,  $L_c$  and  $R_g$  for a shunt reactor having several discretely distributed small air-gaps can be neglected thus permitting practical hand-calculations in the design of such reactors.
- The optimum value of time maximum (peak) flux density in the core is found to be  $B_m = 1.1$  T for the core material M330-35 AP non-oriented steel.

- Min IC design criterion is beneficial only for the reactor manufacturers. Because, the resulting reactor costs more to the user in the long-term (economic life of the reactor).
- Min  $P_t$  design criterion minimizes reactor losses and hence the operating cost of the reactor during its life time.
- Min PVC design criterion minimizes the sum of initial cost and operating cost of the shunt reactor. Although this criterion gives nearly the same economic results with the min  $P_t$  design criterion, it is considered to be the best approach to the reactor design from the viewpoint of macroeconomics and user benefits.
- The target self-inductance values are obtained within  $\pm 5\%$  deviations by using the proposed Practical Design Approach. Moreover, fine tuning is possible in the final manufacturing step by changing number of turns or gap length.
- The graphical tools constructed for leakage inductance percentage estimations give accurate results for both shunt reactor design approaches, i.e., the Practical Design Approach and FEA Design Approach.
- The case studies and the associated results show that, the Practical Design Approach recommended in this research work can be used as a short-cut and simple design method for shunt reactors provided that percentage leakage variations for different reactor sizes, operating voltages and temperature rises above the ambient are available in the form of look-up tables or graphical tools. These approach can be achieved on a personal computer by using some package programs in a few hours time. It is also possible to carry out the design by hand calculations. For this case a few days time can be spend.
- Practical Design Approach eliminates entirely the need to a proper FEA package program and to a powerful digital computer.

- The results presented in this PhD Thesis is applicable only to reactors built up of non-oriented electrical steel (M330-35 AP) and aluminum foil windings and designed at  $B_m=1.1$  T. If the type of the core material and/or winding material or design value of  $B_m$  are changed, a new family of percentage leakage inductance characteristics are to be generated by FEA tools.

Following aspects of shunt reactor design are skipped in this research work:

- The gapped iron-core of the reactor is modeled in the form of solid iron geometry in FEA tools. This is because Maxwell simulation software is run on a powerful personal computer. The model of core consisting of several laminations can also be solved by FEA tools but only on a very powerful computational infrastructure such as a main frame computer or a very powerful server computer. Because of lack of very powerful computational facilities in the laboratory, in this research work the core is modeled as a solid one but the material properties in software are defined as a laminated core (by defining lamination thickness in mm, core density in  $\text{kg/m}^3$ , B-H and loss curves obtained from manufacturer) for core loss calculation. Therefore, in the calculation of the core loss, lamination effect is taken into account by the FEA software automatically. Moreover, since the core loss calculation in 3D consumes too much time (at least 2-3 days for each model) it can be calculated using 2D modeling by defining the depth of the core. If one computes core losses by using the approximate core model and Maxwell Transient Analysis tool in 2D, the error does not exceed 5% of the actual value calculated in 3D. In order to avoid this drawback in the Practical Design Approach, core losses are calculated from the experimental data given by the manufacturer of the laminated core material.
- Because of the lack of a powerful computer infrastructure, all results obtained by the aid of FEA is applied only to isotropic (non-oriented) core materials. If anisotropic (oriented) core materials could be used in the design of shunt reactors, equivalent reactors with lower Present Value Cost would be obtained.

## REFERENCES

- [1] Electrical Power Transformer Engineering, Edited by James H. Harlow, CRC press LLC, 2004
- [2] H.F. Bilgin, M. Ermis, Current Source Converter Based STATCOM: Operating Principles, Design and Field Performance, Electric Power Systems Research, Vol. 81, pp. 478-487, 2011.
- [3] Bilgin, H.F., Ermis, M., Design and Implementation of a Current-Source Converter for Use in Industry Applications of D-STATCOM, IEEE Transactions on Power Electronics, Vol. 25, Issue 8, pp. 1943-1957, 2010.
- [4] Cetin, A., Ermis, M., VSC-Based D-STATCOM With Selective Harmonic Elimination, IEEE Transactions on Industry Applications, Vol. 45, Issue 3, pp. 1000-1015, 2009.
- [5] G.W.Alexander, R.H.Hopkinson, A.U.Welch, Design and Application of EHV Shunt Reactors, IEEE Transactions on Power Apparatus and Systems, PAS-85, No 12, pp. 1247-1258, 1966.
- [6] Yue Hao, Xu Yonghai, Liu Yingying, Zhu Yongqiang, Xiao Xiangning, Study of Nonlinear Model of Shunt Reactor in 1000kV AC Transmission System, International Conference on Energy and Environment Technology, Vol. 2, pp. 305-308, 2009.
- [7] Shingo Saizen, Kazunori Hashiba, Morihiko Iwagami, 500/ $\sqrt{3}$  kV 50/3 MVA Shunt Reactors for CTM Argentina, Fuji Electric Review, Vol. 25, No 2, pp. 49-52, 1979.
- [8] Atilla Donuk, Mihai Rotaru, Jan K. Sykulski, Defining And Computing Equivalent Inductances Of Gapped Iron Core Reactors, Przegląd Elektrotechniczny (Electrical Review), Vol. 88, No 7b, pp.52-55, 2012.
- [9] F. W. Lanchester, The Air-Gap Transformer and Choke, Proceedings of the Institution of Electrical Engineers - Wireless Section, Vol. 8, Issue 24, pp.195-200, 1933
- [10] MIT Members, Magnetic Circuits and Transformers, MIT press, 1943.
- [11] Anil K.Ohri, Thomas G. Wilson, Harry A. Owen, Jr., Design of Air-Gapped Magnetic-Core Inductors for Superimposed Direct and Alternating Currents, IEEE Transactions on Magnetics, Vol. Mag-12, No. 5, pp. 564-574, 1976.
- [12] Anil K.Ohri, Thomas G. Wilson, Harry A. Owen, Jr., Design of a Single-Winding Energy-Storage Reactors for DC-to-DC Converters Using Air-



- Gapped Magnetic-Core Structures, IEEE Transactions on Magnetics, Vol. Mag-13, No. 5, pp. 1214-1216, 1977.
- [13] Stefan F. Szuba, Computer-Aided Design of Air-Gapped Magnetic Core Inductors with Minimum DC Winding Resistance, IEEE Transactions on Magnetics, Vol. Mag-15, No. 3, pp. 1085-1095, 1979.
- [14] Hubert,J., Kakalec,R. Computer Design of AC and DC Inductors, Electrical Electronics Insulation Conference and Electrical Manufacturing & Coil Winding Conference, EEIC/ICWA Exposition, pp. 707 – 712, 1993.
- [15] Bartoli, M., Reatti, A., Kazimierczuk, M.K., Minimum Copper and Core Losses Power Inductor Design, IEEE Industry Applications Conference, Vol.3, pp. 1369 -1376, 1996.
- [16] Introduction to Maxwell, Maxwell 3D Technical Notes, Maxwell Online Help
- [17] Wikipedia, [http://en.wikipedia.org/wiki/Finite\\_element\\_method](http://en.wikipedia.org/wiki/Finite_element_method). August, 2012.
- [18] Z Nami, C H Ahn and M G Allen, An Energy-Based Design Criterion For Magnetic Microactuators, Journal of Micromechanics and Microengineering, Vol.6, No. 3, pp. 337-344, 1996.
- [19] H. Tsai, A. Keyhani and A.B. Proca, Design of Saturable Reactors in Power Conditioning Systems, Electric Machines and Power Systems, Vol.25, pp. 1089-1101, 1996.
- [20] Han-Jong Kim, Geun-Ho Lee, Cheol-Ho Jang and Jea-Pil Lee, Cost-Effective Design of an Inverter Output Reactor in ASD Applications, IEEE Transactions on Industrial Electronics, Vol. 48, No. 6, pp. 1128-1135, 2001.
- [21] A.V. Bossche, V. Valchev, T. Filchev, Improved Approximation for Fringing Permeances in Gapped Inductors, IEEE Industrial Applications Conference, pp. 932-938, 2002.
- [22] Y. Ishihara, T. Morino, T. Todaka, Analysis of Magnetic Fields of a Delta Type Shunt Reactor, IEEE Transactions on Magnetics, Vol. 25, No. 4, pp. 2846-2848, 1989.
- [23] C.M. Arturi, M. Ubaldini, Finite Element Analysis and Calculation of the Magnetic Field Distribution in Smoothing Inductors for Electric Traction, IEEE Transactions on Magnetics, Vol. 25, No. 4, pp. 2864-2866, 1989.
- [24] H.D. Gersem, K. Hameyer, A Finite Element Model for Foil Winding Simulation, IEEE Transactions on Magnetics, Vol. 37, No. 5, pp. 3427-3432, 2001.
- [25] A. Balakrishnan, W.T. Joines, T.G. Wilson, Air-Gap Reluctance and Inductance Calculations for Magnetic Circuits Using a Schwarz-Christoffel

- Transformation, IEEE Transactions on Power Electronics, Vol. 12, No. 4, pp. 654-663, 1997.
- [26] M. Albach, A. Stadler, The Minimization of Magnetic Stray Fields from Toroids with Air Gaps, IEEE International Symposium on Electromagnetic Compatibility, Vol.3, pp. 881-886, 2004
- [27] W.A. Roshen, Fringing Field Formulas and Winding Loss Due to an Air Gap, IEEE Transactions on Magnetics, Vol. 43, No. 8, pp. 3387-3394, 2007.
- [28] J. Driesen, W. Ruythooren, R. Belmans, J.D. Boeck, J.P. Celis, K. Hameyer, Electric and Magnetic FEM Modeling Strategies for Micro-Inductors, IEEE Transactions on Magnetics, Vol. 35, No. 5, pp. 3577-3579, 1999.
- [29] K. Hameyer, J. Driesen, H.D. Gersem, R. Belmans, The Classification of Coupled Field Problems, IEEE Transactions on Magnetics, Vol. 35, No. 3, pp. 1618-1621, 1999.
- [30] H.V. Sande, T. Boonen, I. Podoleanu, F. Henrotte, K. Hameyer, Simulation of a Three-Phase Transformer Using an Improved Anisotropy Model, IEEE Transactions on Magnetics, Vol. 40, No. 2, pp. 850-855, 2004.
- [31] J. Driesen, G. Deliege, R. Belmans, K. Hameyer, Coupled Thermo-Magnetic Simulation of a Foil-Winding Transformer Connected to a Non-Linear Load, IEEE Transactions on Magnetics, Vol. 36, No. 4, pp. 1381-1385, 2000.
- [32] Chen, G.H., Design of Wheel Motor using Maxwell 2D Simulation, International Conference on Energy Management and Power Delivery, Vol.2, pp.634-639,1995.
- [33] A.J. Moses, B. Thomas, Problems in the Design of Power Transformers, IEEE Transactions on Magnetics, Vol. Mag-10, No. 2, pp. 148-150, 1974.
- [34] T. Nakata, Numerical Analysis of Flux and Loss Distributions in Electrical Machinery, IEEE Transactions on Magnetics, Vol. Mag-20, No. 5, pp. 1750-1755, 1984.
- [35] X. Su, N. Zhang, S. Zhang, B. Gao, Design Method of Shading Coil in Electromagnetic Mechanism of AC Contactor Based on FEA, International Conference on Electrical Machines and Systems, pp. 201-204, 2008.
- [36] E. Lesniewska, W. Jalmuzny, Influence of the Number of Core Air Gaps on Transient State Parameters of TPZ Class Protective Current Transformers, IET Science, Measurement and Technology, Vol. 3, Issue 2, pp. 105-112, 2008.
- [37] J.G. Hayes, N. O'Donovan, M.G. Egan, T. O'Donnell, Inductance Characterization of High-Leakage Transformers, IEEE Applied Power Electronics Conference and Exposition, Vol. 2, pp. 1150 -1156, 2003.

- [38] Dina M.M. Ahmad, I. Daut, S. Taib, Flux Simulation on 100kVA Three-Phase Transformer Core, *International Review on Modeling and Simulations (IREMOS)*, Vol. 3, n.3, pp. 340-343, 2010
- [39] E.T. Rakgati, T. Tsalaile, E. Gower, Modeling of Six-Phase Reluctance DC Machine Using Finite Element Method, *International Review on Modeling and Simulations (IREMOS)*, Vol. 4, n.4, pp. 1610-1615, 2011
- [40] B. Tomczuk, D. Koteras, Influence Of The Air Gap Between Coils On The Magnetic Field In The Transformer With Amorphous Modular Core, *Studia Materialy*, Vol.62, No. 28, pp. 92-96, 2008.
- [41] H. Bülent Ertan, Bülent Dag, Gerard Capolino; “Calculation of Parameters of Single Phase PM Motor for Design Optimization”, *IEEE Trans. On Energy Conversion*, Vol. 20, No. 3, pp. 538-548, 2005.
- [42] McLyman, T., *Transformer and Inductor Design Handbook*, (Mercel Dekker, Inc., 2004).
- [43] H.J. Williams, W. Shockley, C. Kittel, Studies of the Propagation Velocity of a Ferromagnetic Domain Boundary, *Physical Review*, Vol. 80, No. 6, pp. 1090-1094, 1950.
- [44] R.H. Pry, C.P. Bean, Calculation of Energy Loss in Magnetic Sheet Materials Using a Domain Model, *Journal of Applied Physics*, Vol. 29, No. 3, pp. 532-533, 1958.
- [45] Bertotti, G., General properties of power losses in soft ferromagnetic materials, *IEEE Transactions on Magnetics*, Vol. 24, pp. 621 – 630, 1988.
- [46] Lee, R.; Stephens, D., Influence of core gap in design of current-limiting transformers, *IEEE Transactions on Magnetics*, Vol. 9, Issue 3, pp. 408 - 410, 1973.
- [47] S.H. Charap, F.F. Judd, A Core Loss Model for Laminated Transformers, *IEEE Transactions on Magnetics*, Vol. Mag-10, No. 3, pp. 678–681, 1974.
- [48] D.C. Jiles, Frequency Dependence of Hysteresis Curves in ‘Non-Conducting’ Magnetic Materials, *IEEE Trans. Magnetics*, Vol. 29, No. 6, pp. 3490–3492, 1993.
- [49] T. Kohsaka, N. Takahashi, S. Nogawa, M. Kuwata, Analysis of Magnetic Characteristics of Three-Phase Reactor Made of Grain-Oriented Silicon Steel, *IEEE Transactions on Magnetics*, Vol. 36, No. 4, pp. 1894–1897, 2000.
- [50] Kutkut, N.H.; Divan, D.M., Optimal air-gap design in high-frequency foil windings, *IEEE Transactions on Power Electronics*, Volume: 13, Issue: 5, pp. 942 – 949, 1998.

- [51] I. Wooley, Eddy-current Losses in Reactor Flux Shields, IEE Proceedings, Vol. 117, No. 11, pp. 2142-2150, 1970.
- [52] J. Li, T. Abdallah, C.R. Sullivan, Improved Calculation of Core Loss with Nonsinusoidal Waveforms, IEEE Industry Applications Society Annual Meeting, pp. 2203-2210, 2001.
- [53] D.M. Ionel, M. Popescu, S.J. Dellinger, T.J.E. Miller, R.J. Heideman, M.I. McGilp, On the Variation with Flux and Frequency of the Core Loss Coefficients in Electrical Machines, IEEE Transactions on Industry Applications, Volume: 42, No: 3 , pp. 658–667, 2006.
- [54] Y. Chen, P. Pillay, An Improved Formula for Lamination Core Loss Calculations in Machines Operating with High Frequency and High Flux Density Excitation, IEEE Industry Applications Society Annual Meeting, pp. 759–766, 2002.
- [55] Y. Gao, K. Muramatsu, K. Shida, K. Fujiwara, S. Fukuchi, T. Takahata, Loss Calculation of reactor Connected to Inverter Power Supply Taking Account of Eddy Currents in Laminated Steel Core, IEEE Transactions on Magnetics, Vol. 45, No. 3, pp. 1044-1047, 2009.
- [56] J.H. Claassen, A Novel Technique for Measurement of Core Loss in Low Permeability Materials, Journal of Magnetism and Magnetic Materials, Vol. 301, pp. 541-545, 2006.
- [57] L. Zeng, L. Zhang, C.D. Xie, D.S. Bai, E.Y. Wu, F.Y. Xia, Separation Calculation of High-Voltage Dry-Type Smoothing Reactor Under Harmonic Magnetic Fields, International Conference on Electrical Machines and Systems, pp. 1-4, 2009.
- [58] Nogawa, S., Kuwata M., Nakau, T., Miyagi D., Takahashi N., Study of Modeling Method of Lamination of Reactor Core, IEEE Transactions on Magnetics, Vol.42, No. 4, pp. 1455-1458, 2006.
- [59] Z. Cheng, N. Takahashi, B. Forghani, G. Gilbert, Y. Du, Y. Fan, L. Liu, Z. Zhai, W. Wu, J. Zhang, Effect of Excitation Patterns on Both Iron Loss and Flux in Solid and Laminated Steel Configurations, IEEE Transactions on Magnetics, Vol.46, No. 8, pp. 3185-3188, 2010.
- [60] B.You, J. Kim, B. Lee, G. Choi, D. Yoo, Optimization of Powder Core Inductors of Buck-Boost Converters for Hybrid Electric Vehicles, IEEE Conference on Vehicle Power and Propulsion, pp. 730-735, 2009.
- [61] G. Grandi, M.K. Kazimierczuk, A. Massarini, U. Reggiani, G. Sancineto, Model of Laminated Iron-Core Inductors for High Frequencies, IEEE Transactions on Magnetics, Vol.40, No. 4, pp. 1839-1845, 2004.
- [62] G. Chen, K.M. Smedley, Z. Qian, Tuned Power Inductors for Hybrid Active Power Filter With Structure of Hybrid Magnetic Core, Distributed Air Gaps

- and Three-Phase Five-Column, IEEE Conference on Industrial Electronics, pp. 2023-2028, 2003.
- [63] S. Nogawa, M. Kuwata, D. Miyagi, T. Hayashi, H. Tounai, T. Nakau, N. Takahashi, Study of Eddy-Current Loss Reduction by Slit in Reactor Core, IEEE Transactions on Magnetics, Vol.41, No. 5, pp. 2024-2027, 2005.
- [64] A.V. Bossche, V.C. Valchev, Improved Calculation of Winding Losses in Gapped Inductors, Journal of Applied Physics, Vol.97, No. 10, pp. 10Q703 - 10Q703-3, 2005.
- [65] A. W. Lotfi, F.C. Lee, Two Dimensional Skin Effect in Power Foils for High-Frequency Applications, IEEE Transactions on Magnetics, Vol. 31, No. 2, pp. 1003-1006, 1995.
- [66] Z.Q. Wang, Z.D. Yin, L.X. Zhou, Z.J. Wang, L.R. Ma, Study on Controllable Reactor Magnetic Structure and Loss Based on ANSYS, IEEE Conference on Industrial Electronics and Applications, pp. 201-205, 2009.
- [67] Z. Cheng, N. Takahashi, B. Forghani, G. Gilbert, J. Zhang, L. Liu , Y. Fan, X. Zhang, Y. Du, J. Wang, C. Jiao, Analysis and Measurements of Iron Loss and Flux Inside Silicon Steel Laminations, IEEE Transactions on Magnetics, Vol.45, No. 3, pp. 1222-1225, 2009.
- [68] Y. Oda, M. Kohno, A. Honda, Recent Development of Non-Oriented Electrical Steel Sheet for Automobile Electrical Devices, Journal of Magnetism and Magnetic Materials, Vol. 320, Issue 20, pp. 2430-2435, 2008.
- [69] D. Lin, P. Zhou, Q.M. Chen, The Effects of Steel Lamination Core Losses on Transient Magnetic Fields Using T- $\Omega$  Method, IEEE Vehicle Power and Propulsion Conference, pp. 1-4, 2008.
- [70] Lin, D.; Zhou, P.; Fu, W.N.; Badics, Z.; Cendes, Z.J., A Dynamic Core Loss Model for Soft Ferromagnetic and Power Ferrite Materials in Transient Finite Element Analysis, IEEE Transactions on Magnetics, Vol. 40, Issue 2, pp. 1318-1321, 2004.
- [71] K.Zakrzewski, B.Tomczuk, On The Use of the FEM and BIE Methods in the 3D Magnetic Field Computation of the Reactors with Air Gaps, Compel, Vol. 17, No. 1/2/3, pp. 116-120, 1998.
- [72] Szczerbanowski, R., Flux Density in Multi-airgap Network Reactor, Electromagnetic Fields in Electrical Engineering, Vol. 22, pp. 295-300, 2002.
- [73] B. Tomczuk, K. Babczyk, Calculation of Self and Mutual Inductances and 3-D Magnetic Fields of Chokes with Air Gaps in Core, Electrical Engineering, Volume:83, pp.41-46, 2001.
- [74] International Standard, Reactors, IEC 289, 1988.

- [75] International Standard, Reactors, IEC 6076-6, Power Transformers-Part6:Reactors, 2007.
- [76] IEEE Loss Evaluation Guide for Power Transformers and Reactors, IEEE Std C57.120-1991.
- [77] Transformer Life Cycle Cost, <http://abb.com.tr>, March, 2012.
- [78] <http://electrical-engineering-portal.com/life-cycle-cost-of-transformers>, March, 2012.
- [79] Nevzat Özay, Nezih Güven, Elektrik Dağıtım Sistemlerinde Orta Gerilim Seviyesinin Belirlenmesi, Elektrik Mühendisliği-397, s. 7-14, ([http://www.emo.org.tr/ekler/4e422f05b68cc01\\_ek.pdf?dergi=270](http://www.emo.org.tr/ekler/4e422f05b68cc01_ek.pdf?dergi=270), September 2012)
- [80] [http://www.aykonelektrik.com/abb/ABB\\_Yagli\\_Tip\\_Trafo\\_Fiyat\\_Listesi.pdf](http://www.aykonelektrik.com/abb/ABB_Yagli_Tip_Trafo_Fiyat_Listesi.pdf), September, 2012.
- [81] [http://books.mcgrawhill.com/downloads/products/0071467890/0071467890\\_ch15.pdf](http://books.mcgrawhill.com/downloads/products/0071467890/0071467890_ch15.pdf), September, 2012.

# APPENDIX A

## MAGNETIZATION AND CORE LOSS CURVES OF M330-35AP NON GRAIN ORIENTED STEEL (THYSSENKRUPP)

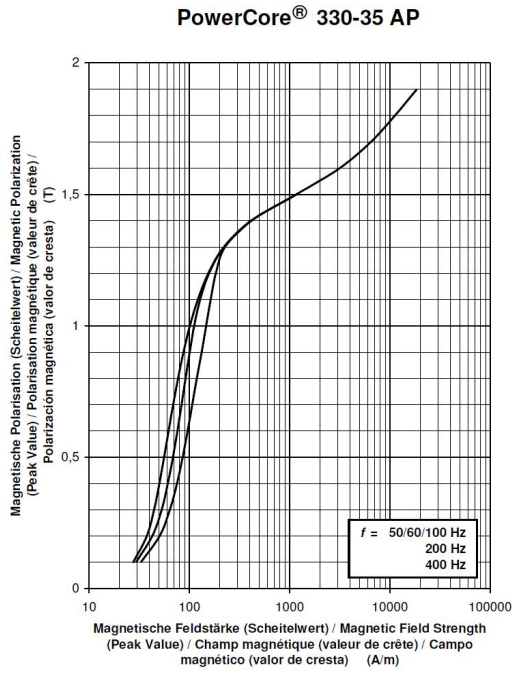


Figure A.1 Magnetization Curve of  
M330-35 AP NGO Steel

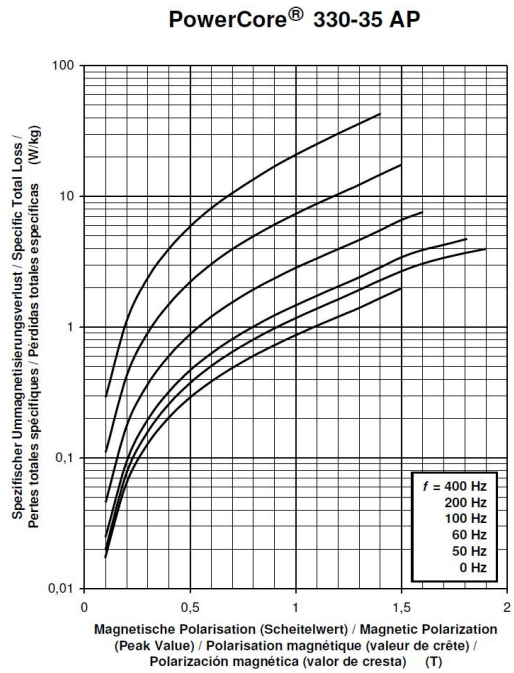


Figure A.2 Loss Curves of  
M330-35 AP NGO Steel

## APPENDIX B

### ITERATION RESULTS PERFORMED FOR THE THREE DESIGN CRITERIA GIVEN IN CHAPTER 3

Table B.1 Design parameters of minimum total loss criterion for 0.8 T

	Design results	iteration 1	iteration 2	iteration 3	iteration 4	Design results	iteration 1
target flux density (T)	0,8	0,8	0,8	0,8	0,8	0,8	0,8
kVAR	46	46	46	46	46	46	46
Voltage (l-l) kV	1,1	1,1	1,1	1,1	1,1	1,1	1,1
Current (A rms)	72,43	72,43	72,43	72,43	72,43	72,43	72,43
L (mH)	27,92	27,92	27,92	27,92	27,92	27,92	27,92
Lleak (%)	5	5	5	5	5	15	15
gap number (G)	2	2	20	20	20	2	20
turns number (N)	100	96	96	102	96	102	108
t (mm)	0,5	0,5	0,5	0,5	0,5	0,5	0,5
insulation (mm)	0,15	0,15	0,15	0,15	0,15	0,15	0,15
J (A/mm <sup>2</sup> )	1,1	1,1	1,1	1,1	1,1	1,1	1,1
A (mm <sup>2</sup> )	35761,8	35761,8	35761,8	35761,8	35761,8	32027,8	32027,8
A <sub>eff</sub> (mm <sup>2</sup> )	34331,4	34331,4	34331,4	34331,4	34331,4	30746,7	30746,7
winding h (mm)	133	133	133	133	133	133	133
l <sub>gap</sub> (mm)	16,9	16,9	16,9	16,9	14,7	16,9	16,9
winding thickness (mm)	65	62,4	62,4	66,3	62,4	66,3	70,2
window (mm)	80	77,4	77,4	81,3	77,4	81,3	85,2
w (mm)	142,1	142,1	142,1	142,1	142,1	134,5	134,5
d (mm)	241,6	241,6	241,6	241,6	241,6	228,6	228,6
temperature rise (K)	32					32	32
winding clearance (mm)	5	5	5	5	5	5	5
yoke clearance (mm)	20	20	20	20	20	20	20
tube (mm)	5	5	5	5	5	5	5
winding-limb clearance	0	0	0	0	0	0	0
total loss (W)	500					457	
initial cost (Euro)	1730					1524	
PV Cost (Euro)	4787					4322	
Winding Loss (W)	264	256	256	268	256	256	
Simulation results							
L <sub>total</sub> (mH)	29,86	27,50	24,40	27,57	27,87	28,04	27,75
L <sub>gap</sub> (mH)		23,00		26,42	26,46	23,27	26,17
L <sub>iron</sub> (mH)		0,30		0,26	0,30	0,32	0,26
L <sub>leakage</sub> (mH)		4,20	24,40	0,89	1,11	4,45	1,32
% leakage		15,27	100,00	3,23	3,98	15,87	4,76
Core Loss (W)		173		166	190	174	164
Total Loss (W)	264	429	256	434	446	430	431
target inductance %		1,52%	12,62%	1,27%	0,19%	-0,42%	0,62%



Table B.2 Design parameters of minimum total loss criterion for 1 T

	Design results	iteration 1	iteration 2	iteration 3	iteration 4	Design results	iteration 1
target flux density (T)	1	1	1	1	1	1	1
kVAR	46	46	46	46	46	46	46
Voltage (l-l) kV	1,1	1,1	1,1	1,1	1,1	1,1	1,1
Current (A rms)	72,43	72,43	72,43	72,43	72,43	72,43	72,43
L (mH)	27,92	27,92	27,92	27,92	27,92	27,92	27,92
Lleak (%)	5	5	5	5	5	17	17
gap number (G)	2	2	20	20	2	2	20
turns number (N)	120	116	120	122	100	120	130
t (mm)	0,5	0,5	0,5	0,5	0,5	0,4	0,4
insulation (mm)	0,15	0,15	0,15	0,15	0,15	0,15	0,15
J (A/mm <sup>2</sup> )	1,1	1,1	1,1	1,1	1,1	1,1	1,1
A (mm <sup>2</sup> )	23861,0	23861,0	23861,0	23861,0	23861,0	20841,0	20841,0
A_eff (mm <sup>2</sup> )	22906,5	22906,5	22906,5	22906,5	22906,5	20007,4	20007,4
winding h (mm)	133	133	133	133	133	133	133
l_gap (mm)	16,2	16,2	16,2	16,2	12	16,2	16,2
winding thickness (mm)	78	75,4	78	79,3	65	66	71,5
window (mm)	93	90,4	93	94,3	80	81	86,5
w (mm)	116,1	116,1	116,1	116,1	116,1	108,5	108,5
d (mm)	197,3	197,3	197,3	197,3	197,3	184,4	184,4
temperature rise (K)	40						
winding clearance (mm)	5	5	5	5	5	5	5
yoke clearance (mm)	20	20	20	20	20	20	20
tube (mm)	5	5	5	5	5	5	5
winding-limb clearance	0	0	0	0	0	0	0
total loss (W)	493					446	
initial cost (Euro)	1167					1040	
PV Cost (Euro)	4188					3774	
Winding Loss (W)	277	270	277	281	241	256	275
Simulation results							
Ltotal (mH)	31,00	28,76	26,70	27,74	27,65	27,33	27,42
Lgap (mH)		23,30	25,00	25,92	23,00	21,73	25,67
Liron (mH)		0,37	0,26	0,28	0,56	0,39	0,28
Lleakage (mH)	31,00	5,09	1,44	1,54	4,09	5,21	1,47
% leakage	100,00	17,70	5,39	5,55	14,79	19,06	5,36
Core Loss (W)		181		163	228	180	166
Total Loss (W)	277	451	277	444	469	436	441
target inductance %	-11,02%	-2,99%	4,38%	0,66%	0,98%	2,13%	1,80%

Table B.3 Design parameters of minimum total loss criterion for 1.2 T

	Design results	iteration 1	iteration 2	iteration 3	Design results	iteration 1	iteration 2
target flux density (T)	1,2	1,2	1,2	1,2	1,2	1,2	1,2
kVAR	46	46	46	46	46	46	46
Voltage (I-I) kV	1,1	1,1	1,1	1,1	1,1	1,1	1,1
Current (A rms)	72,43	72,43	72,43	72,43	72,43	72,43	72,43
L (mH)	27,92	27,92	27,92	27,92	27,92	27,92	27,92
Lleak (%)	5	5	5	5	20	20	20
gap number (G)	2	2	20	20	2	2	20
turns number (N)	140	132	144	132	120	124	134
t (mm)	0,4	0,4	0,4	0,4	0,5	0,5	0,5
insulation (mm)	0,15	0,15	0,15	0,15	0,15	0,15	0,15
J (A/mm <sup>2</sup> )	1,1	1,1	1,1	1,1	1,1	1,1	1,1
A (mm <sup>2</sup> )	17044,9	17044,9	17044,9	17044,9	16736,6	16736,6	16736,6
A_eff (mm <sup>2</sup> )	16363,1	16363,1	16363,1	16363,1	16067,2	16067,2	16067,2
winding h (mm)	166	166	166	166	133	133	133
l_gap (mm)	15,8	15,8	15,8	13,5	13,5	13,5	13,5
winding thickness (mm)	77	72,6	79,2	72,6	78	80,6	87,1
window (mm)	92	87,6	94,2	87,6	93	95,6	102,1
w (mm)	98,1	98,1	98,1	98,1	97,2	97,2	97,2
d (mm)	166,8	166,8	166,8	166,8	165,3	165,3	165,3
temperature rise (K)	48				46	46	46
winding clearance (mm)	5	5	5	5	5	5	5
yoke clearance (mm)	20	20	20	20	20	20	20
tube (mm)	5	5	5	5	5	5	5
winding-limb clearance	0	0	0	0	0	0	0
total loss (W)	495				436		
initial cost (Euro)	900				811		
PV Cost (Euro)	3934				3484		
Winding Loss (W)	285	271	292	271	243	250	268
Simulation results							
Ltotal (mH)	31,24	27,89	28,40	27,50	25,70	27,24	27,94
Lgap (mH)		21,40	26,40	25,70		21,23	26,00
Liron (mH)		0,86	0,30	0,40		1,10	0,43
Lleakage (mH)	31,24	5,63	1,70	1,40	25,70	4,91	1,51
% leakage	100,00	20,19	5,99	5,09	100,00	18,02	5,40
Core Loss (W)		188	172	193		200	187
Total Loss (W)	285	459	464	464	243	450	455
target inductance %	-11,88%	0,12%	-1,70%	1,52%	7,96%	2,45%	-0,06%

Table B.4 Design parameters of minimum total loss criterion for 1.4 T

	Design results	iteration 1	iteration 2	Design results	iteration 1	iteration 2
target flux density (T)	1,4	1,4	1,4	1,4	1,4	1,4
kVAR	46	46	46	46	46	46
Voltage (l-l) kV	1,1	1,1	1,1	1,1	1,1	1,1
Current (A rms)	72,43	72,43	72,43	72,43	72,43	72,43
L (mH)	27,92	27,92	27,92	27,92	27,92	27,92
Lleak (%)	5	5	5	18	18	18
gap number (G)	2	20	20	2	2	20
turns number (N)	140	144	140	140	150	154
t (mm)	0,4	0,4	0,4	0,4	0,4	0,4
insulation (mm)	0,15	0,15	0,15	0,15	0,15	0,15
J (A/mm <sup>2</sup> )	1,1	1,1	1,1	1,1	1,1	1,1
A (mm <sup>2</sup> )	14603,7	14603,7	14603,7	12607,3	12607,3	12607,3
A_eff (mm <sup>2</sup> )	14019,5	14019,5	14019,5	12103,0	12103,0	12103,0
winding h (mm)	166	166	166	166	166	166
l_gap (mm)	13,5	13,5	12,5	13,5	13,5	13,5
winding thickness (mm)	77	79,2	77	77	82,5	84,7
window (mm)	92	94,2	92	92	97,5	99,7
w (mm)	90,8	90,8	90,8	84,4	84,4	84,4
d (mm)	154,4	154,4	154,4	143,4	143,4	143,4
temperature rise (K)	54					
winding clearance (mm)	5	5	5	5	5	5
yoke clearance (mm)	20	20	20	20	20	20
tube (mm)	5	5	5	5	5	5
winding-limb clearance	0	0	0	0	0	0
total loss (W)	499			448		
initial cost (Euro)	777			677		
PV Cost (Euro)	3833			3426		
Winding Loss (W)	257	263	257	256	272	279
Simulation results						
Ltotal (mH)	28,67	28,08	28,18	24,00	27,45	27,37
Lgap (mH)	20,48	25,93	25,77		18,51	24,67
Liron (mH)	3,14	0,55	0,91		4,11	1,00
Lleakage (mH)	5,05	1,60	1,50		4,83	1,70
% leakage	17,61	5,70	5,32	0,00	17,60	6,21
Core Loss (W)	224	192	206		209	183
Total Loss (W)	481	455	463	256	481	462
target inductance %	-2,67%	-0,56%	-0,92%	14,05%	1,70%	1,98%

Table B.5 Selected design parameters from iterations given for minimum total loss criterion

G=2 / High Leakage							
				maxwell	matlab		
B <sub>m</sub> (T)	Total loss	Int. Cost	PV Cost	Core loss	Winding loss	N/t	L <sub>s</sub> (mH)
0,8	430	1524	4160	174	256	102/0,5	28,04
1	436	1040	3713	180	256	120/0,4	27,33
1,2	450	811	3569	200	250	124/0,5	27,24
1,4	481	677	3625	209	272	150/0,4	27,45

a)

G=2 / Low Leakage							
				maxwell	matlab		
B <sub>m</sub> (T)	Total loss	Int. Cost	PV Cost	Core loss	Winding loss	N/t	L <sub>s</sub> (mH)
0,8	429	1730	4360	173	256	96/0,5	27,5
1	451	1167	3932	181	270	116/0,5	28,76
1,2	459	900	3714	188	271	132/0,4	27,89
1,4	481	777	3725	224	257	140/0,4	28,67

b)

G=20 / High Leakage							
				maxwell	matlab		
B <sub>m</sub> (T)	Total loss	Int. Cost	PV Cost	Core loss	Winding loss	N/t	L <sub>s</sub> (mH)
0,8	431	1524	4166	164	267	108/0,5	27,75
1	441	1040	3743	166	275	130/0,4	27,42
1,2	455	811	3600	187	268	134/0,5	27,94
1,4	462	677	3509	183	279	154/0,4	27,37

c)

G=20 / Low Leakage							
				maxwell	matlab		
B <sub>m</sub> (T)	Total loss	Int. Cost	PV Cost	Core loss	Winding loss	N/t	L <sub>s</sub> (mH)
0,8	434	1730	4390	166	268	102/0,5	27,57
1	444	1167	3889	163	281	122/0,5	27,74
1,2	464	900	3744	172	292	144/0,4	28,4
1,4	468	777	3646	192	276	144/0,4	28,08

d)

Table B.6 Design parameters of minimum present value cost criterion for 0.8 T

	Design results	iteration 1	iteration 2	iteration 3	Design results	iteration 1	iteration 2
target flux density (T)	0,8	0,8	0,8	0,8	0,8	0,8	0,8
kVAR	46	46	46	46	46	46	46
Voltage (I-I) kV	1,1	1,1	1,1	1,1	1,1	1,1	1,1
Current (A rms)	72,43	72,43	72,43	72,43	72,43	72,43	72,43
L (mH)	27,92	27,92	27,92	27,92	27,92	27,92	27,92
Lleak (%)	5	5	5	5	15	15	15
gap number (G)	2	2	20	20	2	2	20
turns number (N)	150	138	144	150	150	146	158
t (mm)	0,4	0,4	0,4	0,4	0,4	0,4	0,4
insulation (mm)	0,15	0,15	0,15	0,15	0,15	0,15	0,15
J (A/mm <sup>2</sup> )	1,1	1,1	1,1	1,1	1,1	1,1	1,1
A (mm <sup>2</sup> )	23861	23861	23861	23861	21342	21342	21342
A_eff (mm <sup>2</sup> )	22907	22907	22907	22907	20489	20489	20489
winding h (mm)	166	166	166	166	166	166	166
l_gap (mm)	25,4	25,4	25,4	25,4	25,4	25,4	25,4
winding thickness (mm)	82,5	75,9	79,2	82,5	82,5	80,3	86,9
window (mm)	97,5	90,9	94,2	97,5	97,5	95,3	101,9
w (mm)	116,1	116,1	116,1	116,1	109,8	109,8	109,8
d (mm)	197,3	197,3	197,3	197,3	186,6	186,6	186,6
temperature rise (K)	40				40		
winding clearance (mm)	5	5	5	5	5	5	5
yoke clearance (mm)	20	20	20	20	20	20	20
tube (mm)	5	5	5	5	5	5	5
winding-limb clearance	0	0	0	0	0	0	0
total loss (W)	507				473		
initial cost (Euro)	1296				1158		
PV Cost (Euro)	4404				4058		
Winding Loss (W)	351	328	339	351	336	329	351
Simulation results							
Ltotal (mH)	33,25	28,13	25,09	27,24	30,00	28,46	27,20
Lgap (mH)		21,25		25,17		21,26	24,98
Liron (mH)		0,25		0,18		0,25	0,18
Lleakage (mH)		6,63	25,09	1,89	30,00	6,95	2,04
% leakage		23,57	100,00	6,94	100,00	24,42	7,50
Core Loss (W)		126		112		126	110
Total Loss (W)	351	454	339	463	336	455	461
target inductance %		-0,74%	10,15%	2,45%	-7,43%	-1,92%	2,59%

Table B.7 Design parameters of minimum present value cost criterion for 1 T

	Design results	iteration 1	iteration 2	Design results	iteration 1	iteration 2
target flux density (T)	1	1	1	1	1	1
kVAR	46	46	46	46	46	46
Voltage (I-I) kV	1,1	1,1	1,1	1,1	1,1	1,1
Current (A rms)	72,43	72,43	72,43	72,43	72,43	72,43
L (mH)	27,92	27,92	27,92	27,92	27,92	27,92
Lleak (%)	5	5	5	15	15	15
gap number (G)	2	2	20	2	2	20
turns number (N)	150	140	150	150	146	158
t (mm)	0,4	0,4	0,4	0,4	0,4	0,4
insulation (mm)	0,15	0,15	0,15	0,15	0,15	0,15
J (A/mm <sup>2</sup> )	1,1	1,1	1,1	1,1	1,1	1,1
A (mm <sup>2</sup> )	19084	19084	19084	17072	17072	17072
A_eff (mm <sup>2</sup> )	18321	18321	18321	16390	16390	16390
winding h (mm)	166	166	166	166	166	166
l_gap (mm)	20,3	20,3	20,3	20,3	20,3	20,3
winding thickness (mm)	82,5	77	82,5	82,5	80,3	86,9
window (mm)	97,5	92	97,5	97,5	95,3	101,9
w (mm)	103,8	103,8	103,8	98,2	98,2	98,2
d (mm)	176,5	176,5	176,5	166,9	166,9	166,9
temperature rise (K)	45			46		
winding clearance (mm)	5	5	5	5	5	5
yoke clearance (mm)	20	20	20	20	20	20
tube (mm)	5	5	5	5	5	5
winding-limb clearance	0	0	0	0	0	0
total loss (W)	500			465		
initial cost (Euro)	1036			930		
PV Cost (Euro)	4098			3780		
Winding Loss (W)	323	305	323	310	303	324
Simulation results						
Ltotal (mH)		28,75	27,16		28,16	27,17
Lgap (mH)		21,73	25,10		21,00	24,90
Liron (mH)		0,34	0,23		0,47	0,23
Lleakage (mH)	0,00	6,68	1,83	0,00	6,69	2,04
% leakage	#SAYI/0!	23,23	6,74	#SAYI/0!	23,76	7,51
Core Loss (W)		153	133		150	131
Total Loss (W)	323	458	456	310	453	455
target inductance %	100,00%	-2,96%	2,74%	100,00%	-0,85%	2,70%

Table B.8 Design parameters of minimum present value cost criterion for 1.2 T

	Design results	iteration 1	iteration 2	Design results	iteration 1	iteration 2	iteration 3
target flux density (T)	1,2	1,2	1,2	1,2	1,2	1,2	1,2
kVAR	46	46	46	46	46	46	46
Voltage (I-I) kV	1,1	1,1	1,1	1,1	1,1	1,1	1,1
Current (A rms)	72,43	72,43	72,43	72,43	72,43	72,43	72,43
L (mH)	27,92	27,92	27,92	27,92	27,92	27,92	27,92
Lleak (%)	5	5	5	20	20	20	20
gap number (G)	2	2	20	2	2	20	20
turns number (N)	150	140	152	140	144	148	156
t (mm)	0,4	0,4	0,4	0,4	0,4	0,4	0,4
insulation (mm)	0,15	0,15	0,15	0,15	0,15	0,15	0,15
J (A/mm <sup>2</sup> )	1,1	1,1	1,1	1,1	1,1	1,1	1,1
A (mm <sup>2</sup> )	15909	15909	15909	14344	14344	14344	14344
A_eff (mm <sup>2</sup> )	15272	15272	15272	13770	13770	13770	13770
winding h (mm)	166	166	166	166	166	166	166
l_gap (mm)	16,9	16,9	16,9	15,8	15,8	15,8	15,8
winding thickness (mm)	82,5	77	83,6	77	79,2	81,4	85,8
window (mm)	97,5	92	98,6	92	94,2	96,4	100,8
w (mm)	94,8	94,8	94,8	90	90	90	90
d (mm)	161,1	161,1	161,1	153	153	153	153
temperature rise (K)	50			49			
winding clearance (mm)	5	5	5	5	5	5	5
yoke clearance (mm)	20	20	20	20	20	20	20
tube (mm)	5	5	5	5	5	5	5
winding-limb clearance	0	0	0	0	0	0	0
total loss (W)	498			439			
initial cost (Euro)	869			764			
PV Cost (Euro)	3921			3455			
Winding Loss (W)	302	285	306	268	274	281	295
Simulation results							
Ltotal (mH)		28,65	27,72		27,49	25,30	28,10
Lgap (mH)		21,66	25,68		20,24		25,91
Liron (mH)		0,89	0,28		1,66		0,37
Lleakage (mH)	0,00	6,10	1,76	0,00	5,59	25,30	1,82
% leakage	#SAYI/0!	21,29	6,35	#SAYI/0!	20,33	100,00	6,48
Core Loss (W)		177	157		188		168
Total Loss (W)	302	462	463	268	462	281	463
target inductance %	100,00%	-2,60%	0,73%	100,00%	1,55%	9,40%	-0,63%

Table B.9 Design parameters of minimum present value cost criterion for 1.4 T

	Design results	iteration 1	iteration 2	iteration 3	iteration 4	iteration 5
target flux density (T)	1,4	1,4	1,4	1,4	1,4	1,4
kVAR	46	46	46	46	46	46
Voltage (l-l) kV	1,1	1,1	1,1	1,1	1,1	1,1
Current (A rms)	72,43	72,43	72,43	72,43	72,43	72,43
L (mH)	27,92	27,92	27,92	27,92	27,92	27,92
Lleak (%)	5	5	5	18	18	18
gap number (G)	2	2	20	2	2	20
turns number (N)	150	148	152	140	150	154
t (mm)	0,4	0,4	0,4	0,4	0,4	0,4
insulation (mm)	0,15	0,15	0,15	0,15	0,15	0,15
J (A/mm <sup>2</sup> )	1,1	1,1	1,1	1,1	1,1	1,1
A (mm <sup>2</sup> )	13621	13621	13621	12607	12607	12607
A_eff (mm <sup>2</sup> )	13076	13076	13076	12103	12103	12103
winding h (mm)	166	166	166	166	166	166
l_gap (mm)	14,5	14,5	14,5	13,5	13,5	13,5
winding thickness (mm)	82,5	81,4	83,6	77	82,5	84,7
window (mm)	97,5	96,4	98,6	92	97,5	99,7
w (mm)	87,7	87,7	87,7	84,4	84,4	84,4
d (mm)	149,1	149,1	149,1	143,4	143,4	143,4
temperature rise (K)	56			54		
winding clearance (mm)	5	5	5	5	5	5
yoke clearance (mm)	20	20	20	20	20	20
tube (mm)	5	5	5	5	5	5
winding-limb clearance	0	0	0	0	0	0
total loss (W)	500			448		
initial cost (Euro)	753			677		
PV Cost (Euro)	3817			3426		
Winding Loss (W)	286	283	290	256	272	260
Simulation results						
Ltotal (mH)	28,93	28,39	27,39		27,45	27,37
Lgap (mH)		19,90	25,20		18,51	24,67
Liron (mH)		0,31	0,48		4,11	1,00
Lleakage (mH)	28,93	8,18	1,71		4,83	1,70
% leakage	100,00	28,81	6,24	#SAYI/0!	17,60	6,21
Core Loss (W)		208	175		209	183
Total Loss (W)	286	491	465	256	481	443
target inductance %	-3,60%	-1,67%	1,91%	100,00%	1,70%	1,98%



Table B.10 Selected design parameters from iterations given for minimum Present value cost criterion

G=2 / High Leakage							
				maxwell	matlab		
B <sub>m</sub> (T)	Total loss	Int. Cost	PV Cost	Core loss	Winding loss	N/t	L <sub>s</sub> (mH)
0,8	455	1158	3947	126	329	146/0,4	28,46
1	453	930	3707	150	303	146/0,4	28,16
1,2	462	764	3596	188	274	144/0,4	27,49
1,4	481	677	3625	209	272	150/0,4	27,45

a)

G=2 / Low Leakage							
				maxwell	matlab		
B <sub>m</sub> (T)	Total loss	Int. Cost	PV Cost	Core loss	Winding loss	N/t	L <sub>s</sub> (mH)
0,8	454	1296	4079	126	328	138/0,4	28,13
1	458	1036	3843	153	305	140/0,4	28,75
1,2	462	869	3701	177	285	140/0,4	28,65
1,4	491	753	3763	208	283	148/0,4	28,39

b)

G=20 / High Leakage							
				maxwell	matlab		
B <sub>m</sub> (T)	Total loss	Int. Cost	PV Cost	Core loss	Winding loss	N/t	L <sub>s</sub> (mH)
0,8	461	1158	3984	110	351	158/0,4	27,2
1	455	930	3719	131	324	158/0,4	27,17
1,2	463	764	3602	168	295	156/0,4	28,1
1,4	462	677	3509	183	279	154/0,4	27,37

c)

G=20 / Low Leakage							
				maxwell	matlab		
B <sub>m</sub> (T)	Total loss	Int. Cost	PV Cost	Core loss	Winding loss	N/t	L <sub>s</sub> (mH)
0,8	463	1296	4134	112	351	150/0,4	27,24
1	456	1036	3831	133	323	150/0,4	27,16
1,2	463	869	3707	157	306	152/0,4	27,72
1,4	465	753	3603	175	290	152/0,4	27,39

d)

Table B.11 Design parameters of minimum initial cost criterion for 0.8 T

	Design results	iteration 1	iteration 2	iteration 3	Design results	iteration 1	iteration 2
target flux density (T)	0,8	0,8	0,8	0,8	0,8	0,8	0,8
kVAR	46	46	46	46	46	46	46
Voltage (l-l) kV	1,1	1,1	1,1	1,1	1,1	1,1	1,1
Current (A rms)	72,43	72,43	72,43	72,43	72,43	72,43	72,43
L (mH)	27,92	27,92	27,92	27,92	27,92	27,92	27,92
Lleak (%)	5	5	5	5	15	15	15
gap number (G)	2	2	2	20	2	2	20
turns number (N)	200	170	176	200	200	186	208
t (mm)	0,3	0,3	0,3	0,3	0,3	0,3	0,3
insulation (mm)	0,15	0,15	0,15	0,15	0,15	0,15	0,15
J (A/mm <sup>2</sup> )	1,6	1,6	1,6	1,6	1,6	1,6	1,6
A (mm <sup>2</sup> )	17891	17891	17891	17891	16009	16009	16009
A_eff (mm <sup>2</sup> )	17175	17175	17175	17175	15368	15368	15368
winding h (mm)	152	152	152	152	152	152	152
l_gap (mm)	33,8	33,8	33,8	33,8	33,8	33,8	33,8
winding thickness (mm)	90	76,5	79,2	90	90	83,7	93,6
window (mm)	105	91,5	94,2	105	105	98,7	108,6
w (mm)	100,5	100,5	100,5	100,5	95,1	95,1	95,1
d (mm)	170,9	170,9	170,9	170,9	161,6	161,6	161,6
temperature rise (K)	65				67		
winding clearance (mm)	5	5	5	5	5	5	5
yoke clearance (mm)	20	20	20	20	20	20	20
tube (mm)	5	5	5	5	5	5	5
winding-limb clearance	0	0	0	0	0	0	0
total loss (W)	733				696		
initial cost (Euro)	947				851		
PV Cost (Euro)	5441				5114		
Winding Loss (W)	624		559	624	600	562	621
Simulation results							
Ltotal (mH)	34	25,94	28,1	28,32		28,63	27,66
Lgap (mH)			19,6	25,32		19,56	24,50
Liron (mH)			0,19	0,13		0,20	0,13
Lleakage (mH)	34,00	25,94	8,31	2,87	0,00	8,87	3,03
% leakage	100,00	100,00	29,57	10,13	#SAYI/0!	30,98	10,95
Core Loss (W)			90	81		91	77
Total Loss (W)	624	0	649	705		653	698
target inductance %					100,00%	-2,53%	0,95%

Table B.12 Design parameters of minimum initial cost criterion for 1 T

	Design results	iteration 1	iteration 2	Design results	iteration 1	iteration 2
target flux density (T)	1	1	1	1	1	1
kVAR	46	46	46	46	46	46
Voltage (l-l) kV	1,1	1,1	1,1	1,1	1,1	1,1
Current (A rms)	72,43	72,43	72,43	72,43	72,43	72,43
L (mH)	27,92	27,92	27,92	27,92	27,92	27,92
Lleak (%)	5	5	5	15	15	15
gap number (G)		2	20		2	20
turns number (N)	200	176	200	200	186	208
t (mm)	0,2	0,2	0,2	0,2	0,2	0,2
insulation (mm)	0,15	0,15	0,15	0,15	0,15	0,15
J (A/mm <sup>2</sup> )	1,6	1,6	1,6	1,6	1,6	1,6
A (mm <sup>2</sup> )	14309	14309	14309	12803	12803	12803
A_eff (mm <sup>2</sup> )	13737	13737	13737	12291	12291	12291
winding h (mm)	228	228	228	228	228	228
l_gap (mm)	27,0	27,0	27,0	27,0	27,0	27,0
winding thickness (mm)	70	61,6	70	70	65,1	72,8
window (mm)	85	76,6	85	85	80,1	87,8
w (mm)	89,9	89,9	89,9	85	85	85
d (mm)	152,8	152,8	152,8	144,6	144,6	144,6
temperature rise (K)	66			67		
winding clearance (mm)	5	5	5	5	5	5
yoke clearance (mm)	20	20	20	20	20	20
tube (mm)	5	5	5	5	5	5
winding-limb clearance	0	0	0	0	0	0
total loss (W)	682			644		
initial cost (Euro)	813			732		
PV Cost (Euro)	4994			4680		
Winding Loss (W)	544	490	544	523	492	541
Simulation results						
Ltotal (mH)		28,37	28,05		28,68	27,16
Lgap (mH)		19,30	25,25		19,00	24,42
Liron (mH)		0,48	0,19		0,68	0,18
Lleakage (mH)	0,00	8,59	2,61	0,00	9,00	2,56
% leakage	#SAYI/0!	30,28	9,30	#SAYI/0!	31,38	9,43
Core Loss (W)		131	108		132	104
Total Loss (W)	544	621	652	523	624	645
target inductance %	100,00%	-1,60%	-0,45%	100,00%	-2,71%	2,74%

Table B.13 Design parameters of minimum initial cost criterion for 1.2 T

	Design results	iteration 1	iteration 2	Design results	iteration 1	iteration 2	iteration 3
target flux density (T)	1,2	1,2	1,2	1,2	1,2	1,2	1,2
kVAR	46	46	46	46	46	46	46
Voltage (l-l) kV	1,1	1,1	1,1	1,1	1,1	1,1	1,1
Current (A rms)	72,43	72,43	72,43	72,43	72,43	72,43	72,43
L (mH)	27,92	27,92	27,92	27,92	27,92	27,92	27,92
Lleak (%)	5	5	5	20	20	20	20
gap number (G)		2	20		2	20	20
turns number (N)	200	178	202	200	202	210	214
t (mm)	0,2	0,2	0,2	0,2	0,2	0,2	0,2
insulation (mm)	0,15	0,15	0,15	0,15	0,15	0,15	0,15
J (A/mm <sup>2</sup> )	1,4	1,4	1,4	1,4	1,4	1,4	1,4
A (mm <sup>2</sup> )	11930	11930	11930	10040	10040	10040	10040
A_eff (mm <sup>2</sup> )	11453	11453	11453	9638	9638	9638	9638
winding h (mm)	261	261	261	261	261	261	261
l_gap (mm)	22,5	22,5	22,5	22,5	22,5	22,5	22,5
winding thickness (mm)	70	62,3	70,7	70	70,7	73,5	74,9
window (mm)	85	77,3	85,7	85	85,7	88,5	89,9
w (mm)	82,1	82,1	82,1	75,3	75,3	75,3	75,3
d (mm)	139,5	139,5	139,5	128	128	128	128
temperature rise (K)	65			66			
winding clearance (mm)	5	5	5	5	5	5	5
yoke clearance (mm)	20	20	20	20	20	20	20
tube (mm)	5	5	5	5	5	5	5
winding-limb clearance	0	0	0	0	0	0	0
total loss (W)	636			554			
initial cost (Euro)	744			639			
PV Cost (Euro)	4476			4033			
Winding Loss (W)	446	404	450	420	424		446
Simulation results							
Ltotal (mH)		27,55	28,46		28,58	26,00	27,22
Lgap (mH)		18,30	25,64		17,10		24,18
Liron (mH)		1,60	0,24		3,62		0,26
Lleakage (mH)	0,00	7,65	2,58	0,00	7,86	26,00	2,78
% leakage	#####	27,77	9,07	#####	27,50	100,00	10,21
Core Loss (W)		166	136		174		128
Total Loss (W)	446	570	586	420	598	0	574
target inductance %	#####	1,34%	-1,92%	#####	-2,35%	6,89%	2,52%

Table B.14 Design parameters of minimum initial cost criterion for 1.4 T

	Design results	iteration 1	iteration 2	Design results	iteration 1	iteration 2
target flux density (T)	1,4	1,4	1,4	1,4	1,4	1,4
kVAR	46	46	46	46	46	46
Voltage (l-l) kV	1,1	1,1	1,1	1,1	1,1	1,1
Current (A rms)	72,43	72,43	72,43	72,43	72,43	72,43
L (mH)	27,92	27,92	27,92	27,92	27,92	27,92
Lleak (%)	5	5	5	18	18	18
gap number (G)		2	20		2	20
turns number (N)	150	148	152	150	160	164
t (mm)	0,3	0,3	0,3	0,3	0,3	0,3
insulation (mm)	0,15	0,15	0,15	0,15	0,15	0,15
J (A/mm <sup>2</sup> )	1,5	1,5	1,5	1,5	1,5	1,5
A (mm <sup>2</sup> )	13621	13621	13621	11767	11767	11767
A_eff (mm <sup>2</sup> )	13076	13076	13076	11296	11296	11296
winding h (mm)	162	162	162	162	162	162
l_gap (mm)	14,5	14,5	14,5	14,5	14,5	14,5
winding thickness (mm)	67,5	66,6	68,4	67,5	72	73,8
window (mm)	82,5	81,6	83,4	82,5	87	88,8
w (mm)	87,7	87,7	87,7	81,5	81,5	81,5
d (mm)	149,1	149,1	149,1	138,6	138,6	138,6
temperature rise (K)	64			65	65	65
winding clearance (mm)	5	5	5	5	5	5
yoke clearance (mm)	20	20	20	20	20	20
tube (mm)	5	5	5	5	5	5
winding-limb clearance	0	0	0	0	0	0
total loss (W)	620			523		
initial cost (Euro)	663			575		
PV Cost (Euro)	4210			3803		
Winding Loss (W)	373	369	377	354	374	383
Simulation results						
Ltotal (mH)		28,36	27,32		27,56	27,23
Lgap (mH)		19,96	25,25		18,19	25,00
Liron (mH)		0,31	0,46		4,21	0,86
Lleakage (mH)	0,00	8,09	1,61	0,00	5,16	1,37
% leakage	#SAYI/0!	28,53	5,89	#SAYI/0!	18,72	5,03
Core Loss (W)		200	168		189	163
Total Loss (W)	373	569	545	354	563	546
target inductance %	100,00%	-1,56%	2,16%	100,00%	1,30%	2,49%

Table B.15 Selected Design Parameters from iterations given for minimum initial cost criterion

G=2 / High Leakage							
				maxwell	matlab		
B <sub>m</sub> (T)	Total loss	Int. Cost	PV Cost	Core loss	Winding loss	N/t	L <sub>s</sub> (mH)
0,8	653	851	4854	91	562	186/0,3	28,63
1	624	732	4557	132	492	186/0,2	28,68
1,2	598	639	4305	174	424	202/0,2	28,58
1,4	563	575	4026	189	374	160/0,3	27,56

a)

G=2 / Low Leakage							
				maxwell	matlab		
B <sub>m</sub> (T)	Total loss	Int. Cost	PV Cost	Core loss	Winding loss	N/t	L <sub>s</sub> (mH)
0,8	649	947	4925	90	559	176/0,3	28,1
1	621	813	4620	131	490	176/0,2	28,37
1,2	570	744	4238	166	404	178/0,2	27,55
1,4	569	663	4151	200	369	148/0,3	28,36

b)

G=20 / High Leakage							
				maxwell	matlab		
B <sub>m</sub> (T)	Total loss	Int. Cost	PV Cost	Core loss	Winding loss	N/t	L <sub>s</sub> (mH)
0,8	698	851	5130	77	621	208/0,3	27,66
1	645	732	4686	104	541	208/0,2	27,16
1,2	574	639	4157	128	446	214/0,2	27,22
1,4	546	575	3922	163	383	164/0,3	27,23

c)

G=20 / Low Leakage							
				maxwell	matlab		
B <sub>m</sub> (T)	Total loss	Int. Cost	PV Cost	Core loss	Winding loss	N/t	L <sub>s</sub> (mH)
0,8	705	947	5268	81	624	200/0,3	28,32
1	652	813	4810	108	544	200/0,2	28,05
1,2	586	744	4336	136	450	202/0,2	28,46
1,4	545	663	4004	168	377	152/0,3	27,32

d)

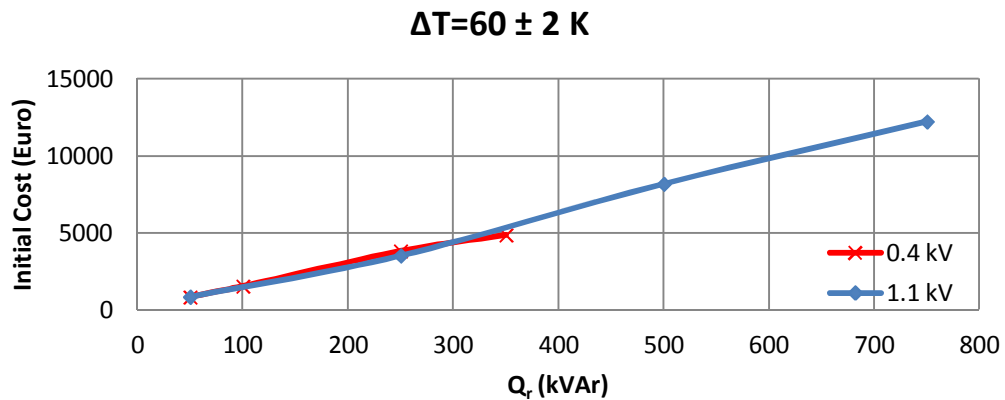
## APPENDIX C

### VARIOUS SHUNT REACTOR DESIGNS OPTIMIZED ACCORDING TO MINIMUM PVC DESIGN OBJECTIVE

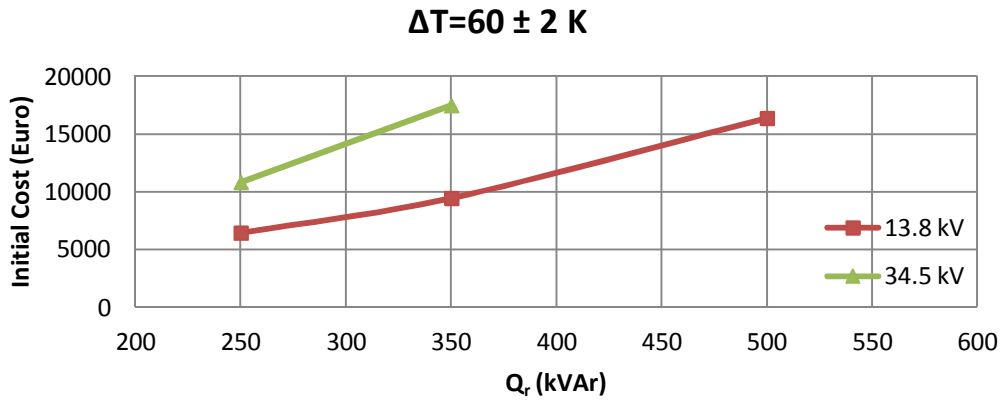
Characteristic curves presented in this section are obtained by the aid of FEA as described in Chapter 3. The associated variations in percentage leakage inductances for these optimum reactors against  $Q_r$  are already given in Figs.4.2-4.8 in Chapter 4. The practical design approach described in Chapter 4 is based on those percentage leakage inductance variations. Other design details of these reactors are given in this Appendix section.

#### C.1 Variations in Parameters Against kVAr Rating of the Reactor

The resulting initial cost variations against kVAr rating of the reactor under design and in terms of temperature rise above the ambient are given in Figs.C.1-C.3.

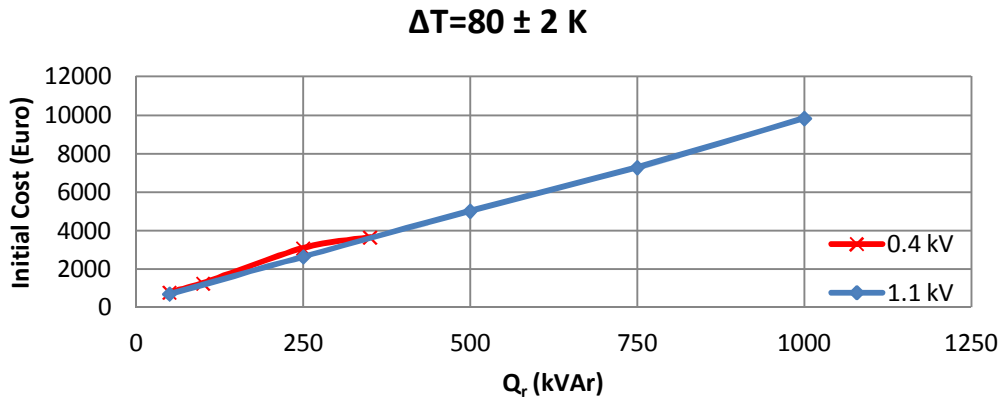


- a) Initial Cost variations against kVAr rating of the reactor for 60 K temperature rise above the ambient (low voltage)

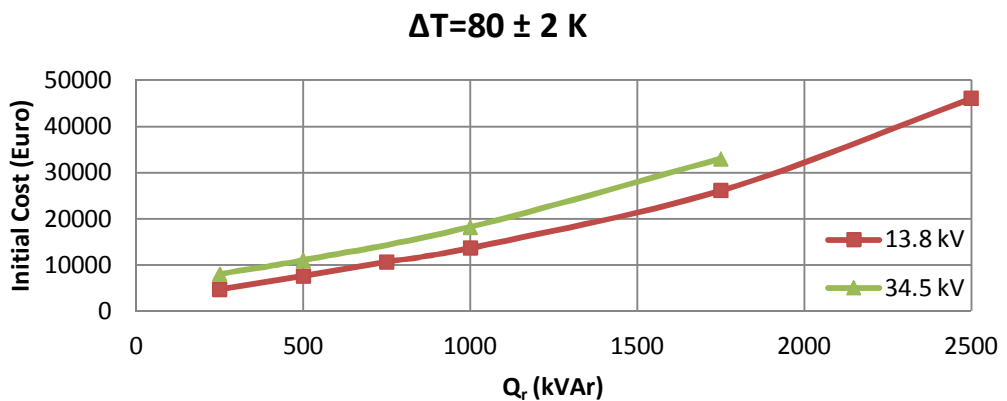


b) Initial Cost variations against kVAr rating of the reactor for 60 K temperature rise above the ambient (medium voltage)

Figure C.1 Initial Cost variations against kVAr rating of the reactor for 60 K temperature rise above the ambient



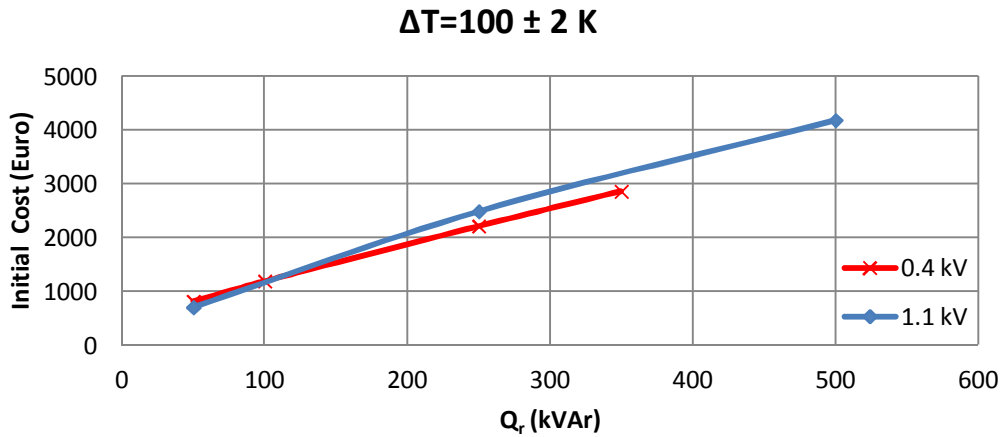
a) Initial Cost variations against kVAr rating of the reactor for 80 K temperature rise above the ambient (low voltage)



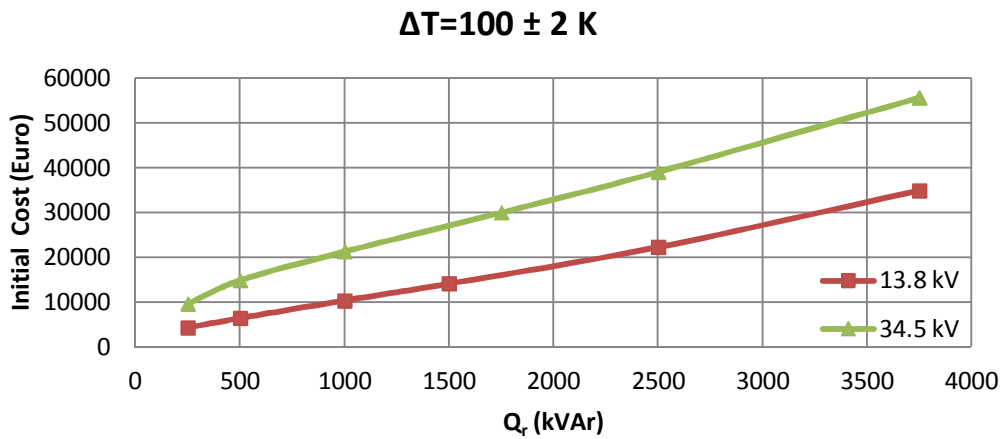
b) Initial Cost variations against kVAr rating of the reactor for 80 K temperature rise above the ambient (medium voltage)

Figure C.2 Initial Cost variations against kVAr rating of the reactor for 80 K temperature rise above the ambient





a) Initial Cost variations against kVAr rating of the reactor for 100 K temperature rise above the ambient (low voltage)



b) Initial Cost variations against kVAr rating of the reactor for 100 K temperature rise above the ambient (medium voltage)

Figure C.3 Initial Cost variations against kVAr rating of the reactor for 100 K temperature rise above the ambient

Following conclusions can be drawn from the results of Figs.C.1-C.3;

- For 0.4 and 1.1 kV operating voltage levels, initial cost of the reactor is very close for all power ratings.
- The initial cost increases with increasing power rating for all operating voltage levels.

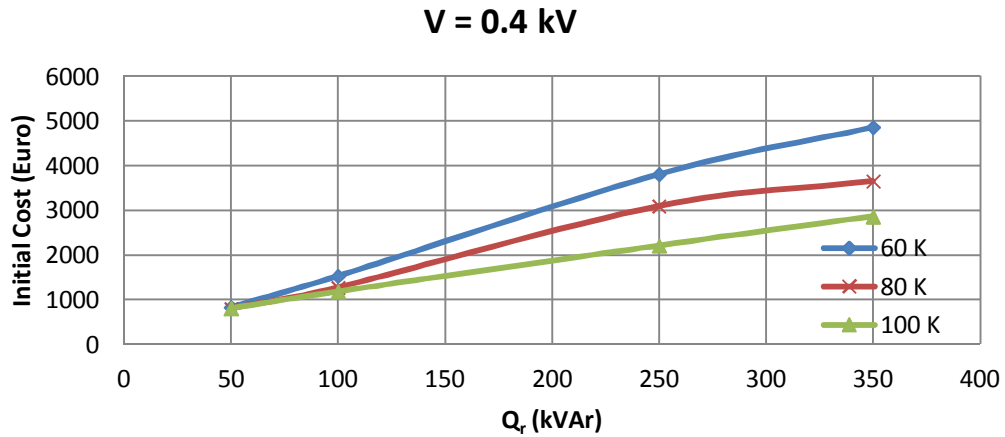


Figure C.4 Initial Cost variations against kVAr rating of the reactor for 0.4 kV operating voltage

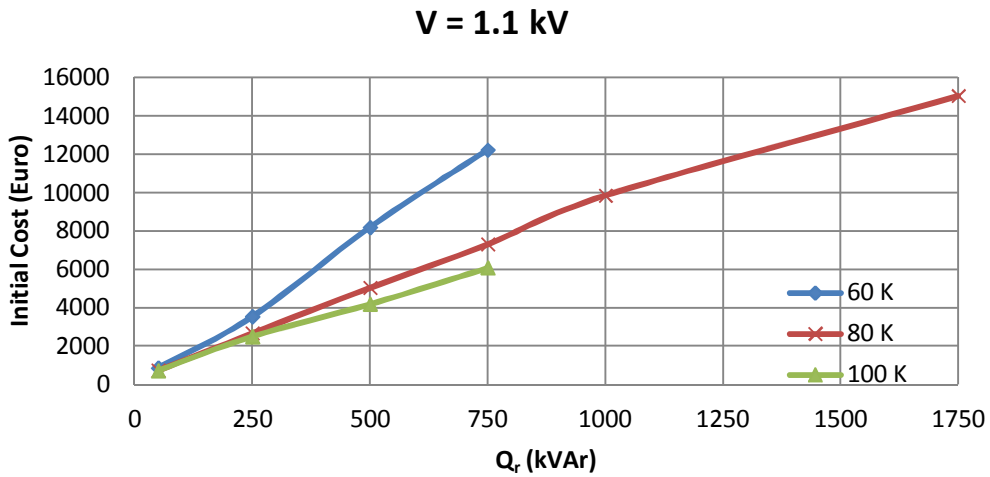


Figure C.5 Initial Cost variations against kVAr rating of the reactor for 1.1 kV operating voltage

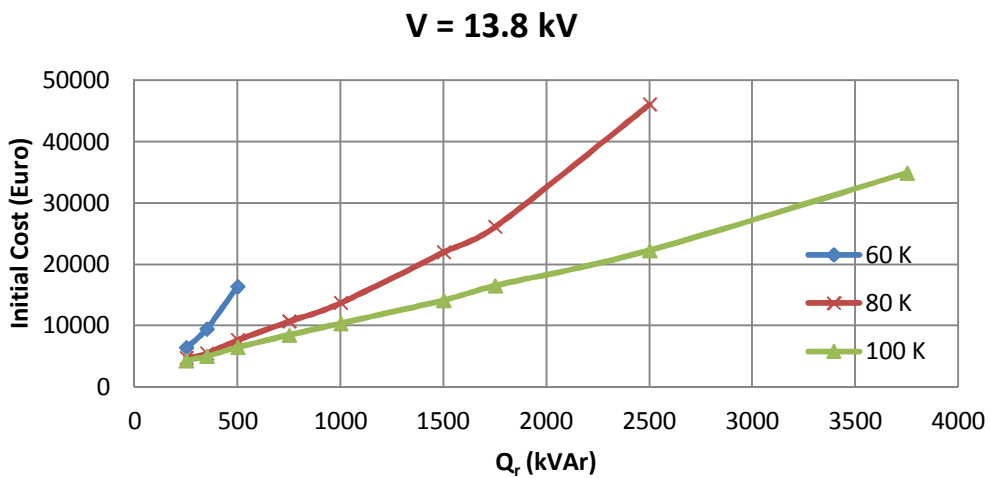


Figure C.6 Initial Cost variations against kVAr rating of the reactor for 13.8 kV operating voltage

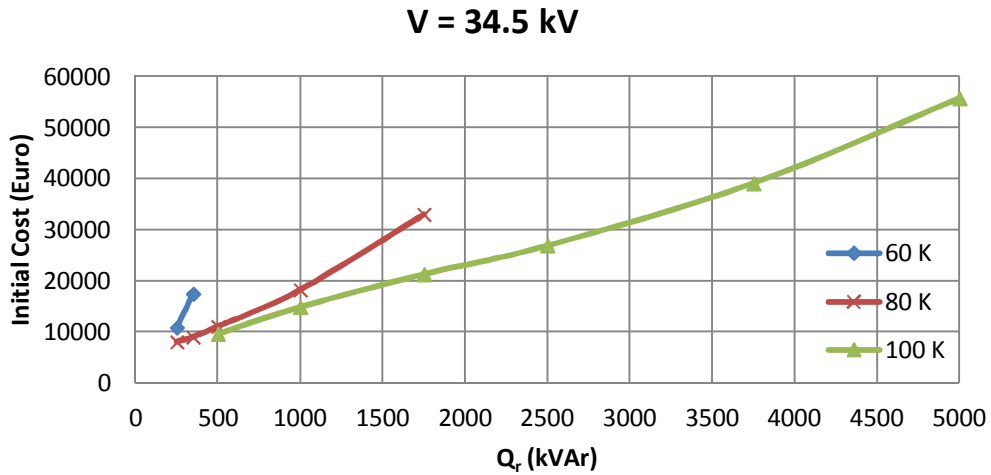
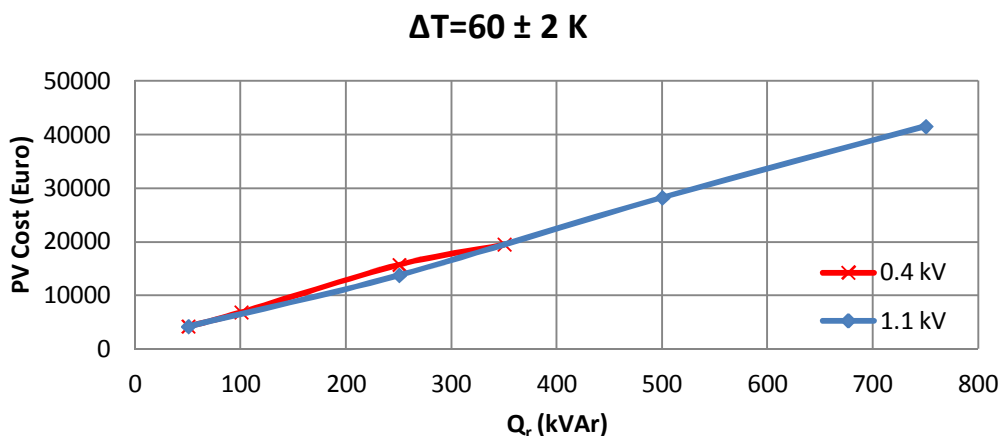


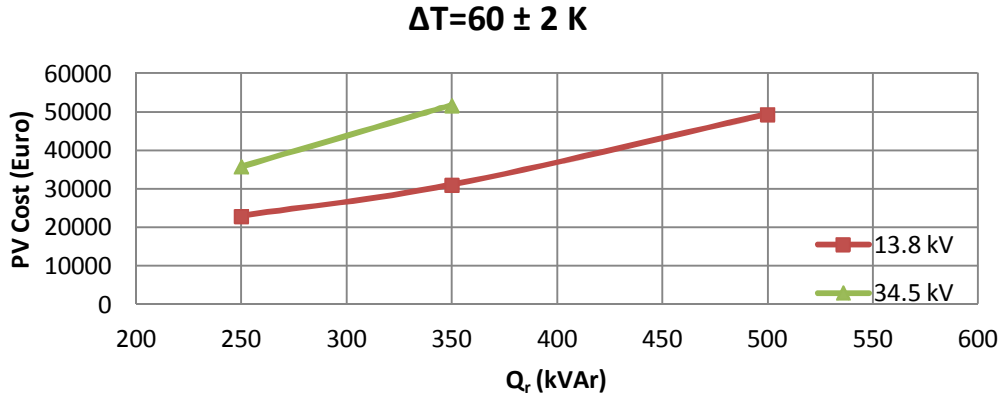
Figure C.7 Initial Cost variations against kVAr rating of the reactor for 34.5 kV operating voltage

The variations in initial cost against kVAr rating of the reactor under design and in terms of operating voltage levels are given in Figs.C.4-C.7. The initial costs of the reactor for all temperature classes are very close at low power rating. As the power rating increases the initial cost of the reactor designed for 60 K becomes highest whereas those of for 100 K becomes lowest for all power ratings. The initial cost increases as the power rating increases for all temperature classes.

The variations in present value cost against kVAr rating of the reactor under design and in terms of temperature rise above the ambient are given in Figs.C.8-C.10.

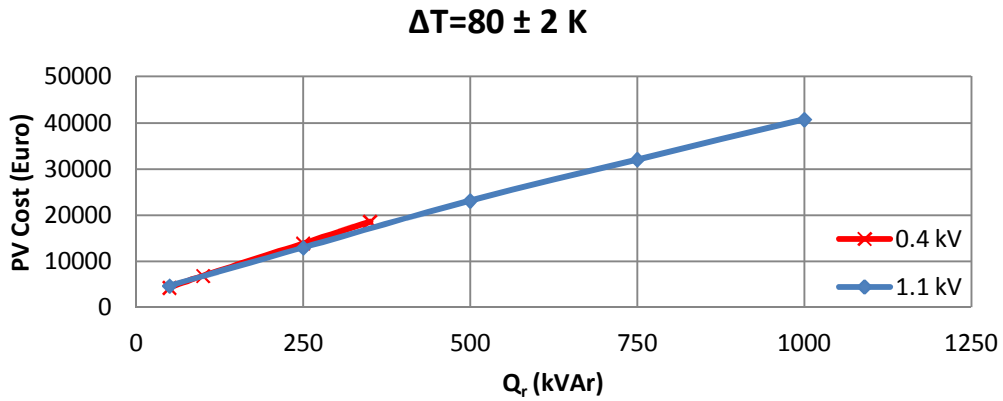


a) Present Value Cost variations against kVAr rating of the reactor for 60 K temperature rise above the ambient (low voltage)

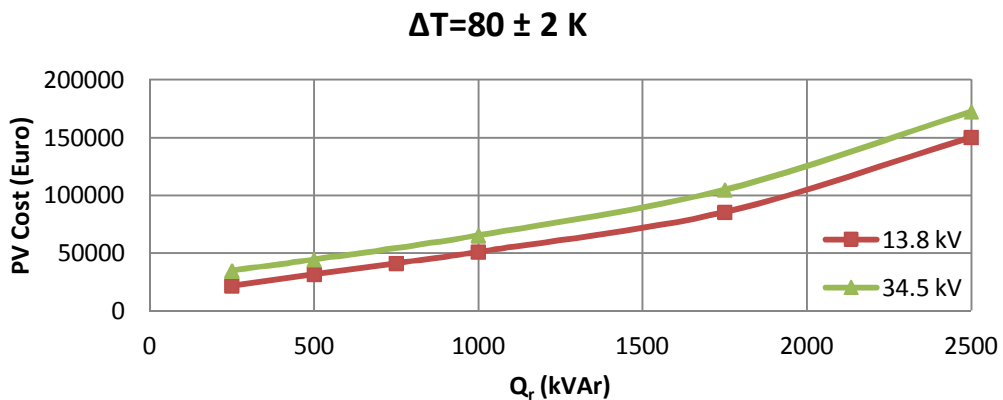


b) Present Value Cost variations against kVAr rating of the reactor for 60 K temperature rise above the ambient (medium voltage)

Figure C.8 Present Value Cost variations against kVAr rating of the reactor for 60 K temperature rise above the ambient

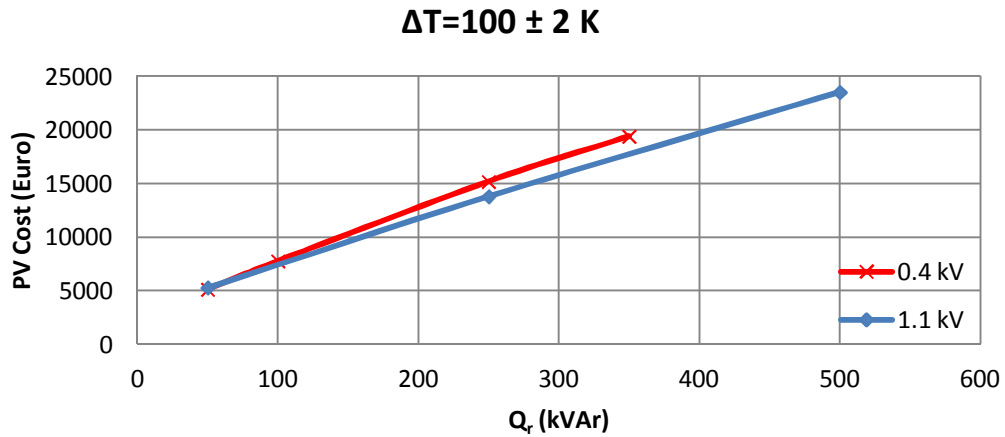


a) Present Value Cost variations against kVAr rating of the reactor for 80 K temperature rise above the ambient (low voltage)

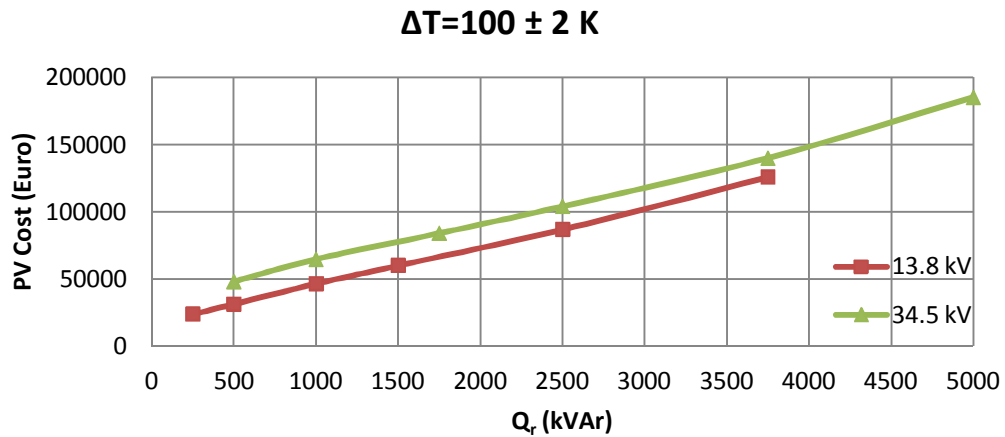


b) Present Value Cost variations against kVAr rating of the reactor for 80 K temperature rise above the ambient (medium voltage)

Figure C.9 Present Value Cost variations against kVAr rating of the reactor for 80 K temperature rise above the ambient



a) Present Value Cost variations against kVAr rating of the reactor for 100 K temperature rise above the ambient (low voltage)



b) Present Value Cost variations against kVAr rating of the reactor for 100 K temperature rise above the ambient (medium voltage)

Figure C.10 Present Value Cost variations against kVAr rating of the reactor for 100 K temperature rise above the ambient

Following conclusions can be drawn from the results of Figs.C.8-C.10;

- Present value cost of the reactor under design increases as the power rating of the reactor increases for all operating voltage levels..
- For 0.4 and 1.1 kV operating voltage levels, present value cost of the reactor is very close for all power ratings.
- The present value costs of the reactors designed at 13.8 kV operating voltage are lower than those of at 34.5 kV.

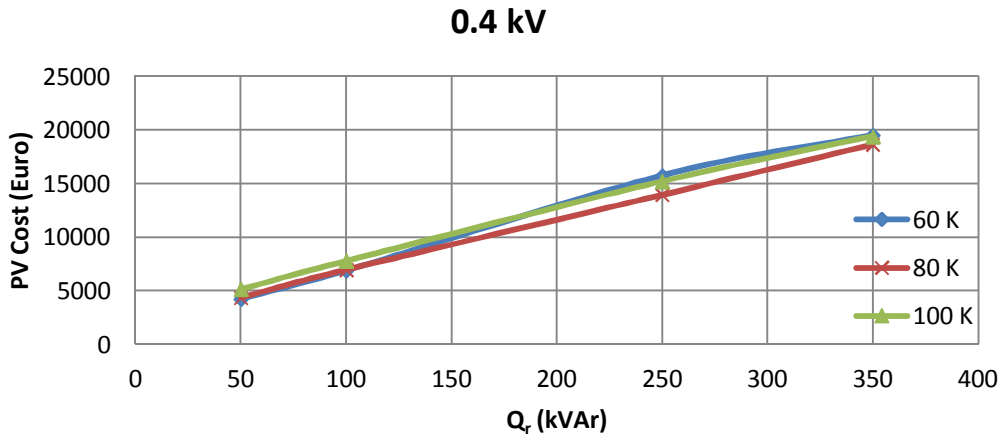


Figure C.11 Present Value Cost variations against kVAr rating of the reactor for 0.4 kV operating voltage

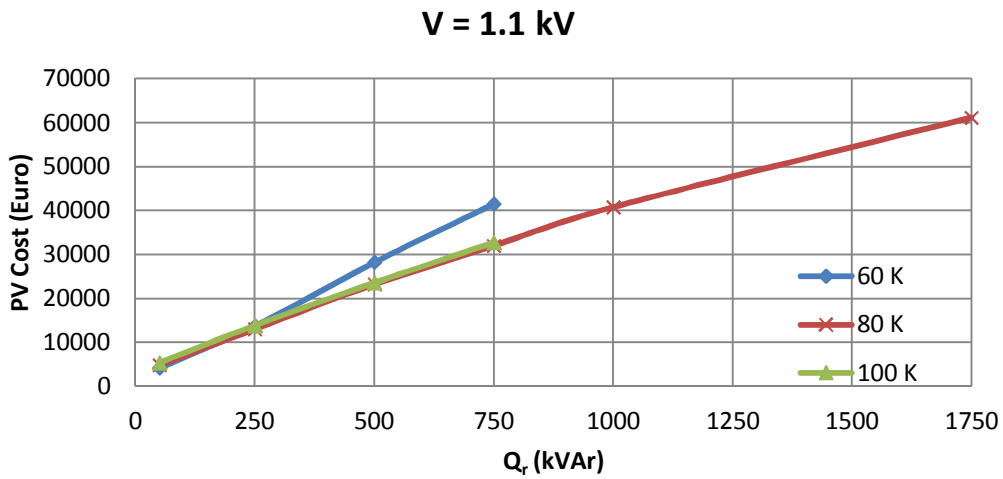


Figure C.12 Present Value Cost variations against kVAr rating of the reactor for 1.1 kV operating voltage

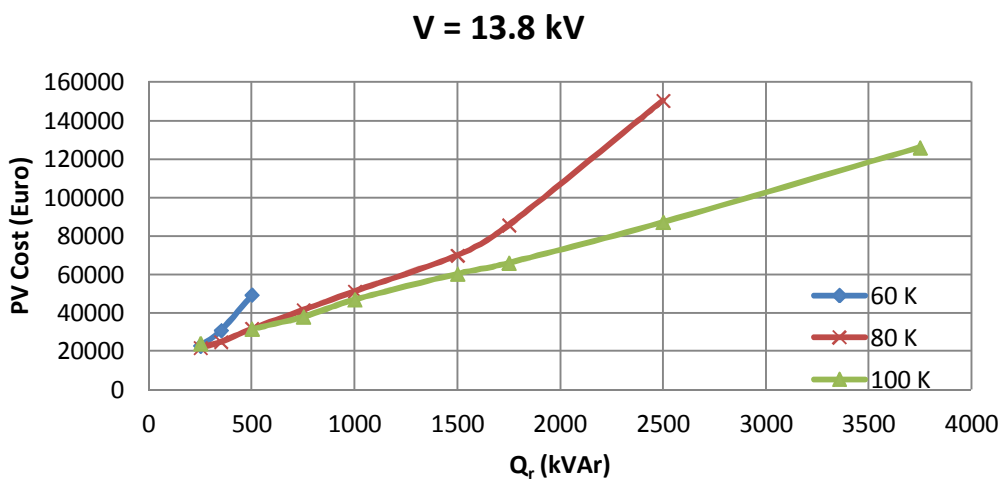


Figure C.13 Present Value Cost variations against kVAr rating of the reactor for 13.8 kV operating voltage

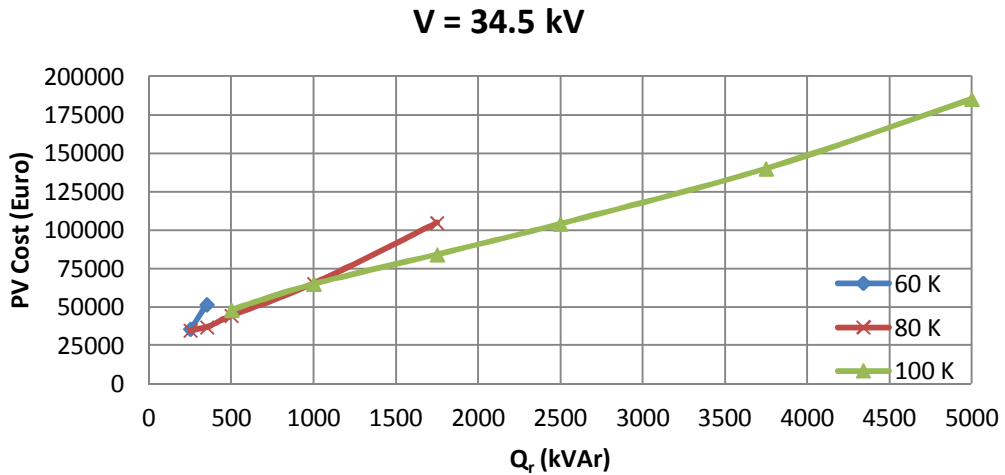


Figure C.14 Present Value Cost variations against kVAr rating of the reactor for 34.5 kV operating voltage

The variations in present value cost against kVAr rating of the reactor under design and in terms of operating voltage levels are given in Figs.C.11-V.14. The present value cost of the reactor for all temperature classes is very close at low power rating. As the power rating increases the present value cost of the reactor designed for 60 K becomes highest whereas those of for 100 K becomes lowest for all power ratings. Although the present value cost at 80 K and 100 K temperature classes are very close for low power ratings, as the power rating increases the cost at 80 K increases much more than the cost at 100 K. The present value cost increases as the power rating increases for all temperature classes.

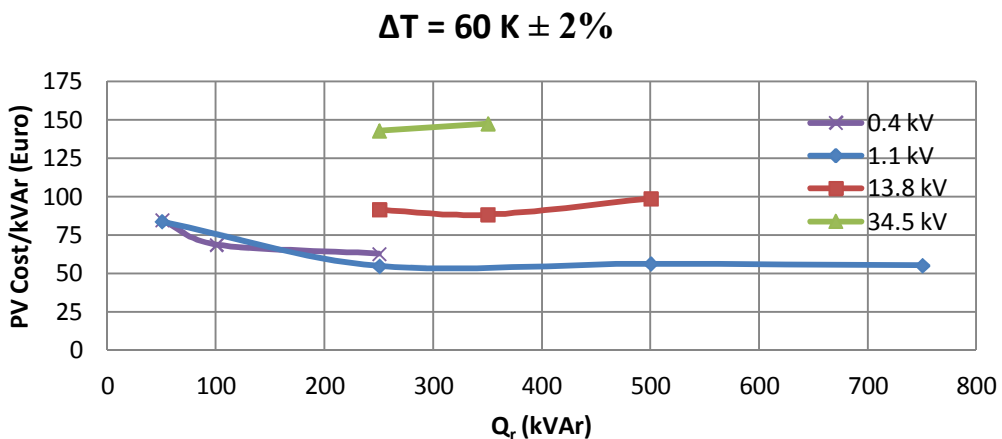


Figure C.15 PV Cost/kVAr variations against kVAr rating of the reactor for 60 K temperature rise above the ambient

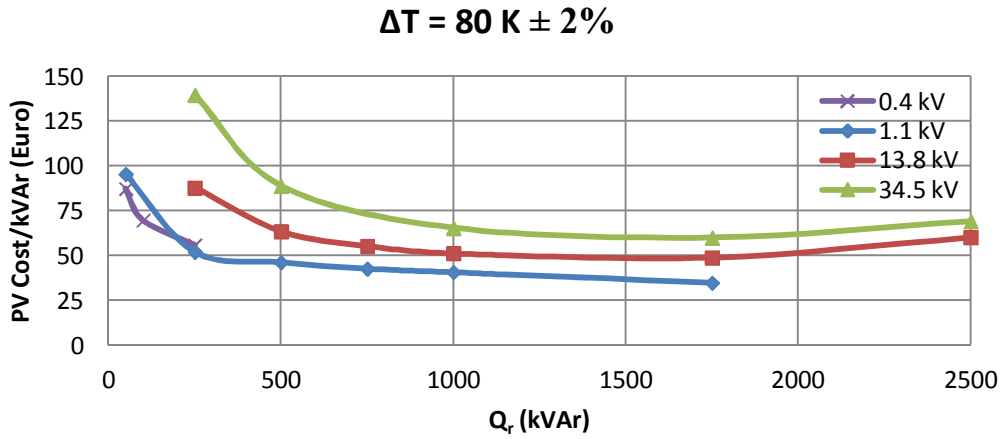


Figure C.16 PV Cost/kVAr variations against kVAr rating of the reactor for 80 K temperature rise above the ambient

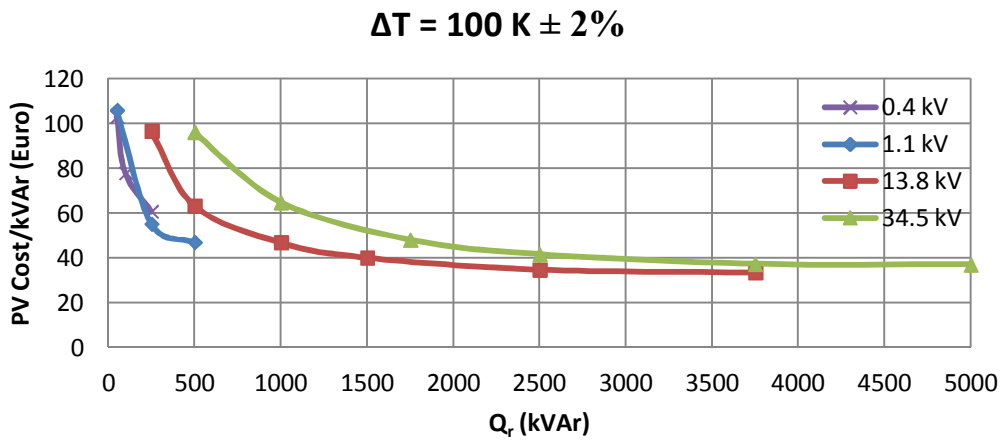


Figure C.17 PV Cost/kVAr variations against kVAr rating of the reactor for 100 K temperature rise above the ambient

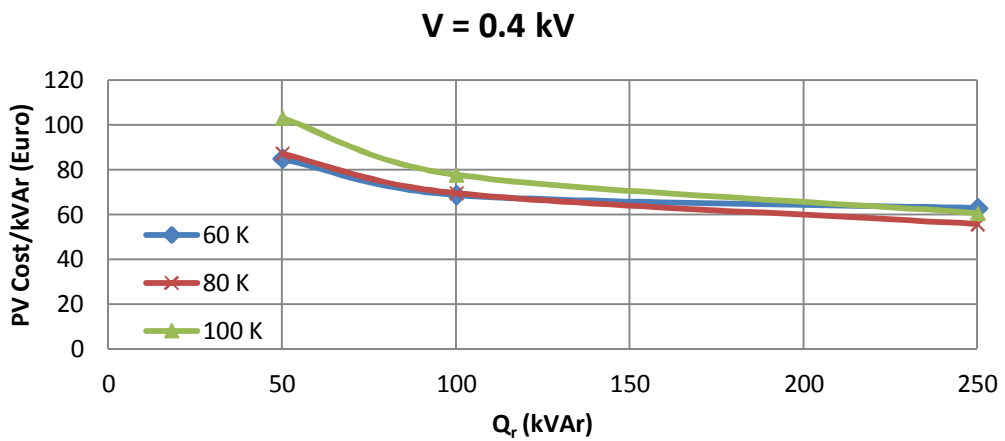


Figure C.18 PV Cost/kVAr variations against kVAr rating of the reactor for 0.4 kV operating voltage



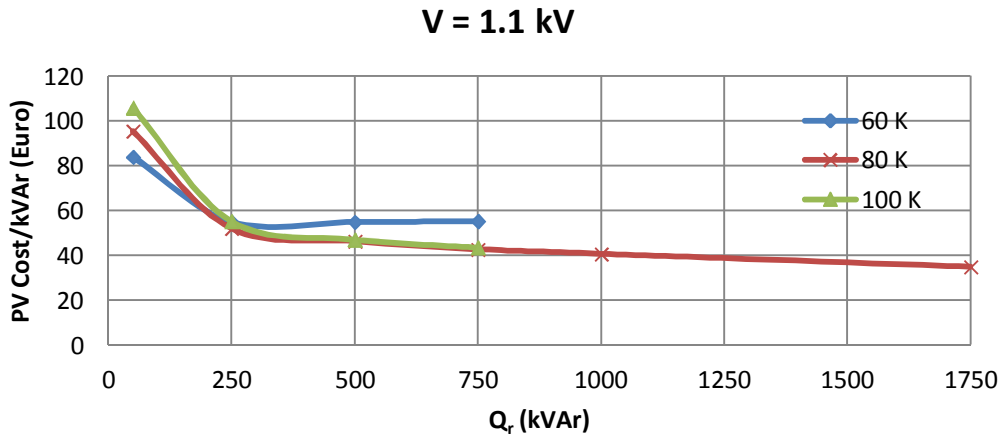


Figure C.19 PV Cost/kVAr variations against kVAr rating of the reactor for 1.1 kV operating voltage

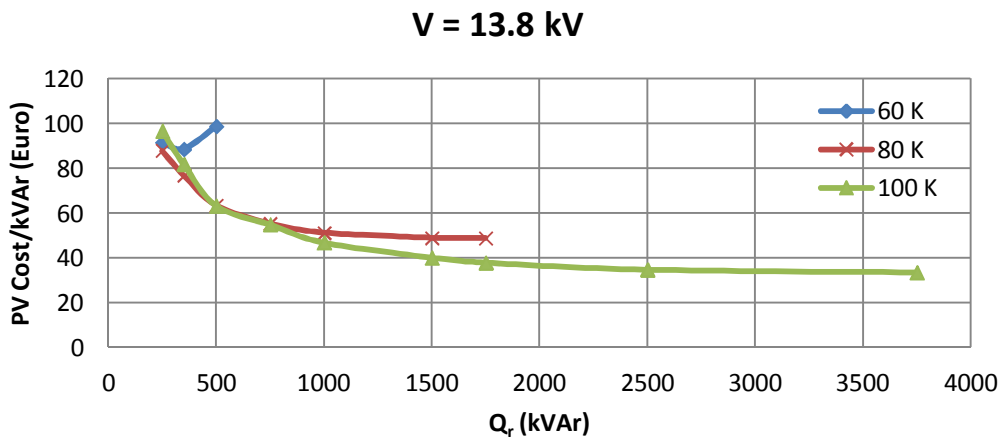


Figure C.20 PV Cost/kVAr variations against kVAr rating of the reactor for 13.8 kV operating voltage

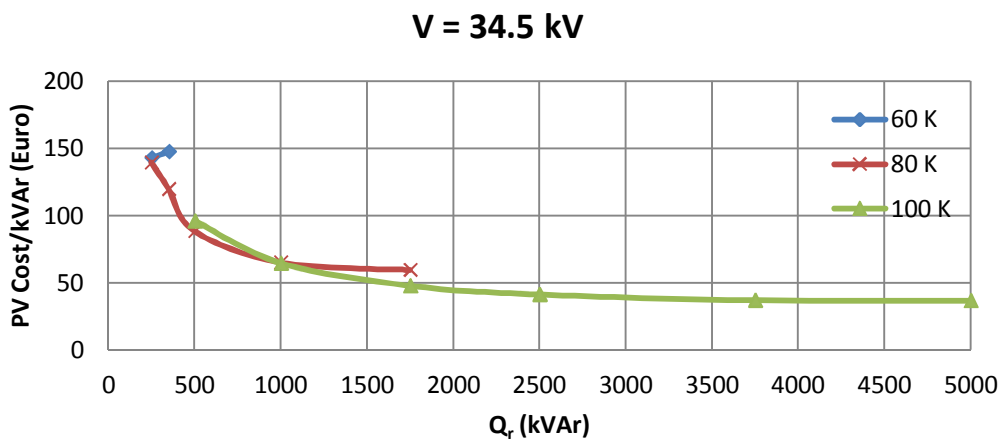


Figure C.21 PV Cost/kVAr variations against kVAr rating of the reactor for 34.5 kV operating voltage

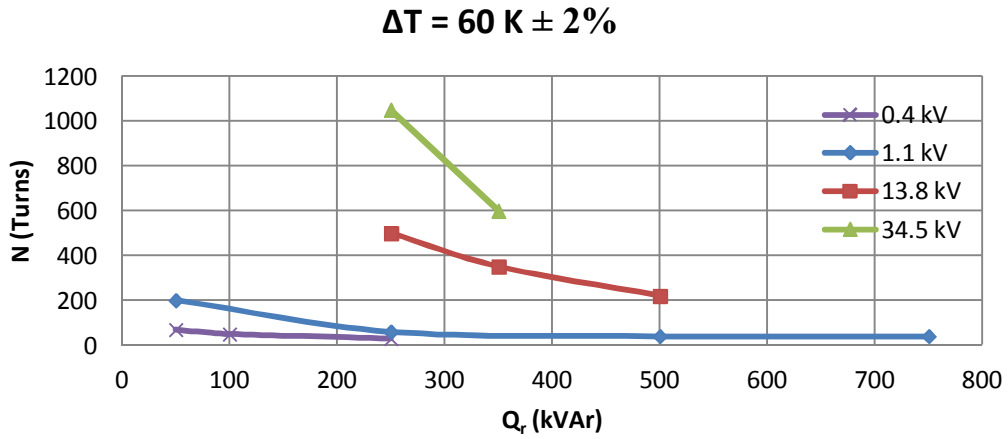


Figure C.22 Number of turns variations against kVAr rating of the reactor for 60 K temperature rise above the ambient

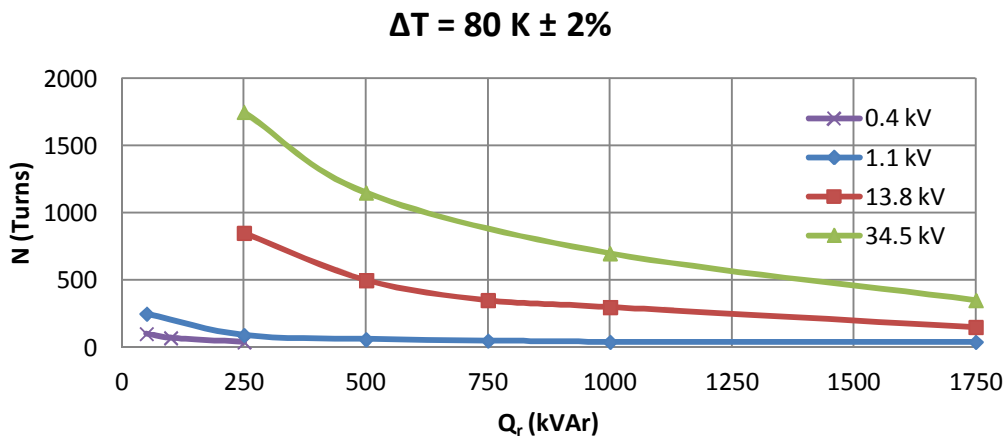


Figure C.23 Number of turns variations against kVAr rating of the reactor for 80 K temperature rise above the ambient

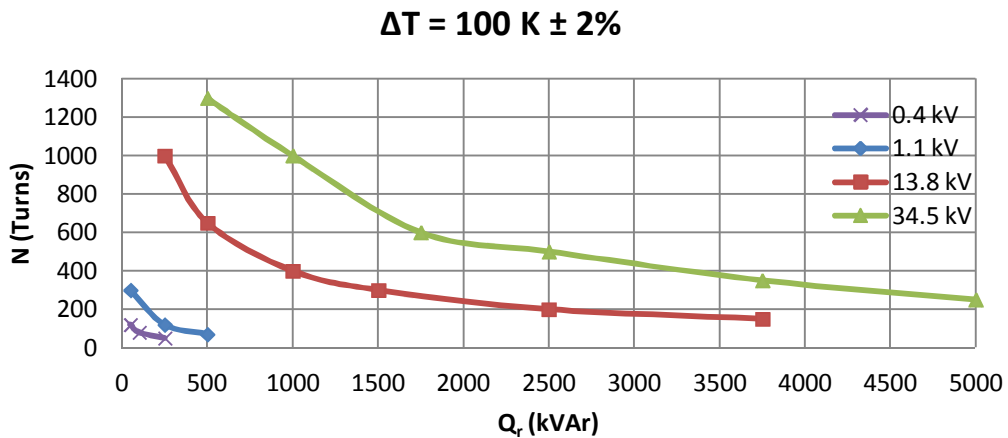


Figure C.24 Number of turns variations against kVAr rating of the reactor for 100 K temperature rise above the ambient

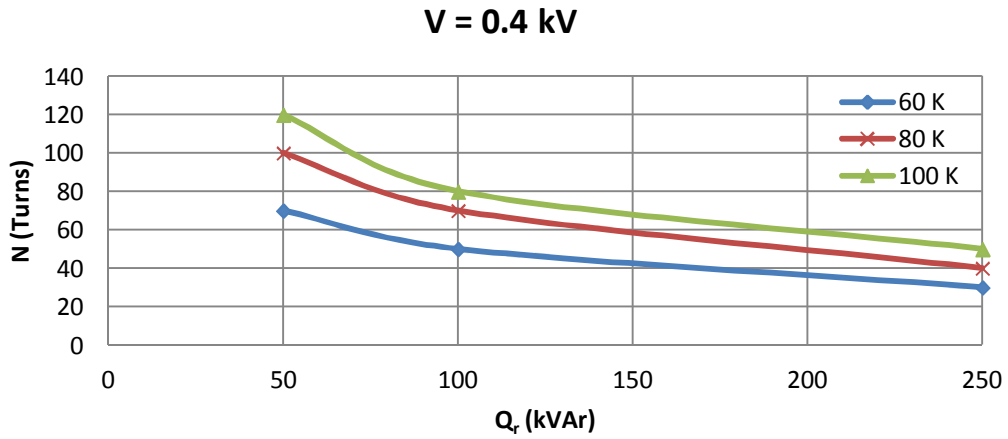


Figure C.25 Number of turns variations against kVAr rating of the reactor for 0.4 kV operating voltage

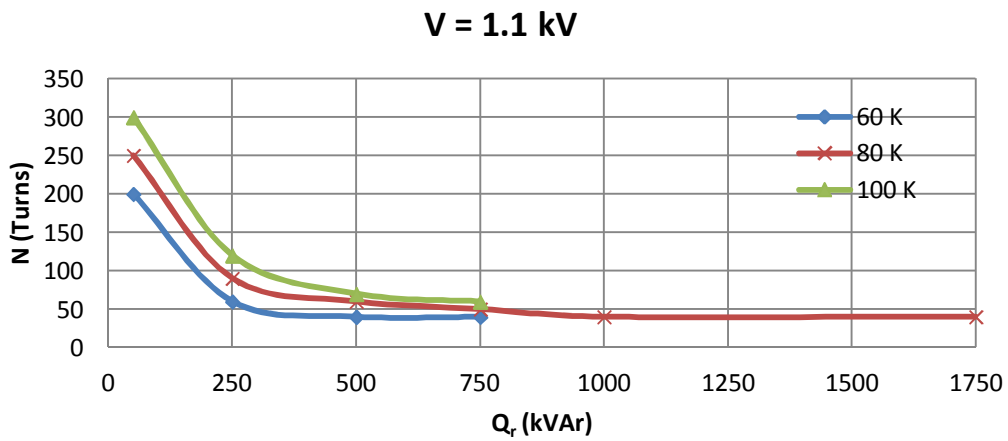


Figure C.26 Number of turns variations against kVAr rating of the reactor for 1.1 kV operating voltage

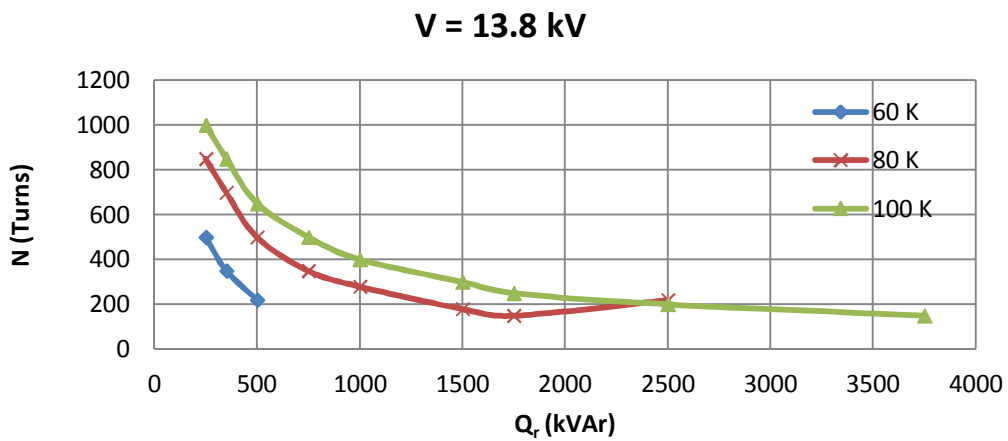


Figure C.27 Number of turns variations against kVAr rating of the reactor for 13.8 kV operating voltage

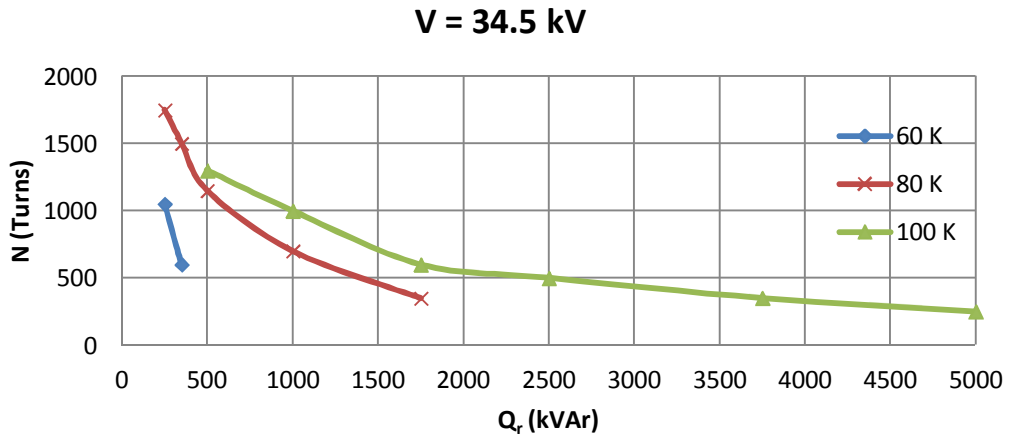


Figure C.28 Number of turns variations against kVAr rating of the reactor for 34.5 kV operating voltage

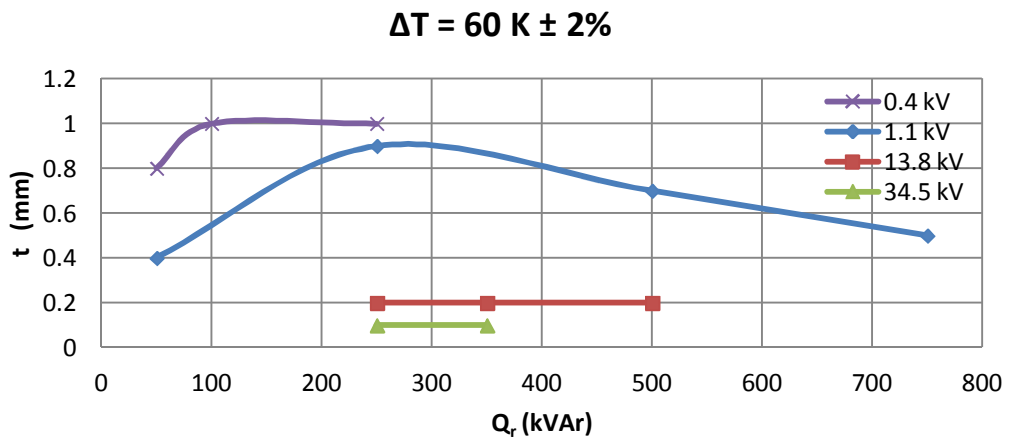


Figure C.29 Foil thickness variations against kVAr rating of the reactor for 60 K temperature rise above the ambient

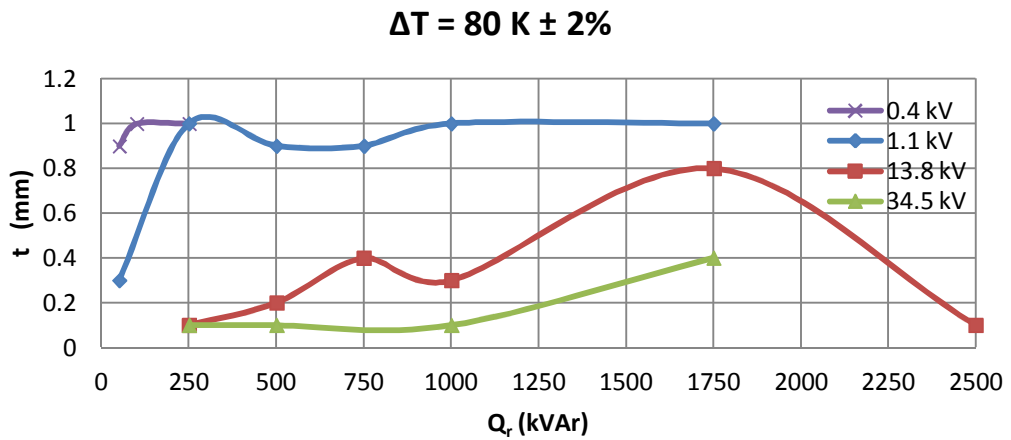


Figure C.30 Foil thickness variations against kVAr rating of the reactor for 80 K temperature rise above the ambient

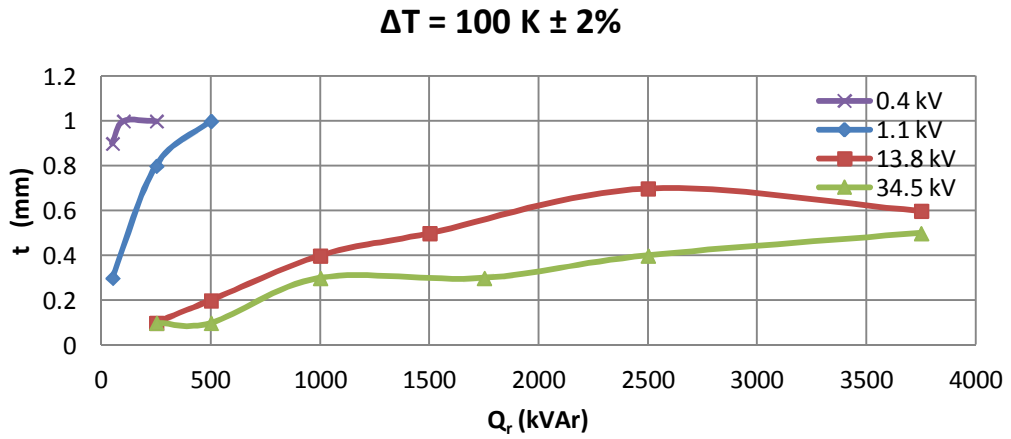


Figure C.31 Foil thickness variations against kVAr rating of the reactor for 100 K temperature rise above the ambient

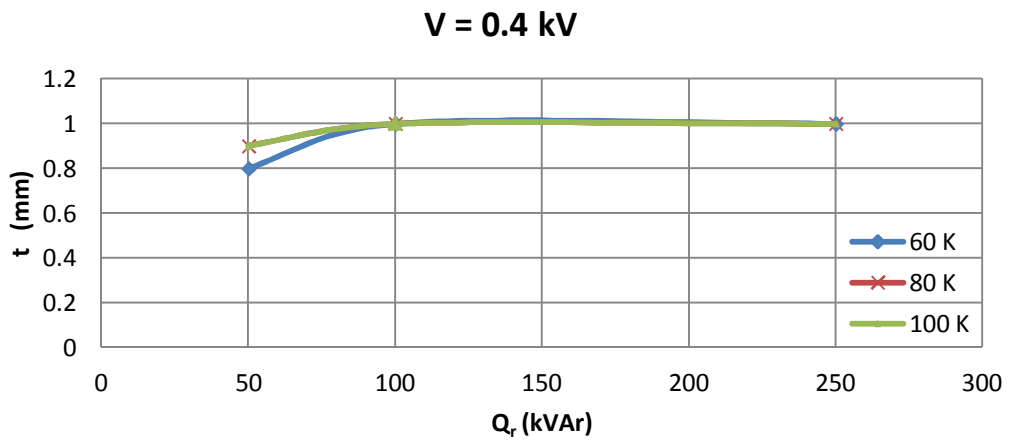


Figure C.32 Foil thickness variations against kVAr rating of the reactor for 0.4 kV operating voltage

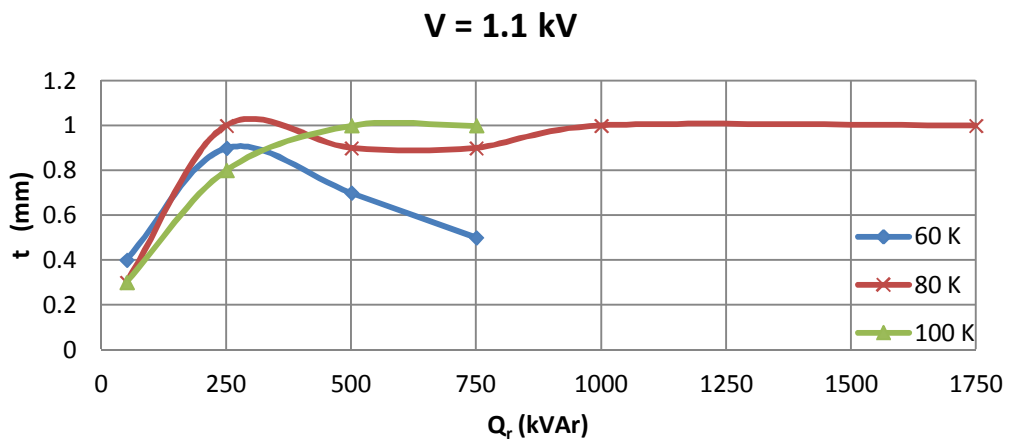


Figure C.33 Foil thickness variations against kVAr rating of the reactor for 1.1 kV operating voltage

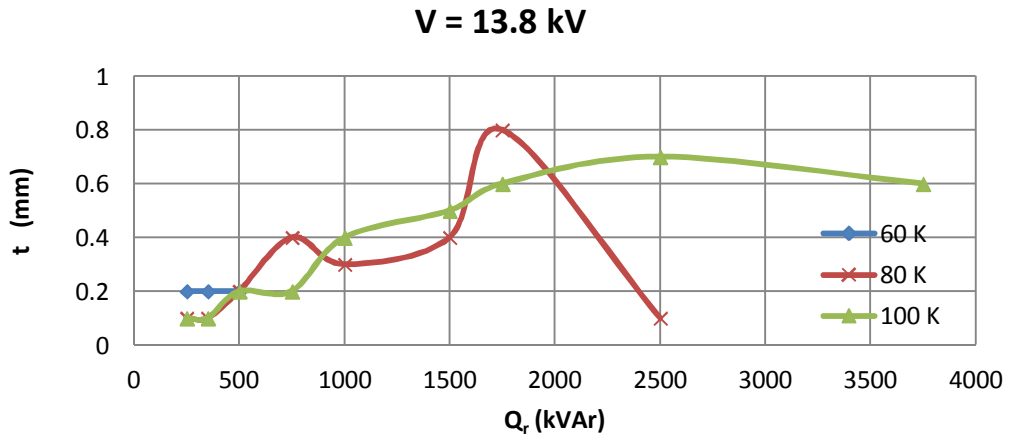


Figure C.34 Foil thickness variations against kVAr rating of the reactor for 13.8 kV operating voltage

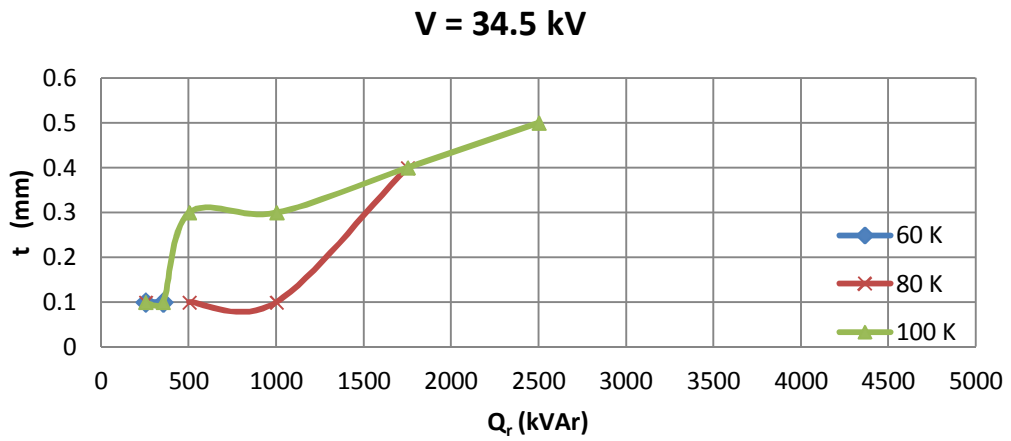


Figure C.35 Foil thickness variations against kVAr rating of the reactor for 34.5 kV operating voltage

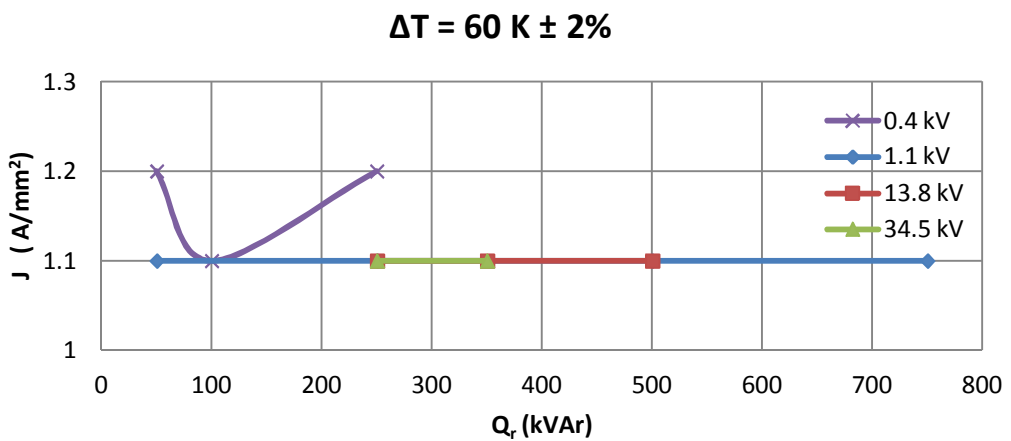


Figure C.36 Current density variations against kVAr rating of the reactor for 60 K temperature rise above the ambient

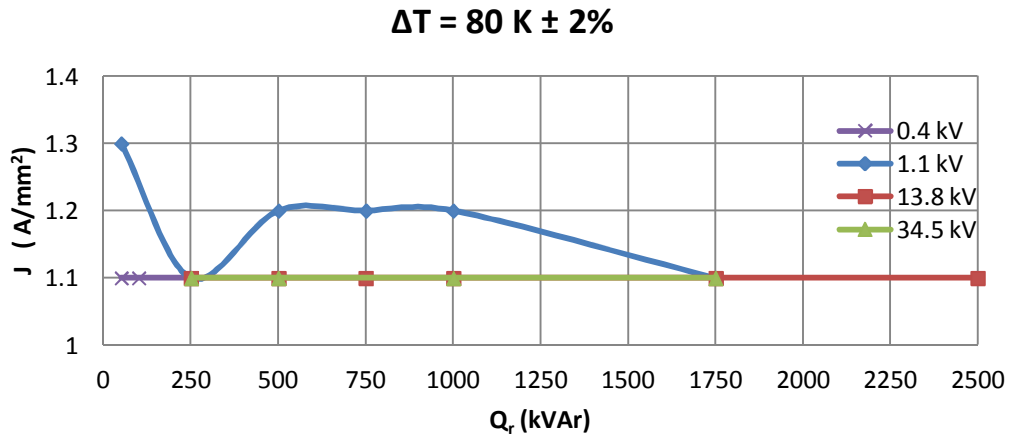


Figure C.37 Current density variations against kVAr rating of the reactor for 80 K temperature rise above the ambient

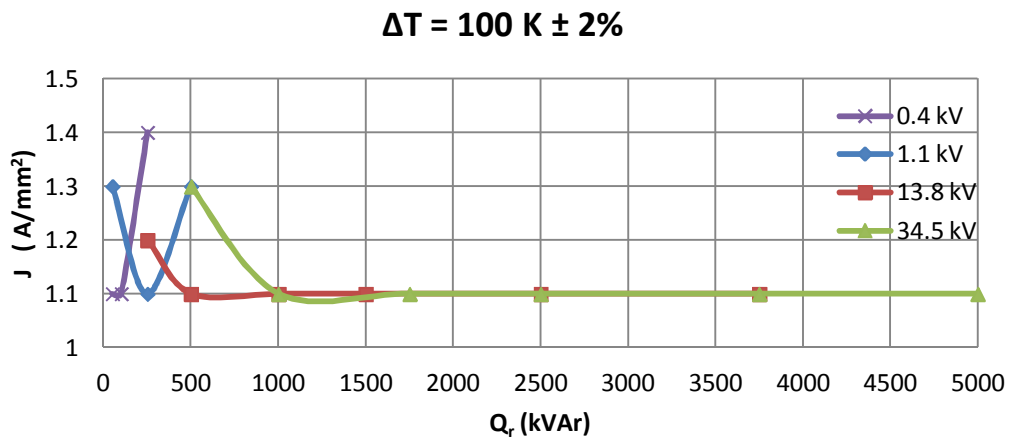


Figure C.38 Current density variations against kVAr rating of the reactor for 100 K temperature rise above the ambient

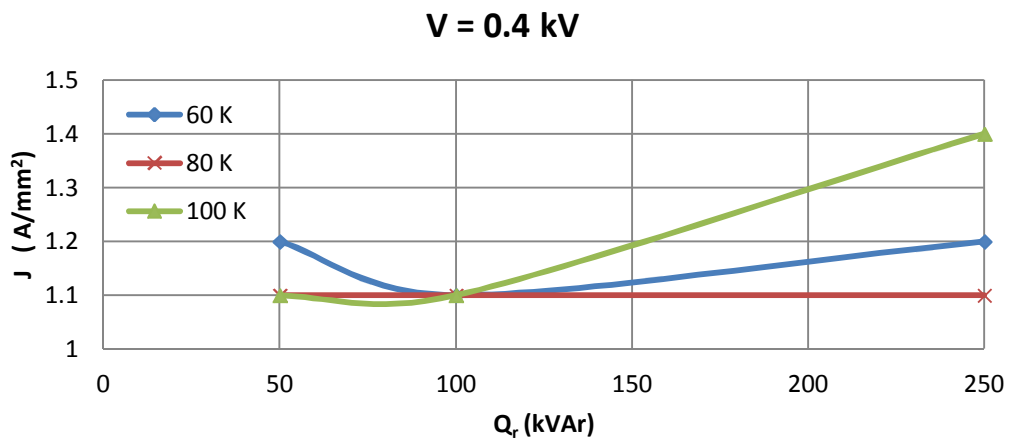


Figure C.39 Current density variations against kVAr rating of the reactor for 0.4 kV operating voltage

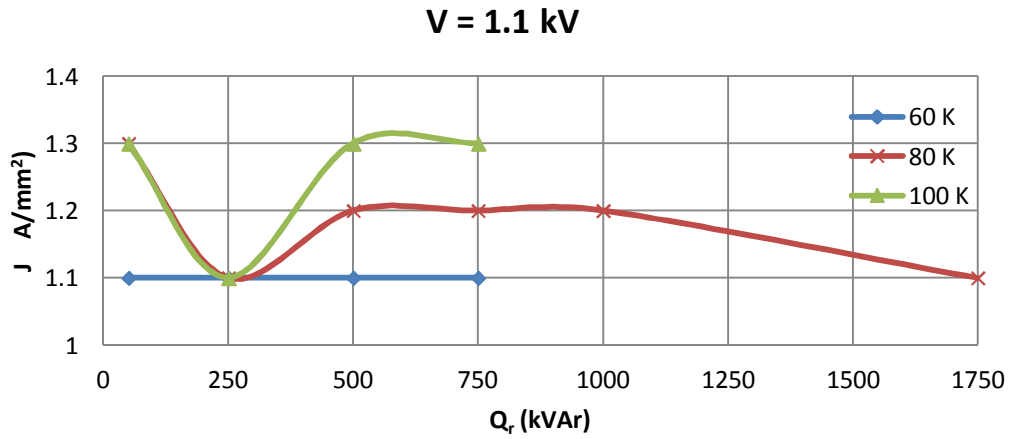


Figure C.40 Current density variations against kVAr rating of the reactor for 1.1 kV operating voltage

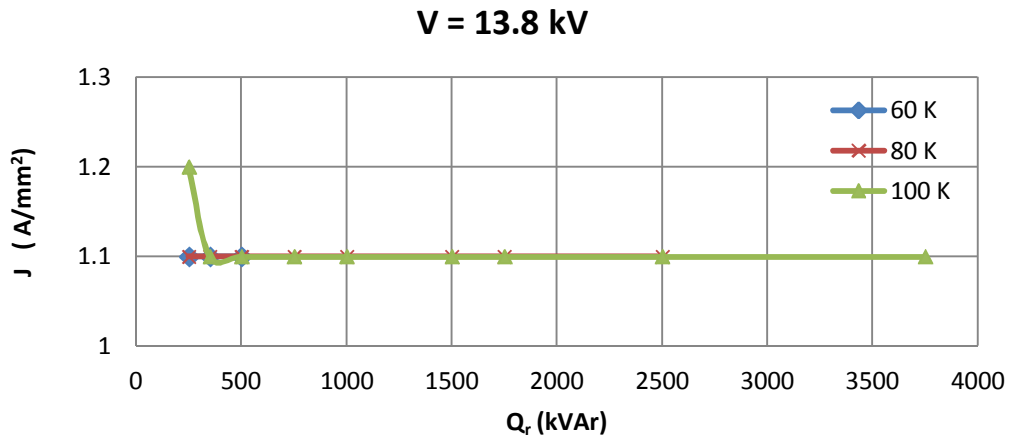


Figure C.41 Current density variations against kVAr rating of the reactor for 13.8 kV operating voltage

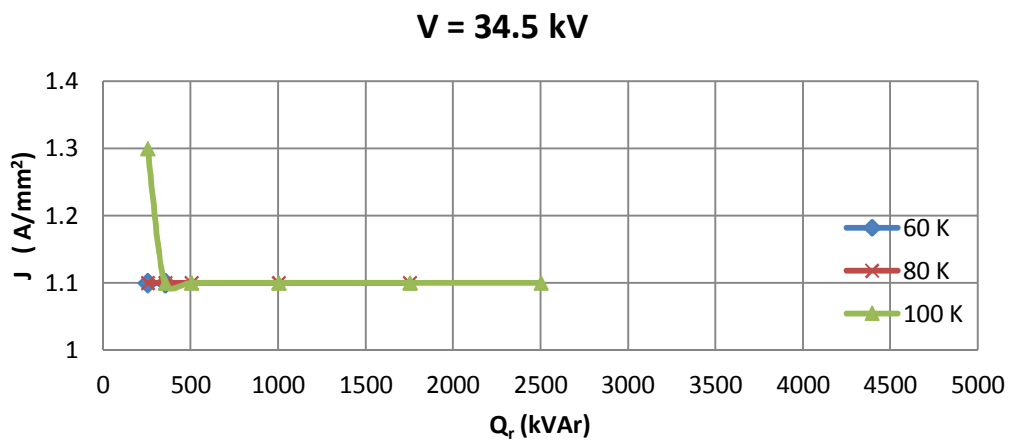


Figure C.42 Current density variations against kVAr rating of the reactor for 34.5 kV operating voltage



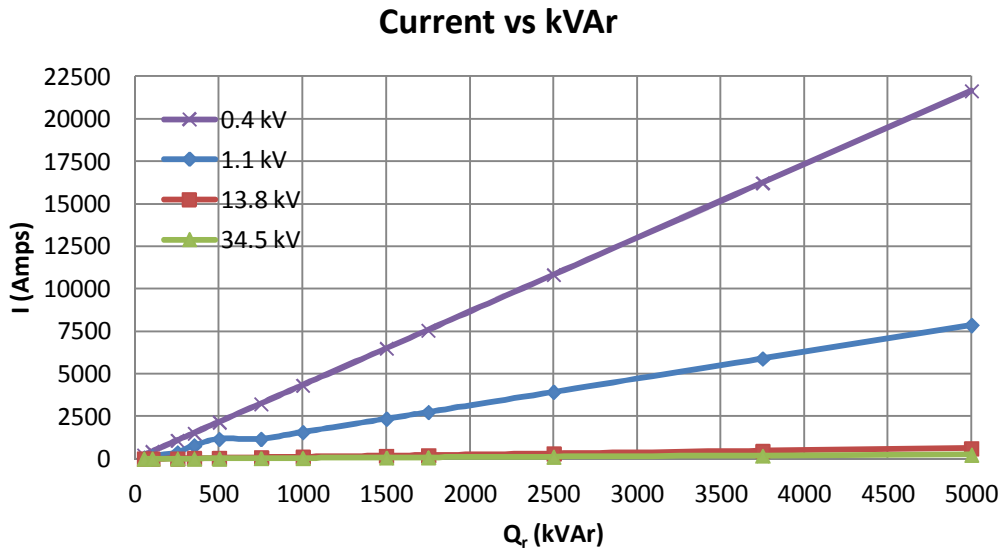
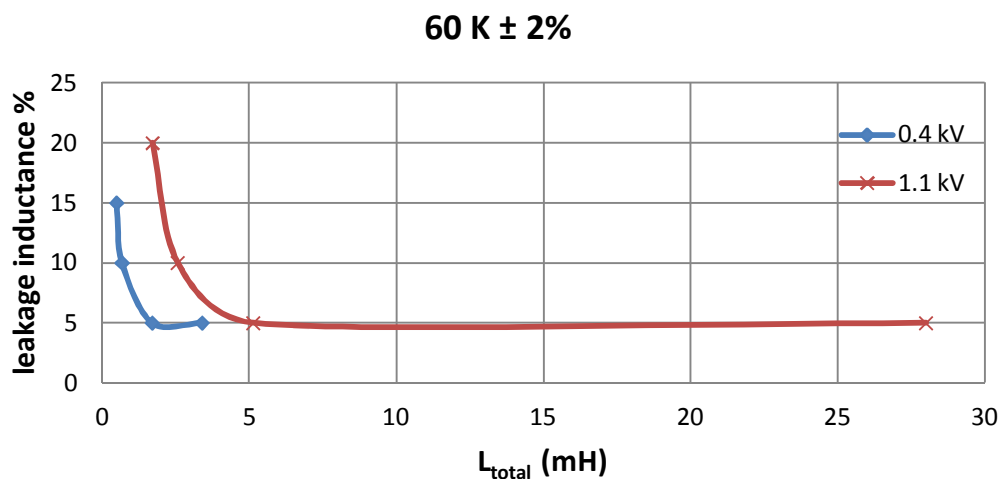


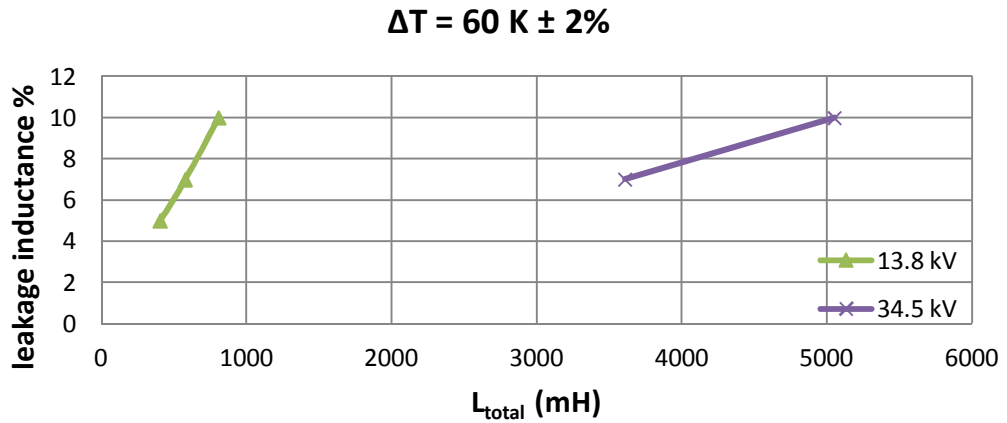
Figure C.43 Variations in reactor current against kVAr rating of the reactor

### C.2 Variations in Parameters against Total Inductance of the Reactor

The resulting percentage leakage inductance variations against total inductance value of the reactor under design and in terms of standard line-to-line operating voltages and temperature rise above the ambient are given in Figs.C.44-C.50.

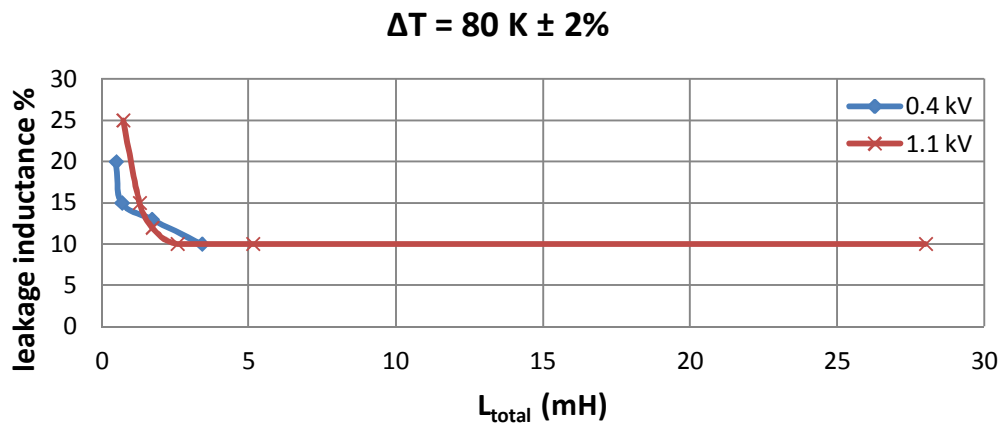


a) Leakage inductance percentage variations against total inductance of the reactor for 60 K temperature rise above the ambient (low voltage)

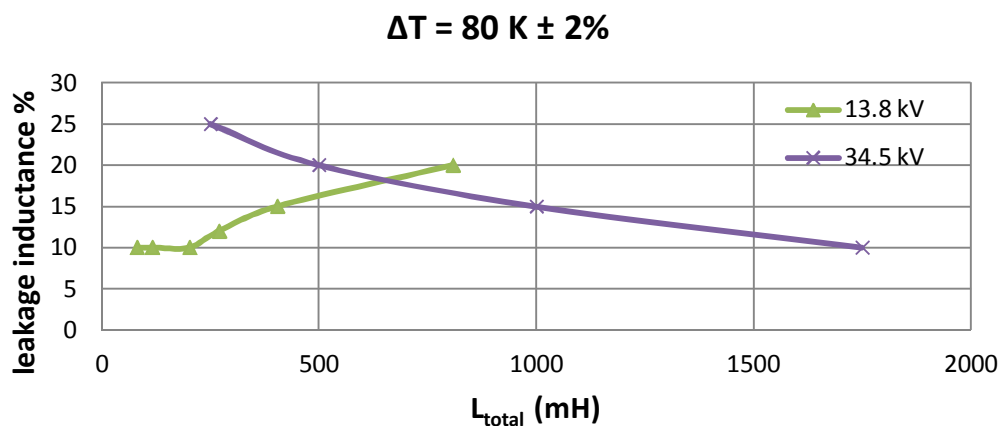


b) Leakage inductance percentage variations against total inductance of the reactor for 60 K temperature rise above the ambient (medium voltage)

Figure C.44 Leakage inductance percentage variations against total inductance of the reactor for 60 K temperature rise above the ambient

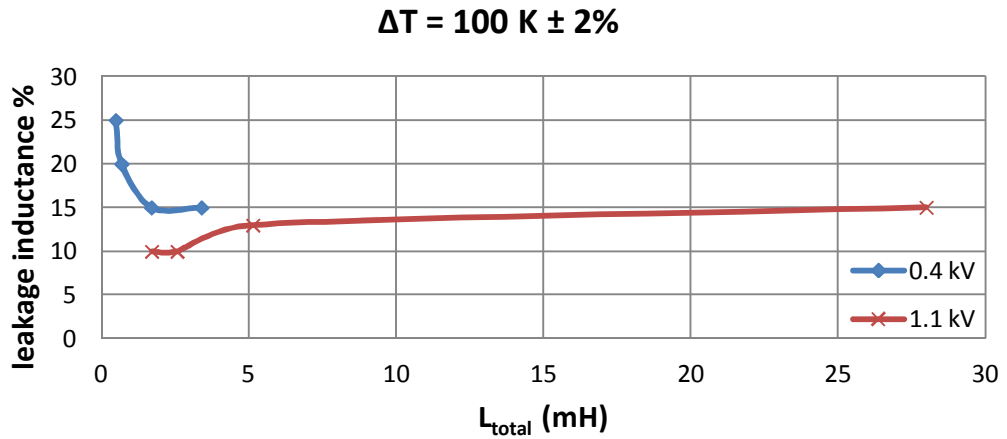


a) Leakage inductance percentage variations against total inductance of the reactor for 80 K temperature rise above the ambient (low voltage)

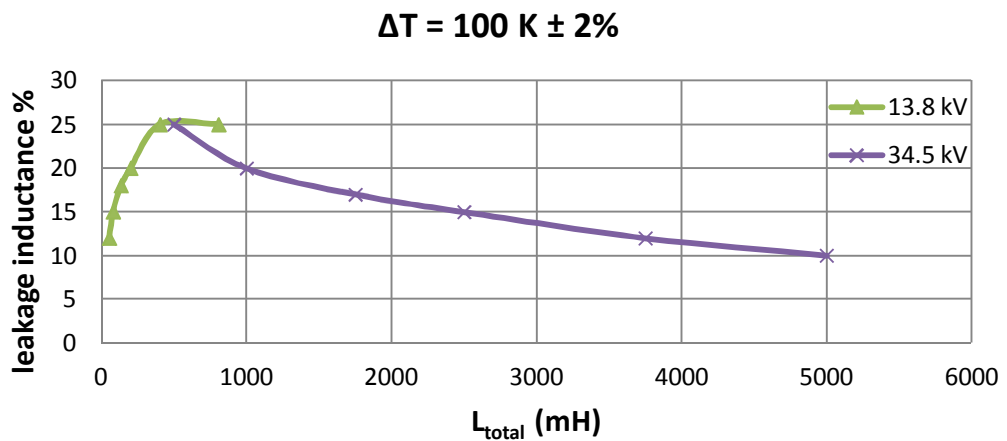


b) Leakage inductance percentage variations against total inductance of the reactor for 80 K temperature rise above the ambient (medium voltage)

Figure C.45 Leakage inductance percentage variations against total inductance of the reactor for 80 K temperature rise above the ambient



a) Leakage inductance percentage variations against total inductance of the reactor for 100 K temperature rise above the ambient (low voltage)



b) Leakage inductance percentage variations against total inductance of the reactor for 100 K temperature rise above the ambient (medium voltage)

Figure C.46 Leakage inductance percentage variations against total inductance of the reactor for 100 K temperature rise above the ambient

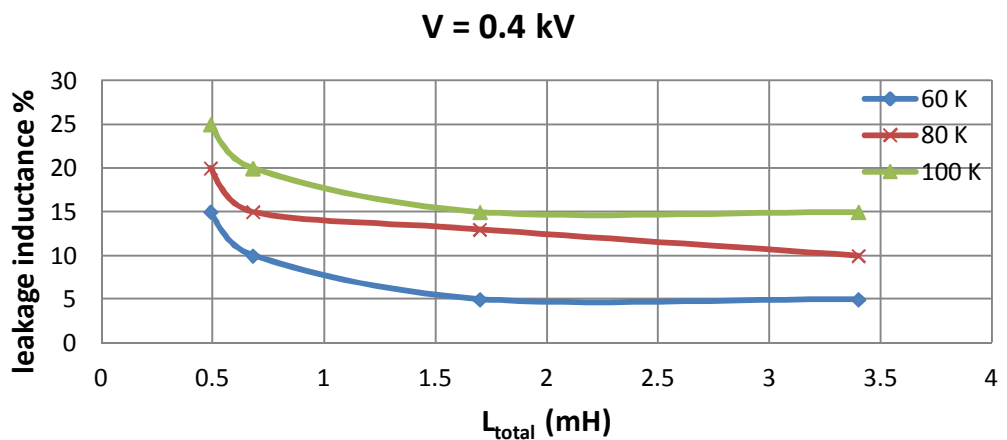


Figure C.47 Leakage inductance percentage variations against total inductance of the reactor for 0.4 kV operating voltage

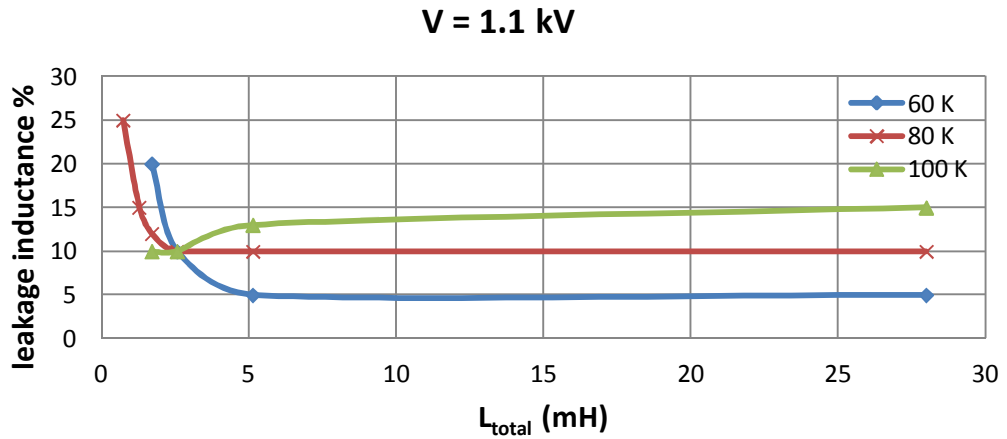


Figure C.48 Leakage inductance percentage variations against total inductance of the reactor for 1.1 kV operating voltage

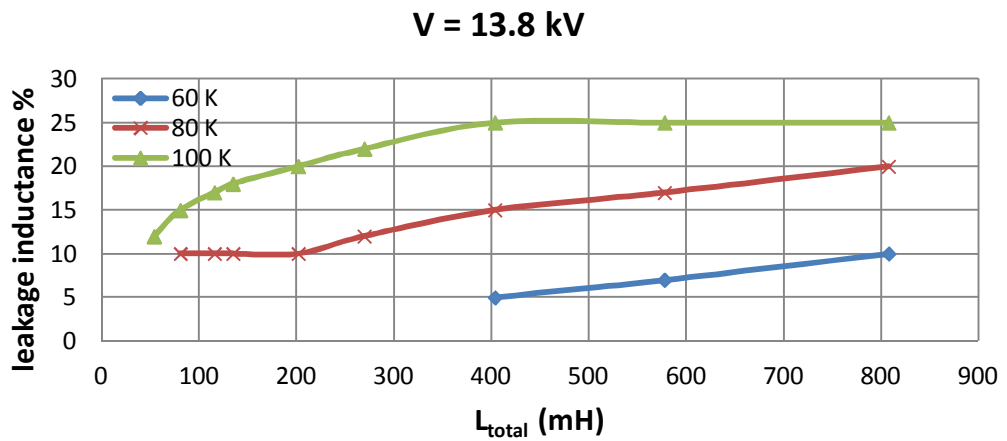


Figure C.49 Leakage inductance percentage variations against total inductance of the reactor for 13.8 kV operating voltage

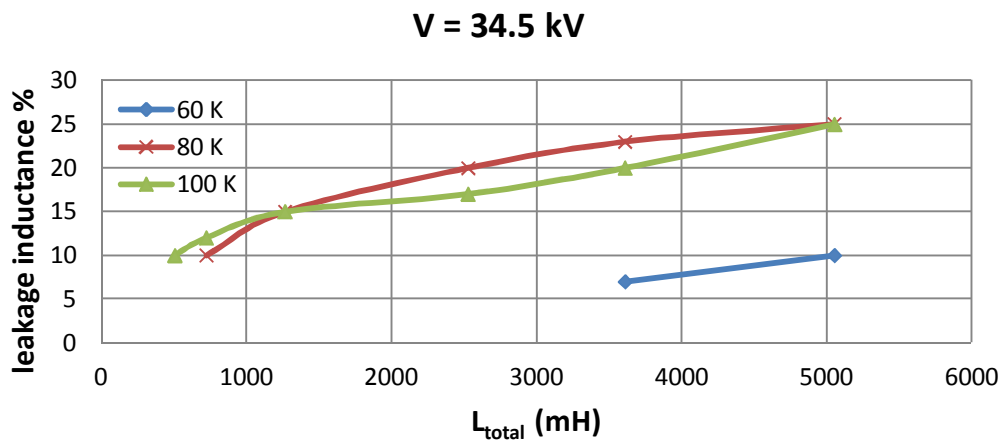
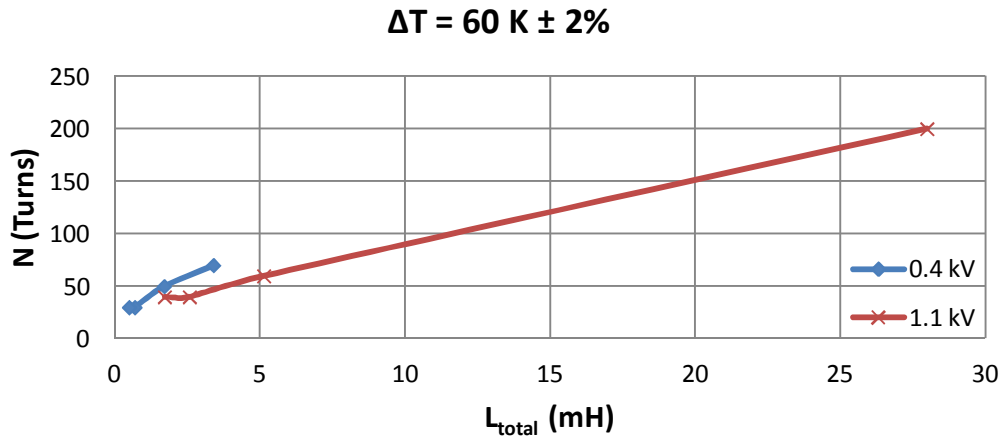
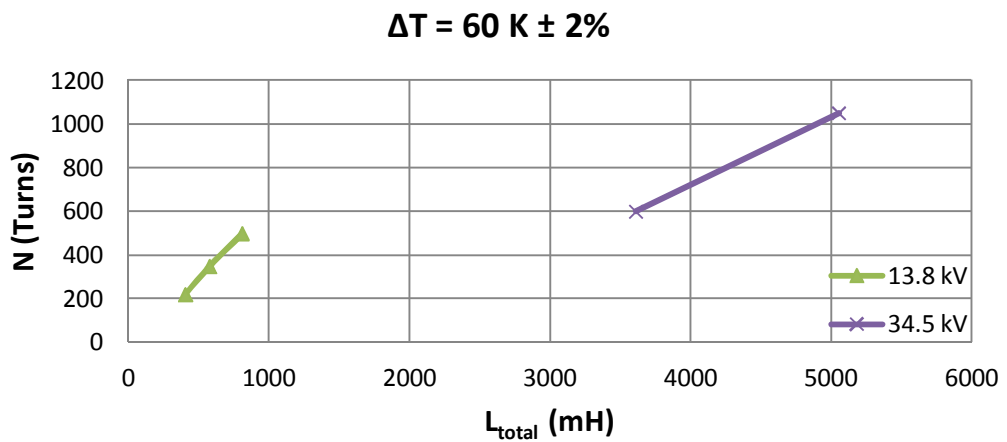


Figure C.50 Leakage inductance percentage variations against total inductance of the reactor for 34.5 kV operating voltage

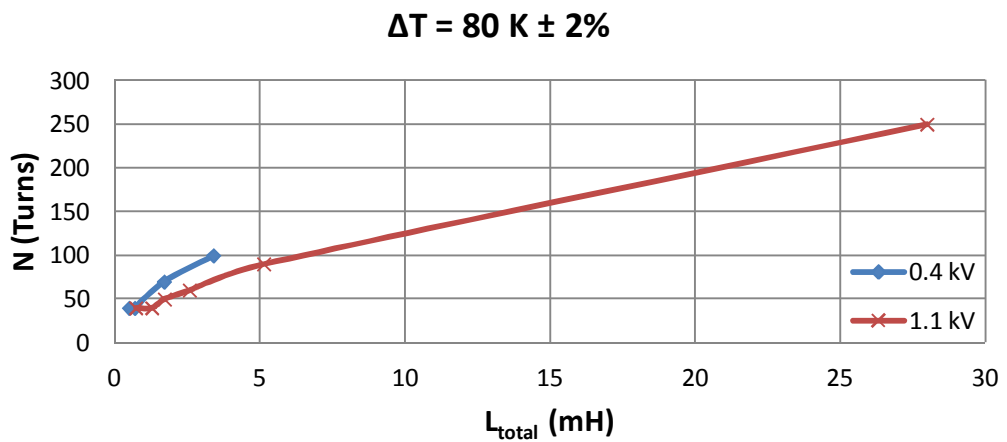


a) Number of turns variations against total inductance of the reactor

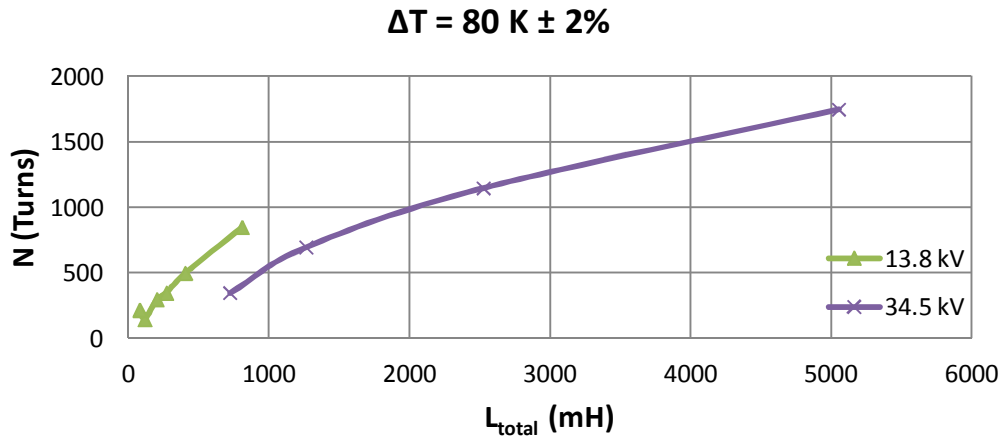


b) Number of turns variations against total inductance of the reactor (medium voltage)

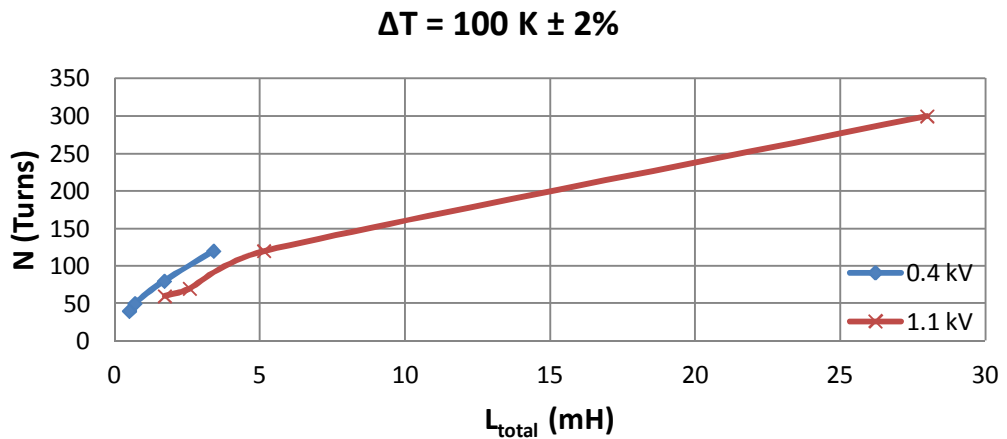
Figure C.51 Number of turns variations against total inductance of the reactor for 60 K temperature rise above the ambient



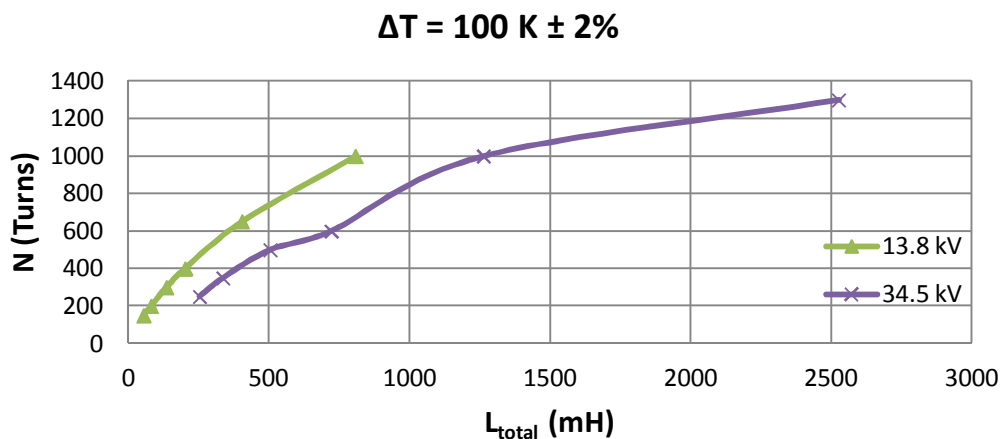
a) Number of turns variations against total inductance of the reactor (low voltage)



b) Number of turns variations against total inductance of the reactor (med. voltage)  
 Figure C.52 Number of turns variations against total inductance of the reactor for 80 K temperature rise above the ambient (medium voltage)



a) Number of turns variations against total inductance of the reactor (low voltage)



b) Number of turns variations against total inductance of the reactor (med. voltage)

Figure C.53 Number of turns variations against total inductance of the reactor for 100 K temperature rise above the ambient (medium voltage)

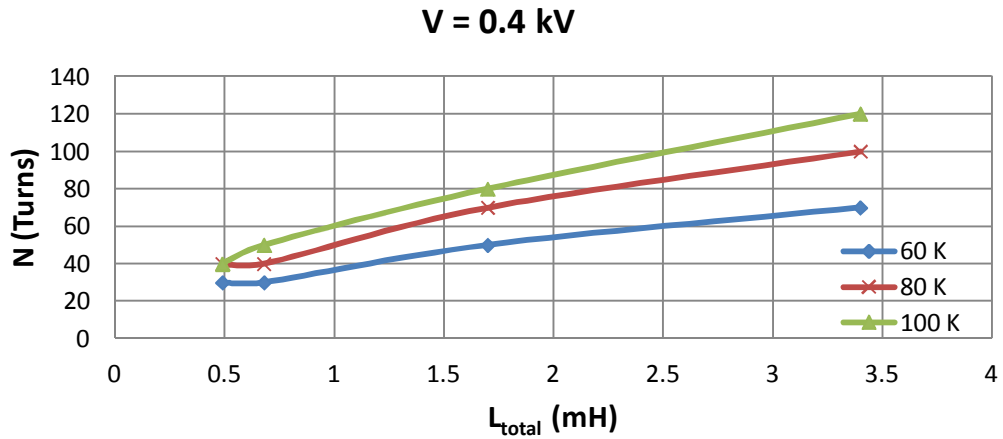


Figure C.54 Number of turns variations against total inductance of the reactor for 0.4 kV operating voltage

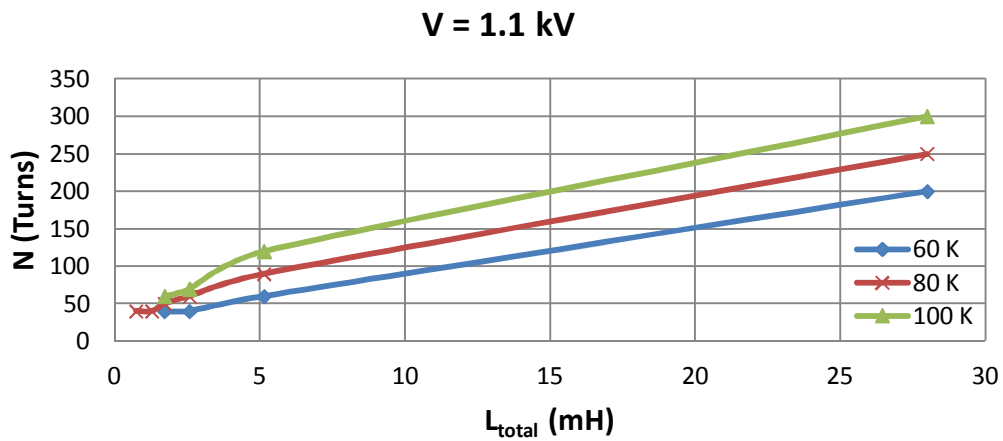


Figure C.55 Number of turns variations against total inductance of the reactor for 1.1 kV operating voltage

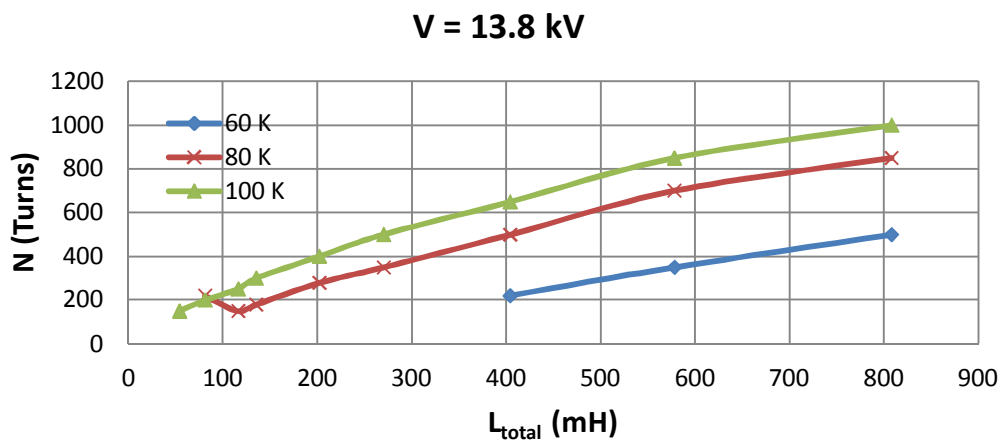


Figure C.56 Number of turns variations against total inductance of the reactor for 13.8 kV operating voltage

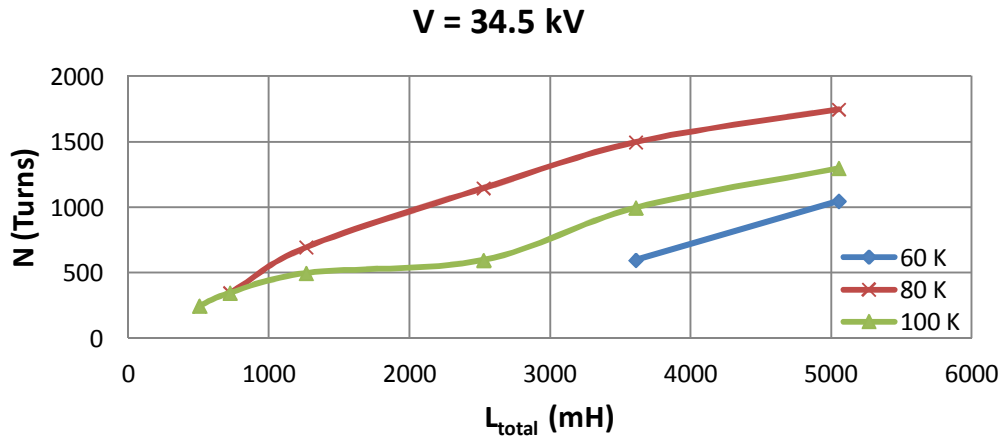


Figure C.57 Number of turns variations against total inductance of the reactor for 34.5 kV operating voltage

### C.3 Iteration Results of FEA Optimizations Performed in Chapter 4

As already mentioned, a few hundreds of optimization study have been carried out by using FEM analysis (Maxwell 3D) in order to find out percent value of  $L_1$  with respect to hundred percent self inductance for various technical specifications of the reactor by using the design objective described in Chapter 4. Therefore, large amounts of data such as; the inductance components calculated in Maxwell 3D, losses, dimensions of the designed reactors, leakage inductance percentage, number of turns, present value cost, initial cost, thickness of the winding material, current density etc. have been obtained. The data of selected optimization work is given in the following tables.



Table C.1 Selected design parameters for 60 K temperature rise above the ambient at 1.1 kV

Temperature Rise	60	60	60	60	60	60	60	60	60
# distributed gap	G=40	G=40	G=40	G=40	G=40	G=40	G=40	G=40	G=40
kVAR	47	250	500	1000	47	500	750	750	750
Voltage (I-I) kV	1,1	1,1	1,1	1,1	1,1	1,1	1,1	1,1	1,1
Current Amps	73,22	393,65	787,30	1574,59	73,22	787,30	1180,94	1180,94	1180,94
L (mH)	27,62	5,14	2,57	1,28	27,62	2,57	1,71	1,71	1,71
L <sub>leak</sub>	0,05	0,05	0,05	0,05	0,10	0,10	0,12	0,15	0,20
B <sub>m</sub> (T)	1,100	1,100	1,100	1,100	1,100	1,100	1,100	1,100	1,100
A mm <sup>2</sup>	13007	43051	65206,02	42767	11735	61780,21	59548	57514	54115,2
A <sub>eff</sub> mm <sup>2</sup>	12486	41329	62597,78	41057	11266	59309	57166	55213	51950,6
foil thickness (mm)	0,40	0,90	0,70	0,30	0,30	0,70	0,50	0,50	0,50
J (A/mm <sup>2</sup> )	1,1	1,1	1,1	1,1	1,1	1,1	1,1	1,1	1,1
foil height (mm)	166	398	1024	4773	221	1024	2147	2147	2147
N (turns)	200	60	40	60	210	40	40	40	40
l <sub>gap</sub> (mm)	23,6	38,2	51	152,8	24,8	51	76,4	76,4	76,4
winding width (mm)	110	63,0	34	27	94,5	34	26	26	26
window (mm)	125	78,0	49	42	109,5	49	41	41	41
w (mm)	85,7	155,9	191,9	155,4	81,4	186,8	183,4	180,2	174,8
d (mm)	145,7	265,1	326,2	264,2	138,4	317,5	311,7	306,4	297,2
Temp rise (K)	60	60	60	60	60	60	60	60	60
wind-wind clearance	5	5	5	5	5	5	5	5	5
yoke clearance (mm)	20	20	20	20	20	20	20	20	20
tube (mm)	5	5	5	5	5	5	5	5	5
limb-wind clearance	0	0	0	0	0	0	0	0	0
PVC (Euro)	4201	13763	29650	68470	4060	28240	45170	43810	41540
<b>Simulation Results</b>									
L <sub>total</sub> (mH)	28,65	5,11	2,87		27,12	2,63	1,818	1,940	1,690
L <sub>gap</sub> (mH)	26,20	4,85	2,45		24,92	2,32	1,491	1,422	1,355
L <sub>iron</sub> (mH)	0,21	0,036	0,025		0,20	0,024	0,020	0,143	0,018
L <sub>leakage</sub> (mH)	2,24	0,22	0,40	0,00	2,01	0,29	0,31	0,38	0,32
Leakage %	7,82	4,38	13,76	#####	7,39	10,87	16,89	19,33	18,76
Inductance decline %	-3,72%	0,55%	-11,72%	#####	1,82%	-2,37%	-6,15%	-13,27%	1,32%

Table C.2 Selected design parameters for 60 K temperature rise above the ambient at 13.8 kV

<b>Temperature Rise</b>	60	60	60	60
<b># distributed gap</b>	<i>G=40</i>	<i>G=40</i>	<i>G=40</i>	<i>G=40</i>
<b>kVAR</b>	250	350	500	250
<b>Voltage (I-I) kV</b>	13,8	13,8	13,8	13,8
<b>Current Amps</b>	31,38	43,93	62,76	31,38
<b>L (mH)</b>	808,66	577,62	404,33	808,66
<b>Lleak</b>	<i>0,05</i>	<i>0,07</i>	<i>0,05</i>	<i>0,10</i>
<b>Bm (T)</b>	1,100	1,100	1,100	1,100
<b>A mm<sup>2</sup></b>	64876,6	90534,2	147294	61460
<b>A_eff mm<sup>2</sup></b>	62281,6	86912,8	141403	59001
<b>foil thickness (mm)</b>	0,20	0,20	0,20	0,20
<b>J (A/mm<sup>2</sup>)</b>	1,1	1,1	1,1	1,1
<b>foil height (mm)</b>	143	200	286	143
<b>N (turns)</b>	500	350	220	500
<b>l_gap (mm)</b>	25,5	24,9	22,4	25,5
<b>winding width (mm)</b>	250	175	110	250
<b>window (mm)</b>	395	320	255	395
<b>w (mm)</b>	191,4	226,1	288,4	186,3
<b>d (mm)</b>	325,4	384,4	490,3	316,7
<b>Temp rise (K)</b>	60	60	60	60
<b>wind-wind clearance</b>	25	25	25	25
<b>yoke clearance (mm)</b>	120	120	120	120
<b>tube (mm)</b>	10	10	10	10
<b>limb-wind clearance</b>	50	50	50	50
<b>PVC (Euro)</b>	23988	31021	49414	22929
<b>Simulation Results</b>				
<b>L<sub>total</sub> (mH)</b>	837,64	567,90	393,90	797,77
<b>L<sub>gap</sub> (mH)</b>	745,80	519,63	368,86	703,86
<b>L<sub>iron</sub> (mH)</b>	12,50	8,88	7,59	11,77
<b>L<sub>leakage</sub> (mH)</b>	79,34	39,39	17,45	82,14
<b>Leakage %</b>	9,47	6,94	4,43	10,30
<b>Inductance decline %</b>	-3,58%	1,68%	2,58%	1,35%

Table C.3 Selected design parameters for 60 K temperature rise above the ambient at 34.5 kV

Temperature Rise	60	60	60	60	60	60	60	60
# distributed gap	<i>G=40</i>	<i>G=40</i>	<i>G=40</i>	<i>G=40</i>	<i>G=40</i>	<i>G=40</i>	<i>G=40</i>	<i>G=40</i>
kVAR	250	350	350	500	1000	2500	5000	250
Voltage (I-I) kV	34,5	34,5	34,5	34,5	34,5	34,5	34,5	34,5
Current Amps	12,55	17,57	17,57	25,10	50,20	125,51	251,02	12,55
L (mH)	5054,14	3610,10	3610,10	2527,07	1263,54	505,41	252,71	5054,14
L <sub>leak</sub>	0,05	0,12	0,07	0,05	0,05	0,05	0,05	0,10
B <sub>m</sub> (T)	1,100	1,100	1,100	1,100	1,100	1,100	1,1	1,100
A mm <sup>2</sup>		65343	131978					
A <sub>eff</sub> mm <sup>2</sup>		62729	126699					
foil thickness (mm)	0,10	0,10	0,10					0,10
J (A/mm <sup>2</sup> )	1,1	1,1	1,1					1,1
foil height (mm)	115	160	160					115
N (turns)	1000	700	600					1050
l <sub>gap</sub> (mm)	20,4	19,9	17,1					21,4
winding width (mm)	600	420	360					630
window (mm)	770	590	530					800
w (mm)	214,0	245,9	273,0					203,2
d (mm)	363,7	255,1	464,1					345,5
Temp rise (K)	60	80	80	<b>65</b>	<b>72</b>	<b>85</b>	<b>96</b>	60
wind-wind clearance	50	50	50	50	50	50	50	50
yoke clearance (mm)	200	200	200	200	200	200	200	200
tube (mm)	10	10	10	10	10	10	10	10
limb-wind clearance	50	50	50	50	50	50	50	50
PVC (Euro)	37964	44695	51744					35801
<b>Simulation Results</b>								
L <sub>total</sub> (mH)	5120,00	3335,20	3421,00					4910,3
L <sub>gap</sub> (mH)	4510,00	3012,65	3138,00					4278
L <sub>iron</sub> (mH)	147,10	84,71	108,47					136,6
L <sub>leakage</sub> (mH)	462,90	237,84	174,53	0,00	0,00	0,00	0,00	495,70
Leakage %	9,04	7,13	5,10	#SAYI/0!	#SAYI/0!	#SAYI/0!	#SAYI/0!	10,10
Inductance decline %	-1,30%	7,61%	5,24%	100,00%	100,00%	100,00%	100,00%	2,85%

Table C.4 Selected design parameters for 60 K temperature rise above the ambient at 1.1/13.8/34.5 kV

Temperature Rise	60	60	60	60	60	60	60	60	60
# distributed gap	G=40	G=40	G=40	G=40	G=40	G=40	G=40	G=40	G=40
kVAR	47	250	500	500	1000	2500	500	2500	5000
Voltage (I-I) kV	1,1	1,1	1,1	13,8	13,8	13,8	34,5	34,5	34,5
Current Amps	73,22	393,65	787,30	62,76	125,51	313,78	25,10	125,51	251,02
L (mH)	27,62	5,14	2,57	404,33	202,17	80,87	2527,07	505,41	252,71
Lleak	0,15	0,15	0,15	0,15	0,15	0,15	0,15	0,15	0,15
Bm (T)	1,100	1,100	1,100	1,100	1,100	1,100	1,100	1,100	1,1
A mm <sup>2</sup>	11082	38519	58345	152559			144517		
A_eff mm <sup>2</sup>	10639	36978	56011	146457			138736		
foil thickness (mm)	0,30	0,90	0,70	0,30			0,10		
J (A/mm <sup>2</sup> )	1,1	1,1	1,1	1,1			1,1		
foil height (mm)	220	398	1024	191			228		
N (turns)	210	60	40	190			500		
l_gap (mm)	24,8	38,2	51	19,4			20,3		
winding width (mm)	94,5	63,0	34	114			300		
window (mm)	109,5	78,0	49	259			470		
w (mm)	79,1	147,5	181,5	293,5			285,7		
d (mm)	134,5	250,7	308,6	499,0			485,6		
Temp rise (K)	60	60	60	60	<b>70</b>	<b>80</b>	<b>62,5</b>	<b>83</b>	<b>80</b>
wind-wind clearance	5	5	5	25	25	25	50	50	50
yoke clearance (mm)	20	20	20	120	120	120	200	200	200
tube (mm)	5	5	5	10	10	10	10	10	10
limb-wind clearance	0	0	0	50	50	50	50	50	50
PVC (Euro)	3926	12567	26826	47360			58170		
<b>Simulation Results</b>									
L <sub>total</sub> (mH)	25,55	4,59	2,40	349,93			2191,55		
L <sub>gap</sub> (mH)	23,42	4,32	2,18	327,54			2031,70		
L <sub>iron</sub> (mH)	0,19	0,032	0,023	7,38			58,20		
L <sub>leakage</sub> (mH)	1,94	0,24	0,20	15,01	0,00	0,00	101,65	0,00	0,00
Leakage %	7,59	5,19	8,21	4,29	#####	#####	4,64	#####	#####
Inductance decline %	7,51%	10,67%	6,58%	13,45%	#####	#####	13,28%	#####	#####

Table C.5 Selected design parameters for 80 K temperature rise above the ambient at 1.1 kV

<b>Temperature Rise</b>	80	80	80	80	80	80	80	80	80	80
<b># distributed gap</b>	G=40	G=40	G=40	G=40	G=40	G=40	G=40	G=40	G=40	G=40
<b>kVAR</b>	47	250	500	1000	750	1000	1750	47	250	500
<b>Voltage (I-I) kV</b>	1,1	1,1	1,1	1,1	1,1	1,1	1,1	1,1	1,1	1,1
<b>Current Amps</b>	73,22	393,65	787,30	1574,59	1180,94	1574,59	2755,54	73,22	393,65	787,30
<b>L (mH)</b>	27,62	5,14	2,57	1,28	1,71	1,28	0,73	27,62	5,14	2,57
<b>Lleak</b>	0,05	0,05	0,05	0,05	0,13	0,15	0,20	0,10	0,10	0,10
<b>Bm (T)</b>	1,100	1,100	1,100	1,100	1,100	1,100	1,100	1,100	1,100	1,100
<b>A mm<sup>2</sup></b>	10410	25834	37273	51338	47095	57425,6	53913,2	9861,188	27193	41190,9
<b>A_eff mm<sup>2</sup></b>	9994	24800	35782	49285	45211	55128,6	51756,7	9466,74	26106	39543,3
<b>foil thickness (mm)</b>	0,30	0,70	0,80	0,90	0,90	1,00	1,00	0,30	1,00	0,90
<b>J (A/mm<sup>2</sup>)</b>	1,3	1,1	1,1	1,1	1,2	1,2	1,1	1,3	1,1	1,2
<b>foil height (mm)</b>	187	512	895	1590	1193	1312,5	2505	187	358	730
<b>N (turns)</b>	250	100	70	50	50	40	40	250	90	60
<b>l_gap (mm)</b>	29,5	63,7	89,2	127,3	95,5	101,8	178,2	29,5	57,3	76,4
<b>winding width (mm)</b>	112,5	85,0	66,5	52,5	52,5	46	46	112,5	103,5	63
<b>window (mm)</b>	127,5	100,0	81,5	67,5	67,5	61	61	127,5	118,5	78
<b>w (mm)</b>	76,7	120,8	145,1	170,3	163,1	180,1	174,5	74,6	123,9	152,5
<b>d (mm)</b>	130,3	205,3	246,6	289,4	277,2	306,1	296,6	126,9	210,7	259,3
<b>Temp rise (K)</b>	80	80	80	80	80	80	80	80	80	80
<b>wind-wind clearance</b>	5	5	5	5	5	5	5	5	5	5
<b>yoke clearance (mm)</b>	20	20	20	20	20	20	20	20	20	20
<b>tube (mm)</b>	5	5	5	5	5	5	5	5	5	5
<b>limb-wind clearance</b>	0	0	0	0	0	0	0	0	0	0
<b>PVC (Euro)</b>	4902	13871	24129	43820	32090	40760	64160	4774	13016	23176
<b>Simulation Results</b>										
<b>L<sub>total</sub> (mH)</b>	29,37	5,37	2,73	1,57	1,742	1,273	0,833	28,06	5,063	2,585
<b>L<sub>gap</sub> (mH)</b>	26,30	4,84	2,45	1,22	1,483	1,08	0,60	24,92	4,610	2,32
<b>L<sub>iron</sub> (mH)</b>	0,20	0,03	0,01	0,01	0,01	0,01	0,0043	0,17	0,020	0,01
<b>L<sub>leakage</sub> (mH)</b>	2,87	0,50	0,27	0,34	0,25	0,18	0,23	2,97	0,43	0,26
<b>Leakage %</b>	9,77	9,31	9,89	21,86	14,29	14,38	27,45	10,58	8,55	9,86
<b>Inductance decline %</b>	4,90%	4,27%	5%	20%	-1,71%	0,50%	-13,49%	0,21%	1,69%	0,58%

Table C.6 Selected design parameters for 80 K temperature rise above the ambient at 13.8 kV

<b>Temperature Rise</b>	80	80	80	80	80	80	80	80	80
<b># distributed gap</b>	<i>G=40</i>	<i>G=40</i>	<i>G=40</i>	<i>G=40</i>	<i>G=40</i>	<i>G=40</i>	<i>G=40</i>	<i>G=40</i>	<i>G=40</i>
<b>kVAR</b>	250	500	1000	2500	750	250	1000	1750	2500
<b>Voltage (I-I) kV</b>	13,8	13,8	13,8	13,8	13,8	13,8	13,8	13,8	13,8
<b>Current Amps</b>	31,38	62,76	125,51	313,78	94,13	31,38	125,51	219,64	313,78
<b>L (mH)</b>	808,66	404,33	202,17	80,87	269,55	808,66	202,17	115,52	80,87
<b>L<sub>leak</sub></b>	0,15	0,15	0,15	0,15	0,12	0,20	0,10	0,10	0,10
<b>B<sub>m</sub> (T)</b>	1,100	1,100	1,100	1,100	1,100	1,100	1,100	1,100	1,100
<b>A mm<sup>2</sup></b>	34160,7	57995,4	96226,6	144847	85538,83	32132	101908	205197	139423
<b>A<sub>eff</sub> mm<sup>2</sup></b>	32794,3	55675,6	92377,5	139053	82117,28	30846	97831,2	196989	133846
<b>foil thickness (mm)</b>	0,10	0,20	0,30	0,10	0,40	0,10	0,30	0,80	0,10
<b>J (A/mm<sup>2</sup>)</b>	1,1	1,1	1,1	1,1	1,1	1,1	1,1	1,1	1,1
<b>foil height (mm)</b>	286	286	380	2855	214,0	286	380	250,0	2855
<b>N (turns)</b>	850	500	300	200	350	850	300	150	220
<b>l<sub>gap</sub> (mm)</b>	43,3	50,9	60,9	101,5	53,2	43,3	60,9	53,3	111,7
<b>winding width (mm)</b>	340	250	180	80	245	340	180	165	88
<b>window (mm)</b>	485	395	325	225	390	485	325	310	233
<b>w (mm)</b>	138,9	181,0	233,1	286,0	219,8	134,7	239,9	340,4	280,6
<b>d (mm)</b>	236,1	307,6	396,3	486,2	373,6	229,0	407,8	578,7	477,0
<b>Temp rise (K)</b>	80	80	80	80	80	80	80	80	80
<b>wind-wind clearance</b>	25	25	25	25	25	25	25	25	25
<b>yoke clearance (mm)</b>	120	120	120	120	120	120	120	120	120
<b>tube (mm)</b>	10	10	10	10	10	10	10	10	10
<b>limb-wind clearance</b>	50	50	50	50	50	50	50	50	50
<b>PVC (Euro)</b>	22738	31793	49029	151290	41537	21992	51314	85670	150360
<b>Simulation Results</b>									
<b>L<sub>total</sub> (mH)</b>	836,96	401,71	192,58	75,83	272,66	795,91	202,23	112,62	80,20
<b>L<sub>gap</sub> (mH)</b>	673,22	337,62	167,62	67,14	233,60	632,91	177,34	102,58	71,04
<b>L<sub>iron</sub> (mH)</b>	8,14	3,28	1,40	1,00	2,10	7,70	1,50	0,97	0,98
<b>L<sub>leakage</sub> (mH)</b>	155,60	60,81	23,56	7,69	36,96	155,30	23,39	9,07	8,18
<b>Leakage %</b>	18,59	15,14	12,23	10,15	13,56	19,51	11,57	8,05	10,20
<b>Inductance decline %</b>	3,50%	1,00%	4,66%	6,40%	-1,15%	1,62%	-0,11%	2,51%	0,99%

Table C.7 Selected design parameters for 80 K temperature rise above the ambient at 34.5 kV

Temperature Rise	80	80	80	80	80	80	80	80	80	80	80
# distributed gap	G=40	G=40	G=40	G=40	G=40	G=40	G=40	G=40	G=40	G=40	G=40
kVAR	250	500	1000	2500	250	500	1750	250	500	1000	2500
Voltage (I-I) kV	34,5	34,5	34,5	34,5	34,5	34,5	34,5	34,5	34,5	34,5	34,5
Current Amps	12,55	25,10	50,20	125,51	12,55	25,10	87,86	12,55	25,10	50,20	125,51
L (mH)	5054,14	2527,07	1263,54	505,41	5054,14	2527,07	722,02	5054,14	2527,07	1263,54	505,41
Lleak	0,15	0,15	0,15	0,15	0,25	0,20	0,10	0,05	0,05	0,05	0,05
Bm (T)	1,100	1,100	1,100	1,100	1,100	1,100	1,100	1,100	1,100	1,100	1,100
A mm <sup>2</sup>	40302,88	62839,25	103266	300747,1	36568,66	59111,06	218944,3	46320,313	73402,0417	115416,9	368220
A_eff mm <sup>2</sup>	38690,76	60325,68	99135,8	288717,3	35105,91	56746,62	210186,5	44467,5	70465,96	110800,2	353491,2
foil thickness (mm)	0,10	0,10	0,10	0,30	0,10	0,10	0,40	0,10	0,10	0,10	0,40
J (A/mm <sup>2</sup> )	1,1	1,1	1,1	1,1	1,1	1,1	1,1	1,2	1,2	1,1	1,1
foil height (mm)	115	228	456	380	115	228	200	105	209	456	286
N (turns)	1800	1150	700	240	1750	1150	350	1750	1100	700	220
l_gap (mm)	36,7	46,7	56,8	48,7	35,6	46,7	49,8	35,6	44,6	56,8	44,8
winding width (mm)	1080	690	420	192	1050	690	315	1050	660	420	198
window (mm)	1250	860	590	362	1220	860	485	1220	830	590	368
w (mm)	150,9	188,4	241,5	412,1	143,7	182,7	351,6	161,7	203,6	255,3	456,0
d (mm)	256,4	320,2	410,5	700,6	244,3	310,6	597,8	275,0	346,1	434,0	775,2
Temp rise (K)	80	80	80	83	80	80	80	80	80	80	85
wind-wind clearance	50	50	50	50	50	50	50	50	50	50	50
yoke clearance (mm)	200	200	200	200	200	200	200	200	200	200	200
tube (mm)	10	10	10	10	10	10	10	10	10	10	10
limb-wind clearance	50	50	50	50	50	50	50	50	50	50	50
PVC (Euro)	37987	46189	65391	145730	34923	44411	104860	41204	50648	71524	172640
<b>Simulation Results</b>											
L <sub>total</sub> (mH)	5975,30	2629,80	1203,60	448,65	5075,70	2481,00	701,68	6413,60	2854,80	1334,60	499,35
L <sub>gap</sub> (mH)	3993,50	2082,51	1001,60	417,77	3561,60	1956,80	634,00	4510,00	2342,80	1173,80	466,79
L <sub>iron</sub> (mH)	177,12	34,86	13,36	5,66	132,28	32,65	7,94	172,85	39,62	15,10	6,76
L <sub>leakage</sub> (mH)	1804,68	512,43	188,64	25,22	1381,82	491,55	59,74	1730,75	472,38	145,70	25,80
Leakage %	30,20	19,49	15,67	5,62	27,22	19,81	8,51	26,99	16,55	10,92	5,17
Inductance decline %	18,00%	4%	4,78%	11,15%	-0,43%	1,82%	2,82%	26,90%	13%	5,60%	1,10%

Table C.8 Selected design parameters for 100 K temperature rise above the ambient at 1.1 kV

Temperature Rise	100	100	100	100	100	100	100	100	100	100	100	100	100	100	100
# distributed gap	G=40	G=40	G=40	G=40	G=40	G=40	G=40	G=40	G=40	G=40	G=40	G=40	G=40	G=40	G=40
kVAR	47	250	500	1000	500	1000	1000	500	1000	500	500	750	750	750	750
Voltage (l-l) kV	1,1	1,1	1,1	1,1	1,1	1,1	1,1	1,1	1,1	1,1	1,1	1,1	1,1	1,1	1,1
Current Amps	73,22	393,65	787,30	1574,59	787,30	1574,59	1574,59	787,30	1574,59	787,30	787,30	1180,94	1180,94	1180,94	1180,94
L (mH)	27,62	5,14	2,57	1,28	2,57	1,28	1,28	2,57	1,28	2,57	2,57	1,71	1,71	1,71	1,71
Leak	0,15	0,15	0,15	0,15	0,05	0,10	0,10	0,25	0,25	0,10	0,10	0,10	0,10	0,20	0,00
Bm (T)	1,100	1,100	1,100	1,100	1,100	1,100	1,100	1,100	1,100	1,100	1,100	1,100	1,100	1,100	1,100
A mm <sup>2</sup>	7757,8	19263	23342,7	38266	32610,4	40536	34748	25753,1	33777	27145,7	34895,3	34801,7	40594	36076,3	45103,6
A <sub>eff</sub> mm <sup>2</sup>	7447,5	18492	22409	36735	31306	38914	33358	24723	32425,9	26059,9	33499,4	33409,7	38970	34633,3	43299,5
foil thickness (mm)	0,30	0,80	0,70	1,00	1,00	1,00	1,00	0,9	1,00	0,9	1,0	0,9	1,0	1,0	1,0
J (A/mm <sup>2</sup> )	1,3	1,1	1,1	1,2	1,2	1,2	1,1	1,2	1,2	1,1	1,3	1,2	1,3	1,3	1,3
foil height (mm)	187	448	1023,4	1312,5	657	1312,5	1432	730	1313	796	606	1094	910	910	910
N (turns)	300	120	100	60	80	60	70	80	60	90	70	70	60	60	60
l <sub>gap</sub> (mm)	35,4	76,4	127,4	152,8	101,9	152,8	178,2	101,9	152,8	114,7	89,2	133,6	114,6	114,6	114,6
winding width (mm)	135	114,0	85	69	92	69	80,5	84	69	94,5	94,5	73,5	69	69	69
window (mm)	150	129,0	100	84	107	84	95,5	99	84	109,5	109,5	88,5	84	84	84
w (mm)	66,2	104,3	114,8	147,0	135,7	151,3	140,1	120,6	138,1	123,8	140,4	140,2	151,4	142,7	159,6
d (mm)	112,5	177,3	195,2	249,9	230,7	257,2	238,1	205,0	234,8	210,5	238,6	238,3	257,4	242,7	271,3
Temp rise (K)	100	100	100	100	100	100	100	100	100	100	100	100	100	100	100
wind-wind clearance	5	5	5	5	5	5	5	5	5	5	5	5	5	5	5
yoke clearance (mm)	20	20	20	20	20	20	20	20	20	20	20	20	20	20	20
tube (mm)	5	5	5	5	5	5	5	5	5	5	5	5	5	5	5
limb-wind clearance	0	0	0	0	0	0	0	0	0	0	0	0	0	0	0
PVC (Euro)	5303	13820	24187	39880	24509	41370	41390	21405	36860	23708	23535	33080	32704	30328	35050
Simulation Results															
L <sub>total</sub> (mH)	27,99	5,05	3,36	1,40	2,783	1,61	1,60	2,43	1,475	2,75	2,567	2,256	1,770	1,620	2,040
L <sub>gap</sub> (mH)	23,57	4,35	2,41	1,10	2,460	1,21	1,15	1,96	1,030	2,30	2,30	1,61	1,53	1,36	1,71
L <sub>iron</sub> (mH)	0,14	0,02	0,01	0,01	0,010	0,01	0,01	0,01	0,005	0,01	0,01	0,007	0,007	0,006	0,008
L <sub>leakage</sub> (mH)	4,28	0,68	0,94	0,29	0,31	0,39	0,44	0,46	0,44	0,44	0,26	0,64	0,24	0,25	0,32
Leakage %	15,29	13,47	27,98	20,71	11,25	24,22	27,36	18,93	29,83	16,00	10,01	28,32	13,33	15,56	15,78
Inductance decline %	-1,33%	1,71%	-30,79%	-8,99%	-8,33%	-25,34%	-24,33%	5,41%	-14,83%	-7,05%	0,08%	-31,72%	-3,35%	5,41%	-19,11%



Table C.9 Selected design parameters for 100 K temperature rise above the ambient at 13.8 kV

Temperature Rise	100	100	100	100	100	100	100	100	100	100
# distributed gap	<b>G=40</b>	<b>G=40</b>	<b>G=40</b>	<b>G=40</b>	<b>G=40</b>	<b>G=40</b>	<b>G=40</b>	<b>G=40</b>	<b>G=40</b>	<b>G=40</b>
kVAR	250	500	1000	2500	500	250	500	1500	3750	1000
Voltage (I-I) kV	<b>13,8</b>	<b>13,8</b>	<b>13,8</b>	<b>13,8</b>	<b>13,8</b>	13,8	13,8	13,8	13,8	13,8
Current Amps	31,38	62,76	125,51	313,78	62,76	31,38	62,76	188,27	470,67	125,51
L (mH)	<b>808,66</b>	<b>404,33</b>	<b>202,17</b>	<b>80,87</b>	<b>404,33</b>	808,66	404,33	134,78	53,91	202,17
Leak	0,15	0,15	0,15	0,15	0,20	0,25	0,25	0,18	0,12	0,20
Bm (T)	<b>1,100</b>	<b>1,100</b>	<b>1,100</b>	<b>1,100</b>	<b>1,100</b>	1,100	1,100	1,100	1,100	1,100
A mm <sup>2</sup>	29000	44601,31	72179	144847	41981,04	25613,88	39356,19	92952,55	199437,3	67952,81
A_eff mm <sup>2</sup>	<b>27840</b>	<b>42817,26</b>	<b>69292</b>	<b>139053</b>	<b>40301,8</b>	24589,32	37781,94	89234,45	191459,8	65234,7
foil thickness (mm)	0,10	0,30	0,40	0,70	0,20	0,10	0,20	0,5	0,6	0,40
J (A/mm <sup>2</sup> )	<b>1,2</b>	<b>1,1</b>	<b>1,1</b>	<b>1,1</b>	<b>1,1</b>	1,2	1,1	1,1	1,1	1,1
foil height (mm)	262,5	191	285	408	286	262,5	286	342	713	285
N (turns)	<b>1000</b>	<b>650</b>	<b>400</b>	<b>200</b>	<b>650</b>	1000	650	300	150	400
l_gap (mm)	50,9	66,2	81,2	101,5	66,2	50,9	66,2	91,2	114,1	81,2
winding width (mm)	<b>400</b>	<b>390</b>	<b>280</b>	<b>200</b>	<b>325</b>	400	325	240	135	280
window (mm)	545	535	425	345	470	545	470	385	280	425
w (mm)	<b>128,0</b>	<b>158,7</b>	<b>201,9</b>	<b>286,0</b>	<b>154,0</b>	120,3	149,1	229,1	335,6	195,9
d (mm)	217,5	269,8	343,2	486,2	261,7	204,4	253,4	389,5	570,5	333,0
Temp rise (K)	100	100	100	100	100	100	100	100	100	100
wind-wind clearance	25	25	25	25	25	25	25	25	25	25
yoke clearance (mm)	<b>120</b>	<b>120</b>	<b>120</b>	<b>120</b>	<b>120</b>	120	120	120	120	120
tube (mm)	10	10	10	10	10	10	10	10	10	10
limb-wind clearance	<b>50</b>	<b>50</b>	<b>50</b>	<b>50</b>	<b>50</b>	50	50	50	50	50
PVC (Euro)	25557	34978	48704	87200	32758	24198	31688	60359	126060	46921
Simulation Results										
L <sub>total</sub> (mH)	910,59	464,56	211,08	78,94	416,48	829,13	392,74	132,00	52,25	200,26
L <sub>gap</sub> (mH)	673,22	338,62	169,65	68,17	318,47	595,00	298,82	109,47	46,95	160,00
L <sub>iron</sub> (mH)	7,58	2,87	1,10	0,38	2,60	6,70	2,42	0,64	0,28	1,03
L <sub>leakage</sub> (mH)	229,79	123,07	40,33	10,39	95,41	227,43	91,50	21,89	5,02	39,23
Leakage %	25,24	26,49	19,11	13,16	22,91	27,43	23,30	16,58	9,61	19,59
Inductance decline %	-12,60%	-14,90%	-4,41%	2,38%	-3,00%	-2,53%	2,87%	2,06%	3,08%	0,94%

Table C.10 Selected design parameters for 100 K temperature rise above the ambient at 34.5 kV

Temperature Rise	100	100	100	100	100	100	100	100	100	100	100	100
# distributed gap	G=40	G=40	G=40	G=40	G=40	G=40	G=40	G=40	G=40	G=40	G=40	G=40
kVAR	1000	2500	5000	250	500	1000	1750	2500	5000	1000	5000	3750
Voltage (l-l) kV	34,5	34,5	34,5	34,5	34,5	34,5	34,5	34,5	34,5	34,5	34,5	34,5
Current Amps	50,20	125,51	251,02	12,55	25,10	50,20	87,86	125,51	251,02	50,20	251,02	188,27
L (mH)	1263,54	505,41	252,71	5054,14	2527,07	1263,54	722,02	505,41	252,71	1263,54	252,71	336,94
l <sub>leak</sub>	0,15	0,15	0,15	0,25	0,25	0,25	0,17	0,25	0,25	0,20	0,10	0,12
B <sub>m</sub> (T)	1,100	1,100	1,1	1,100	1,100	1,100	1,100	1,100	1,1	1,100	1,1	1,100
A mm <sup>2</sup>	76096,38	144355,9	288178,9	27836,19	49036	75009,81	117774,3	141526,7	254257,7	68028,33	305141,7	213455,7
A <sub>eff</sub> mm <sup>2</sup>	73052,52	138581,7	276651,7	26722,74	47074,56	72009,42	113063,4	135865,6	244087,4	65307,2	292936,1	204917,4
foil thickness (mm)	0,20	0,30	0,50	0,10	0,10	0,2	0,3	0,50	0,60	0,1	0,50	0,4
J (A/mm <sup>2</sup> )	1,1	1,1	1,1	1,1	1,3	1,2	1,1	1,1	1,1	1,1	1,1	1,1
foil height (mm)	228	380	456	115	193	210	267	228	380	456	456	427
N (turns)	950	500	250	2300	1300	850	600	450	250	1000	250	350
l <sub>gap</sub> (mm)	77,1	101,4	101,4	46,9	52,8	69,0	85,4	91,3	101,4	81,2	101,4	106,4
winding width (mm)	665	400	250	1380	780	595	480	450	275	600	250	315
window (mm)	835	570	420	1550	950	765	650	620	445	770	420	485
w (mm)	207,3	285,5	403,4	125,4	166,4	205,8	257,9	282,7	378,9	196,0	415,1	347,2
d (mm)	352,4	485,4	685,8	213,1	282,9	349,9	438,4	480,6	644,2	333,2	705,7	590,2
Temp rise (K)	100	100	100	100	100	100	100	100	100	100	100	100
wind-wind clearance	50	50	50	50	50	50	25	50	50	50	50	25
yoke clearance (mm)	200	200	200	200	200	200	120	200	200	200	200	120
tube (mm)	10	10	10	10	10	10	10	10	10	10	10	10
limb-wind clearance	50	50	50	50	50	50	50	50	50	50	50	50
PVC (Euro)	66615	104110	175630	43550	48130	61419	84180	96450	154690	64861	185340	140080
Simulation Results												
L <sub>total</sub> (mH)	1421,10	508,77	236,19	6399,40	2557,70	1209,50	728,00	456,75	211,77	1277,10	249,73	338,48
L <sub>gap</sub> (mH)	1054,00	423,87	211,49	3200,00	1834,90	928,56	589,90	373,33	186,73	992,10	223,90	292,90
L <sub>iron</sub> (mH)	11,20	3,02	1,49	404,38	32,20	10,20	4,95	2,84	1,27	10,17	1,59	1,97
L <sub>leakage</sub> (mH)	355,90	81,88	23,21	2795,02	690,60	270,74	133,15	80,58	23,77	274,83	24,24	43,61
Leakage %	25,04	16,09	9,83	43,68	27,00	22,38	18,29	17,64	11,22	21,52	9,71	12,88
Inductance decline %	-12,47%	-0,66%	6,54%	-26,62%	-1,21%	4,28%	-0,83%	9,63%	16,20%	-1,07%	1,18%	-0,46%

## APPENDIX D

### THE MOST COMMON STANDARD TRANSFORMER RATINGS

Table D1. Distribution Transformers of Beyoğlu Region [79]

Voltage (kV)	Total number of transformers	Unit x power (kVA)	Total power (MVA)
10.5/0.4	652	3x2000 71x1600 82x1250 76x1000 48x800 260x630 25x500 76x400 3x230 9x150	545.2
34.5/0.4	40	Sale	56.83

Table D.2 Dispersion of MV/LV Distribution Transformers Installed in Turkish Electricity Grid Related to Voltage Levels [79]

MV/LV (kV/kV)	Unit	Total		Average Power (MVA)
		Unit (%)	Installed Capacity (MVA)	
30/0.4	86388	73.2	14182.8	164.1
15/0.4	19191	16.3	3565.3	185.8
10.5/0.4	4770	4.0	3271.5	685.8
6.3/0.4	7610	6.5	4560.6	599.3
Total	117459	100.0	25580.2	

Table D.3 ABB Oil Immersed Transformer Power Rating (34.5/0.4 kV) [80]

Power (kVA)	Price (USD)
50	4500
100	5500
160	7000
250	8500
400	11000
630	14000
800	16000
1000	18000
1250	20000
1600	25000
2000	30000
2500	34000

Table D.4 Standard Ratings of Distribution Transformers (kVA) [81]

Overhead type		Pad-mounted type	
Single-phase	Three-phase	Single-phase	Three-phase
5	15	25	75
10	30	37 <sup>1/2</sup>	112 <sup>1/2</sup>
15	45	50	150
25	75	75	225
37 <sup>1/2</sup>	112 <sup>1/2</sup>	100	300
50	150	167	500
75	225		750
100	300		1000
167	500		1500
250			2000
333			2500
500			

## APPENDIX E

### MAXWELL SOFTWARE OVERVIEW [16]

“Maxwell is a high-performance interactive software package that uses finite element analysis (FEA) to solve three-dimensional (3D) electric, magnetostatic, eddy current, and transient problems.

#### **Electric 3D fields:**

- Electrostatic 3D fields in dielectrics caused by a user-specified distribution of voltages and charges. Additional computed quantities you can specify include torque, force, and capacitances.
- Electric 3D fields in conductors, characterized by a spatial distribution of voltage, electric field, and DC current density. The main additional quantity in this case is power loss.
- A combination of the first two with conduction solutions being used as boundary conditions for an electrostatic problem.

#### **Magnetostatic:**

- Linear and nonlinear 3D magnetostatic fields caused by a user-specified distribution of DC current density, voltage, permanent magnets, or externally applied magnetic fields. Additional computed quantities you can specify include torque, force, and inductances (self and mutual).
- Applications that use Magnetostatic Analysis can be solenoids, inductors, motors, actuators, permanent magnets, stray field calculations and many others.
- The magnetostatic solver computes static (DC) magnetic fields.

- All objects are stationary.
- The source of the static magnetic field can be:
  - DC current in conductors
  - Permanent magnets
  - Static magnetic fields represented by external boundary conditions.
- The quantity solved is the magnetic field (H).
- Current density (J) and magnetic flux density (B) are automatically calculated from the magnetic field (H).
- Derived quantities such as forces, torques, energy, and inductances may be calculated from these basic field quantities.
- Material permeabilities can be nonlinear and/or anisotropic.

**Eddy current:**

- Harmonic (sinusoidal variation in time) steady state 3D magnetic fields with pulsation-induced eddy currents in massive (solid) conductors caused by one of the following: by a user-specified distribution of AC currents (all with the same frequency but with possibly different initial phase angles), or by externally applied magnetic fields. The eddy solution is a full wave solution that includes electromagnetic wave radiation effects.
- Applications that use Eddy Current Analysis can be solenoids, inductors, motors, stray field calculations and many others.
- The eddy current solver computes steady-state, time-varying (AC) magnetic fields at a given frequency – this is a frequency domain solution.
- All objects are stationary.
- The source of the static magnetic field can be:
  - Sinusoidal AC current (peak) in conductors.
  - Time-varying external magnetic fields represented by external boundary conditions.
- The quantities solved are the magnetic field (H) and the magnetic scalar potential ( $\Omega$ ).
- Current density (J) and magnetic flux density (B) are automatically calculated
- from the magnetic field (H).

- Derived quantities such as forces, torques, energy, and inductances may be
- calculated from these basic field quantities.
- Material permeabilities and conductivities can be anisotropic, but must be linear.

**Transient:**

- Time domain 3D magnetic fields caused by permanent magnets and windings supplied by voltage and/or current sources with arbitrary variation as functions of time; electrical circuits will be connected with the windings. Rotational or translational motion effects can also be included in the simulation.
- Applications that use Transient Analysis can be solenoids, inductors, motors, actuators, permanent magnets and many others.
- The Transient solver computes magnetic fields in the time domain (instantaneously at each time step).
- The solver formulation is based on a current vector potential in solid conductors, and a scalar potential over the entire field domain.
- The source of the static magnetic field can be:
  - Arbitrary time-varying current in conductors.
  - Permanent magnets.
- Field Quantities are strongly coupled with circuit equations to allow voltage sources and/or external driving circuits.
- The quantity solved is the magnetic field (H) and the current density (J) while magnetic flux density (B) is automatically calculated from the H-field.
- Derived quantities such as forces, torques, flux linkage and core loss may be calculated from these basic field quantities.
- Material permeabilities can be nonlinear and/or anisotropic.
- Permanent magnets are considered.
- Excitations can be sinusoidal or non-sinusoidal including:
  - Voltages and currents applied to windings.
  - External circuits attached to windings.
  - Permanent magnets.”

## CIRRICULUM VITAE

### PERSONAL INFORMATION

Surname, Name : Dönük, Atilla  
Nationality : Turkish (TC)  
Date and Place of Birth : 17 February 1977, Malatya  
Marital Status : Married  
Phone : +90 312 210 46 21  
Fax : +90 312 210 23 04  
email : atilla@metu.edu.tr

### EDUCATION

Degree	Institution	Year of Graduation
BS	Inonu University, Electrical and Electronics Engineering	2000
High School	H.H.K. Anadolu Ticaret High School, Malatya	1995

### WORK EXPERIENCE

Year	Place	Enrollment
2002 Sept.-Present	METU Electrical and Electronics Eng. Dept.	Research Assistant
2010 Nov.-2011 Oct.	University of Southampton School of ECS	Visiting Researcher
2000 Nov.-2002 Aug.	Çalık Holding	Maintenance Engineer
1999 August	Çalık Holding	Intern Eng. Student
1999 July	Türk Telekom	Intern Eng. Student

### FOREIGN LANGUAGES

English

### PUBLICATIONS

1. Donuk Atilla, Rotaru Mihai, Sykulski Jan K., *Defining And Computing Equivalent Inductances Of Gapped Iron Core Reactors*, XV International Symposium on Electromagnetic Fields in Mechatronics, Electrical and Electronic Engineering (ISEF), September 2011, Funchal, Madeira.
2. Atilla Donuk, Mihai Rotaru, Jan K. Sykulski, *Defining And Computing Equivalent Inductances Of Gapped Iron Core Reactors*, Przegląd Elektrotechniczny (Electrical Review), Vol.88, No.7b, pp.52-55, 2012.
3. A. Donuk, H.F. Bilgin, M. Ermis, *Effects of Distributed Air-Gaps in the Iron-Core of Shunt Reactors on Inductance Components and Losses*, International Review of Electrical Engineering (IREE), Vol.7, No.3, pp. 4428-4436, 2012.